

1996

A PALAEOMAGNETIC STUDY OF CRUSTAL ROTATIONS AND THEIR RELATIONSHIP TO THE TECTONICS OF THE ATACAMA AND DOMEYKO FAULT SYSTEMS, NORTHERN CHILE

RANDALL, DARREN EDWARD

<http://hdl.handle.net/10026.1/1728>

<http://dx.doi.org/10.24382/4592>

University of Plymouth

All content in PEARL is protected by copyright law. Author manuscripts are made available in accordance with publisher policies. Please cite only the published version using the details provided on the item record or document. In the absence of an open licence (e.g. Creative Commons), permissions for further reuse of content should be sought from the publisher or author.

**A PALAEO-MAGNETIC STUDY OF CRUSTAL ROTATIONS AND THEIR
RELATIONSHIP TO THE TECTONICS OF THE ATACAMA AND DOMEYKO
FAULT SYSTEMS, NORTHERN CHILE**

DARREN EDWARD RANDALL

A thesis submitted to the University of Plymouth

in partial fulfilment for the degree of

DOCTOR OF PHILOSOPHY

DARREN EDWARD RANDALL
Department of Geological Sciences

Faculty of Science

In collaboration with

Servicio Nacional de Geología y Minería (SERNAGEOMIN), Chile

June 1996

LIBRARY STORE

REFERENCE ONLY

UNIVERSITY OF SOUTH	
Item No.	900 2789755
Date	25 OCT 1988
Class No.	551.87098
Contl. No.	X703358226
LIBRARY SERVICES	

3 RAN

90 0278975 5



A PALAEOMAGNETIC STUDY OF CRUSTAL ROTATIONS AND THEIR
RELATIONSHIP TO THE TECTONICS OF THE ATACAMA AND DOMEYKO
FAULT SYSTEMS, NORTHERN CHILE

DARREN EDWARD RANDALL

ABSTRACT

A total of 178 sites have been collected for palaeomagnetic analysis from within two strike-slip fault systems in northern Chile (25.4°S - 26.4°S); the Atacama Fault System in the Coastal Cordillera, and the Domeyko Fault System in the Andean pre-Cordillera. In the Coastal Cordillera, analysis of Middle Jurassic lavas (La Negra Formation) and Middle Jurassic to Early Cretaceous dyke swarms reveal a consistent clockwise rotation of approximately 42°. The remanence from the La Negra Formation passes both fold and reversal tests and is interpreted as a pre-folding remanence. Four of the five dyke swarms have mixed polarity, suggesting that they too carry a primary or very early remanence. The clockwise rotation of the area is interpreted as occurring due to a domino-type mechanism where the blocks are bounded by sinistral faults operating in a crustal scale strike-slip duplex structure. The rotation is the result of sinistral transpression during the middle Cretaceous as a result of the Peruvian Orogeny leading to abandonment of the Jurassic-Early Cretaceous magmatic arc in the Coastal Cordillera and its subsequent eastward migration.

The Domeyko Fault System (DFS) comprises the Domeyko Fault Zone (DFZ), and a series of subsidiary faults to the east which define two distinct but slightly overlapping domains: a fold-and-thrust belt in the north and a domain of sinistral strike-slip faults in the south. Samples were collected from the volcanic rocks of the Sierra Fraga Formation (Middle Jurassic) west of the DFZ, and from the lavas of the Quebrada Vicuña Formation (Late Jurassic) and Cerro Valiente Formation (Palaeocene) from both domains of the DFS. Also sampled in the southern domain, and in a small area between the two domains were sandstones of the Quebrada Monardes Formation (Early Cretaceous). All of the volcanic units have been remagnetised and no tectonic interpretation is made from them. The sandstones in the southern domain record a clockwise rotation of approximately 24° . This is interpreted as being due to compression across the DFS causing the sinistral strike-slip faults, and the blocks between them to rotate clockwise towards the major tectonic structure, the DFS. The sandstones in the central area between the two domains record an anticlockwise rotation of approximately 28° . This is explained by small-scale rotation of thrust sheets or slip on minor dextral strike-slip faults. The deformation and rotation in the pre-Cordillera occurred in response to the Incaic Orogeny during the Miocene-Oligocene.

LIST OF CONTENTS

ABSTRACT 1

LIST OF CONTENTS..... 3

LIST OF FIGURES..... 10

LIST OF TABLES 16

LIST OF PLATES..... 18

ACKNOWLEDGEMENTS 19

DECLARATION..... 20

1. INTRODUCTION..... 23

 1.1 Selection of sampling regions..... 27

 1.1.1 The Coastal Cordillera 29

 1.1.2 The pre-Cordillera..... 29

 1.2 The wider context of this work 31

 1.3 Geological background to South America 32

 1.3.1 The Andean margin..... 33

 1.3.2 The geology of northern Chile 34

 1.3.3 The Arica Deflection..... 37

2. THE GEOMAGNETIC FIELD, SAMPLING TECHNIQUES AND

PALAEOMAGNETIC METHODS..... 38

 2.1 Introduction..... 38

 2.2 The geomagnetic field and acquisition of magnetisation 38

 2.2.1 Acquisition of magnetisation 41

2.3 Sample collection and preparation.....	43
2.4 Specimen measurement	44
2.5 Demagnetisation.....	44
2.5.1 Thermal demagnetisation	45
2.5.2 Alternating field demagnetisation	48
2.6 Magnetic mineralogy studies	49
2.6.1 Identification of magnetic minerals	49
2.6.2 Grain size determination	51
2.6.3 Measurements of the decay of viscous remanent magnetisation	52
2.6.4 Anisotropy of magnetic susceptibility.....	53
2.7 Data interpretation and statistics.....	53
2.7.1 Calculation of rotation, flattening and associated errors	55
 3. PALAEOMAGNETIC REFERENCE POLES AND REFERENCE DIRECTIONS .	57
3.1 Introduction.....	57
3.2 Reliability criteria	59
3.3 Review of previous APWPs and reference directions	66
3.4 Calculating a new reference direction	69
3.4.1 Jurassic reference directions	73
i) Early Jurassic (208-178 Ma).....	73
ii) Middle Jurassic (178-157.1 Ma).....	76
iii) Late Jurassic (157.1-145.6 Ma).....	76
3.4.2 Cretaceous reference directions	77
i) Early Cretaceous (145.6-131.8 Ma).....	77

- ii) mid-Cretaceous (131.8-88.5 Ma)..... 77
 - iii) Late Cretaceous (88.5-65 Ma) 78
 - 3.4.3 Cenozoic reference directions 79
 - i) The early Cenozoic (Palaeogene)..... 79
 - ii) The late Cenozoic (Neogene)..... 80
 - 3.5 Conclusions 80

- 4. CAUSES OF VERTICAL AXIS ROTATION 83
 - 4.1 Introduction..... 83
 - 4.2 Rigid bending of the continental margin..... 84
 - 4.2.1 Oroclinal bending..... 84
 - 4.2.2 Differential shortening 86
 - 4.3 Mechanisms and models for small-scale
 - in situ* vertical axis rotations..... 88
 - 4.3.1 The role of strike-slip faults in *in situ* vertical axis rotation..... 88
 - 4.3.2 Definitions of models..... 92
 - 4.3.3 Continuum versus discrete deformation..... 98
 - 4.3.4 Discrete models of *in situ* vertical axis rotation..... 99
 - 4.3.5 *In situ* rotation on thrust sheets 107
 - 4.4 Mechanisms and models for large-scale
 - in situ* vertical axis rotation 107
 - 4.5 Conclusions..... 110

- 5. THE COASTAL CORDILLERA AND THE ATACAMA FAULT SYSTEM 111
 - 5.1 Introduction..... 111

5.2 The geology of the Coastal Cordillera	
and the Atacama Fault System.....	113
5.2.1 Geology and petrology	113
5.2.2 Structural geology and the Atacama Fault System.....	122
5.3 Structural and palaeostress analysis of the dykes	127
5.3.1 Dyke emplacement and orientation.....	127
5.3.2 Palaeostress analysis.....	129
5.3.3 Discussion of the palaeostress analysis results.....	132
5.4 Palaeomagnetic results.....	137
5.4.1 La Negra Formation.....	137
i) Palaeomagnetic sampling localities	137
ii) Magnetic mineralogy	137
iii) Anisotropy of magnetic susceptibility	142
iv) Palaeomagnetic remanence measurements.....	148
v) Discussion of results.....	158
5.4.2 Magnetic mineralogy of dyke samples.....	159
5.4.3 Low and intermediate coercivity/unblocking	
temperature components in the dyke samples	165
5.4.4 Dykes in the Vetado pluton.....	166
i) Palaeomagnetic sampling localities	166
ii) Palaeomagnetic remanence measurements.....	166
iii) Discussion of results	171
5.4.5 Dykes from the Flamenco pluton	174
i) Palaeomagnetic sampling localities	174
ii) Palaeomagnetic remanence measurements.....	174

iii) Discussion of results	177
5.4.6 Dykes from the Las Animas pluton	182
i) Palaeomagnetic sampling localities	182
ii) Palaeomagnetic remanence measurements.....	182
iii) Discussion of results	185
5.4.7 Dykes from the Las Tazas pluton	190
i) Palaeomagnetic sampling localities	190
ii) Palaeomagnetic remanence measurements.....	192
iii) Discussion of results	195
5.4.8 Dykes from the Remolino pluton	200
i) Palaeomagnetic sampling localities	200
ii) Palaeomagnetic remanence measurements.....	201
ii) Discussion of Results	210
5.5 Discussion and conclusions.....	211
6. THE PRE-CORDILLERA AND THE DOMEYKO FAULT SYSTEM	214
6.1 Introduction.....	214
6.2 The geology and structure of the Cordillera	
de Domeyko and the Domeyko Fault System.....	216
6.2.1 Geology and petrology of lithologies in the study area.....	217
6.2.2 Structural geology and the Domeyko Fault System	225
6.3 Palaeomagnetic results.....	229
6.3.1 Sierra Fraga Formation.....	229
i) Palaeomagnetic sampling localities	229
ii) Magnetic mineralogy	229

iii) Palaeomagnetic remanence measurements.....	232
iv) Discussion of results.....	238
6.3.2 Quebrada Vicuña Formation.....	241
i) Palaeomagnetic sampling localities.....	241
ii) Magnetic mineralogy	241
iii) Palaeomagnetic remanence measurements.....	248
iv) Discussion of results.....	259
6.3.3 Quebrada Monardes Formation.....	261
i) Palaeomagnetic sampling localities.....	261
ii) Magnetic mineralogy	263
iii) Palaeomagnetic remanence measurements.....	263
iv) Discussion of results.....	274
6.3.4 Cerro Valiente Sequence.....	276
i) Palaeomagnetic sampling localities.....	276
ii) Magnetic mineralogy	279
iii) Palaeomagnetic remanence measurements.....	284
iv) Discussion of results.....	291
6.4 Discussion and Conclusions.....	295
 7. MODELS FOR ROTATION IN THE ATACAMA AND DOMEYKO FAULT	
SYSTEM	298
7.1 Introduction.....	298
7.2 Rigid bending of the Andean margin	303
7.3 Large-scale <i>in situ</i> rotation models	308
7.4 Small-scale <i>in situ</i> rotation models.....	311

7.5 Proposed models for rotation in the	
Atacama and Domeyko Fault Systems	315
7.5.1 The Atacama Fault System.....	317
7.5.2 The Domeyko Fault System	321
7.6 Conclusions	326
 8. SUMMARY AND CONCLUSIONS	 327
8.1 Introduction	327
8.2 The Coastal Cordillera	327
8.3 The pre-Cordillera.....	329
8.4 The Andean margin.....	331
8.5 Recommendations for future work	332
 APPENDICES	 334
APPENDIX 1 THIN SECTION DESCRIPTIONS	335
APPENDIX 2 PALAEOMAGNETIC DATA	345
 REFERENCES	 346

LIST OF FIGURES

1. INTRODUCTION

1.1	Map of South America	24
1.2	Tectonic map of Nazca plate	25
1.3	Generalised geological map of study area	28
1.4	Map of magmatic arcs in northern Chile	36

2. THE GEOMAGNETIC FIELD, SAMPLING TECHNIQUES AND

PALAEOMAGNETIC METHODS

2.1	Description of the Earth's magnetic field	40
2.2	Graph of hold time requirement for thermal samples	47
2.3	Oven temperature calibration	47
2.4	Examples of IRM plots	50

3. PALAEOMAGNETIC REFERENCE POLES AND REFERENCE DIRECTIONS

3.1	Plot of previously published APWPs for South America	70
3.2	Plot of reference directions for this thesis	81

4. CAUSES OF VERTICAL AXIS ROTATION

4.1	The oroclinal bending model	85
4.2	The differential shortening model	85
4.3	Cross-sections through the Andean margin	87
4.4	Model of displacing conjugate faults	89
4.5	Domain formation in strike-slip faults	89

4.6	Orientation of fractures in transpressional shear zones.....	91
4.7	General models of accommodating strike-slip deformation	93
4.8	The major classes of strike-slip faults	94
4.9	Terminology of strike-slip deformation zones	96
4.10	The ball-bearing model.....	100
4.11	The slat model	103
4.12	The two domain model.....	103
4.13	The soft block model	105
4.14	Mechanisms for avoiding sphenochasms	106
4.15	Transtensional rotation model	108
4.16	The buttress model	108

5. THE COASTAL CORDILLERA AND THE ATACAMA FAULT SYSTEM

5.1	Geological map of the study area in the Coastal Cordillera.....	112
5.2	The timing of events in the Coastal Cordillera.....	114
5.3	Map of Atacama Fault Zone and subsidiary faults.....	123
5.4	Map of the Atacama Fault System.....	125
5.5	Morphology of dykes.....	130
5.6	Features of a side-stepping dyke and construction of the dilation plane.....	131
5.7	Structural data from the dykes.....	133
5.8	Map of sampling sites in the La Negra Fm.....	138
5.9	IRM data for the La Negra Fm.	139
5.10	Shape Parameters of anisotropy, La Negra Fm.	145
5.11	Plot of principle susceptibility axes, La Negra Fm.....	147

5.12	Plot of low temperature components, La Negra Fm.....	151
5.13	Demagnetisation plots of two samples in La Negra Fm.....	152
5.14	Plot of site mean directions, La Negra Fm..	154
5.15	Demagnetisation plots, La Negra Fm..	155
5.16	IRM data for dyke samples.....	160
5.17	Map of sampling sites in the Vetado pluton.....	167
5.18	Plot of low temperature components, dykes in Vetado pluton.....	169
5.19	Plot of site mean directions, dykes in Vetado pluton	170
5.20	Demagnetisation plots, dykes in Vetado pluton	172
5.21	Map of sampling sites in the Flamenco pluton.....	175
5.22	Plot of low temperature components, dykes from Flamenco pluton....	178
5.23	Plot of site mean directions, dykes in Flamenco pluton.....	179
5.24	Demagnetisation plots, dykes in Flamenco pluton.....	180
5.25	Map of sampling sites in the Las Animas pluton	183
5.26	Plot of site mean directions, dykes in Las Animas pluton.....	186
5.27	Plot of low temperature components, dykes in Las Animas pluton	187
5.28	Demagnetisation plots, dykes in Las Animas pluton.....	188
5.29	Map of sampling sites in the Las Tazas pluton.....	191
5.30	Plot of site mean directions, dykes in Las Tazas pluton.....	194
5.31	Plot of low temperature components, dykes in Las Tazas pluton	196
5.32	Demagnetisation plots, dykes in Las Tazas pluton.....	197
5.33	Map of sampling sites in the Remolino pluton.....	199
5.34	Plot of site mean directions, dykes in Remolino pluton.....	203
5.35	Down core variation in demagnetisation behaviour.....	204
5.36	Plot of low temperature components, dykes in Remolino pluton	205

5.37	Demagnetisation plots, dykes in Remolino pluton.....	207
------	--	-----

6. THE PRE-CORDILLERA AND THE DOMEYKO FAULT SYSTEM

6.1	Geological map of the study area in the pre-Cordillera	215
6.2	Stratigraphy in the sampling region.....	218
6.3	Map of the Domeyko Fault System	226
6.4	Map of the sampling sites for the Sierra Fraga Fm.....	230
6.5	IRM data, Sierra Fraga Fm.	231
6.6	Plot of low coercivity components, Sierra Fraga Fm.	235
6.7	Demagnetisation plots, Sierra Fraga Fm.....	236
6.8	Plot of site mean directions, Sierra Fraga Fm.....	239
6.9	Plot showing tilt correction of site mean directions.....	240
6.10	Map of sampling sites for the Quebrada Vicuña Fm. (north)	242
6.11	Map of sampling sites for the Quebrada Vicuña Fm. (south)	243
6.12	Cross-section showing sampling sites in Quebrada Asientos (west)....	244
6.13	Cross-section showing sampling sites in Quebrada Asientos (east)....	245
6.14	IRM data, Quebrada Vicuña Fm.	246
6.15	VRM decay in samples from the Quebrada Vicuña Fm.	250
6.16	Plot of low coercivity components, Quebrada Vicuña Fm.	254
6.17	Demagnetisation plots, Quebrada Vicuña Fm.....	256
6.18	Plot of site mean directions, Quebrada Vicuña Fm. (north)	258
6.19	Plot of site mean directions, Quebrada Vicuña Fm. (south)	260
6.20	Map of sampling sites in the Quebrada Monardes Fm.....	262
6.21	IRM data, Quebrada Monardes Fm.	264
6.22	Plot of low temperature components, Quebrada Monardes Fm.	269

6.23	Demagnetisation plots, Quebrada Monardes Fm.	270
6.24	Plot of site mean directions, Quebrada Monardes Fm. (south).....	273
6.25	Plot of site mean directions, Quebrada Monardes Fm. (central).....	275
6.26	Map of sampling sites in the Cerro Valiente Fm. (north).....	277
6.27	Map of sampling sites in the Cerro Valiente Fm. (south)	278
6.28	IRM data, Cerro Valiente Fm.	280
6.29	VRM decay in samples from the Cerro Valiente Fm.	283
6.30	Plot of low coercivity components, Cerro Valiente Fm.	287
6.31	Demagnetisation plots, Cerro Valiente Fm.	289
6.32	Plot of site mean directions, Cerro Valiente Fm. (north).....	292
6.33	Plot of site mean directions, Cerro Valiente Fm. (south).....	293

7. MODELS FOR ROTATION IN THE ATACAMA AND DOMEYKO FAULT

SYSTEM

7.1	Map showing palaeomagnetic rotations recorded around the Arica Deflection.....	302
7.2	Large-scale map of Mesozoic directions from around the Arica deflection	304
7.3	Predicted rotations from the differential shortening model	306
7.4	Rotation versus latitude plots for palaeomagnetic data from around the Arica Deflection.....	306
7.5	The transtensional rotation model	309
7.6	The buttressing rotation model	309
7.7	Diagram of stress variations in an arcuate forearc	312
7.8	The <i>in situ</i> rotation model for the Atacama Fault Zone	316

7.9 Proposed model to explain rotations observed in the Coastal
 Cordillera 318

7.10 Proposed model to explain rotations observed in the southern
 domain in the pre-Cordillera 322

7.11 Map of minor structures in the area of overlap between the two
 structural domains..... 324

LIST OF TABLES

3. PALAEOMAGNETIC REFERENCE POLES AND REFERENCE DIRECTIONS

3.1	Palaeomagnetic reference directions from South America	64
3.2	Palaeomagnetic reference directions from Africa.....	72
3.3	Palaeomagnetic reference directions from South America and Africa which pass reliability criteria.....	74
3.4	References for tables 3.1 to 3.3	75
3.5	Mean reference directions calculated for this thesis	82

5. THE COASTAL CORDILLERA AND THE ATACAMA FAULT SYSTEM

5.1	Geochronological ages of plutons in the Coastal Cordillera.....	117
5.2	Anisotropy data from the La Negra Fm.	143
5.3	Sampling and demagnetisation data for La Negra Fm.	149
5.4	Remanence data from the La Negra Fm.	150
5.5	Sampling and demagnetisation data, dykes in Vetado pluton.....	168
5.6	Sampling and demagnetisation data, dykes in Flamenco pluton.....	176
5.7	Sampling and demagnetisation data, dykes in Las Animas pluton	184
5.8	Sampling and demagnetisation data, dykes in Las Tazas pluton.....	193
5.9	Sampling and demagnetisation data, dykes in Remolino pluton.....	202
5.10	Rotation and flattening for units in the Coastal Cordillera	213

6. THE PRE-CORDILLERA AND THE DOMEYKO FAULT SYSTEM

6.1	Sampling and demagnetisation data, Sierra Fraga Fm.	233
6.2	Remanence data from the Sierra Fraga Fm.	234

6.3	Grain size analysis, Quebrada Vicuña Fm.....	248
6.4	VRM decay measurements, Quebrada Vicuña Fm.	249
6.5	Sampling and demagnetisation data, Quebrada Vicuña Fm.	251
6.6	Remanence data from the Quebrada Vicuña Fm.	252
6.7	Sampling and demagnetisation data, Quebrada Monardes Fm.	267
6.8	Remanence data from the Quebrada Monardes Fm.	268
6.9	Grain size analysis, Cerro Valiente Fm.	281
6.10	VRM decay measurements, Cerro Valiente Fm.	282
6.11	Sampling and demagnetisation data, Cerro Valiente Fm.	285
6.12	Remanence data from the Cerro Valiente Fm.	286
6.13	Rotation and flattening for units in the pre-Cordillera.....	297

7. MODELS FOR ROTATION IN THE ATACAMA AND DOMEYKO FAULT SYSTEM

7.1	Mesozoic and Tertiary palaeomagnetic data recorded around the Arica Deflection.....	299
-----	--	-----

LIST OF PLATES

5. THE COASTAL CORDILLERA AND THE ATACAMA FAULT SYSTEM

5.1 Cross-cutting dykes in the Vetado pluton..... 119

5.2 Thin section from La Negra Fm. 121

5.3 Thin section from Vetado pluton..... 121

6. THE PRE-CORDILLERA AND THE DOMEYKO FAULT SYSTEM

6.1a The Early-Late Jurassic units in the sampling region..... 220

6.1b The Late Jurassic-Early Cretaceous units in the sampling region..... 221

6.2 Thin section of a Quebrada Vicuña Fm. lava..... 223

6.3 Thin section of cross-cutting veins in a Quebrada Vicuña Fm. lava.. 223

6.4 Thin section of the Quebrada Monardes Fm.. 224

6.5 Thin section of a Cerro Valiente Fm. lava 224

ACKNOWLEDGEMENTS

My first thanks go to Stephen Caswell, whose recommendation one evening in July 1992 in part gave me the opportunity to carry out this research.

I would like to thank my supervisors, Graeme Taylor and Don Tarling, for their help and support during this work. Many of the ideas developed in this work were done so after lengthy discussions with Graeme concerning the geology of northern Chile. Graeme also commented thoroughly on numerous drafts of this thesis. Thanks also go to Tony Morris for his patience in explaining numerous palaeomagnetic techniques and his meticulous reading of several of the chapters in this thesis. Discussions about stress, strain, faulting and dyke emplacement with Mark Anderson and Dave Peacock greatly increased my understanding of tectonic mechanisms and structural processes. I gratefully acknowledge the support and encouragement of my fellow research students, both past and present, and the help from several members of staff in the Department of Geological Sciences. Conversations with members of the wider palaeomagnetic community allowed me to exchange ideas about many aspects of this work.

Access to the palaeomagnetic facilities at the University of Newcastle-upon-Tyne was arranged by Alan Stephenson and David Collinson, and my knowledge of rock magnetic studies benefited greatly from discussions with Dave Potter.

All figures were drafted by the author except Figures 5.1 and 5.3, drafted by Stella Bignold at the University of Kingston. All thin sections were prepared by Mike Ashton.

Thanks to my family and friends for supporting me during this Ph.D. My final but most important thanks go to Joanne Thomas for putting up with my fixation of rocks, and for her support and help during the long hours involved in the final preparation of this thesis.

AUTHOR'S DECLARATION

At no time during the registration for the degree of Doctor of Philosophy has the author been registered for any other University award. This study was financed with the aid of a studentship from the Faculty of Science, University of Plymouth. During this study relevant conferences and seminars were attended at which this work was presented. One paper was prepared for publication.

Publications:

Randall, D.E., G.K. Taylor, and J. Grocott, Major Crustal Rotations in the Andean Margin: Paleomagnetic Results from the Coastal Cordillera of Northern Chile. *J. Geophys. Res.*, 101 (B7), 15,783-15, 798, 1996.

Conferences Attended:

International Association of Geomagnetism and Aeronomy, Buenos Aires, 1993

Palaeomagnetic Pow-Wow, Southampton, 1993; Edinburgh, 1994.

United Kingdom Geophysical Assembly, Oxford, 1993; Liverpool, 1994;

Manchester 1995.

Tectonic Studies Group, Leeds, 1994

European Union of Geosciences, Strasbourg, 1995

Andean Geosciences Workshop, Kingston University, 1995.

International Union of Geodesy and Geophysics, Boulder, 1995.

Conference Contributions:

Taylor, G.K., D.E. Randall, J. Grocott, P.J. Treloar, and D.P. Dallmeyer, Palaeomagnetic and structural studies of arc tectonics and fault block rotation, northern Chile. *JAG*, 4, 1993.

Taylor, G.K., D.E. Randall, J. Grocott, and P.J. Treloar, Palaeomagnetic studies of transtensional rotations associated with granite emplacement and the Atacama Fault System (26-27°S). *IAGA*, 1993.

Taylor, G.K., D.E. Randall, J. Grocott, and P.J. Treloar, Palaeomagnetic studies of fault block rotations in relation to transtension on the Atacama Fault System and granite emplacement. *2nd ISAG*, 253-254, 1993.

Randall, D.E. and G.K. Taylor, Palaeomagnetically identified block rotations and their relation to sinistral transtension on the Atacama Fault System. *JAG*, 5, 79, 1994.

Randall, D.E., G.K. Taylor, and J. Grocott, Paleomagnetically identified block rotations in the Coastal Cordillera of northern Chile. *Terra Abstracts*, 7, 268, 1995.

Randall, D.E., Palaeomagnetically identified block rotations associated with the Domeyko Fault System, northern Chile. *JAG*, 6, 27, 1995.

Randall, D.E., Palaeomagnetic study of block rotations in the Domeyko Fault System, northern Chile. *Andean Geoscience Workshop*, 1995.

Randall, D.E. and G.K. Taylor, Paleomagnetically identified block rotations in the Coastal Cordillera of northern Chile. *IUGG*, B91, 1995.

Randall, D.E., Paleomagnetic studies of rotations associated with the Domeyko Fault System, northern Chile. *IUGG*, B105, 1995.

Randall, D.E., Paleomagnetism and tectonics of Northern Chile. *IUGG*, Additional contribution, 1995.

Signed.....*Darren E. Rodell*.....

26th June 1996

Chapter 1

INTRODUCTION

Explicit in the plate tectonic model is the concept that the Earth's surface is composed of mobile rigid plates which, for most of their area, undergo slow rates of deformation. The boundaries of the plates, however, undergo rapid and intense deformation to accommodate large amounts of stress. At convergent margins this stress is usually accommodated in a narrow band of deformation. A typical feature often associated with deformation zones in overriding continental plates are crustal-scale strike-slip faults. Motion on these faults causes differential uplift and rotation of crustal blocks. While it is not possible to quantify the stress state in the overriding continental crust from geological observations (Jarrard, 1986; Apperson, 1991), lithologies and structures preserved in the plate give an indication of ancient stress regimes and subduction processes at the margin.

For almost 200 Ma, the Andean margin of South America (Figure 1.1) has been characterised by continuous subduction of normal oceanic lithosphere beneath a continental margin (Dalziel and Forsythe, 1985). The margin has the highest plate convergence rate in the world (Jarrard, 1986) and displays a variety of subduction features, including ridge subduction in southern Chile, variable slab dip and segmentation of the downgoing slab (Figure 1.2). Although little is known about the tectonics of the margin prior to this, it is known that the margin has faced an ocean basin since at least the latest Proterozoic (Dalziel, 1986).

Since the onset of orogenesis in the Late Triassic-Early Jurassic, a variety of subduction deformation related structures have developed. In northern Chile, Miocene-Recent rapid uplift combined with erosion associated with the arid environment, have exposed these structures particularly well. This neotectonic activity also means that there is

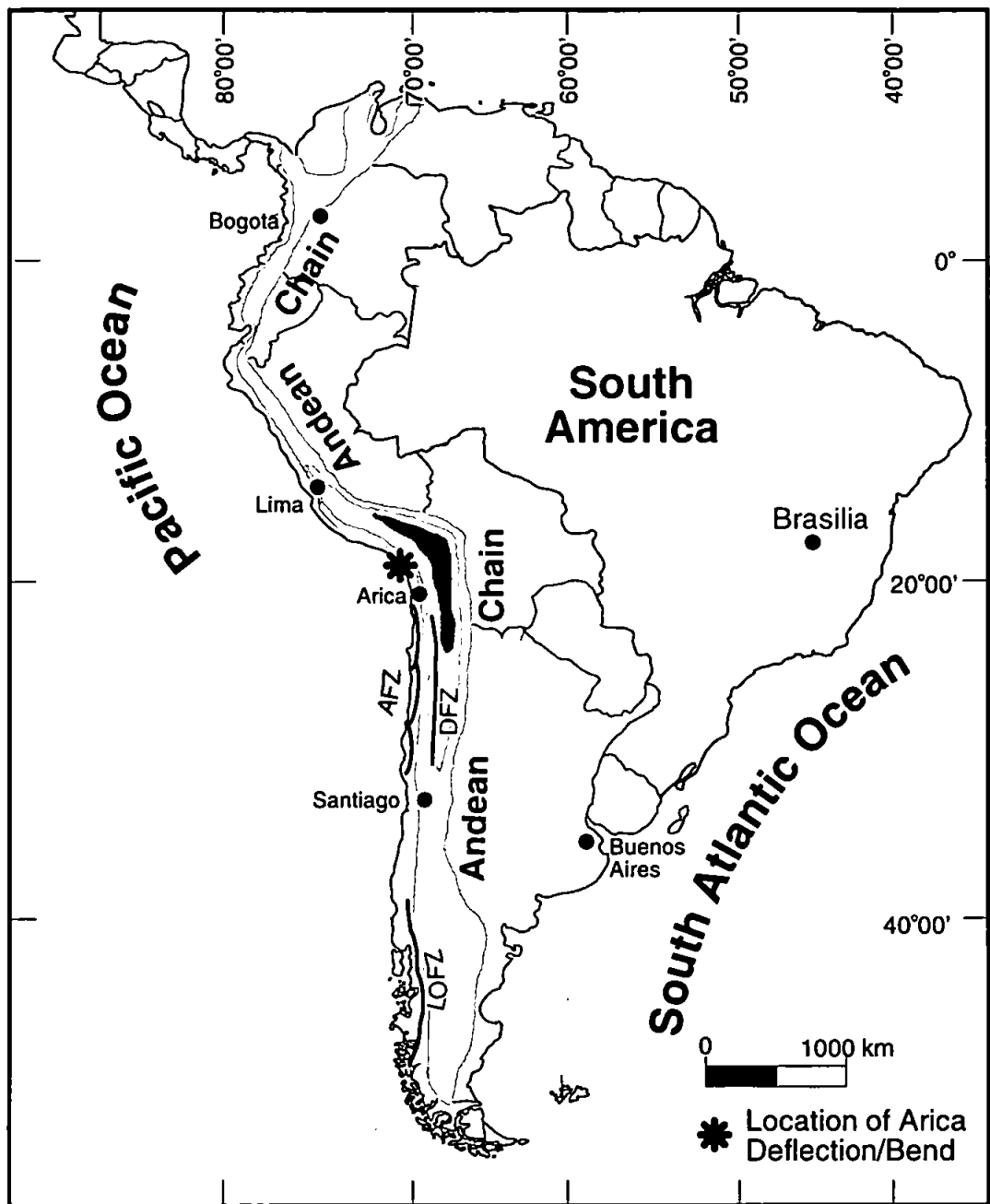


Figure 1.1. Map of South America showing the location of the Arica Deflection. Heights in the Andean chain are represented schematically, darker colour indicates higher mountains. Three of the major faults of Chile are shown. AFZ is the Atacama Fault Zone, DFZ is the Domeyko Fault Zone and LOFZ is the Liquine-Ofqui Fault Zone.

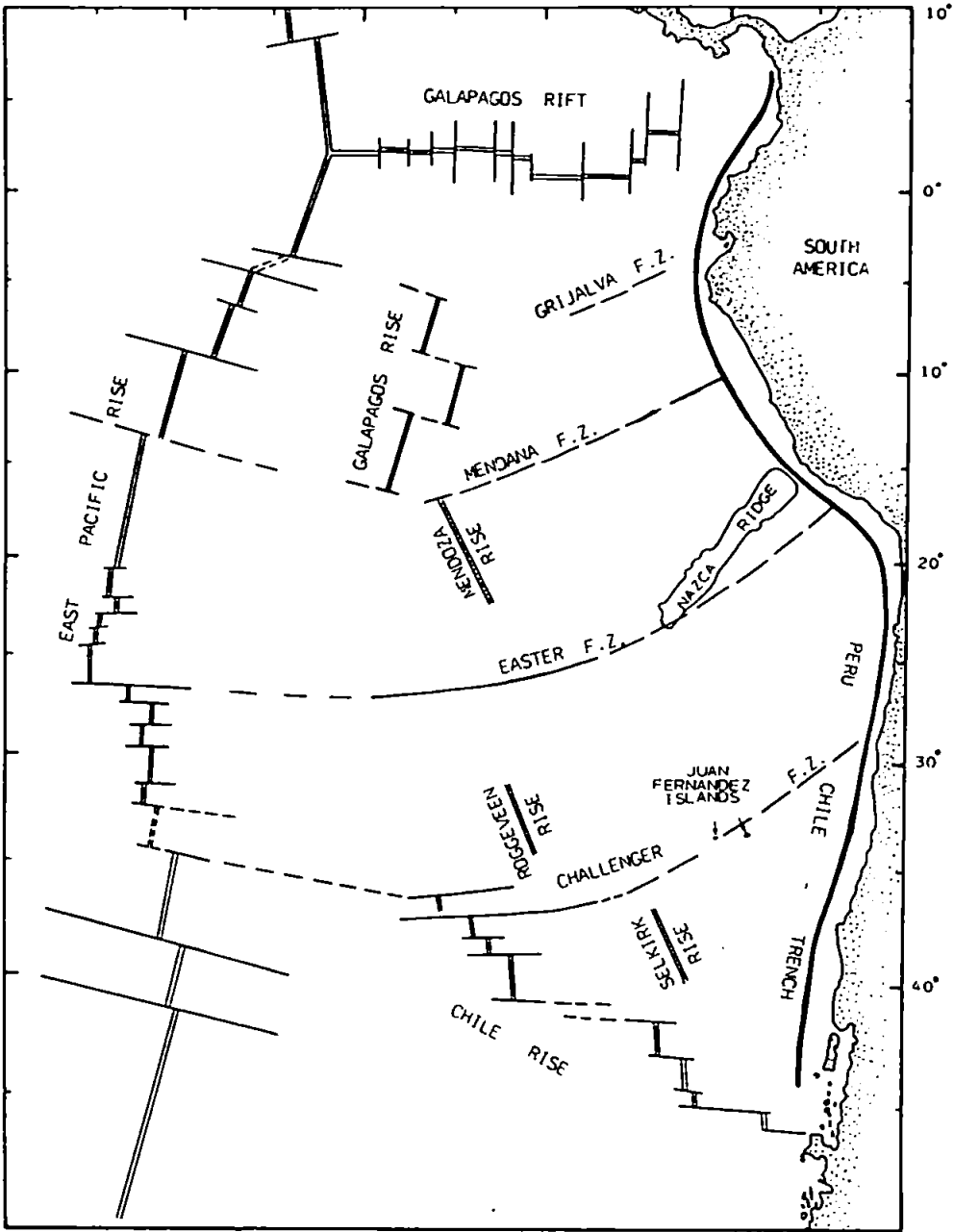


Figure 1.2. Simplified tectonic map of the Nazca plate. Modified from Warsi *et al.* (1983)

good exposure of a variety of lithologies across the Andean margin. Palaeomagnetic studies carried out along the length of the Andean margin indicate the presence of crustal rotations. The problem, however, with many of the previous palaeomagnetic studies of crustal rotations is that they have been limited by poor age constraints, restricted areal coverage, and most importantly the rotations have not been related to known fault systems using structural information.

Previous studies from the margin suggested that a palaeomagnetic study in northern Chile may identify rotations, and that this area is an ideal location to study rotations in relation to the well defined fault systems. Previous geological studies indicate that there are many lithologies suitable for palaeomagnetic investigation and that these are exposed over large areas. A study to identify, quantify and explain rotations thought to be associated with large scale strike-slip fault systems in the northern Chilean section of the Andean margin was therefore undertaken. The basic aims of this research can thus be summarised as follows:

1. To identify a stable characteristic palaeomagnetic remanence direction in sites sampled from Mesozoic units in the Coastal Cordillera and Mesozoic to early Cenozoic units in the Andean pre-Cordillera.
2. To identify and quantify any tectonic rotations by comparing characteristic remanence directions with those from stable South America.
3. To integrate the palaeomagnetic interpretation with the geology of the sampling areas.
4. To suggest tectonic models to account for both the observed rotations and the observed fault patterns in the study area.
5. To consider the rotation models with respect to other rotations identified in the Andean margin and the large-scale tectonic processes operating in the margin.

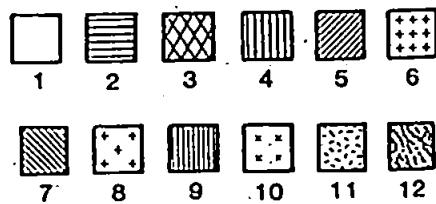
In this thesis, new palaeomagnetic data are presented and interpreted from a study in northern Chile. Chapters two, three and four give an introduction to the ideas and techniques used in this thesis. Chapter two is an introduction to the concepts behind the geomagnetic field and the basic principles of the palaeomagnetic methods used in this work. Chapter three contains a critical review of the available apparent polar wander paths for South America, as the lack of well constrained reference poles has been a major problem in recognising and quantifying rotation in the Andean margin. Chapter four discusses models which have been published to explain rotations in the Andean margin and other tectonically rotated areas. Chapters five, six and seven present the new palaeomagnetic data from northern Chile and models for the rotation are presented.

1.1 Selection of sampling regions

In northern Chile, two of the most important tectonic features are the Atacama Fault System (AFS) in the Coastal Cordillera, and the Domeyko Fault System (DFS) in the Andean pre-Cordillera. The major component of each of these fault systems is a margin parallel large-scale strike-slip fault, these are called the Atacama Fault Zone (AFZ) and the Domeyko Fault Zone (DFZ) respectively (Figure 1.1 and 1.3). Sampling of rocks for palaeomagnetic analysis was carried out from lithologies which outcrop within the two fault systems to identify the presence of any vertical axis rotation. It was intended that by sampling rocks of known age, the amount and timing of any rotation could be elucidated. In the body of this thesis, the sampling areas from the AFS in the Coastal Cordillera and the DFS in the pre-Cordillera are treated as separate and independent sampling regions.

Legend for Figure 1.3

1. Late Cenozoic continental sedimentary rocks
2. Miocene-Oligocene plutonic rocks
3. Early Tertiary plutonic rocks
4. Palaeocene-Eocene volcanic and sedimentary rocks
5. Cretaceous volcanic and sedimentary rocks
6. Cretaceous plutonic rocks
7. Jurassic volcanic rocks
8. Early Cretaceous-Late Jurassic plutonic rocks
9. Jurassic-Triassic sedimentary rocks in the east
10. Early Jurassic plutonic rocks
11. Triassic-Permian plutonic complexes
12. Palaeozoic pre-arc basement



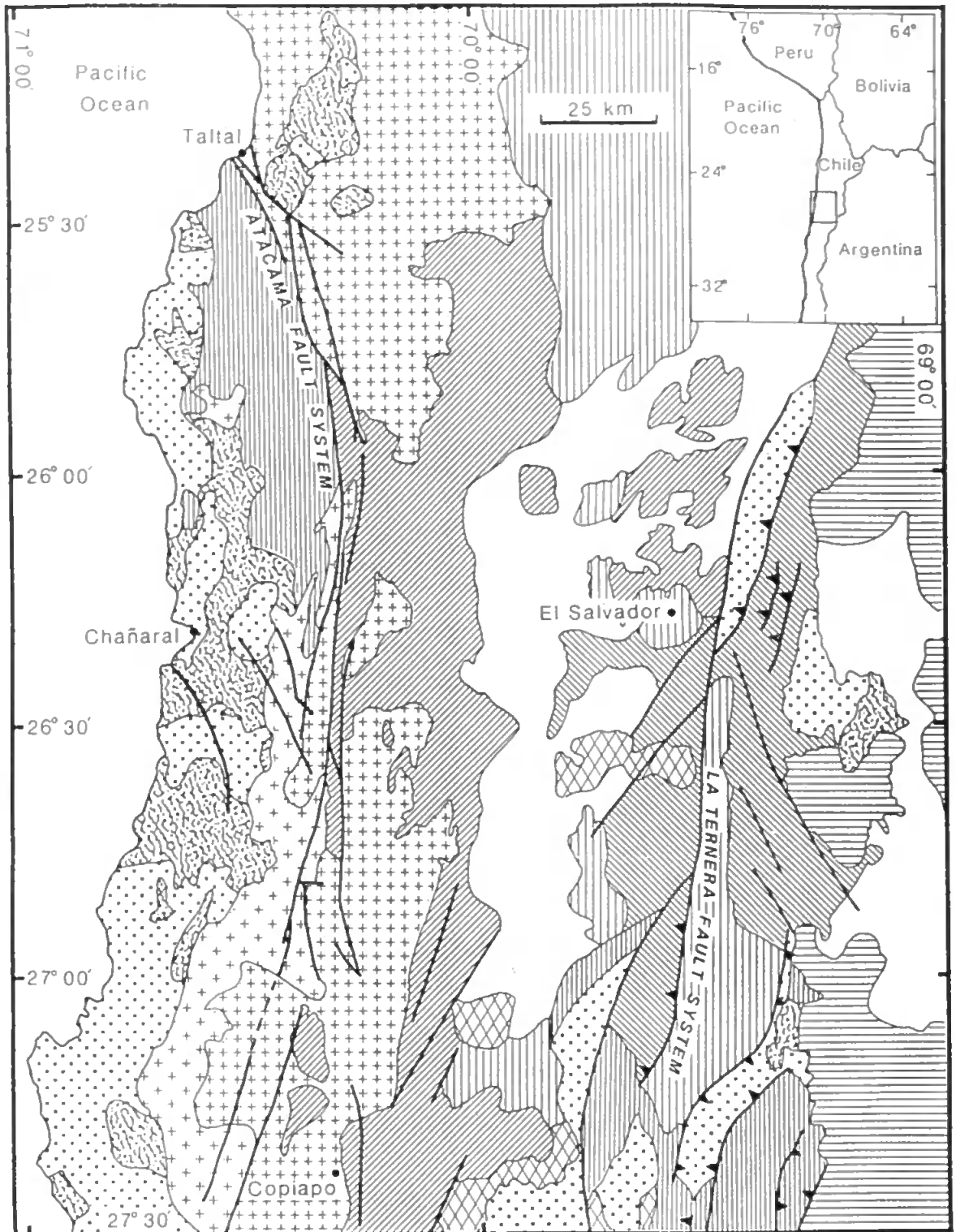


Figure 1.3. Generalised geological map showing the major tectonic features of the study area in northern Chile. The Atacama Fault System comprises the curved Atacama Fault Zone and the NW-SE trending faults to the west. The Domeyko Fault Zone is here marked the La Ternerera Fault System. To the east of this are the NE fold-and-thrust belt domain in the north, and the NW trending faults in the southern domain. Together with the Domeyko Fault Zone this comprises the Domeyko Fault System. The sampling localities are dominantly to the west of the Atacama Fault Zone and east of the Domeyko fault Zone (taken from Dallmeyer *et al.*, 1996, figure 1).

1.1.1 The Coastal Cordillera

The major structural feature in the Coastal Cordillera of northern Chile is the AFZ. The fault zone is defined by a series of sinistral ductile and brittle, sub-parallel and en-echelon north-south faults. The fault zone has been identified over a length of 1100 km, extending from near Iquique (20°S) to La Serena (30°S) and is divided into three seaward concave curvilinear fault segments. From south to north these are the El Salado, Paposo and Salar de Carmen segments (Naranjo, 1987). The sampling region for this study lies in the northern end of the El Salado segment and lies to the east of the coastal town of Chañaral (Figure 1.3). The AFS is a sinistral strike-slip fault system which comprises the AFZ together with a set of subsidiary faults.

This sampling locality was chosen as it had already been studied extensively, and work was ongoing (Berg and Breitzkreuz, 1983; Herve, 1987; Scheuber and Andriessen, 1990; Brown *et al.*, 1993; Grocott *et al.*, 1994; Dallmeyer *et al.*, 1996). These previous studies included geochronological work and detailed lithological and structural mapping. Together these studies indicated a variety of dated lithologies suitable for palaeomagnetic analysis, within a well defined and dated structural setting. Samples for palaeomagnetic analysis were collected from a large area within the fault system dominantly to the west, but also to the east of the main strands of the AFZ. The aim of the study was to identify any rotation in the area and to try and relate this to the fault systems observed in the Coastal Cordillera. The detailed sampling localities and results from this study region are discussed in Chapter 5.

1.1.2 The pre-Cordillera

To the east of the Coastal Cordillera, across the Central Valley, is the Andean pre-Cordillera. In this part of northern Chile, the main structural feature is the DFZ, a large north-south orientated strike-slip fault zone. The fault zone comprises several large faults

including the West Fissure to the north, and in the sampling region, the Sierra-Castillo Fault, the Agua Amarga Thrust and the La Ternera Fault (all marked La Ternera Fault System on Figure 1.3). The sampling locality is SE of the major mining district of El Salvador (Figure 1.3). To the east of the DFZ in this area are two domains of subsidiary faults, these faults form a fold-and-thrust belt in the north and a set of sinistral strike-slip faults in the south. The two subsidiary domains, together with the DFZ define the DFS.

This area of northern Chile has recently been re-mapped by the Servicio Nacional de Geología y Minería (SERNAGEOMIN), the Chilean Geological Survey, and a regional guide is available (Cornejo *et al.*, 1993). The area was targeted for re-mapping to better constrain the distribution and age control on the large number of copper porphyry deposits in the region. The mapping has allowed good kinematic and geochronological controls on the timing of motion on the faults. Similarly, the lithologies have been better defined in terms of their descriptions and ages. This region therefore offers a range of well dated lithologies suitable for palaeomagnetic study. Samples for palaeomagnetic study were collected from units in both of the subsidiary fault domains that lie to the east of the DFZ, and also from one unit to the west. The aim was to test whether there is any difference in the amount or sense of rotation within the subsidiary fault system which could then be related to the overall fault motion. Details of the sampling and results from this study locality are given in Chapter 6.

Palaeomagnetic sampling for this project took place over two field seasons in 1992 and 1993. During the first season, sites were collected from the Coastal Cordillera only. During the second season, additional samples were collected from targeted units in the Coastal Cordillera based on results obtained from the 1992 samples. Most of the second season was spent sampling in the pre-Cordillera. Logistical support for the fieldwork was provided by SERNAGEOMIN, and the fieldwork in the pre-Cordillera was carried out in

collaboration with geologists from the survey. Access to sampling sites was often limited due to the mountainous terrane and the large scree slopes at the base of many of the outcrops. Sampling was carried out by a petrol powered drill or block sampling. There were several problems with using the drill. Firstly, the aridity of the area meant that water for cooling was in short supply, and, secondly there were several mechanical problems with the drill. In the pre-Cordillera these were related to the altitude. The problems of access to the sampling sites and the difficulties with the drill, meant that most sites in both the Coastal Cordillera and the pre-Cordillera were collected as orientated hand samples.

1.2 The wider context of this work

The work from both fault systems forms part of a larger ongoing studies into the geology and tectonics of northern Chile and the Andean margin as a whole. The work in the Coastal Cordillera is related to structural and fault kinematic studies, and associated petrogenic and dating work. Combining the palaeomagnetic study with these data allow development of an integrated model for the behaviour of the Jurassic-Cretaceous magmatic arc in this part of the Andean margin and its mid-Cretaceous deformation. This integrated approach gives information about types, times and duration of deformation and how stress is accommodated within the overriding continental crust. The overall aims are to gain a better understanding of the nature of the magmatic arc in the Coastal Cordillera of northern Chile and hopefully, magmatic arcs in other parts of the world.

The palaeomagnetic data from the DFS in the pre-Cordillera should give more information about the style of deformation and stress accommodation within the fault system. As many of the copper porphyry deposits are associated with, or intruded along the major faults east of the DFZ, understanding and quantifying the rotation and motion on the faults offers potentially valuable geological information with respect to mining prospects in

the region. Overall the SERNAGEOMIN project aims to improve understanding of the geology and structure of this part of northern Chile, particularly with reference to locating and assessing the commercial viability of ore deposits.

It can be seen from this introduction that integrating data from different branches of geology is the only way to solve large-scale tectonic problems. Crucial to these integrated studies of magmatic arcs, crustal-scale fault systems and deformation is the contribution of palaeomagnetism.

1.3 Geological background to South America

This section begins with a brief overview of the tectonic and geological development of the South America margin. The first section deals with some of the large-scale tectonic history of the western margin of South America. In the second section, greater discussion is given to the study area in northern Chile and its development during the Andean Orogeny. One of the most controversial features in the Andean margin, in terms of its origin and significance, is the change in coastline orientation and geological strike at approximately 19°S latitude, the Arica Deflection or Bend. As this feature has been important to many of the models of vertical axis rotation in the Andean margin, some details about these structures are discussed in the final part of this section.

1.3.1 The Andean margin

As stated earlier, the western South American margin has a long history of continuous active subduction (Dalziel and Forsythe, 1985). The most recent subduction phase is the Mesozoic-Recent Andean orogenic cycle which has lasted approximately 200 Ma. This orogeny is the second to affect the margin (Coira *et al.*, 1982) and is discussed further with respect to northern Chile in Section 1.3.2. The margin also underwent an earlier distinct orogenic cycle, termed the Palaeozoic Hercynic cycle (Coira *et al.*, 1982). The geology and tectonics of the Hercynic cycle are not well understood but it was characterised by alternating periods of sedimentary and/or volcanic events separated by short phases of deformation. At least two major regional orogenic phases are known; the late Ordovician Ocluyic phase, and the late Devonian Chanic phase. After this time the geology and structure became variable and more localised, the post Devonian development of northern Chile is therefore discussed further in Section 1.3.2.

During the Palaeozoic, prior to the break up of the Gondwana supercontinent, the western continental margin of South America was increased in width by accretion of exotic terranes (Dalziel and Forsythe, 1985). Although a major allochthonous terrane has been recognised in the Central Andes (Ramos *et al.*, 1986; Mpodozis and Ramos, 1989), the majority recognised so far are located in the south of the continent (Dalziel and Forsythe, 1985; Rapalini *et al.*, 1985). Along most of the length of the Andean margin, terrane accretion appears to have ceased during the Triassic, the exception to this is Ecuador, where accretion of exotic terranes continued until at least the Palaeocene (Daly, 1989).

A major change in the tectonics of the Andean margin began in the early Mesozoic with the onset of the Andean orogenic cycle. At this time, Gondwana began to fragment and South America drifted westwards. This plate reorganisation led to the initiation of the development of the Andean Cordillera. The onset of magmatism in the overriding continental plate was diachronous (Dalziel, 1986) and developed from the north (Middle-

Late Triassic) to the south (Middle-Late Jurassic). This diachroneity was probably related to a north-south change in the motion and direction of the subducting plate (Scheuber and Reutter, 1992). A feature of the Mesozoic evolution of the Andean margin is the variation and tectonic segmentation observed along the length of the margin (Mpodozis and Ramos, 1989). There are changes in structural style and differences in the development of both the magmatic arcs and back-arcs within each of the segments. As this study is based in northern Chile, only the geology of this section of the margin is discussed in detail.

1.3.2 The geology of northern Chile

In northern Chile, after the major tectonic phases of the Hercynic cycle ended in the Late Devonian, Carboniferous to Lower Permian sediments were deposited in a shallow marine environment (Bell, 1987). These were subsequently deformed and metamorphosed by the Early-Middle Permian Saalian phase (Coira *et al.*, 1982). These meta-sedimentary rocks were then intruded by a broad belt of genetically related Middle Permian to Early Triassic granitic plutons (Brown, 1991), possibly part of a magmatic arc (Coira *et al.*, 1982). This intrusion marked the end of the Hercynic cycle in the South American margin (Coira *et al.*, 1982). Collectively, the meta-sediments and plutons form the Palaeozoic basement into which the magmatic arc rocks of the Andean cycle were intruded.

In northern Chile, the Andean cycle was characterised by the development of a series of magmatic arcs which are parallel to the margin. The oldest of these arcs is the Jurassic to Early Cretaceous arc, called the La Negra arc, in the Coastal Cordillera. In the mid-Cretaceous the Peruvian Orogeny (also called Mirano phase, e.g., Dalziel, 1986) resulted in a change from dominantly extensional, to contractional arc tectonics in northern Chile (Scheuber and Reutter, 1992). The orogeny caused the magmatic arc to migrate eastwards and establish a new mid-Cretaceous arc. This orogeny occurred in response to an increase in sea floor spreading rates as a result of the early stages of South Atlantic

ripping (Dalziel, 1986). Since this time, continued growth of the South Atlantic, and shallowing of the subducting Nazca plate has meant that the magmatic arc has continued to migrate eastwards (Dalziel and Forsythe, 1985; Scheuber and Reutter, 1992) to its present position in Argentina (Allmendinger *et al.*, 1983). This eastward migration has preserved four magmatic arcs in northern Chile (Scheuber and Reutter, 1992). The arcs are defined by their age of activity and are sub-divided by Scheuber and Reutter (1992) into; Jurassic to Early Cretaceous, mid-Cretaceous, Late Cretaceous to Palaeogene and Miocene to Recent (Figure 1.4). The mid-Cretaceous arc is poorly defined and in some parts of northern Chile almost absent, becoming indistinct from the Late Cretaceous to Palaeogene arc. Instead, the Jurassic to Early Cretaceous and Late Cretaceous to Palaeogene magmatic arcs are separated by the *Central Valley* (Dalziel, 1986), also called the *Longitudinal Valley* (Scheuber and Reutter, 1992) and the *Central Depression* (Buddin *et al.*, 1993). This is a north-south trending basin approximately 80 km wide which has undergone much less deformation than the arcs to the east and west of it.

Since the Peruvian Orogeny there have been three other major phases of deformation in the Andean margin, all in the Cenozoic. Two of these, the mid-Eocene Incaic phase, and the mid-Miocene Quechua phase (Coira *et al.*, 1982) correlate well with periods of rapid plate convergence (Pardo-Casas and Molnar, 1987). The late Pliocene Diaguita phase (Jordan and Alonso, 1987) is less well defined, and may be a localised late stage part of the Quechua phase (Pardo-Casas and Molnar, 1987).

For this study, samples were collected from the Jurassic to Early Cretaceous arc in the Coastal Cordillera, and from the Late Cretaceous to Palaeogene arc in the pre-Cordillera. A fuller description of the geology, including lithologies and structure for these two sampling localities is given in Chapters 5 and 6.

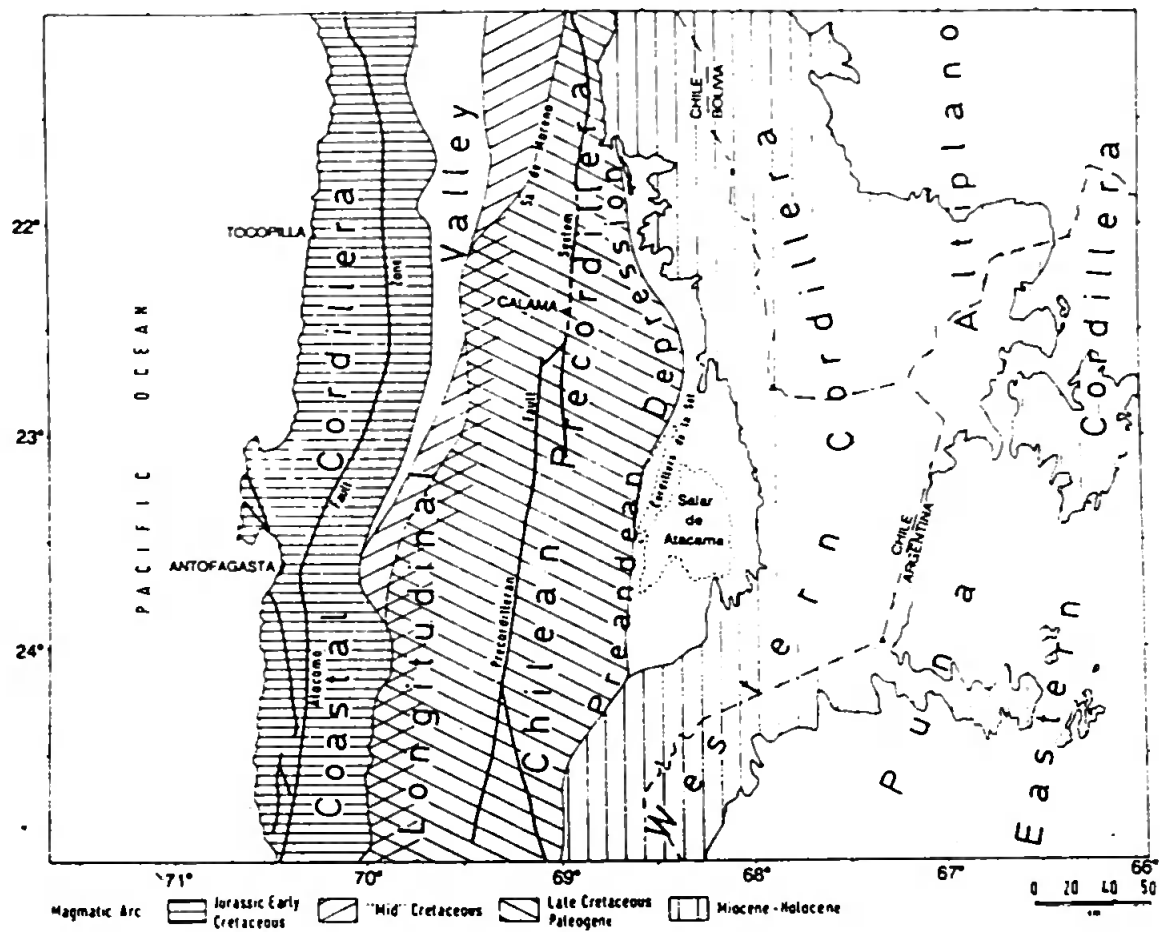


Figure 1.4. Map showing the four magmatic arcs identified in northern Chile (taken from Scheuber and Reutter, 1992, figure 1).

1.3.3 The Arica Deflection

One of the major tectonic and topographic features of the South America margin is the $\sim 50^{\circ}$ - 60° change in the direction of the geological strike, the coastline and the Andean mountain chain near to Arica at the Chile-Peru border ($\sim 19^{\circ}\text{S}$). This has been variously called the Arica Deflection, Arica Bend or Bolivian Orocline (Figure 1.1). It is not known whether this deflection is a primary feature of the shape of the continental crust unrelated to subduction, or is the result of subduction processes bending an originally straight or near straight continental margin. If the bend is an original feature of the margin, the change in strike orientation at the Arica Deflection may be due to changes in the angle of obliquity of the subducting plate along the margin causing different structural responses around the bend. If the bend is not a primary feature, this suggests that an originally straight or near straight margin was bent or modified by a strain impressed by subduction processes.

Many studies have tried to establish whether the Arica Deflection is primary or secondary in origin. Some workers have interpreted the change in palaeomagnetic rotations from anticlockwise north of the bend to clockwise south of the bend as evidence that the structure is secondary, models have then been presented to explain the rotation. Other studies have interpreted the Arica Deflection as a primary feature and a number of mechanisms have been presented to explain the palaeomagnetic rotations as occurring *in situ*, on both local and regional scales. These models, and the applicability of the data obtained in this study are discussed further in Chapter 7.

Chapter 2

THE GEOMAGNETIC FIELD, SAMPLING TECHNIQUES AND PALAEOMAGNETIC METHODS

2.1 Introduction

This chapter begins with a brief discussion of the nature of the Earth's magnetic field and its variability, followed by a discussion of the main assumptions of the palaeomagnetic method, as these influence the interpretation of results. The main part of the chapter deals with the specific palaeomagnetic methods, equipment and analytical methods used in this study.

2.2 The geomagnetic field and acquisition of magnetisation

Central to the palaeomagnetic method is the *geocentric axial dipole model* (GAD). This states that the position of the geomagnetic pole averaged over periods greater than a few millions of years is approximated by the field produced by a single magnetic dipole at the centre of the Earth aligned with the Earth's rotation axis. Mathematical modelling of the geomagnetic field, based on continuous measurements of the magnetic field direction made from fixed observation stations suggests that the GAD model is valid. Over shorter periods of time (milliseconds to a few million years) the geomagnetic field and the position of the geomagnetic poles changes. The present-day geomagnetic field is better described by an *inclined geocentric dipole model* where the dipole is inclined at $\sim 11.5^\circ$ to the rotation axis. This provides the best-fit that can be achieved by a single dipole model, and can account for $\sim 90\%$ of the observed field. This is referred to as the *dipole field*. In addition,

there is a non-dipole field, which is calculated by removing the dipole field from the observed geomagnetic field.

The rapid changes in the geomagnetic field, typically regarded as less than 1 year (Merrill and McElhinny, 1983), are dominantly caused by external sources, while those with periodicities of years to millions of years are considered to be of internal origin. These slower changes are referred to as *geomagnetic secular variation*, or *palaeosecular variation* (PSV) when dealing with rocks containing a record of the past geomagnetic field. Secular variation is generated by changes in both the dipole and non-dipole field, the non-dipole changes generally having a much shorter periodicity. The fluctuations in the non-dipole field are thought to be related to the growth, decay and motion of the fluid eddies that generate this part of the field.

Over longer time periods than are applicable for secular variation, the geomagnetic field direction appears to change polarity through 180° ; this is termed a *magnetic reversal*. The present field configuration is referred to as *normal polarity*, the opposite as *reversed polarity*. If the field direction is $>45^\circ$ away from either its normal or reversed positions, it is said to have *intermediate polarity*. Reversals are world-wide effects and occur at all points on the Earth's surface.

Palaeomagnetic studies also indicate that the pole may undergo large directional departures ($>45^\circ$) from the GAD model that are not associated with polarity reversals. The pole position is said to undergo a *geomagnetic excursion* before returning to the original polarity. Like reversals, these phenomenon are world-wide in effect, and may represent aborted reversals.

The geomagnetic field direction at the Earth's surface can be described in terms of declination and inclination (Figure 2.1). Declination is the angle between the field direction and geographic north measured in the horizontal plane, while inclination is the angle

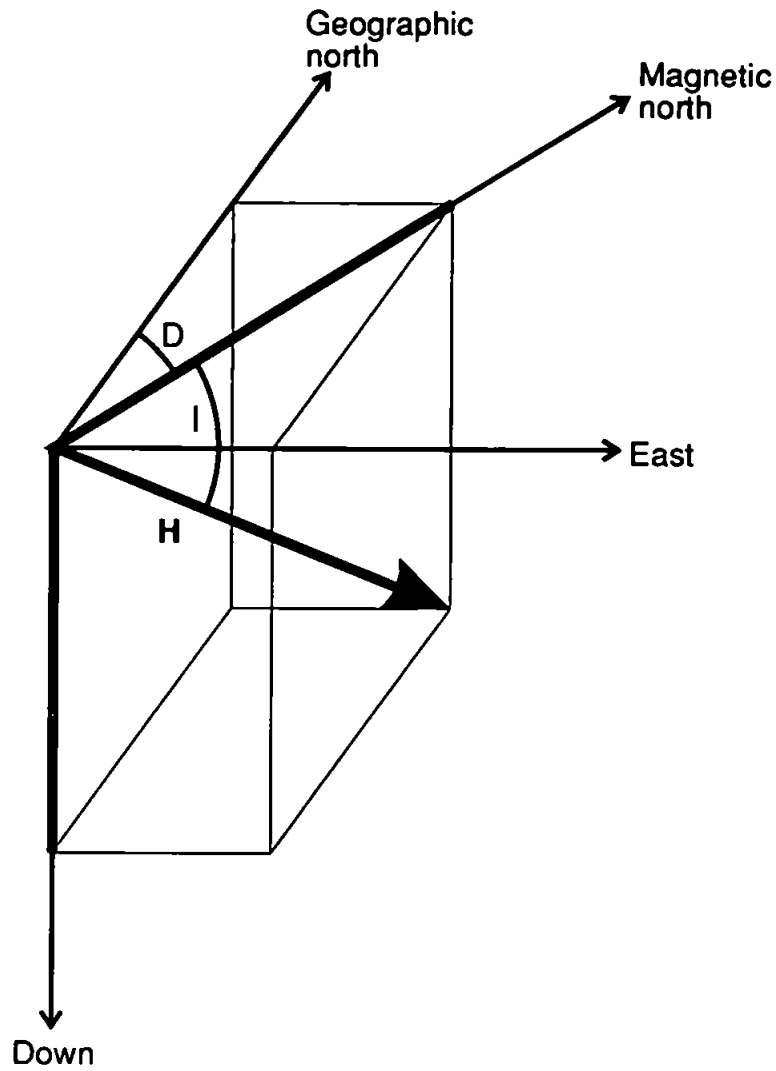


Figure 2.1. Description of the Earth's magnetic field direction. The total field vector **H** can be divided into a horizontal and vertical component. Declination, **D**, is the azimuthal angle between the horizontal component of **H** and geographic north. Inclination, **I**, is the vertical angle between the horizontal and **H**. Redrawn from Butler (1992).

measured in the vertical plane between the field direction and the horizontal. For the GAD model, the declination (D) will be 0° at all points on the Earth's surface, while the inclination (I) is related to latitude (λ) by:

$$\tan I = 2 \tan \lambda$$

2.2.1 Acquisition of magnetisation

Ideally the magnetisation recorded in a rock will have been acquired at the time of rock formation and be in the same direction as the prevailing geomagnetic field which is representative of the GAD. The magnetisation acquired at the time of rock formation is the *primary component of magnetisation*. In igneous rocks, this will normally be a *thermal remanent magnetisation (TRM)*. This is acquired when the magnetic minerals cool below a temperature at which the magnetisation is fixed, this process is discussed further in section 2.5.1. In sedimentary rocks, the remanence is usually acquired initially as a *detrital remanent magnetisation (DRM)*. DRM can be affected by two sedimentary processes; *depositional DRM* and *postdepositional DRM (pDRM)*. Depositional DRM considers the aligning force of the magnetic field on a magnetic grain at the sediment-water interface. It is assumed that the magnetisation of the grain will be aligned with the prevailing field direction. Physical processes which act on the grain after deposition but before consolidation are pDRM's. These processes take place in the upper levels of the sediment where high water content allows re-orientation of the grains. The third major type of remanence acquisition is *chemical remanent magnetisation (CRM)*. In this type of magnetisation the magnetic grains are formed at low temperatures by either alteration of a pre-existing grain, or precipitation of a magnetic grain from solution. This type of magnetisation is most common in sediments.

There are three main reasons why the magnetisation in a rock may not be that predicted from the GAD model. Firstly, if magnetisation is acquired during a geomagnetic excursion, or at the intermediate stage of a polarity reversal, the direction of the magnetisation will not be related to the GAD field. Additionally, if sites are collected from rocks representing a very short time period, PSV may not be averaged out and the mean direction will be biased away from that expected from the GAD model. The effects of geomagnetic variation can usually be eradicated by sampling multiple sites. The sampled sites should cover a time period long enough to average out PSV. This should also identify sites with magnetisations acquired during excursions or reversals as the directions will lie away from the mean direction.

The second problem is that the rock may be anisotropic and therefore not acquire its magnetisation parallel to the geomagnetic field direction. Although all magnetic minerals are anisotropic and will try to acquire their magnetisations along preferentially easy directions, the minerals are normally assumed to be randomly orientated in igneous and sedimentary rocks. This means that the overall rock behaves as if it were isotropic. If the rock is itself strongly anisotropic the orientation of the magnetisation may be affected. Measurement of the magnetic anisotropy of the rock should make this problem evident. Sampling over wide geographical areas may also reduce this problem as significant anisotropy in igneous and sedimentary rocks tends to be localised.

The third problem is that the magnetisation may not have been acquired at the time of rock formation. Commonly, in addition to the primary components of magnetisation a rock will also contain *secondary components of magnetisation*. These are acquired after formation and result from partial remagnetisation of the rock. Remagnetisation may occur due to heating, lightning strikes, fluid or chemical alteration, or by influence of the geomagnetic field in a different direction to that of the primary magnetisation. Most rocks

are *multi-component*, with the *natural remanent magnetisation (NRM)* consisting of a primary component and a mix of secondary components. In laboratory analyses the initial measurement made is of the total NRM. In most palaeomagnetic studies, the aim is to identify each component of the NRM and, ideally, to recover the primary magnetisation. The common characteristic magnetic direction recovered from the majority of samples in a rock unit is termed the *characteristic remanent magnetisation (ChRM)*. The ChRM may not necessarily represent the primary magnetisation because it is possible that a rock will be completely remagnetised with no trace of its original primary magnetisation remaining. Wherever possible, field tests are applied to determine whether the ChRM is a secondary component, or was acquired during, or soon after rock formation.

2.3 Sample collection and preparation

In the field, the plunge and azimuth of the sample, and the tectonic orientation of the sampled unit or bed must be recorded. This is so that the sample's demagnetisation trajectory can be corrected for its field orientation and any tectonic tilting.

In this study, sites were collected as either field-drilled cores or orientated blocks. Block sampling was favoured due to both equipment failure and the logistical problems of aridity and accessibility of exposures. When field drilling, six to eight cores were typically taken at each site. These were oriented using both sun and magnetic compasses. The difference between corrected sun and magnetic compass bearings was always less than 5°. When block sampling, two or three magnetically orientated blocks were collected at each sites. Each was marked with horizontal strike lines and an independent north arrow. A minimum of three 25 mm diameter cores were drilled in each block, which were then re-

orientated to their field position and the cores extracted. Specimens of 22 mm length were cut from the cores.

2.4 Specimen measurement

NRM measurements were carried out using fluxgate magnetometers (Collinson, 1983) which work by slowly spinning a specimen inside a coil detector. The specimen induces a current in the coil, and the direction of magnetisation can be determined from the phase difference between the waveform produced and a reference waveform, while the amplitude is proportional to the intensity of magnetisation. For this study, most specimens were measured using a Molspin MS2 magnetometer which uses a fluxgate coil detector inside a three layer passive shield. The shielding reduces the residual magnetic field inside the shield to approximately 12 nT. Although the MS2 spinner has sensitivity and noise levels quoted at $\sim 0.03 \text{ mAm}^{-1}$, specimens with NRM intensities of less than 10 mAm^{-1} were measured on a Geofyzica JR4 magnetometer. This magnetometer is more sensitive than the MS2, having a sensitivity quoted as 0.004 mAm^{-1} . This is achieved by using longer measurement times at more sensitive ranges to reduce the effects of noise. The residual magnetisation of the specimen holder is measured during calibration and is compensated for during measurement. In practice, the weakest specimen intensities that could be repeatably measured with the JR4 were found to be $\sim 0.01 \text{ mAm}^{-1}$.

2.5 Demagnetisation

To recover the ChRM from the total NRM, specimens are progressively demagnetised to remove secondary components of magnetisation. The most commonly

used techniques are thermal and alternating field (AF) demagnetisation. For this study, all specimens were fully and progressively demagnetised in a stepwise manner. The choice of demagnetisation method for the bulk of the specimens was based on the behaviour of at least two pilot specimens from each site.

2.5.1 Thermal demagnetisation

All magnetic grains have two parameters which are controlled by mineralogy and grain size. Above the *Curie temperature*, saturation magnetisation becomes zero and the grains behave in a *superparamagnetic* manner. Below the *blocking temperature*, the magnetisation is stable. Between these temperatures the grain behaves in a *paramagnetic* manner, it can acquire a magnetisation, but this will quickly decay to zero and the grain is said to have a short *relaxation time*. At temperatures below the blocking temperature, the relaxation time increases rapidly with decreasing temperature and the remanent magnetisation becomes increasingly stable. To hold a stable primary magnetisation the magnetic grains must have relaxation times in excess of the age of the rock. Secondary components of magnetisation which exist in addition to the primary magnetisation will tend to be held by the grains with shorter relaxation times and lower blocking temperatures. A specimen can therefore be demagnetised by heating to progressively higher temperatures and cooling in zero magnetic field between measurement steps. All grains with unblocking temperatures below the maximum applied temperature at each demagnetisation step will have their contribution to the specimen NRM removed.

Most specimens were demagnetised using a Magnetic Measurements MMTD1 oven which has a maximum temperature of 800°C and is encased in a four layer active magnetic shield. Alternatively, a Pyrox oven with a maximum temperature of 720°C and a three layer passive magnetic shield was used. Typically 12 specimens were demagnetised at a time, and

each had a 2 cm gap from its neighbour to reduce magnetic interference between the specimens. The shielding on both of the ovens reduces the residual magnetic field to less than 20 nT.

The length of time that a specimen needed to be held at each temperature setting in the MMTD1 oven was tested experimentally. A typical andesite dyke specimen had a 3 mm by 10 mm hole drilled in it, an iron constantan thermocouple placed inside, and the hole then filled with fire clay. The specimen was placed in the centre of the oven and heated. Once the oven had reached its set temperature, the temperature indicated by the thermocouple in the specimen was recorded every 5 minutes until it stabilised. Figure 2.2 shows a graph of the specimen temperature versus hold time. The experiment showed that 20 minutes was a sufficient hold time for the temperature in the specimen to stabilise for oven temperatures up to 560°C, above this specimens were held for 30 minutes. An unexpected result of this experiment was that the specimen did not seem to reach the temperature set for the oven (Figure 2.2). To check the accuracy of the oven temperature settings, the thermocouple was again put inside the specimen and placed at the centre of the oven. The oven was then heated to increasing temperatures and the temperature recorded by the thermocouple allowed to stabilise. Figure 2.3 shows the temperature recorded by the thermocouple versus the oven temperature setting, for comparison, the thermocouples expected response, including its tolerances (12 mV up to 100°C, 2% above), is also shown. The results indicate that the heating chamber may be failing to reach the set temperature of 700°C by up to 40°C, although the problem of heat affecting the resistance of the wires connecting the thermocouple to the voltmeter is unquantified. This experiment suggests that some compensation must be made when interpreting specimen demagnetisation temperatures.

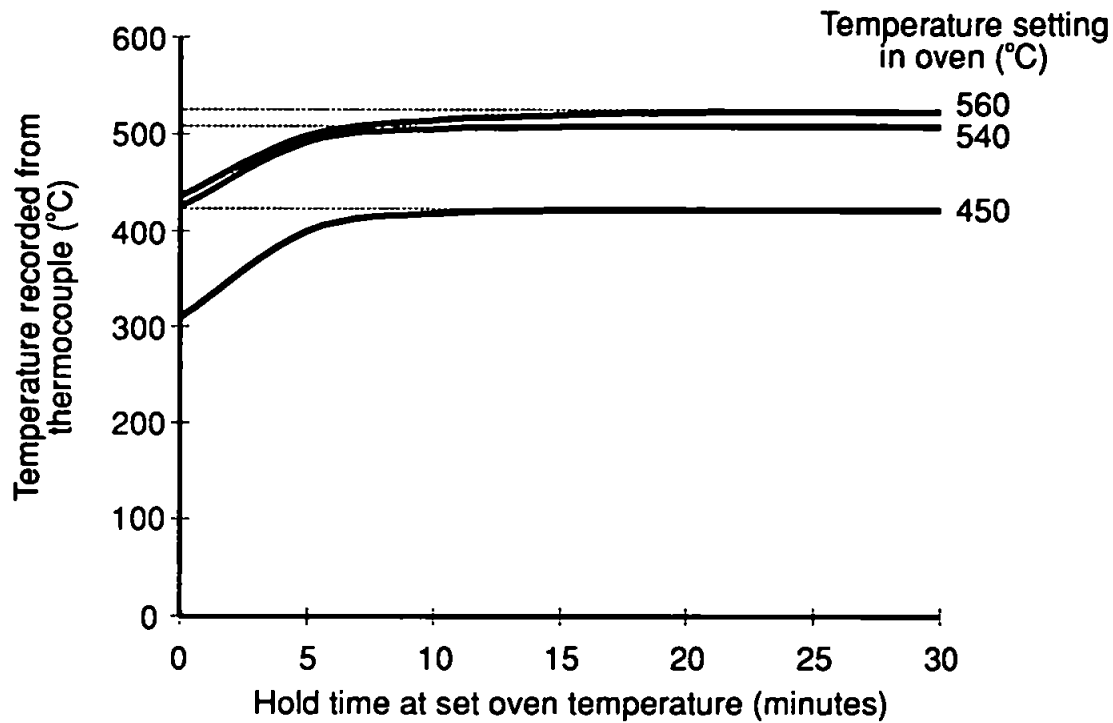


Figure 2.2. Graph showing the amount of time that a typical andesitic dyke sample needs to be held at a specific temperature in order for the temperature to stabilise at its centre.

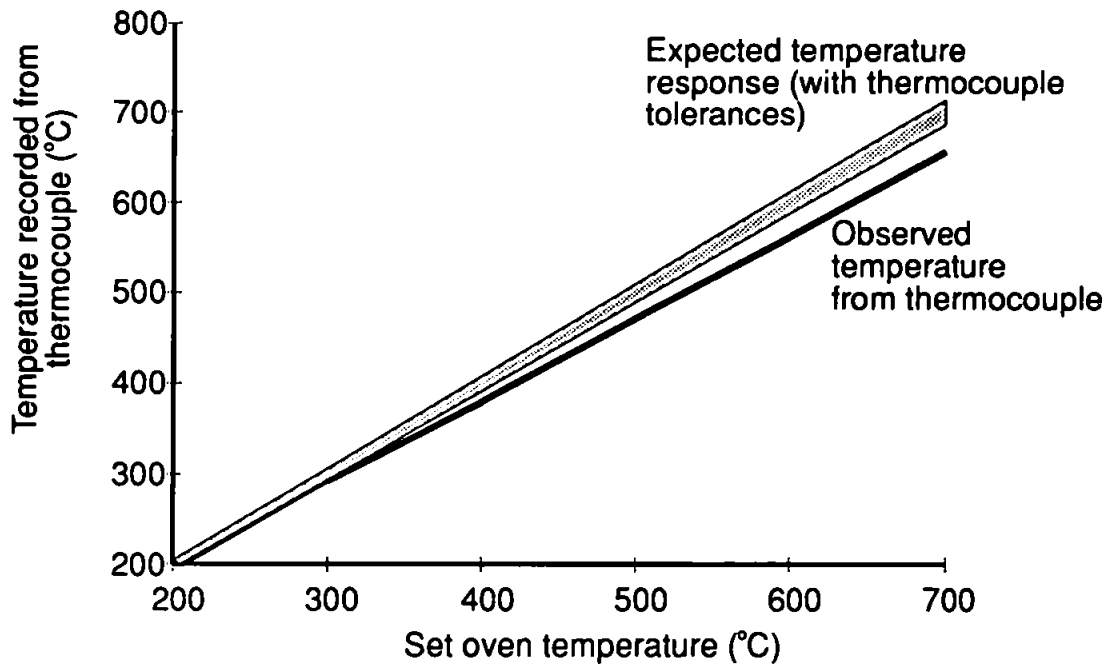


Figure 2.3. Temperature inside the MMTD1 oven measured by an Iron constantan thermocouple. Comparison with the expected response for the thermocouple at the temperatures set shows that the oven is failing to reach the set temperatures.

2.5.2 Alternating field demagnetisation

One of the magnetic parameters of a grain is its *microscopic coercive force*, a measure of the grain's resistance to re-alignment of its magnetisation by an applied field. This force is controlled by shape anisotropy of the grain as well as mineralogy and grain size. If a specimen is put into a magnetic alternating field (AF), all grains with a coercive force less than the peak applied field will be aligned with the applied field. To demagnetise the specimen, the amplitude of the AF is reduced by a small amount during each alternating cycle, such that the field decays to zero linearly with time. This leaves all grains with coercivities less than the peak applied AF remagnetised along the axis of the demagnetiser coil, with half of the grains aligned with the positive AF and half aligned with the negative AF directions. Thus the magnetic moments of these grains will approximately cancel out leaving a net zero magnetisation. Application of the field along three orthogonal axes of the sample in turn results in effective demagnetisation of all grains with coercivities less than the peak applied field. More commonly, the specimen is rotated or 'tumbled' around two axes during the AF decay to present all axes of the sample to the demagnetiser coil, thereby allowing demagnetisation in a single operation. This also reduces the risk of introducing spurious laboratory-induced remanences during demagnetisation. Specimens can be progressively demagnetised by applying AFs of increasing amplitude between measurement steps.

The AF demagnetiser used in this study was a two-axis tumbling type, with a maximum applied field intensity of 100 mT adjustable in 0.1 mT units. The specimen is demagnetised inside a three layer passive shield surrounded by two pairs of Helmholtz coils, the residual field inside the shielding being <15 nT. The decay of the AF can be set at 4, 8, 16 or 32 $\mu\text{T}/\text{cycle}$.

2.6 Magnetic mineralogy studies

2.6.1 Identification of magnetic minerals

Magnetic mineralogy was investigated by observing the behaviour of specimens during demagnetisation, and by conducting rock magnetic experiments. The magnetic mineralogy of representative specimens was identified by acquisition and subsequent thermal demagnetisation of isothermal remanent magnetisation (IRM). Before the IRM acquisition experiments were carried out, the specimen was AF demagnetised to 100 mT to remove the effects of the NRM on the IRM. Progressively increasing fields were applied along the z axis of the specimen, up to a maximum field of 800 mT (the maximum that can be applied in the Plymouth laboratory), and the intensity of IRM measured after each application. The results are presented as shown in Figure 2.4a and b. The line graph shows normalised IRM intensity, while the bar chart shows normalised rate of change in IRM. If the sample is dominated by low coercivity minerals, the graph will have the shape shown in Figure 2.4a; a rapid rise in IRM saturating in the 800 mT applied magnetic field. If the sample is dominated by minerals with coercivities higher than 800 mT, the graph shows a slower rate of IRM acquisition which does not saturate in the 800 mT applied magnetic field (Figure 2.4b).

Lowrie (1990) suggested that demagnetising IRMs of differing magnitudes applied along three orthogonal axes in the specimen gives more information than demagnetising an IRM acquired along a single axis. In this method a large field is applied along one axis of the specimen. An intermediate field is then applied orthogonal to the first. This will remagnetise the magnetic fraction with coercivities lower than the intermediate field. A third, low field is then applied orthogonal to the first two. Although a large field is desirable for this technique (ideally >2 T), 800 mT is the maximum field that can be applied in the

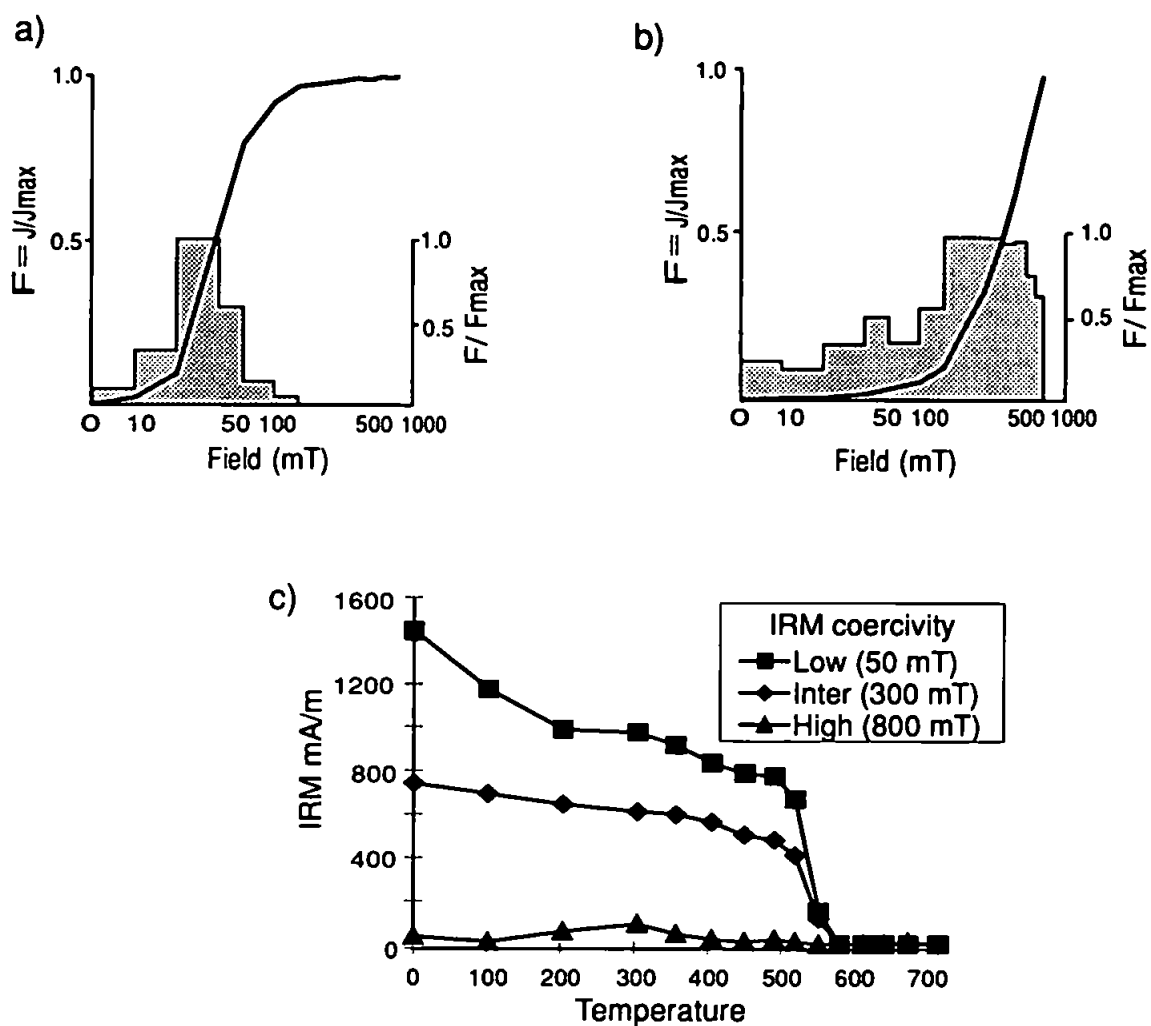


Figure 2.4. a and b) IRM acquisition diagram showing normalised IRM and rate of change of IRM. c) Demagnetisation of three orthogonal IRMs.

Plymouth laboratory. The intermediate value of 300 mT was used to discriminate between magnetite and pyrrhotite. Pyrrhotite has a maximum coercivity of 500-1000 mT, and is therefore less likely to saturate in a 300 mT field. A 50 mT field was the last applied to identify low coercivity multi-domain magnetite which is common in many of the specimens. After acquisition of IRMs, the specimens were stepwise thermally demagnetised and the intensity of the IRM along each axis recorded at each step. The results are presented as shown in Figure 2.4c. The demagnetisation behaviour of the three components gives an indication of the magnetic mineralogy by relating coercivities and blocking temperatures.

When a specimen is exposed to a direct field, all grains capable of being magnetised will be magnetised in the same direction, although some of these grains may not have carried a natural remanence. IRM experiments therefore identify potential carriers of magnetisation, not all of which need contribute to the NRM. In addition, different components of NRM may have been carried by different minerals, or those with different grain sizes. After acquisition of an IRM in a high applied field, all grains become magnetised in the same direction. For these reasons potential carriers identified by IRM experiments may not be fully representative of the original carriers of natural remanence. Comparison of IRM demagnetisation data with that of the NRM therefore gives more information than using IRM data alone.

2.6.2 Grain size determination

Potter and Stephenson (1986) suggested that the average size of magnetic grains can be investigated using a combination of *rotational remanent magnetisation* (RRM) and *anhysteretic remanent magnetisation* (ARM). These experiments were carried out at the University of Newcastle upon Tyne. To generate the RRM, the specimen is exposed to an AF while being rotated at 95 Hz around its z axis. The AF has a frequency of 50 Hz and a

peak amplitude of 80 mT. Two measurements of RRM are obtained, first by spinning the specimen clockwise and then anticlockwise. The two spins average out inhomogeneity in the specimen or in the applied field and also show the presence of any stray direct field. The ARM is produced by rotating the sample anticlockwise again but this time in the presence of a 70 μ T direct field as well as the AF. The RRM/ARM ratio can be used as an estimate of the grain size of the magnetic fraction of a specimen. This technique only works well if the carrier is magnetite because haematite does not acquire RRM, but does acquire ARM. The influence of minor proportions of haematite in magnetite-haematite assemblages is small due to the much larger magnetic susceptibility of magnetite.

2.6.3 Measurements of the decay of viscous remanent magnetisation

Some studies of the decay of *viscous remanent magnetisation* (VRM) were also made during this work, again at the University of Newcastle upon Tyne. This was carried out by applying a 5 mT direct field along the z axis of the specimen. The intensity of the magnetisation along the z axis was then measured over a period of 10 s-1000 s without removing the specimen from the shielding of the magnetometer. A plot of intensity versus time shows the decay of the VRM component present in the sample. This technique offers a quick method of establishing the presence of VRM in specimens. In all cases this technique was applied to the sample after AF demagnetisation only, and after thermal demagnetisation to 700°C. This method gives no information about a samples ability to acquire a VRM. However, the technique allows comparison of viscous decay behaviour both before and after heating, indicating possible changes in VRM presence after thermal demagnetisation.

2.6.4 Anisotropy of magnetic susceptibility

Bulk susceptibility, the ease with which a specimen can be magnetised due to all minerals present, and *anisotropy of magnetic susceptibility* (AMS) measurements were carried out on both igneous and sedimentary rocks. AMS reflects the alignment of elongate or platy minerals within a specimen. This alignment may be due to tectonic foliation, bedding or flow orientations. In this study, AMS was used as a check to see if there was significant anisotropy in any of the specimens as this could potentially influence the palaeomagnetic direction recorded in the rocks. Measurements were made using Molspin Minisep equipment and all AMS experiments were carried out before any demagnetisation of the samples.

2.7 Data interpretation and statistics

The palaeomagnetic remanence directions were analysed using the integrated software of Randy Enkin. These packages allow visual analysis of results as Zijderveld diagrams (Zijderveld, 1967), stereonet and intensity plots. Directions were selected by considering all plots in both field corrected and, where applicable, tilt corrected co-ordinates. The best fit direction was calculated using principal component analysis (Kirschvink, 1980). In most cases stable components of magnetisation were isolated from the specimens. In some sites this was not possible due to the presence of magnetic components with overlapping unblocking temperature or coercivity spectra, or differential demagnetisation of separate components of magnetisation. Where this occurred, great circle analyses was used following the method of McFadden and McElhinny (1988). Typically, the great circle analyses were combined with independent stable end points to calculate the mean direction. Components with coercivities and unblocking temperatures lower than those of the ChRM

are here referred to as *low* and *intermediate* components. The acceptance criteria for these components is that they are defined by a minimum of two points. The ChRM was selected by its identification in the majority of samples from a site. Specimen ChRM directions from within individual sites were combined to give site mean directions using Fisherian statistics (Fisher, 1953). Site mean directions were then combined to give formation mean directions for each geological unit.

Two statistical errors are calculated on the mean direction. The precision parameter, k , is a measure of the concentration of the individual data points around the mean direction and is given by

$$k = (N-1) / (N-R)$$

where N is the number of individual unit vectors and R is the length of the resultant vector. The value of k ranges from 0 where the points are distributed uniformly over the sphere, and approaches ∞ as the directions concentrate to a point. The second statistical parameter is the confidence limit on the mean direction. This is the semi-angle of the cone of confidence surrounding the calculated mean direction. This confidence limit is given a probability level, typically 95 per cent, and is referred to as α_{95} . This confidence limit is given by

$$\cos \alpha_{(1-p)} = \frac{N-R}{R} \left\{ \left(\frac{1}{N} \right)^{\frac{1}{N-1}} - 1 \right\}$$

where a probability level, p , of 0.95 is usually accepted in palaeomagnetic studies; N is the number of individual unit vectors and R is the length of the resultant vector. This statistical parameter suggests that 95 per cent of the time, the true mean direction will lie within cone of confidence calculated around the calculated mean direction.

To identify and quantify any vertical axis rotation, formation mean directions were compared with a *reference direction*. This is the mean direction of magnetisation calculated

from the results of a compilation of palaeomagnetic studies which are assumed to have undergone no vertical axis rotation. It is important that the selected reference direction is well defined and that the age of the sample's magnetisation is well established so the correct reference direction is used. More discussion of reference directions is given in Chapter 3.

2.7.1 Calculation of rotation, flattening and associated errors

The amount of rotation at a site was calculated using the method of Beck (1980). The difference between the mean palaeomagnetic vector observed at a particular sampling site, or from an individual formation, and the mean expected direction for the site calculated from appropriate reference poles is described in terms of *rotation* and *flattening*. The difference in declination is rotation (R). This is measured by comparing the observed site mean direction (D_o) with the expected reference direction (D_x) such that

$$R = D_o - D_x$$

By convention this is described as being positive for clockwise and negative for anticlockwise rotation. The difference in inclination is flattening (F). This is measured by comparing the observed inclination at the site (I_o) with the expected inclination (I_x) such that

$$F = I_x - I_o$$

By convention this is described as being positive for northward and negative for southward latitudinal shift.

As both the observed and expected directions have associated confidence limits, so do R and F. These 95% confidence limits are ΔD and ΔF respectively. Beck (1980) suggests that these confidence limits are of the form

$$\Delta R = \sqrt{\Delta D_o^2 + \Delta D_x^2}$$

for the rotation error and

$$\Delta F = \sqrt{\Delta I_o^2 + \Delta I_x^2}$$

for the flattening error. Demarest (1983) carried out a statistical analysis of these proposed confidence limits of ΔD and ΔF and concluded that they over estimated the errors. The over estimation varies with the number of samples but lies in the range 20% to 25%. Demarest (1983) notes that in most cases, where the magnetic inclination is not close to 90° and α_{95} is small, ideally less than ten degrees, a standard correction factor can be applied. If the number of palaeomagnetic samples lies between 6 and infinity, as is typical in this study, the correction factor varies between 0.78 and 0.8. In this study a correction factor of 0.8 has been applied to all calculations of confidence limits on R and F as this gives the most liberal estimate of the confidence limit. The formulae for the errors ΔR and ΔF on R and F respectively are therefore

$$\Delta R = 0.8 \sqrt{\Delta D_o^2 + \Delta D_x^2}$$

$$\Delta F = 0.8 \sqrt{\Delta I_o^2 + \Delta I_x^2}$$

For the rotation or flattening to be considered statistically discordant, the observed direction must deviate from the expected direction such that $R > \Delta R$ and/or $F > \Delta F$. If R or F lie within their associated confidence limits they are considered concordant and are not significantly different statistically.

Chapter 3

PALAEOMAGNETIC REFERENCE POLES AND REFERENCE DIRECTIONS

3.1 Introduction

One of the major problems with palaeomagnetic studies of tectonic rotations in South America has been the lack of well constrained reference data from the stable craton, as this prevents reliable determination of the amount of any tectonic rotation. Many of the published palaeopoles from South America are poorly constrained and may therefore be unreliable. Problems with the studies include poor age control, insufficient sampling to account for palaeosecular variation, poor laboratory techniques, particularly demagnetisation, and the possible effects of undetected rotation (Beck, 1988). Rotations calculated with respect to these reference poles may therefore be suspect, particularly if they record only a small amount of rotation.

This chapter discusses some of the methods for selecting and using reference poles, and applies this to the data from cratonic South America. A set of mean reference directions is then calculated for use as comparison in this thesis.

A reference palaeopole is taken to represent the direction of the magnetic field at a specific time period. Typically several poles with small discrete time periods will be available from the stable cratonic part of an individual plate. Ideally, with the effects of all geomagnetic variations and local controls removed, the differences in the directions will represent motion of the plate. These poles are therefore said to be recording *apparent polar wander (APW)*. Commonly, a study thought to demonstrate rotation will be from a time period between two fixed reference poles. To allow comparison of the direction or

pole with the reference the most common way of representing and using reference poles is by construction of an *apparent polar wander path (APWP)*. This path represents the sequential position of the palaeopoles from a particular continent. Before constructing an APWP, the available palaeopoles from a continent are first evaluated for their reliability using some form of acceptance criteria (Section 3.2). To construct the APWP a best fit path is fitted through the data points, normally by applying a 'sliding-time-window' to the data (Harrison and Lindh, 1982; Irving and Irving, 1982), or by a least-squares core fitting algorithm (Thompson and Clark, 1981; Jupp and Kent, 1987). These techniques have the advantage of averaging out random errors, or outliers in the data, but will also smooth the data resulting in the suppression of fine detail revealed by the original poles (May and Butler, 1986).

Another method for construction of APWPs is *palaeomagnetic Euler pole (PEP)* analysis (Gordon *et al.*, 1984). In this technique a series of best fit small circle paths, and resulting Euler poles are calculated for an APW track. Assuming a constant angular displacement about the calculated Euler pole allows a series of time incremented reference poles to be calculated whose geometry and age range is constrained by the original palaeomagnetic data set. The main problem with this technique is that it forces the palaeomagnetic data to fit a plate tectonic model which may itself contain inherent inaccuracies (May and Butler, 1986).

An alternative approach is to define reference poles based on a calculated mean pole for a fixed geological period. Although similar in concept to a sliding-time-window, the windows will be of unequal length defined by the length of the individual geological period. This means that the APWP cannot be used to calculate rates of geological processes such as sea floor spreading (May and Butler, 1986). Additionally, the chronostratigraphic boundaries are treated as cut-offs and the data is not averaged across the boundary. This

method of calculating mean poles results in a large amount of data smoothing and the loss of any fine detail. The technique is most suited to instances where there are only a few poles from which to calculate the mean, or there is very little variation in the directional data. The well constrained poles published for South America show that APW of the plate has been slight since at least the Late Triassic (Beck, 1988; Riley *et al.*, 1993), with most of the plate motion occurring along lines of latitude. For this reason, Beck (1988) calculated mean directions from the South American data for fixed geological periods. Beck (1988) calculated discrete directions for the Jurassic and Cretaceous.

3.2 Reliability criteria

While selecting reference palaeopoles for a continent it is usual to subject each pole to a set of minimum reliability criteria to decide whether or not it is to be included in the mean calculations. There is no standard set of criteria as different authors require different qualities from their compilation, the only apparently agreed rejection criterion is that undemagnetised results should not be included. Ideally the reliability criteria applied should be objective, but in many cases the selection of the criteria is itself subjective and is in part controlled by the size and quality of the initial pole data base. The application of reliability criteria is crucial to the development of APW paths, as choice of a data base is the major factor in producing variation in APW paths (Harrison and Lindh, 1982).

Application of any reliability criteria to a data set requires a trade off between the number of poles included and the quality and reliability of each individual pole. Lenient reliability criteria will increase the number of pole determinations that are included in the mean, but may include some unreliable or poorly determined pole positions and these spurious poles may influence the shape of the APW path. Conversely, stringent reliability criteria may reduce the data set to only a few poles leaving the APWP ill defined and

possibly removing or over smoothing important features. When using reliability criteria the aim is to remove 'bad' poles and retain 'good' ones while noting that the exclusion of a pole does not necessarily make it incorrect, merely poorly constrained in terms of the criteria used. In short, although reliability criteria are essential to evaluate a set of poles, consideration of the reliability criteria used is also important when constructing or comparing APWPs.

When constructing APWPs, including those from South America, different authors used different reliability criteria. In most compilations of South American poles the criteria has been lenient, possibly due to the lack of available poles. In this section examples of the criteria previously used for South American poles and those from other continents are discussed. The effects of the application of more lenient and more stringent reliability criteria on the South American pole data base are reviewed.

Beck (1988) applied reliability criteria to the South America pole data base but the paucity of poles for the Mesozoic, and in particular the Jurassic, meant that the reliability criteria were quite lenient. Beck (1988) defined a set of reliability criteria as;

1. Mean directions are based on a minimum three determinations of the geomagnetic field, three samples per site and three sites per mean pole.
2. Directions are based on laboratory demagnetised directions, either AF or thermal.
3. Directions have 95% confidence intervals of $< 20^\circ$.

Accepting that the criteria were lenient, Beck (1988) suggests that these are the minimum acceptable criteria that should be used to evaluate the reliability of a reference pole. Beck's (1988) criteria are also been used by Ernesto *et al.* (1990) and Raposo and Ernesto (1995) when producing an APW path for the Mesozoic, although Raposo and Ernesto (1995) note that for rapidly extruded lavas a minimum ten determinations of the ancient geomagnetic field should be used rather than three.

Besse and Courtillot (1991) constructed an APWP by combining data from Europe, North America, Africa and India. The data from the four continents were rotated into African co-ordinates and used to construct a single APWP. This is referred to as the African Master Curve. Using combined data gave Besse and Courtillot (1991) access to a much larger pole data base than was available to Beck (1988) from South America, and this enabled a much more stringent set of reliability criteria to be used (Besse and Courtillot, 1988; 1991). In considering the data for the African Master Curve, Besse and Courtillot (1991) suggest that four criteria need to be met by an individual pole for it to pass the reliability criteria. The criteria are defined as;

1. Mean directions are based on a minimum of 6 sites and 36 samples.
2. Directions have a 95% confidence interval of $< 10^\circ$ for the Cenozoic, $< 15^\circ$ for the Mesozoic.
3. Direction are based on successful AF or thermal demagnetisation
4. Localities have a maximum dating uncertainty of ± 15 Ma.

Besse and Courtillot (1988; 1991) also include some poles which just fail this criterion, this underlines the subjectivity in data pole selection.

Due to the extensive amount of palaeomagnetic work that has been carried out in the western Cordillera of North America, much attention has been given to establishing a good North American reference pole data base, particularly for the Early and Middle Jurassic. This meant that May and Butler (1986) could use very stringent reliability criteria when evaluating this pole data base. May and Butler (1986) define six criteria that must be passed as;

1. Demonstration that a stable, primary component of magnetisation is isolated through AF or thermal demagnetisation (preferably both).

2. Mean directions are based on ≥ 10 sites or independent geomagnetic field readings, preferably based on multiple samples.
3. Fisher precision associated with VGP dispersion, $20 \leq k \leq 150$.
4. Direction have a 95% confidence interval of $\leq 15^\circ$.
5. The age of the localities is known to within ± 10 Ma.
6. The study contains sufficient discussion of geological setting to demonstrate an appropriate understanding of necessary structural corrections.

May and Butler (1986) comment that the selection of 20 and 150 as limits for k are arbitrary, and a site should not be rejected on this one criteria alone.

Briden and Duff (1981) and Van der Voo (1993) take a different approach to reliability criteria, instead of just accepting or rejecting a pole, each one is graded on seven criteria. The system of Van der Voo (1993) uses a quality or Q rating for each pole depending on how many of the criteria the individual pole passes, with a suggestion that poles with a $Q \geq 3$ should be included. The Q ratings can then be used to produce a weighted average APWP with better constrained poles being given most weight. The seven criteria specified by Van der Voo (1993) are;

1. Well-determined rock age and a presumption that magnetisation is the same age.
2. Sufficient number of samples ($n > 24$), $k \geq 10$ and $\alpha_{95} \leq 16^\circ$.
3. Adequate demagnetisation that demonstrably includes vector subtraction.
4. Field tests that constrain the age of magnetisation.
5. Structural control, and tectonic coherence with craton or block involved.
6. The presence of reversals.
7. No resemblance to palaeopoles of a younger age (by at least a period).

Van der Voo (1993) also excludes any poles not based on demagnetisation of all samples, unpublished or poles presented in abstract form only, and any palaeopoles based on remagnetisations.

The pole data base for South America is given in Table 3.1, including as much age, demagnetisation and geological data as are available. Whenever possible data have been taken from the original publication, however three of the studies are currently unavailable. The direction from the Mafic Dykes in Brazil (Raposo, *In press*) is taken from an abstract, the Central Alkaline Province direction from Paraguay is published, but a copy is not yet available, and the data from the Ceara Mirim Dykes and associated intrusions in Brazil (Ernesto *et al.*, *In prep*) is referenced in Montes-Lauar *et al.* (1994). Also shown in Table 3.1 is whether the poles pass each of the reliability criteria outlined above, and the Q rating of Van der Voo (1993). The lenient criteria of Beck (1988) means that 34 of the 36 available poles are accepted and while this gives a large number of poles from which to compile an APW path, many of the poles are poorly constrained, particularly in terms of either age or statistical parameters.

The more rigorous data selection criteria proposed by Besse and Courtillot (1988; 1991) and May and Butler (1986) excludes more poles from the South American list, 24 and 13 poles are accepted respectively (it is not known whether the unavailable poles would pass the criteria of May and Butler (1986) so they are not included). Most of the poles which fail the criteria do so because they have an insufficient number of sites or samples per site. The requirement for evidence of structural corrections in the criteria of May and Butler (1986) means that several of the studies in the South American data base fail the criteria. This is because most of the South American poles are based on studies of volcanic or intrusive rocks and this means that structural control is difficult and defining what qualifies as 'demonstrating an appropriate understanding' is somewhat arbitrary. For this reason poles can only be rejected on this criteria if there is no discussion of structural

Locality	Age	Stratigraphic/ Age Range	No. of sites	For site at Lat. 26.3°S, Long. 290.1°E				Field / other					Notes	B	BC	M	Q
				Dec.	Inc.	k	α_{95}	Demag	Nor/rev	tests	Ref.						
LATE CRETACEOUS																	
Andacollo tuffs, Argentina	69	69±4	13	348.0	-27.0	-	-	AF	-	? Tilt	1	Remagnetised rocks	F	F	F	F	
Passa Quatro/Itatiaia intrusives, Brazil	70	~70	18	348.7	-48.5	-	5.7	AF/T	16/2	Rm	2		P	P	P	4	
Patagonian Basalts	72	79-64	18	347.9	-49.1	31.6	6.3	AF/T	6/12	R+, Rm	3		P	P	P	4	
Pocos de Caldos intrusives, Brazil	75	~75	6	359.9	-51.1	23.6	14.1	AF	1/5	Rm	4	R. 29	P	P	F	4	
Cerritos Negro Volcanics, Argentina	76	85±5-66±5	12	348.5	-62.6	13.6	12.2	AF	9/3	None	5	< 6 specimens/site	P	F	F	3	
Las Curtiembres Fm., S'st., basalt, Argentina	77	77±1	5	358.5	-40.9	23.7	16.0	AF/T	5/0	None	6		P	F	F	3	
Sao Sebastiao stocks, Brazil	81	80.8±3.1	11	350.3	-54.7	-	7.0	AF/T	11/0	Rm	2		P	P	P	3	
Pocos de Caldos intrusives, Brazil	88	~88	47	356.0	-51.5	64.1	2.6	AF/T	3/44	Rm	2		P	P	P	4	
MID-CRETACEOUS																	
Mafic dykes, Brazil	105	M. Cret	65	359.0	-45.0	47.3	2.6				7		P	P			
Rio los Molinas Dykes, Argentina	106	146-65	7	346.6	-45.7	51	8.0	AF	2/5	None	8	Altered rocks	P	F	F	3	
Cabo de Santo Agostinho, intrusives, Brazil	106	~85-99	9	358.8	-47.3	127	4.5	AF	9/0	None	9		P	P	F	3	
La Yesera Fm, S'st., cong., basalt, Argentina	106	~106	4	21.1	-55.9	59.1	12.0	AF/T	4/0	None	6		P	F	F	2	
Merida Andes, Sediments, Venezuela	111	L.Jur-L.Cret	9	357.4	-47.9	85	5.6	AF/T	6/3	R+,F+,Rm	22	V. poor age	P	F	F	4	
Maranhao Basin Basalt, Brazil	118	118±6	18	356.7	-37.1	289	2.0	AF	18/0	None	10	R. 29	P	F	F	3	
Cerro Barcino sediments, Argentina	118	Aptian	11	5.2	-42.4	66.0	5.6	AF/T	11/0	F+	11		P	P	P	5	
Vulcanites Cerro Colorado, Argentina	120	~120	7	343.9	-46.0	-	12.3	AF/T	0/7	None	12	R. this work	P	P	F	3	
Vulcanites Cerro Colorado, Argentina	120	~120	6	357.1	-38.8	139.0	5.7	AF	6/0	None	13	R. this work	P	P	F	2	
Vulcanites Cerro Colorado, Argentina	123	123±4	10	334.2	-41.3	17.5	11.9	AF	3/7	None	14	R. 29	P	F	F	3	
Cerro Colorado Mean	121		23	350.5	-42.8	35.8	7.0	AF/T	9/14	None	12 & 13	R. this work					
Sao Sebastiao dykes, Brazil	122	122.2±2.8	7	353.4	-51.2	-	8.4	AF/T	7/0	Rm	2		P	P	F	3	
Central Alkaline Province, Paraguay	125	130-120	75	356.3	-40.6	29.0	3.1	AF/T			15		P	P			

Table 3.1

Continued...

Locality	Age	Stratigraphic/ Age Range	No. of sites	For site at Lat. 26.3°S, Long. 290.1°E						Field / other						
				Dec.	Inc.	k	α_{95}	Demag	Nor/rev	tests	Ref.	Notes	B	BC	M	Q
EARLY CRETACEOUS																
Ponta Grossa Dykes, Brazil	131	~135-127	115	351.8	-42.6	42.0	2.0	AF/T	79/36	R+, Psv	17		P	P	P	4
South Parana Basin, Brazil	133	133	197	359.6	-36.5	45.0	1.5	AF/T	-	-	18	R. 17	P	P	P	4
Central Parana Basin, Brazil	133	133-132	106	355.4	-39.1	38.0	2.3	AF/T	222/117	Rm, Psv	18	R. 17	P	P	P	4
North Parana Basin, Brazil	135	137-132	36	356.1	-36.9	29.0	4.5	AF/T	-	-	18	R. 17	P	P	P	4
Ceara Mirim dykes (I, V) and Sardinha intrusions (MC1), Brazil	135	145-125 130-120	29 -	357.8 -	-37.0 -	- -	2.0 -	- -	- -	- -	16 -		P	P		
MIDDLE JURASSIC																
Chon Aike Fm., Argentina, Puerto Descardo	161	160.7±7	22	354.7	-39.9	14.0	4.8	AF/T	21/1	None	19		P	P	P	4
Chon Aike Fm., Argentina, La Reconquista	164	164	14	359.7	-39.7	43.1	6.1	AF/T	14/0	None	20	R. 29	P	P	P	3
Marifil Fm., Argentina, dykes/lavas	169	174-164	14	4.3	-36.9	-	15.0	AF/T	8/6	None	21	R. from 27 & 28	P	P	F	4
Ceara Mirim dykes (III, IV) and Mosquito flows (MC2), Brazil	168	175-160 200-170	39 -	7.7 -	-46.6 -	- -	4.0 -	AF/T -	- -	- -	16 -		P	P		
Porto Franco Volcanics, Brazil	175	175	15	2.5	-49.6	31.8	6.9	AF	15/0	None	10 d. 17		P	P	P	3
EARLY JURASSIC																
Ceara Mirim dykes (II, RN2), Brazil	193	E. Jur	27	349.7	-68.0	-	4.0	AF/T	-	-	16		P	P		
Pescadero rhyolite porphyry, Venezuela	194	193±6	1	0.6	-47.3	22.9	10.9	AF	1/0	Rm	23		F	F	F	2
Guacamayas Volcanics, Venezuela	195	195±3.9	5	354.5	-64.0	41.2	12.1	AF	5/0	Rm	23	< 6 specimens/site	P	F	F	3
Anari and Tapirapua basalt flows, Brazil	197	196.6±0.4	15	21.5	-62.2	102.8	3.8	AF/T	15/0	Rm	24		P	P	P	3
Bolivar Dykes, Venezuela	198	198±4	5	21.3	-60.4	38.9	8.4	AF	5/0	Rm	23	< 6 specimens/site	P	F	F	3
Las Cabras Lavas, Argentina	204	204±3	5	8.5	-59.8	-	13	AF/T	4/1	None	25 d. 26	< 6 specimens/site	P	F	F	2

Table 3.1. Palaeomagnetic reference directions from the South American plate. Dec. and Inc. are declination and inclination of remanence direction; k and α_{95} are Fisher (1953) statistical parameters; demag. is type of demagnetisation used, T is thermal, AF is alternating field; Nor/Rev is number of normally and reversally magnetised samples; Field/other tests are labelled as, R+, reversal; F+, Fold; PSV, Palaeosecular variation; Rm, rock magnetic. References are coded to Table 3.4, d. means age is from another reference. In notes R. means recalculated. Selection criteria are labelled as P, pass and F, Fail with respect to B, Beck (1988); BC, Besse and Courtillot (1988; 1991); M, May and Butler, (1986); Q, rating from Van der Voo (1993).

corrections or the original authors stated that there may be a problem with geological setting and palaeohorizontal control.

Most of the South American poles, 26 of 36, pass the criteria of Van der Voo (1993), but many have a $Q = 3$ rating, indicating that they are poorly constrained (again it is not known which of the criteria the unavailable poles would pass, so they are not included). The two main problems which prevent a higher rating are, firstly, the problem of structural control in intrusive and volcanic rocks and secondly, as APW of the South American craton has been slight since the Triassic (Riley *et al.*, 1993) any palaeopole may well be similar to younger poles, even by more than a period. An additional problem is that poles can achieve a Q rating of greater than three whilst being very poorly constrained in terms of one or more of the criteria. An example of this is shown by the mid-Cretaceous Rio los Molinas Dyke pole of Linares and Valencio (1975). Although the pole has a Q rating of three, it has a very poorly defined age. The individual constraints on poles with the same Q rating may therefore be extremely different, and this will inevitably lead to inconsistencies in the quality of the data selected.

3.3 Review of previous APWPs and reference directions

A review of the previous APWPs for South America, and those from other continents which could be used as a reference for the South American data are discussed. As the rocks in this current study are Mesozoic or Tertiary in age, only APWPs covering this time period are considered. Comparison of APWPs allows a check on the consistency of the data, and the effects of different reliability criteria and construction methods.

An APW path for South America was compiled by Irving and Irving (1982) who averaged individual pole positions using 30 Ma windows to determine a mean pole every 10 Ma. Irving and Irving (1982) do not state their reliability criteria but many of the poles used to calculate this path are poorly constrained. This led Beck (1988) to apply reliability criteria, and publish a new compilation of South America reference directions, calculating two mean reference poles, one for the whole of the Jurassic, the other for the Cretaceous. Since the compilation of Beck (1988), additional poles, particularly for the Cretaceous have been published. Considering this larger data set, Butler *et al.* (1991) suggest that calculating a single mean pole for the whole of the Cretaceous is inappropriate as distinctions can be made between poles of Early and Late Cretaceous age.

Like the South America pole data base, the North American pole list also suffers from a lack of data for the late Middle to Late Jurassic. Van der Voo (1992) suggests a different approach to constructing APWPs which could provide data for this gap. Van der Voo (1992) suggests that poles from Atlantic bordering countries in areas that are likely to have been affected by vertical axis rotations could be used to define a pole for the Middle to Late Jurassic. If a particular site has suffered vertical axis rotation, but no latitudinal shift, the declination will have been rotated and the corresponding pole will lie on a small circle path which would include the true unrotated pole. By compiling enough pole positions from each continent a small circle path is defined. When the Atlantic is closed and the different areas are reconstructed to their original locations, the small circle paths for each continent will cross at the position of the true pole at this time. The small circle path for the South American data lies at approximately 90° to the European data and is therefore vital in defining the true pole position. Despite this, Van der Voo (1992) constructs the South American reference small circle on only four poles, all of which are clustered in an arc on one part of the small circle. Therefore, while this small circle technique is valid for pole

reconstruction, there may be a problem with the South American contribution and the true pole may not be well defined.

As discussed earlier, Besse and Courtillot (1991) generated a synthetic APWP, the African Master Curve, by taking the best constrained poles from Africa, North America, Europe and India. This APWP is constructed by rotating all poles that pass their reliability criteria into African co-ordinates. The APWP is synthetic as it relies on data from more than one continent rotated using plate reconstruction models. This synthetic APWP can be used for reference on any continent by rotating the path into the correct co-ordinates for the continent as defined by plate reconstruction parameters. Roperch and Carlier (1992) rotated poles from the African Master Curve of Besse and Courtillot (1991) for the period 10 Ma-200 Ma by partial and progressive closure of the Atlantic Ocean. The individual calculated poles are separated by 10-30 Ma gaps. The rotated poles from the African Master Curve therefore provide an alternative set of reference directions for South American palaeomagnetic data.

One of the most studied areas for South America reference poles has been the intracratonic basalts of Brazil, particularly from the Serra Geral Formation in the Paraná Basin (Piccirillo and Melfi, 1988, Ernesto *et al.*, 1990). Many of the poles were poorly dated and this made comparison of poles and construction of an APW path difficult (Raposo and Ernesto, 1995). Recently, many of the sites in the basin have been more accurately dated and the area has been divided into three distinct geochemical regions. In addition to publishing data from a new part of the Paraná Basin, Raposo and Ernesto (1995) calculate new mean directions for the three parts already identified. These new poles are then used in association with other published poles from South America to construct mean poles for the Middle Jurassic to the Late Cretaceous.

Poles from the studies of Irving and Irving (1982), Beck (1988), Raposo and Ernesto (1995) and Roperch and Carlier (1992) have been converted into direction space

using a site at 26.3°S, 290.1°E. The mean direction paths from these studies are shown in Figure 3.1. With the exception of the Early Jurassic, the reference poles all show consistent directions and trends in the data. The rotated African Master Curve shows a good correlation with the South America data. As there are no South America data included in the master curve this provides independent evidence that the South America data is an accurate recorder of ancient APW.

It can be seen from Figure 3.1 that APW of the South American plate has been slight since the Jurassic, and the choice of selection criteria and method of APWP construction makes only slight differences to the APWP.

3.4 Calculating a new reference direction

For this thesis rocks have been sampled with ages ranging from Early Jurassic to mid-Cretaceous in the Coastal Cordillera, and from Early Jurassic to Early Cenozoic (Palaeocene-Eocene) in the Pre-Cordillera. It is therefore necessary to construct an APW path or a set of mean pole positions for this period. Although Butler *et al.* (1991) suggest that the reference pole probably did not align with the present axial dipole position until after 10 Ma, given the sparsity of data available for the mid-Late Cenozoic the present axial dipole is used for time periods younger than Eocene in this study. In this thesis the ages of the reference palaeopoles have all been referred to the timescale of Harland *et al.* (1989).

Since the compilation of Beck (1988) more poles have been published and many older poles have been better constrained by radiometric dating. For this reason a more

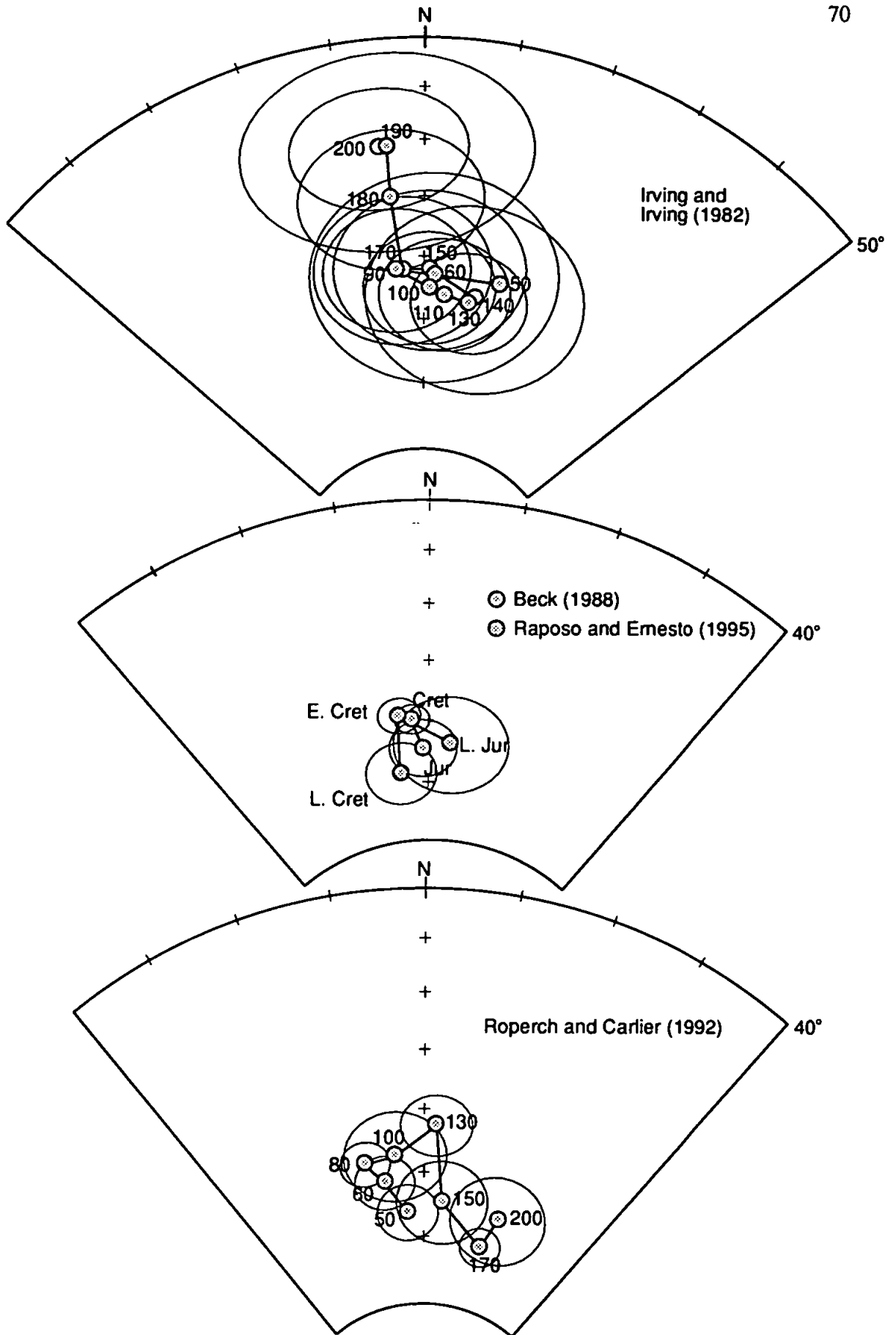


Figure 3.1. Equal area stereographic plots of previously published APWPs and mean palaeomagnetic reference poles converted to direction space for a site at 26.3°S, 290.1°E. All points plot on the upper hemisphere. Confidence limits are for α_{95} ; numbers are Ma. before present.

stringent set of reliability criteria can be used to grade the available poles from South America. Of the reliability criteria discussed in Section 3.2 the 'information' system of rating poles (Van der Voo, 1993) results in a poor Q rating for many of the poles because of the problems with structural corrections. Additionally, as discussed previously, the criteria mean that poles can be very poorly constrained in terms of one or more of the criteria and still gain a Q rating of three or higher. The criteria of May and Butler (1986) significantly reduce the number of poles available to calculate the mean direction, and leave some time periods very poorly defined. The criteria of Besse and Courtillot (1988; 1991) seem to form a sensible middle ground between the criteria of Beck (1988) and May and Butler (1986). For this reason the criteria of Besse and Courtillot (1988; 1991) are used to assess the reliability of palaeopoles in this study.

The South America data set is given in Table 3.1 and those which pass the reliability criteria are indicated in the right-hand column. To supplement the South America data set and increase the number of poles available to calculate the mean direction, African data which passes the selection criteria (Table 3.2) will also be included in the mean calculations. The African poles from the Jurassic to Eocene have been rotated into a South American framework using plate reconstruction parameters given by Cande *et al.* (1986) and Roperch and Carlier (1992), and the final fit from Lawver and Scotese (1987). In some cases it can be seen that there have been multiple studies of the same formation. Where this has occurred, a formation mean has been calculated by averaging all of the site mean virtual geomagnetic poles which pass the selection criteria. This aims to reduce the effect of any bias which may be introduced by including many studies from a single locality. The exception to this is the data from the Serra Geral Formation in the Paraná Basin of Brazil. The poles published by Ernesto *et al.* (1990) include the reworking of many of the older site localities, and the well constrained results obtained supersede those of the older studies.

Locality	Age	Stratigraphic/ Age Range	Pole Africa		Rotation Afr./S. Am.			Pole S. Am.		Reference direction for 26.3°S, 290.1°E				Reference
			Lat. N	Long. E	Lat. N	Long. E	Angle	Lat. S	Long. E	Dec.	Inc.	α_{95}		
EARLY CENOZOIC														
Small circles intersection	50	E. Tert.	73	194	58.5 ¹	-31.5	-19.1	77	323	351	-56	4	30	
Wadi Abut Teireifiya, Egypt	50	E. Tert.	69	189	58.5	-31.5	-19.1	72	325	347	-60	5	31	
LATE CRETACEOUS														
Small circles intersection	68	L.Cret.	67	223	63.0	-33.5	-25.6	77	357	346	-50	4	30	
Fuerteventura	70	L.Cret.	69	221	63.0	-33.5	-26.6	78	350	348	-51	4	32	
Madagascar	70	70±7	63	243	63.0	-33.5	-26.6	75	215	17	-48	11	33	
Madagascar	73	73±7	66	218	63.0	-33.5	-27.9	75	348	345	-53	7	33	
Madagascar	74	74±6	60	212	63.0	-33.5	-27.9	69	348	334	-55	4	33	
Wadi Natash Volcanics, Egypt	85	104-63	65	249	61.8	-34.0	-33.5	81	216	10	-47	11	34	
Madagascar	88	92-84	70	248	61.8	-34.0	-33.5	86	208	15	-45	11	33	
MID-CRETACEOUS														
Madagascar	89	90-88	70	244	61.8	-34.0	-33.5	85	192	5	-44	9	33	
Wadi Natash Volcanics, Egypt	90	111-82	69	258	53.7 ²	-33.1	-41.5	87	196	4	-44	6	35	
Kimberlites (upper age), S. Africa	90	100-81	64	226	53.7	-33.1	-41.5	78	306	356	-57	5	36	
Madagascar	92	94-90	65	230	53.7	-33.1	-41.5	80	304	357	-55	6	33	
Kuoko Volcanics, SW. Africa	122	131-113	48	267	53.7	-33.1	-41.5	71	248	7	-59	3	37	
Mlanje Massif Lupata Volcanics	122	128-116	61	261	53.7	-33.1	-41.5	84	257	357	-38	6	38 & 39	
Kimberlites (Lower age), S. Africa	130	145-113	48	270	45.5 ³	-32.2	-58.2	83	293	357	-53	10	36	
LATE JURASSIC														
Karoo Dolerite Lavas, Mozambique	157	165-150	65	255	45.5	-32.2	-58.2	75	223	16	-51	12	40	
EARLY JURASSIC														
Liberia Diabases	182	192-173	69	242	45.5	-32.2	-58.2	69	234	21	-56	5	41	
Draa Valley Sills, Morocco	183	186-180	66	230	45.5	-32.2	-58.2	68	249	19	-60	4	42	
Zimbabwe Mateke/Marangudzi	186	186	60	270	45.5	-32.2	-58.2	79	189	12	-41	8	43 & 44	
Mauritania S. Dolerites	187	187±5	71	240	45.5	-32.2	-58.2	67	233	24	-56	6	45	
Mauritania N. Dolerite	187	187±5	69	232	45.5	-32.2	-58.2	67	241	23	-59	4	45	

Table 3.2. Palaeomagnetic reference poles/directions from Africa. Euler rotation parameters from; ¹Cande *et al.* (1986); ²Roperch and Carlier (1992); ³Lawver and Scotese (1987). Dec. and Inc. are declination and inclination of remanence vector; α_{95} is according to Fisher (1953). References are coded to Table 3.4.

In this thesis all of the palaeomagnetic data are considered in direction space rather than pole space, this is because variations and patterns in the data are more apparent when considered in direction space. This approach requires the calculation of reference directions from the poles relative to the geographic position of the study area. To calculate the reference directions from the published reference palaeopoles all directions have been referred to a sampling locality of 26.3°S, 290.1°E, approximately mid-way between the study areas of the Coastal Cordillera and the Pre-Cordillera. The two study areas are sufficiently close so as to make it unnecessary to calculate separate reference directions for each.

The full set of reference directions, both from South America and Africa, which pass the selection criteria are given in Table 3.3. It is obvious from Table 3.3 that, for the most part, there is very little variation in the directions within each Epoch. For this reason mean reference direction are calculated for each Epoch identified in Table 3.3 rather than constructing an APWP.

3.4.1 Jurassic reference directions

i) Early Jurassic (208-178 Ma)

There are seven reference directions available for the Early Jurassic, dominantly from the rotated African data set. The directions are fairly consistent and lie east of north. The direction from the Ceara-Mirim dykes lies away from the main group approximately 30° anticlockwise. The direction from these dykes also has the steepest inclination, possibly indicating a problem with undetected and uncorrected structural deformation of the sampling region. Although the reason for this directional outlier is unknown, M. Ernesto (*Pers. comm.*) notes that there is a problem with correlating the $\text{Ar}^{39}\text{-Ar}^{40}$ age of

Locality	Age	Age Range	Dec.	Inc.	α_{95}	Ref.
EARLY CENOZOIC						
Small circles intersection	50	E. Tert.	351	-56	4	30
Wadi Abun Teireifiya, Egypt	50	E. Tert.	347	-60	5	31
LATE CRETACEOUS						
Small circles intersection	68	L.Cret.	346	-50	4	30
Passa Quatro/Itatiaia intrusives, Brazil	70	~70	349	-49	6	2
Fuerteventura	70	L.Cret.	348	-51	4	32
Madagascar	70	70±7	17	-48	11	33
Patagonian Basalts	72	79-64	348	-49	6	3
Madagascar	73	73±7	345	-53	7	33
Madagascar	74	74±6	338	-55	4	33
Pocos de Caldos intrusives, Brazil	75	~75	0	-51	14	4
Sao Sebastiao stocks, Brazil	81	80.8±3.1	350	-55	7	2
Wadi Natash Volcanics, Egypt	85	104-63	10	-47	11	34
Madagascar	88	92-84	15	-45	11	33
Pocos de Caldos intrusives, Brazil	88	~88	356	-52	3	2
MID-CRETACEOUS						
Madagascar	89	90-88	5	-44	9	33
Wadi Natash Volcanics, Egypt	90	111-82	4	-44	6	35
Kimberlites (upper age), S. Africa	90	100-81	356	-57	5	36
Madagascar	92	94-90	357	-55	6	33
Mafic dykes, Brazil	105	M. Cret	359	-45	3	7
Cabo de Santo Agostinho, intrusives, Brazil	106	~85-99	359	-47	5	9
Cerro Barcino sediments, Argentina	118	Aptian	5	-42	6	11
Cerro Colorado Mean	121	123-120	351	-43	7	12 & 13
Sao Sebastiao dykes, Brazil	122	122.2±2.8	353	-51	8	2
Kaoko Volcanics, SW. Africa	122	131-113	7	-59	3	37
Mlanje Massif Lupata Volcanics	122	128-116	357	-38	6	38 & 39
Central Alkaline Province, Paraguay	125	130-120	356	-41	3	15
Kimberlites (Lower age), S. Africa	130	145-113	357	-53	10	36
EARLY CRETACEOUS						
Ponta Grossa Dykes, Brazil	131	~135-127	352	-43	2	17
South Parana Basin, Brazil	133	133	0	-37	2	18
Central Parana Basin, Brazil	133	133-132	355	-39	2	18
North Parana Basin, Brazil	135	137-132	356	-37	5	18
Ceara Mirim dykes (I, V) and Sardhina intrusions (MC1), Brazil	135	145-125 130-120	358 -	-37 -	2 -	16 -
LATE JURASSIC						
Karoo Dolerite Lavas, Mozambique	157	165-150	16	-51	12	40
MIDDLE JURASSIC						
Chon Aike Fm., Argentina, Puento Descardo	161	160.7±7	355	-40	5	19
Chon Aike Fm., Argentina, La Reconquista	164	164	0	-40	6	20
Marifil Fm., Argentina, dykes/lavas	169	174-164	4	-37	15	21
Ceara Mirim dykes (III, IV) and Mosquito flows (MC2), Brazil	168	175-160 200-170	8 -	-47 -	4 -	16 -
Porto Franco Volcanics, Brazil	175	175	3	-50	7	10
EARLY JURASSIC						
Liberia Diabases	182	192-173	21	-56	5	41
Draa Valley Sills, Morocco	183	186-180	19	-60	4	42
Zimbabwe Mateke / Marangudzi	186	186	12	-41	8	43 & 44
Mauritania S. Dolerites	187	187±5	24	-56	6	45
Mauritania N. Dolerite	187	187±5	23	-59	4	45
Ceara Mirim dykes (II, RN2), Brazil*	193	E. Jur	350	-68	4	16
Anari and Tapirapua basalt flows, Brazil	197	196.6±0.4	22	-62	4	24

Table 3.3. Palaeomagnetic reference directions from South America and Africa (in South American co-ordinates) which pass the selection criteria of Besse and Courtillot (1988; 1991). Column headings as in Table 3.2. The ages quoted are either the specific age quoted by the original author, or the mid-point if an age range or chronostratigraphic stage is given.

* indicates that the direction is not included in the calculation.

- | | |
|--------------------------------------|--|
| 1. Vilas and Valencio (1978) | 23. MacDonald and Opdyke (1974) |
| 2. Montes-Lauar <i>et al.</i> (1995) | 24. Montes-Lauar <i>et al.</i> (1994) |
| 3. Butler <i>et al.</i> (1991) | 25. Valencio (1969) |
| 4. Opdyke and MacDonald (1973) | 26. Valencio and Vilas (1972) |
| 5. Valencio <i>et al.</i> (1983a) | 27. Mena (1990) |
| 6. Valencio <i>et al.</i> (1977) | 28. Rapalini and Vilas (1991) |
| 7. Raposo (In press) | 29. Beck (1988) |
| 8. Linares and Valencio (1975) | 30. Besse and Courtillot (1991) |
| 9. Schult and Guerrieiro (1980) | 31. Gouda-Hussein <i>et al.</i> (1979) |
| 10. Schult and Guerrieiro (1979) | 32. Storedveldt <i>et al.</i> (1979) |
| 11. Somoza (1994) | 33. Andiamirado (1971) |
| 12. Valencio (1972) | 34. Resselar <i>et al.</i> (1981) |
| 13. Vilas (1976) | 35. Schult <i>et al.</i> (1981) |
| 14. Mendia (1978) | 36. Hargraves (1989) |
| 15. Ernesto <i>et al.</i> (1995) | 37. Gidskehaug <i>et al.</i> (1975) |
| 16. Ernesto <i>et al.</i> (In Prep.) | 38. Gough and Opdyke (1963) |
| 17. Raposo and Ernesto (1995) | 39. Briden (1967) |
| 18. Ernesto <i>et al.</i> (1990) | 40. McElhinny and Jones (1965) |
| 19. Valencio and Vilas (1970) | 41. Dalrymple <i>et al.</i> (1975) |
| 20. Vilas (1974) | 42. Hailwood and Mitchell (1971) |
| 21. Rapalini <i>et al.</i> (1993) | 43. Gough and Brock (1964) |
| 22. Castillo <i>et al.</i> (1991) | 44. Brock (1981) |
| | 45. Sichler <i>et al.</i> (1980) |

Table 3.4. References for data quoted in Tables 3.1 to 3.3.

the Early Jurassic sites with the palaeomagnetic direction. For these reasons the direction is considered to be unreliable and is excluded from the mean calculation.

All of the calculated reference directions, except that from Zimbabwe, have inclinations that are steeper than would be expected at the current site latitude, yielding palaeolatitudes in the range 37° - 51° S. This suggests a more southerly location for the South American plate during this time period, consistent with plate tectonic reconstructions for the Late Triassic-Early Jurassic (Smith and Briden, 1977; Scotese, 1990). The mean direction is calculated from six studies, excluding the Ceara-Mirim dyke direction, lies at $\text{dec} = 20^{\circ}$, $\text{inc} = -56^{\circ}$, $\alpha_{95} = 7^{\circ}$.

ii) Middle Jurassic (178-157.1 Ma)

The Middle Jurassic is represented by five directions, all from South America which yield a mean direction at $\text{dec} = 2^{\circ}$, $\text{inc} = -43^{\circ}$, $\alpha_{95} = 6^{\circ}$. This direction is substantially different to the Early Jurassic direction, the declination lies much closer to north being approximately 15° anticlockwise of the Early Jurassic mean direction, and the inclination is also shallower. The difference between the inclinations suggests $\sim 14^{\circ}$ of northward latitudinal transport. Given the short time gap between the mean directions from the Early and Middle Jurassic, the directions must be indicating a period of rapid motion of the South American Plate.

iii) Late Jurassic (157.1-145.6 Ma)

Only one direction of Late Jurassic age passes the reliability criteria, that of the Karoo Lavas at $\text{dec} = 16^{\circ}$, $\text{inc} = -51^{\circ}$, $\alpha_{95} = 12^{\circ}$. Both the declination and inclination appear anomalous when compared to the directions from the Middle Jurassic and Early Cretaceous. This study was carried out some time ago (McElhinny and Jones, 1965) and

the analytical procedures used may not have been as rigorous as those currently in use. As a consequence this direction may not be accurate and is treated with some scepticism. For this reason no reliable Late Jurassic mean direction is recognised.

3.4.2 Cretaceous reference directions

i) Early Cretaceous (145.6-131.8)

The five studies which comprise the Early Cretaceous results are all from South America, four of them (excluding the Ceara-Mirim dykes) are from the Paraná Basin of Brazil. Although the age of the Paraná Basin volcanic province as a whole is poorly constrained (Rocha-Campos *et al.*, 1988) the palaeomagnetic sampling localities have been well dated and subdivided into distinct geochemical regions (Ernesto *et al.*, 1990; Raposo and Ernesto, 1995).

Considering the extensive sampling and rigorous analytical procedures involved in these five studies, the directions must be regarded as very well constrained. The mean direction calculated from the five studies lies at $\text{dec} = 356^\circ$, $\text{inc} = -39^\circ$, $\alpha_{95} = 3^\circ$.

ii) mid-Cretaceous (131.8-88.5)

Directions from 13 studies are available for the mid-Cretaceous, 6 of which are from South America. The data are spread throughout the time period and the directions are fairly consistent, both in declination and inclination. In most cases the directions calculated from the African data have steeper inclinations than the South American directions for the corresponding age. The Euler rotation pole used to rotate the African data into South American co-ordinates for the majority of this time period was the 100 Ma pole of Roperch and Carlier (1992). The position of this Euler pole was calculated as lying between the earliest fracture zone Euler pole at 84 Ma (Cande *et al.*, 1988) and the final-fit

pole of Lawver and Scotese (1987). The calculation assumed that the position of the Euler rotation pole followed a linear track with constant velocity between these two times. If the motion of the Euler pole between these times was more complicated, the position of 100 Ma pole may be inaccurate, this may have resulted in the steeper inclinations displayed by the directions from the African data set after rotation into South American co-ordinates around this pole.

The mean direction calculated from the 13 studies lies at $\text{dec} = 359^\circ$, $\text{inc} = -48^\circ$, $\alpha_{95} = 4^\circ$, close to the direction from the Early Cretaceous.

iii) Late Cretaceous (88.5-65)

There are a total of 12 directions for the Late Cretaceous, five of these are from the South American data set. All of the data have inclinations steeper than would be expected for the current site latitude, the mean inclination gives a palaeolatitude of 32°S . In addition, the data show a 25° spread of directions, much greater than is observed for any other time period. Beck (1988) commented on the elongate or 'streaked' distribution of the Cretaceous South American data set and discussed possible explanations. Valencio *et al.*, (1983b) and Oviedo *et al.*, (1991) suggest that the distribution represents true APW, but this seems unlikely as the South Atlantic fracture zones show no evidence of backward-and-forward motion, or 'fish-tailing', during this time period (Beck, 1988; Cande *et al.*, 1988). Beck (1988) also considered the possibility that geomagnetic effects caused the variation, again this is unlikely as the same streaked pattern is not seen in the Cretaceous data from North America (Beck, 1988, based on data from Irving and Irving, 1982). The possibility that intracratonic block rotations may have caused the elongation of the data seems unlikely given the range of localities from which the data comes. This explanation was rejected by Beck (1988) for the South America data. Beck (1988) explained the

outliers by a series of problems specific to each study, but notes that these were highly speculative and tenuous.

The African data also show a large spread of directions and these tend to lie at the extremities of the data spread, particularly the directions from Madagascar. The Euler rotation parameters are very well constrained for the Late Cretaceous (Cande *et al.*, 1988) so it is unlikely that this is an additional source of error in the rotated African data. So, while the variation in the directions for the Late Cretaceous is acknowledged, no definitive interpretation can be given as to its origin.

As there is no explanation for the variation in the Late Cretaceous data none of the directions are excluded and the mean has been calculated from all 12 directions. The mean direction for the Late Cretaceous lies at $\text{dec} = 356^\circ$, $\text{inc} = -51^\circ$, $\alpha_{95} = 5^\circ$.

3.4.3 Cenozoic reference direction

i) The early Cenozoic (Palaeogene)

The Palaeogene is very poorly constrained in terms of the number of available palaeomagnetic reference directions. For previous studies authors have variously used North American poles rotated to South American co-ordinates (Riley *et al.*, 1993), the Late Cretaceous pole (Hartley *et al.*, 1992a), the average present day pole (Hartley *et al.*, 1992a) or, most commonly, the time averaged present day field direction with no associated error (e.g., Heki *et al.*, 1983, 1984, 1985; Kono *et al.*, 1985; MacFadden *et al.*, 1990, 1995).

Butler *et al.* (1991) suggest that using the time averaged present day direction is inappropriate as South America underwent significant APW between 70 and 10 Ma.

Calculation of a new Palaeogene direction is hampered by there being no South American poles specifically dated as early Cenozoic. Butler *et al.* (1991) argue that their Patagonian Basalt pole, data at 79-64 Ma should also be used for at least the Palaeocene as

it is in good agreement with both the North American and African Palaeocene poles when they are rotated into South American co-ordinates. However, none of the African Palaeocene poles passed the reliability criteria of Besse and Courtillot (1988; 1991). There are though two Eocene directions in the African data base with direction close to that of Butler *et al.* (1991). As the Early Cenozoic rocks considered in this study are dated as Palaeocene-Eocene, and the data appears to be consistent, it seems logical to calculate an Early Cenozoic direction based on the combined Late Cretaceous-Palaeocene and the Eocene data. The mean direction for this time period lies at $\text{dec} = 349^\circ$, $\text{inc} = -55^\circ$, $\alpha_{95} = 9^\circ$.

ii) The late Cenozoic (Neogene)

After a review of the available South American reference pole data for the late Cenozoic, Somoza *et al.* (1996) conclude that the mean direction was indistinguishable from the time-averaged GAD position. This can therefore be used as a reference direction for direction of Neogene age. For this study, the direction for the GAD is given an α_{95} of zero, as was also done by Heki *et al.*, (1983, 1984, 1985); Kono *et al.*, (1985); MacFadden *et al.*, (1990, 1995).

3.5 Conclusions

The mean reference directions calculated are given in Table 3.5, along with the position of the present axial dipole direction. Figure 3.2 shows an equal area plot of the directions. It is apparent that the amount of APW of the South America plate has been fairly small, recording a general westward drift due to clockwise rotation of the entire South American plate since the Jurassic. The similarity of the directions, at least since the

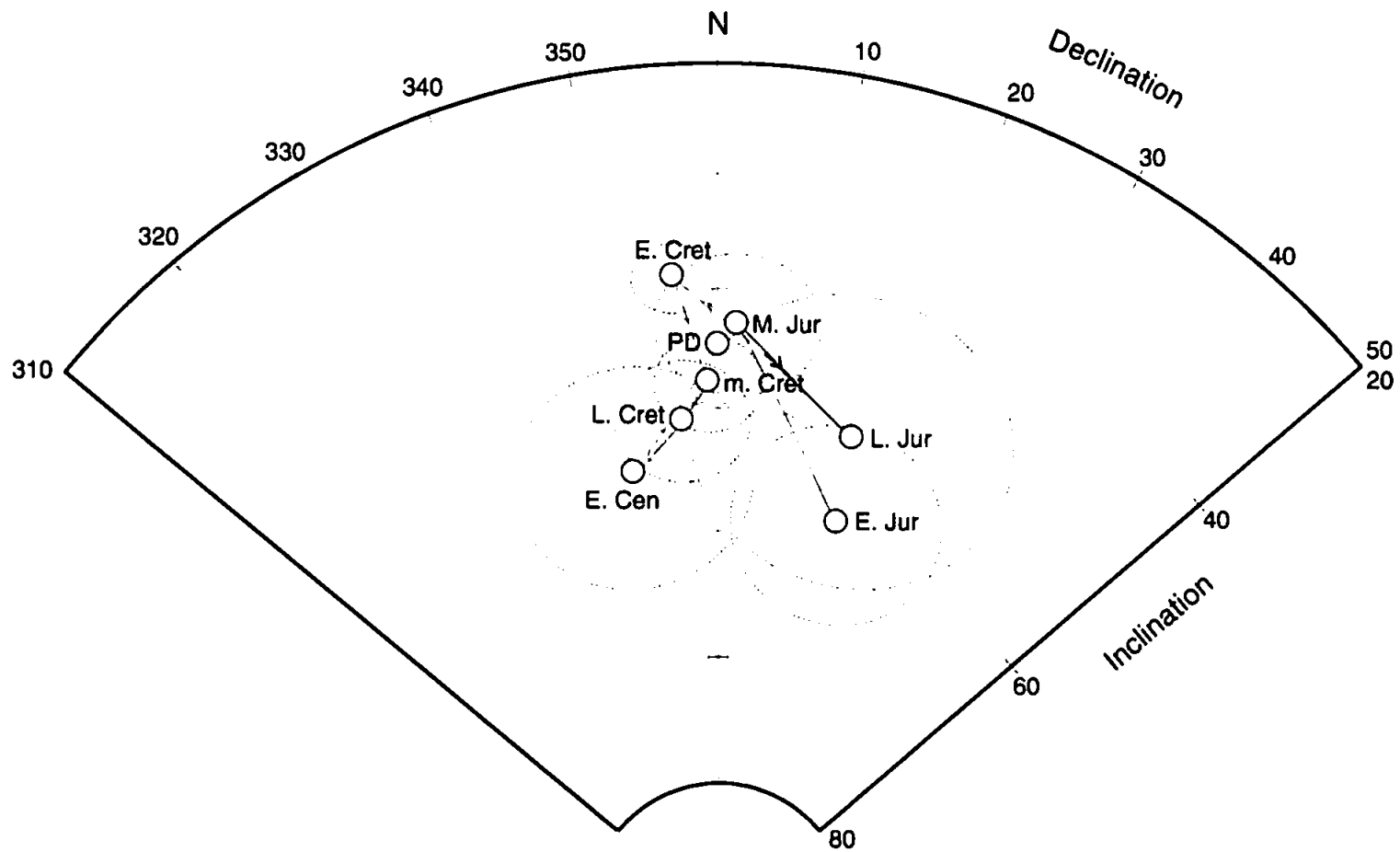


Figure 3.2. Equal area plot of reference directions calculated for this thesis. α_{95} cones of confidence are shown. Open symbols denote upper hemisphere projections.

Middle Jurassic, means that if,significant local vertical axis rotation ($>20^{\circ}$) has occurred since the acquisition of the remanence, this will be evident no matter which reference direction is used. This means that rotation can still be recognised with reasonable security even if the palaeomagnetic remanence was acquired some time after formation of the rock.

Time period	No.	Declination ($^{\circ}$)	Inclination ($^{\circ}$)	α_{95} ($^{\circ}$)
Present Day	-	0	-45	0
Early Cenozoic	3	349	-55	9
Late Cretaceous	12	356	-51	5
mid-Cretaceous	13	359	-48	4
Early Cretaceous	5	356	-39	3
Late Jurassic	1	16	-51	12
Middle Jurassic	5	2	-43	6
Early Jurassic	6	20	-56	7

Table 3.5. Reference directions calculated in this Chapter, and present day direction assuming a dipolar field. No. is number of studies included in the mean.

Chapter 4

CAUSES OF VERTICAL AXIS ROTATION

4.1 Introduction

Studies from tectonic zones around the world have demonstrated that crustal rotations around vertical axes are a common component of crustal deformation. These rotations may be recognised from discrepancies between observed and expected palaeomagnetic declinations (e.g., Luyendyk *et al.*, 1980; Ron *et al.*, 1984, 1986; Beck, 1976, 1988; Forsythe and Chisholm, 1994; Sonder *et al.*, 1994) or from fault geometries (e.g., Sanderson *et al.*, 1991; Jackson and Sanderson, 1992). The scale and distribution of rotations varies in every different deformation zone and the models proposed to account for the vertical axis rotations are therefore often case specific.

This chapter reviews the major tectonic models that have been suggested to explain vertical axis rotations, both from the South American margin and from deformation zones in continental margins around the world. The rotation models, particularly those proposed for the South America margin, can be broadly divided into three categories differentiated by the scale at which the rotation mechanisms operate. In the first category, it is suggested that rigid bending of an originally near-straight continental margin accounts for both palaeomagnetically identified rotations and the presence of the Arica Deflection; in the second category, the rotations occur *in situ* and at a much smaller scale in response to motion on strike-slip faults; and in the third category the rotation occurs *in situ* but in response to large-scale tectonic processes.

4.2 Rigid bending of the continental margin

4.2.1 Oroclinal bending

Carey (1958) suggested that bending of an originally straight continental margin could be achieved by impressing a strain in to the continental crust, this process being termed *oroclinal bending*. Rotation is by large-scale, essentially rigid bending of the continental margin around a fixed point which then becomes the hinge zone of the bend (Figure 4.1). The bending therefore causes different senses of rotation on either side of the hinge which should be reflected in the palaeomagnetic directions from the two limbs. Not only can this type of rigid rotation be used to account for palaeomagnetically identified rotations but also, in the case of South America, the rotation could account for the marked change in geological strike at the Arica Deflection.

Carey (1958) does not define a kinematic mechanism for the model, and no attempt is made to relate the rotations to the fault systems in the deforming zone. Oroclinal bending only effects the leading edge of the deforming margin and not the stable cratonic area behind. Bending should therefore cause triangular shaped extensional zones to develop between the rotating margin and the stable craton block (Figure 4.1). These extensional zones should be preserved in the geological record either by plutonic or sedimentary infilling. Extensional zones such as this are not obvious in the Andean margin and this led Isacks (1988) to suggest a modification of the model based on differential shortening rather than rigid rotation and extension.

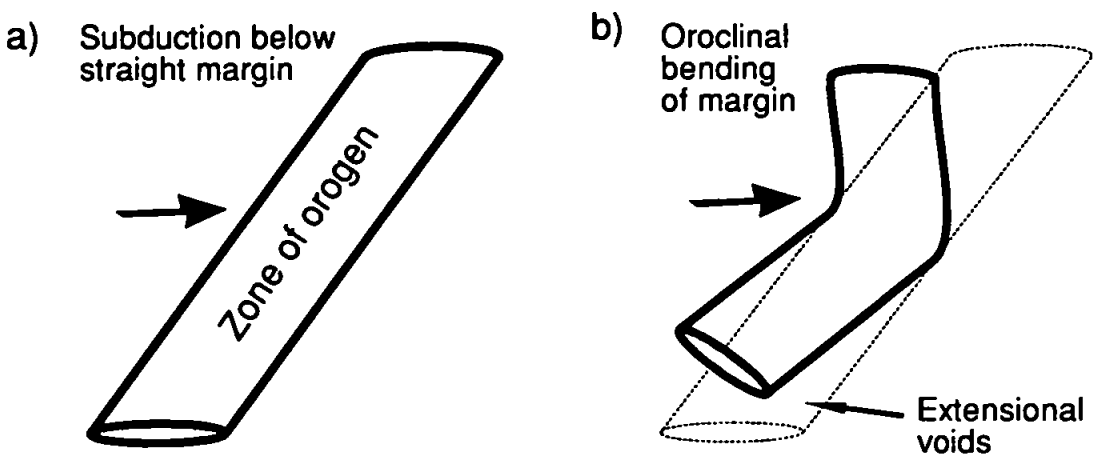


Figure 4.1. The oroclinal bending model of Carey (1958). An originally straight continental margin (a) is bent by subduction (b). The bend results from passive rotation of both limbs around a fixed hinge point. The rotation causes triangular voids to develop behind the deformation zone.

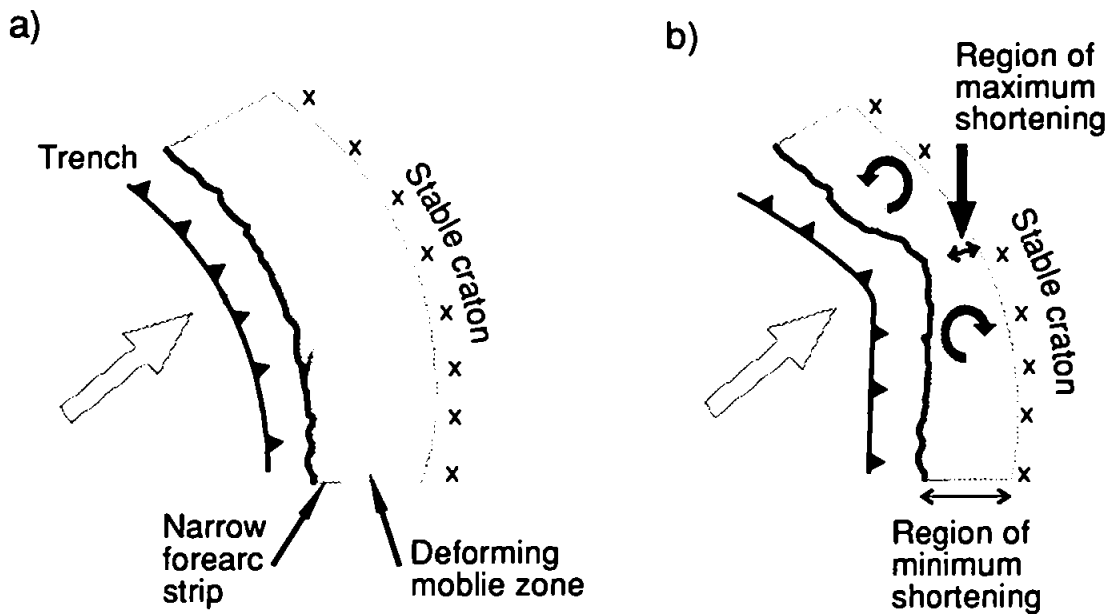


Figure 4.2. The differential shortening model of Isacks (1988). a) Original bend in the Andean margin. b) Differential shortening along the margin causes enhancement of the bend and rotation of the forearc. The surface area of the thermally weakened zone (light shading) is reduced in size to accommodate the rotation.

4.2.2 Differential shortening

Isacks (1988) suggests a kinematic model to explain the Arica Deflection in which an original bend in the Andean margin close to Arica is enhanced by *differential shortening* along the length of the margin (Figure 4.2). The orocline develops by bending a narrow forearc strip and the space loss behind the forearc is accommodated by differential shortening, crustal thickening and uplift of a mobile belt between the forearc and the cratonic foreland. The variation in the amount of shortening accommodated along the margin of the overriding continental crust is controlled by the width of the thermally weakened zone (Figure 4.3). This weak zone results from magmatic and convective processes in the asthenospheric wedge between the colliding plates. Changes in the dip of the subducting oceanic plate along the margin cause differences in the width of the weakened zone and therefore, differential shortening along the margin. Maximum shortening occurs near Arica and decreases both north and south away from the bend. This causes the Andean mountain chain to be both higher and wider closer to the bend (Figure 4.3, topographic plots). As with the oroclinal bending model, rotation of the limbs should be recorded in the palaeomagnetic directions. Isacks (1988) envisaged all of the rotation as occurring during the Neogene (dominantly 23 to 5 Ma), and selected palaeomagnetic data of varying ages from Peru, Bolivia and Chile to support the model.

Although the kinematics of the shortening are well documented for the model, Isacks (1988) makes no explanation of how the shortening is accommodated mechanically, either within or behind the forearc. The shortening should produce obvious structural features which become more dominant closer to Arica, due to the increasing deformation, but Isacks (1988) does not discuss how the shortening relates to the geology or the observed fault patterns in Chile and Peru.

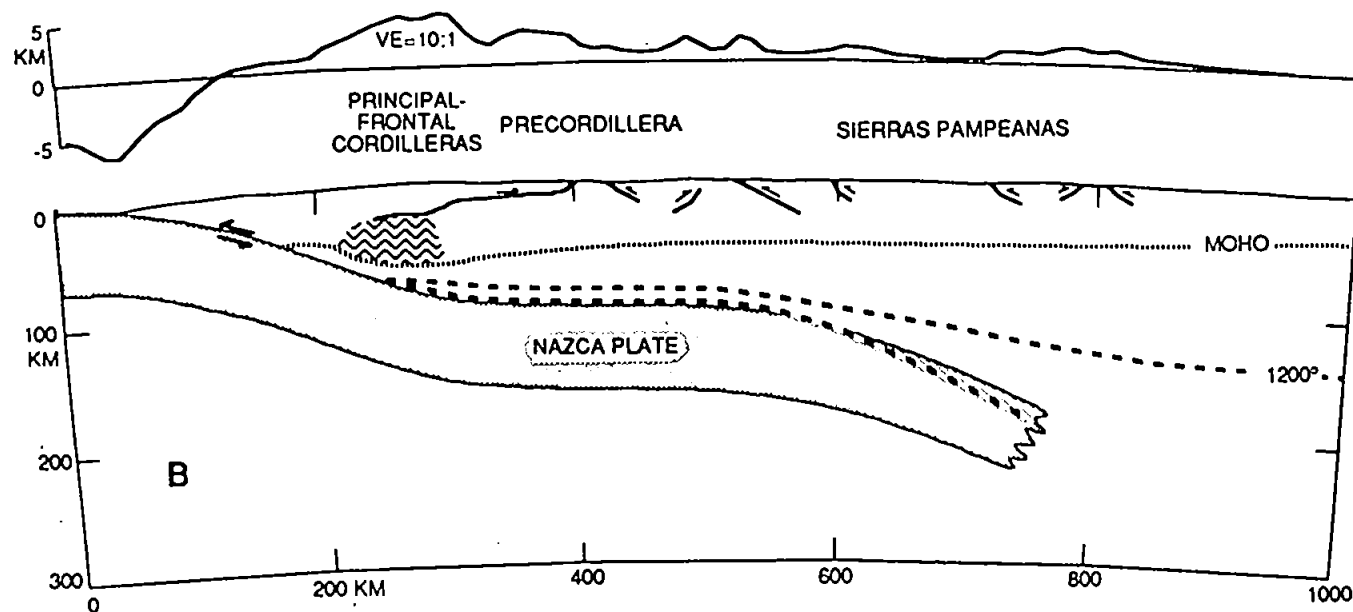
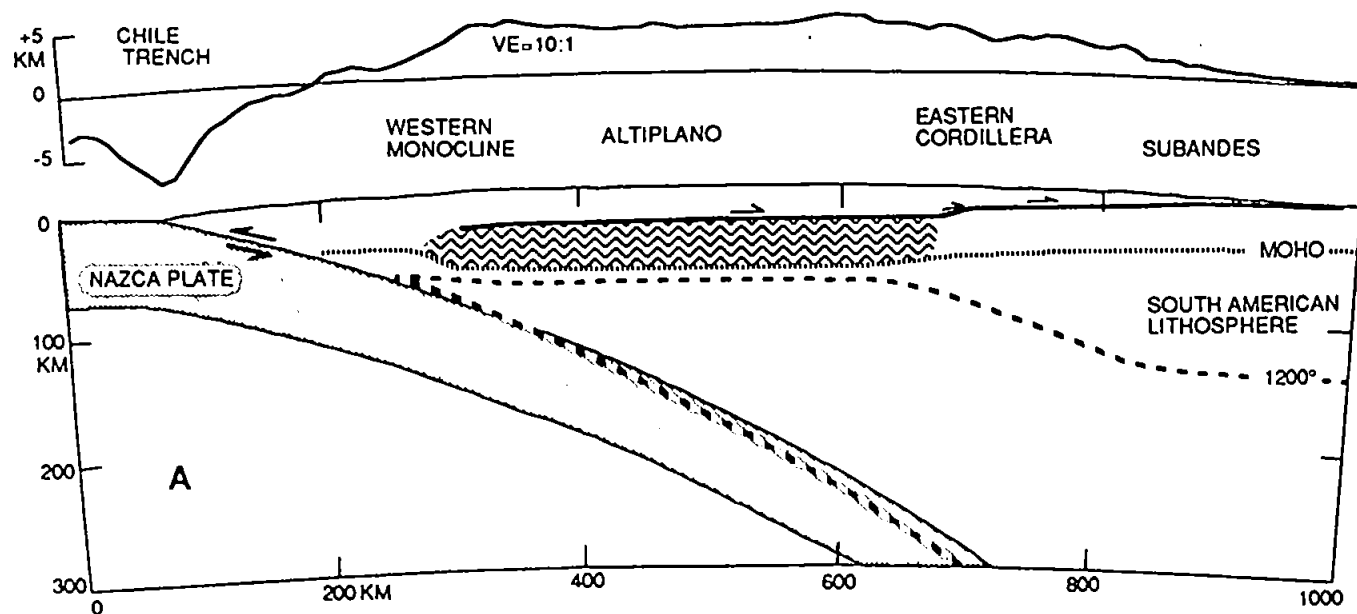


Figure 4.3. Cross-sections through the Andean margin showing, in each case, topography (upper plot) and hypothesised deep structure (lower plot). A) Section through the Altiplano area (approx. 20.5°S). B) Section through the Pampean flat slab segment (approx. 31°S). The wiggly line areas indicate areas of shortened and thickened lower crust. The dashed line shows the position of the 1200°C isograd (diagram taken from Isacks, 1988, figure 3).

4.3 Mechanisms and models for small-scale *in situ* vertical axis rotations

An alternative to the large-scale bending models are those which consider the rotation to occur *in situ* and at much smaller scales. In terms of their applicability to the Andean margin, these models do not attempt to explain the origins of the Arica Deflection. This is presumed to be a primary feature of the margin pre-dating rotation. In these types of models the *in situ* vertical axis rotation occurs in response to strike-slip fault movement in the overriding continental plate. These models are often referred to as *vertical axis rotation* models (Nelson and Jones, 1987; Sonder *et al.*, 1994) or *fault block rotation* models (Ron *et al.*, 1984, 1986; Garfunkel, 1989). It is noted however, that although the models consider the rotation to be occurring around a vertical axis, in many strike-slip shear zones the orientations of the faults will be such that the rotation occurs around an axis inclined to the vertical. The size of the rotating bodies may range from the rotation of individual grains to terrane and micro-plate rotations, but between these two end members are the 1-100 km crustal block scale rotations normally considered in models of continental plate deformation. Before discussing the *in situ* vertical axis rotation models, the role of strike-slip faulting in the overriding plate is considered.

4.3.1 The role of strike-slip faults in *in situ* vertical axis rotation

The ideal stress conditions for strike-slip faulting are when σ_1 (the maximum principle compressive stress) and σ_3 (the minimum principle compressive stress) are horizontal, and σ_2 (the intermediate principle compressive stress) is vertical (Anderson, 1951). According to the Coulomb failure criteria, this stress regime will generate two sets of sub-vertical faults which are conjugate. If there is no volume loss during fault motion (Odonne and Massonnat, 1992), the two fault sets must either operate in sequence and

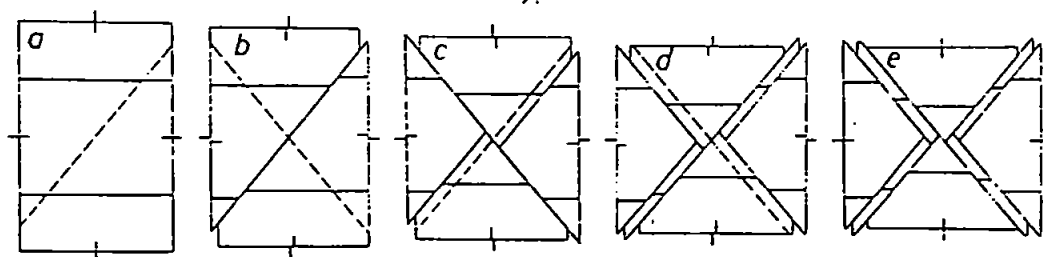


Figure 4.4. Geometrical model of conjugate faults which operate in sequence from an initial undeformed block (a) to sets of displaced faults (e). The faults do not rotate, but displace each other. From Freund (1974, figure 17).

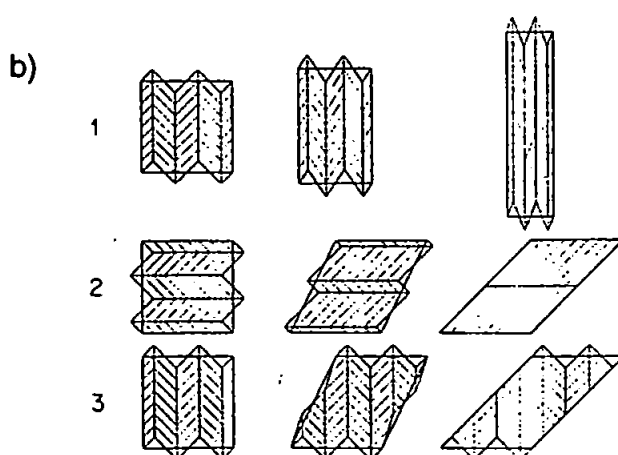
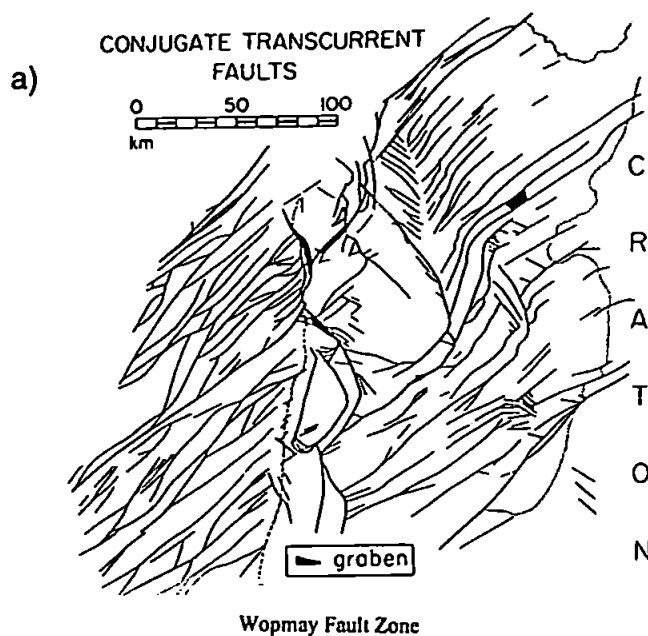


Figure 4.5. Faults avoid transecting by forming domains. a) An example from Wopmay orogen, Canada. The domain containing the NE trending dextral faults dominates over the domain of NW trending sinistral faults (taken from Sylvester, 1988, figure 11). b) Theoretical models of two domain systems undergoing three modes of deformation; 1. boundary-parallel stretching; 2. boundary-parallel shearing; 3. across-boundary shearing. It is noted that faults do rotate in domain systems, the faults in each domain will rotate away from each other towards the extension direction (taken from Cobbold and Gapais, 1986, figure 3).

displace one another (Figure 4.4), or the faults must avoid transecting by forming domains (Figure 4.5). In domains the displacement is achieved by setting up uneven sized domains with only one set of faults in each (Freund, 1974). Over time one domain becomes dominant and takes up most of the stress (Tchalenko, 1970; Cobbold and Gapais, 1986).

Strike-slip fault zones are usually much more complicated than predicted by the Coulomb failure criteria (e.g., Aydin and Page, 1984). More commonly, at crustal scales, the deformation will be influenced by the end effects at fault terminations, and interaction between the faults, regions of extension or contraction at step-overs between fault segments (Wilcox *et al.*, 1973; Segall and Pollard, 1980; Peacock, 1991). The overall nature of the fault system is also complicated by horizontal extension or contraction across the deforming zone. This is because the effect of the pure shear component is to accommodate some stress applied to the overriding crust by the development of extensional or contractional structures. This will reduce the amount of stress within the overriding plate in the simple shear orientation and therefore the amount of displacement that is required on the strike-slip faults. The combination of pure and simple shear will lead to either a transpressive stress regime, where there is horizontal shortening and vertical lengthening along the shear plane (Sanderson and Marchini, 1984) or to transtension, where there is extension in the horizontal plane. The pure shear will effect the development and orientation of secondary features within the fault system (Figure 4.6).

The secondary faults and the effects of pure shear will normally define a more complicated fault system, rather than a simple margin-parallel strike-slip fault. As a result, a common deformation pattern is a diffuse zone in which fault-bound blocks experience rotation around a vertical axis and differential uplift (Jarrard, 1986). Indeed any displacement on the fault, other than pure strike-slip motion parallel to the simple shear direction, must generate vertical axis rotations or the fault domain will become distorted and will no longer be in contact with the boundary of the deformation zone (Ron *et al.*,

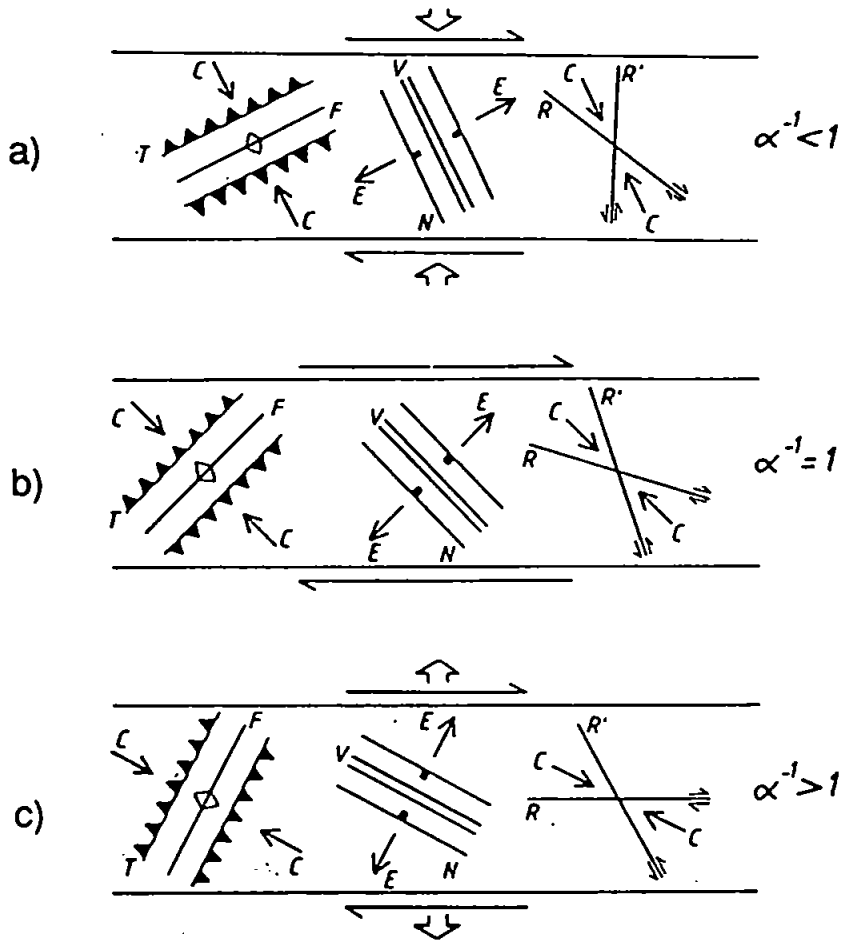


Figure 4.6. The orientations of fractures in shear zones (from Sanderson and Marchini, 1984, figure 5). a) Dextral transpression. b) Simple shear. c) Transtension. C=compression direction; E=extension direction; N=normal faults; T= thrust faults; R, R'=shears in Riedel orientation; V=extension fractures; F=fold axes.

1984). When vertical axis rotation occurs associated with discrete faults, the faults bounding the rotating blocks must also rotate to preserve the area. It is possible for strike-slip motion to occur along parallel shear planes resulting in no vertical axis rotations (Figure 4.7b). An example of this may be parts of the North Anatolian Fault in Turkey (Platzman *et al.*, 1995), where palaeomagnetic studies across the fault zone suggest that no rotation has occurred.

Large scale strike-slip faults near active plate margins can be divided into four major types (Woodcock, 1986), as shown in Figure 4.8. In belts of regional simple shear in continental margins, strike-slip faults often cut both crust and lithosphere. These are referred to as *trench-linked* strike-slip faults (Woodcock, 1986). A trench-linked strike-slip fault defines a *forearc sliver*, which is a margin-parallel strip of the overriding crust decoupled from the main plate and allowed to move independently of the plate. The forearc sliver is bounded by the trench-linked strike-slip fault and the trench. Trench-linked strike-slip faults develop in response to even slightly oblique subduction, a common feature of most subduction margins (Jarrard, 1986; Woodcock, 1986). The faults are usually located within the magmatic arc (Jarrard, 1986) as this is the weakest region of the crust. Here, high geothermal gradients cause a thinned lithosphere and the volcanic arc generates a 'thermally softened' crust (Beck, 1980).

4.3.2 Definitions of models

The kinematics of small crustal scale *in situ* vertical axis rotations are controversial (Ron *et al.*, 1984; Lamb, 1987; Nelson and Jones, 1987; King *et al.* 1994; Sonder *et al.*, 1994). Models published to account for the distribution of vertical axis rotations in continental lithosphere can be divided into two end members (King *et al.*, 1994); *continuum models*, are where the deformation is distributed over a wide area (Figure 4.7c-d), and *discrete* or *non-continuum models* are where undeformed blocks are bound by faults

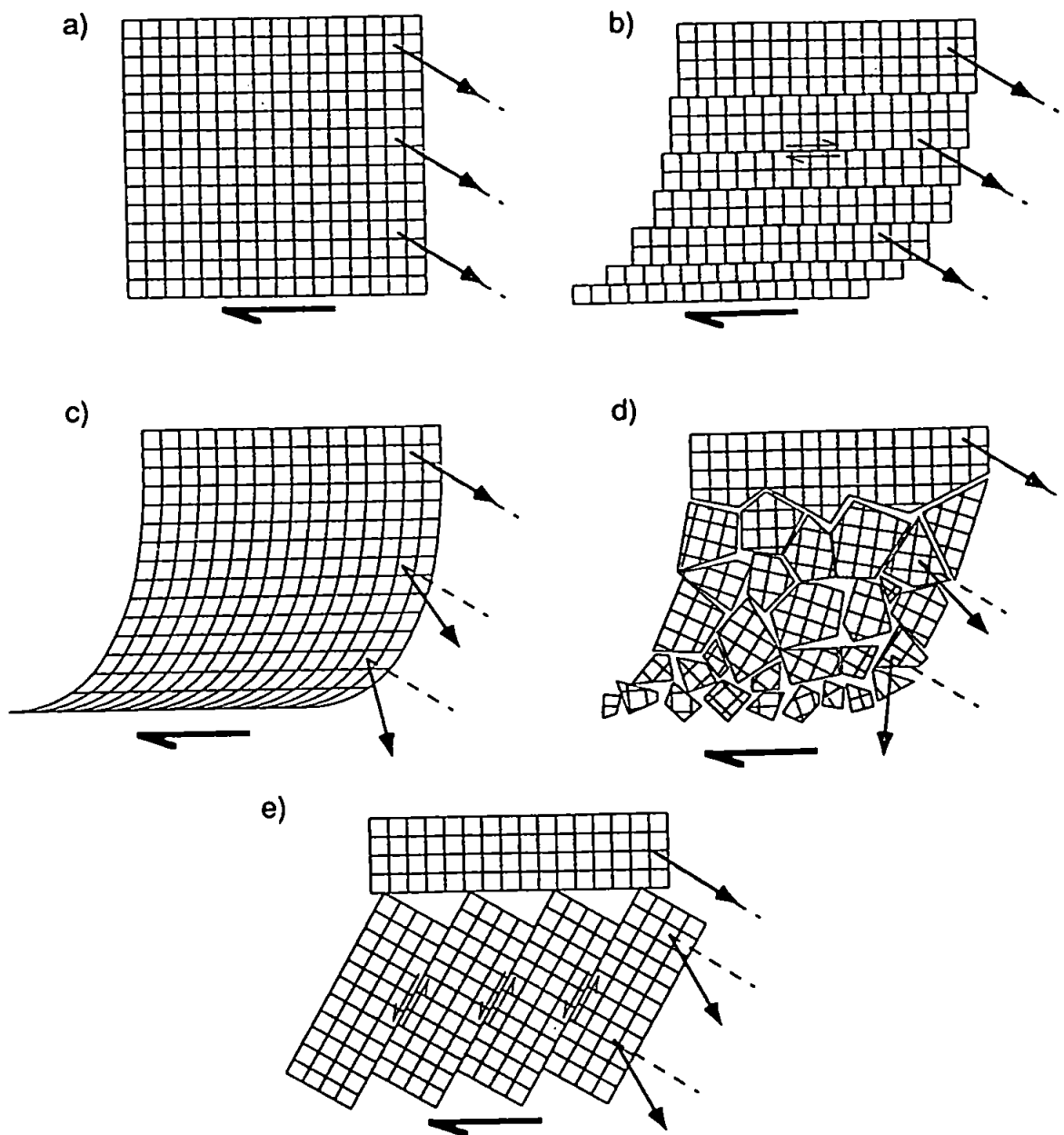


Figure 4.7. General models for accommodating strike-slip deformation (from Nelson and Jones, 1987, figure 6). Dashed lines show declination of unrotated palaeomagnetic directions within each region, and solid arrows show rotated direction. a) Undeformed block. b) Deformation accommodated on parallel faults, with no rotation of palaeomagnetic direction. c) Pervasive continuum deformation, the amount of rotation increases with proximity to the main fault. d) Small-block model. The amount of rotation generally increases with proximity to the deforming zone. e) *In situ* rigid block rotation model. Rotations are driven by motion on bounding faults. Rotation is constant within the deforming blocks and within the domain. Stippled area shows affect of rotation on a marker horizon.

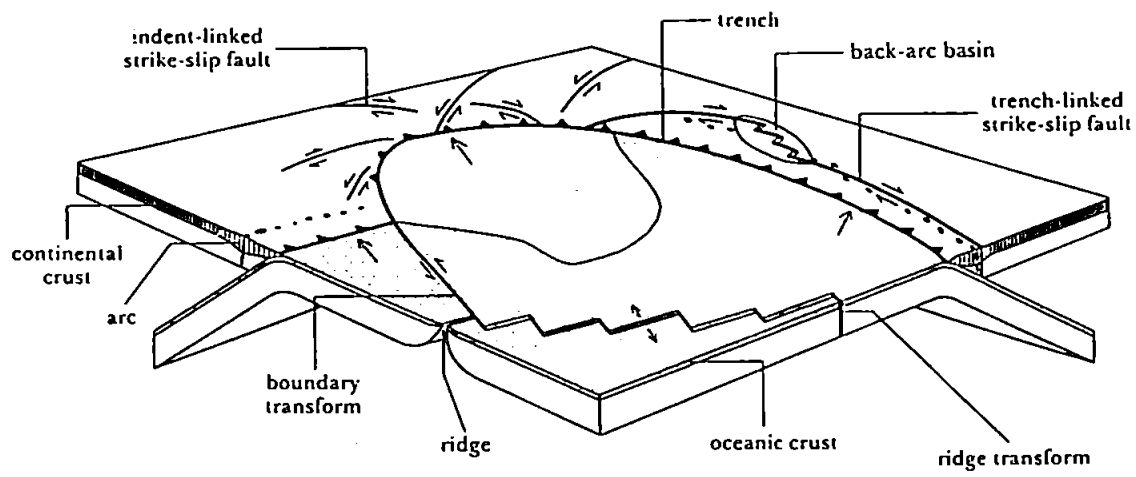


Figure 4.8. The major classes of strike-slip faults in their plate tectonic setting (from Woodcock, 1986, figure 6).

(Figure 4.7e). In reality, these two end members are theoretical ideals and most crustal deformation is the result of a combination of the two (King *et al.*, 1994). The most important difference between the mechanisms in term of classifying the models is the driving force for the rotations (see section 4.3.3). In continuum models the rotation of passive, 'floating' blocks occurs in response to deformation in an underlying medium, but in discrete models the rotation is driven by fault motion at the edges of the blocks (Nelson and Jones, 1987).

In continuum rotation models (Nelson and Jones, 1987; King *et al.*, 1994; Sonder *et al.*, 1994), the rotating blocks are significantly smaller than the size of the deforming zone and shear is distributed across the shear zone with no major through-going faults (Figure 4.7c). The most extreme model of this type is *pervasive continuum deformation*, in which the deformation is accommodated by crystalline plasticity and diffusive mass transfer, usually developing mylonitic fabrics. As stated above, in continuum models, the rotation occurs passively in response to motion of an underlying medium which may itself be continuous (McKenzie and Jackson, 1983) or brittle (King *et al.*, 1994). Pervasive continuous deformation can only occur if there is sufficient heat source for the processes of crystalline plasticity and diffusive mass transfer to occur. In continuous deformation models, palaeomagnetic vectors will be rotated and the amount of rotation will decrease away from the main fault.

In discrete models the deformation is taken up on rigid crustal blocks, the length of which is comparable to the width of the deforming zone (Figure 4.7e). The rotation and deformation occurs in response to shear applied along the edges of the blocks by strike-slip faults. All blocks and block-bounding faults within the same fault domain will rotate by the same amount and in the same direction, although if the strike-slip faults form two domains, the sense of rotation will be opposite within each domain (Ron *et al.*, 1984). The terminology used in previously published models has been inconsistent and Figure 4.9

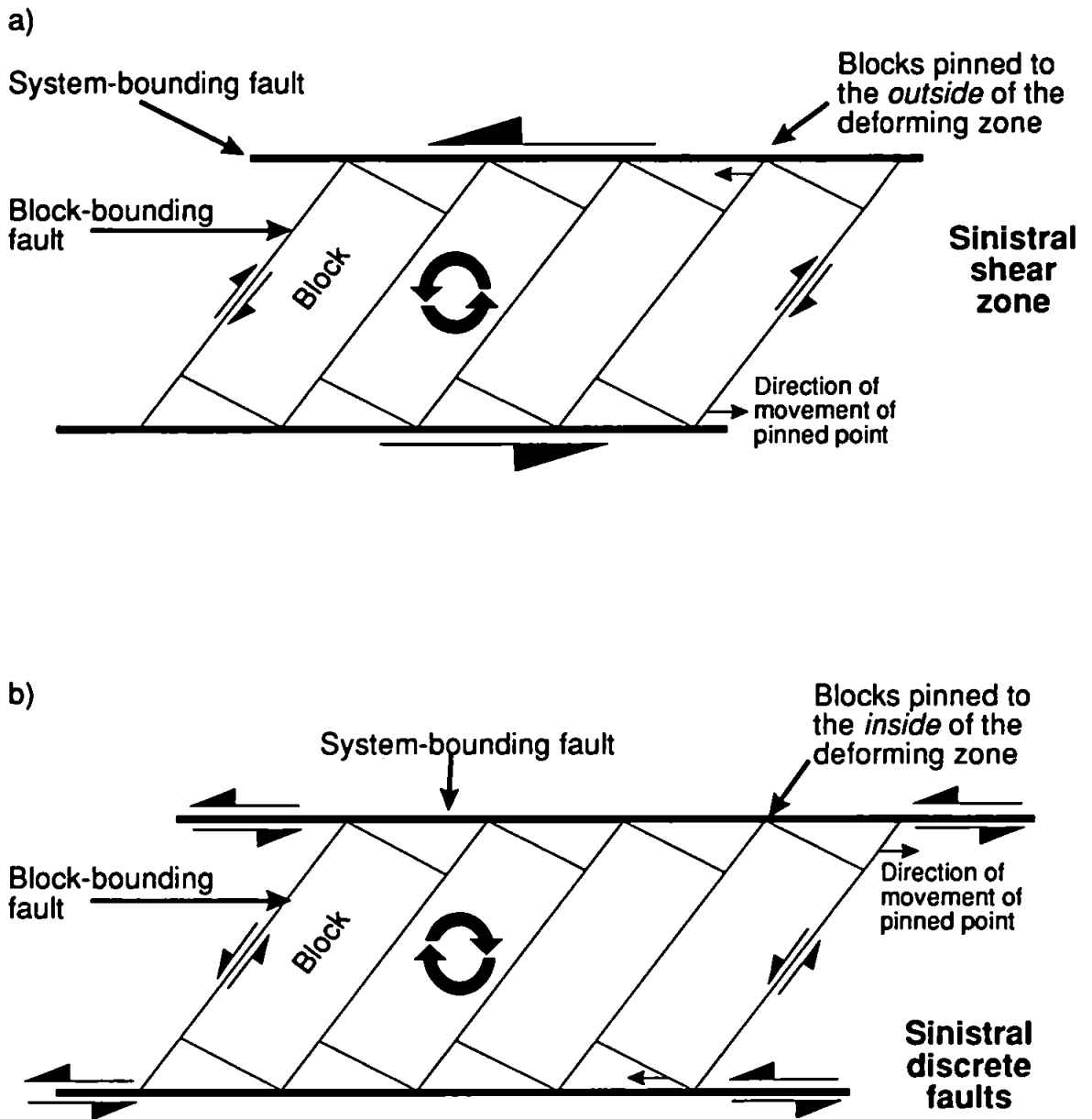


Figure 4.9. a) Anticlockwise rotation generated in a sinistral shear zone with dextral block-bounding faults. The blocks are 'pinned' to the outside of the deformation zone. b) Clockwise rotation generated by sinistral shear on discrete system-bounding faults with sinistral block-bounding faults. The blocks are 'pinned' to the inside of the deforming and therefore the faults. Opposite senses of rotation can therefore be explained in terms of the detailed behaviour of apparently identical faults. The terminology used in these diagrams is that used in the rest of this thesis in reference to small-scale *in situ* rotation models.

shows the terminology used in the rest of this thesis. An area of rotating rock is here referred to as a *block*, equivalent to the *slat* of McKenzie and Jackson (1986), and the *domino* of Ron *et al.* (1984) and Forsythe and Chisholm (1994). The faults between the blocks are *block-bounding faults*, equivalent to the *cross faults* of McKenzie and Jackson (1986) and the *system-bounding faults* are the large-scale margin parallel strike-slip faults that define the deforming zone. In this environment, the *system-bounding faults* are likely to be crustal scale strike-slip faults.

A common assumption in many published rotation models is that rotation will be clockwise in regions of net dextral shear and anticlockwise in net sinistral shear (Nelson and Jones, 1987; Scanlan and Turner, 1992; Riley *et al.*, 1993; Sonder *et al.*, 1994). But as is demonstrated in Figure 4.9, this is not necessarily the case. The sense of fault motion on the block-bounding faults, and therefore controlling the rotation need not necessarily be the same as the motion sense on the system-bounding faults (Mandl, 1987). The controlling factors are; the initial orientation of the block-bounding faults with respect to the system-bounding faults, and whether the system-bounding faults are acting as the margins of a wide shear zone (Figure 4.9a) or discrete faults either side of the rotating blocks (Figure 4.9b). If the block-bounding faults have the same sense of motion to discrete system-bounding faults (Figure 4.9b), the blocks can rotate in the direction opposite to that suggested by the bulk shear of the deformation zone. Sinistral block-bounding faults can therefore cause clockwise rotations even in zones of apparently bulk sinistral shear (Figure 4.9b; also Ron *et al.*, 1984; Shreurs, 1994).

Another class of model which lies between these two end members is the *small block* model (McKenzie and Jackson, 1983; Lamb, 1987; Nelson and Jones, 1987), a mixture of both continuum and discrete rotations (Figure 4.7d). This rotation model has been developed from experimental studies attempting to replicate behaviour of a deforming crust over large areas. In these experiments, the upper crust is regarded as being broken

into small rigid blocks that are much smaller than the width of the deforming zone. These are considered to be 'floating' in a highly viscous fluid which represents the intensely deformed continuum material below. Lamb (1987) showed that in this model the pattern of rotations produced can be very complex and rotations with variable rates and directions were observed between adjacent blocks. In addition, some blocks can rotate in the opposite direction to that applied by the bulk shear. Lamb (1987) also notes that it is difficult to define and quantify all of the variables involved in the rotation, although the interactions between the blocks and changes in their aspect ratios had a major effect on the pattern produced. Although developed as an experimental model, this type of deformation rotation has been suggested for some strike-slip fault systems in the Western Cordillera of the USA (Nelson and Jones, 1987; Sonder *et al.*, 1994).

4.3.3 Continuum versus discrete deformation

The division of models into continuum or discrete is based on the driving mechanism for the rotation rather than the type of deformation produced, this is because there has been disagreement in the literature about what constitutes continuous deformation (King *et al.*, 1994). The main cause of disagreement and confusion has been the scale of observation. At the smallest scale, crystals can deform by crystalline plasticity or diffusive mass transfer which are ductile (Garfunkel, 1989). At larger scales, all deformation is discrete and brittle but rotations may be too small to detect and the deformation appears continuous (Cobbold and Gapais, 1986; Rutter, 1986). This problem has led to the upper limit of continuous deformation being defined as the *continuous approximation*, where the number of faults increases indefinitely and their spacing tends towards zero (Garfunkel, 1989). If the rock is considered to be deforming as a ductile medium, there must be no tendency for the strain to be localised into bands and form discrete faults (Rutter, 1986). If this is the case, the deformation is truly pervasive and there are no blocks as the rock will be mylonitic.

At the largest scale, when averaged over long time periods, the Earth's surface can be treated as if it were a thin viscous sheet which deforms in a continuous manner (England and McKenzie, 1982; McKenzie and Jackson, 1983; Sonder and England, 1986). When viewed in more detail, the number of brittle structures observed increases, but it is possible that the brittle structures will be below the threshold of field observation, so the deformation is considered as continuous in terms of crustal scale tectonic models (Nelson and Jones, 1987). In the past it was considered that for continuous deformation to occur, the rock must be heated to a state where it can behave in a ductile way (Nelson and Jones, 1987), but this is not necessarily the case. For example, cataclastic flow is ductile and can occur at low temperatures, hence depth and temperature of deformation are not necessarily controls on whether deformation is continuous or discrete and may not be as important as the scale of observation employed.

4.3.4 Discrete models of *in situ* vertical axis rotation

All of the *in situ* vertical axis rotation models that have previously been applied to the Andean margin are discrete. The presence of obvious fault systems in the margin suggests that if rotations are present and the result of *in situ* vertical axis rotation, then a discrete model is more applicable than continuous deformation one. In this section discrete models which have been applied to the Andean margin, or which may be applicable, are discussed.

Ball-bearing rotation. Beck (1976) proposed a model for the North American Coastal Cordillera where circular blocks (hence the name ball-bearing model) are translated and rotated by motion on parallel strike-slip faults (Figure 4.10a). Beck (1988) modified this model in applying it to South America by removing the component of latitudinal block translation, allowing the blocks to rotate *in situ*. The sense of rotation is controlled by the plate convergence direction which comprises a trench-normal component, responsible for

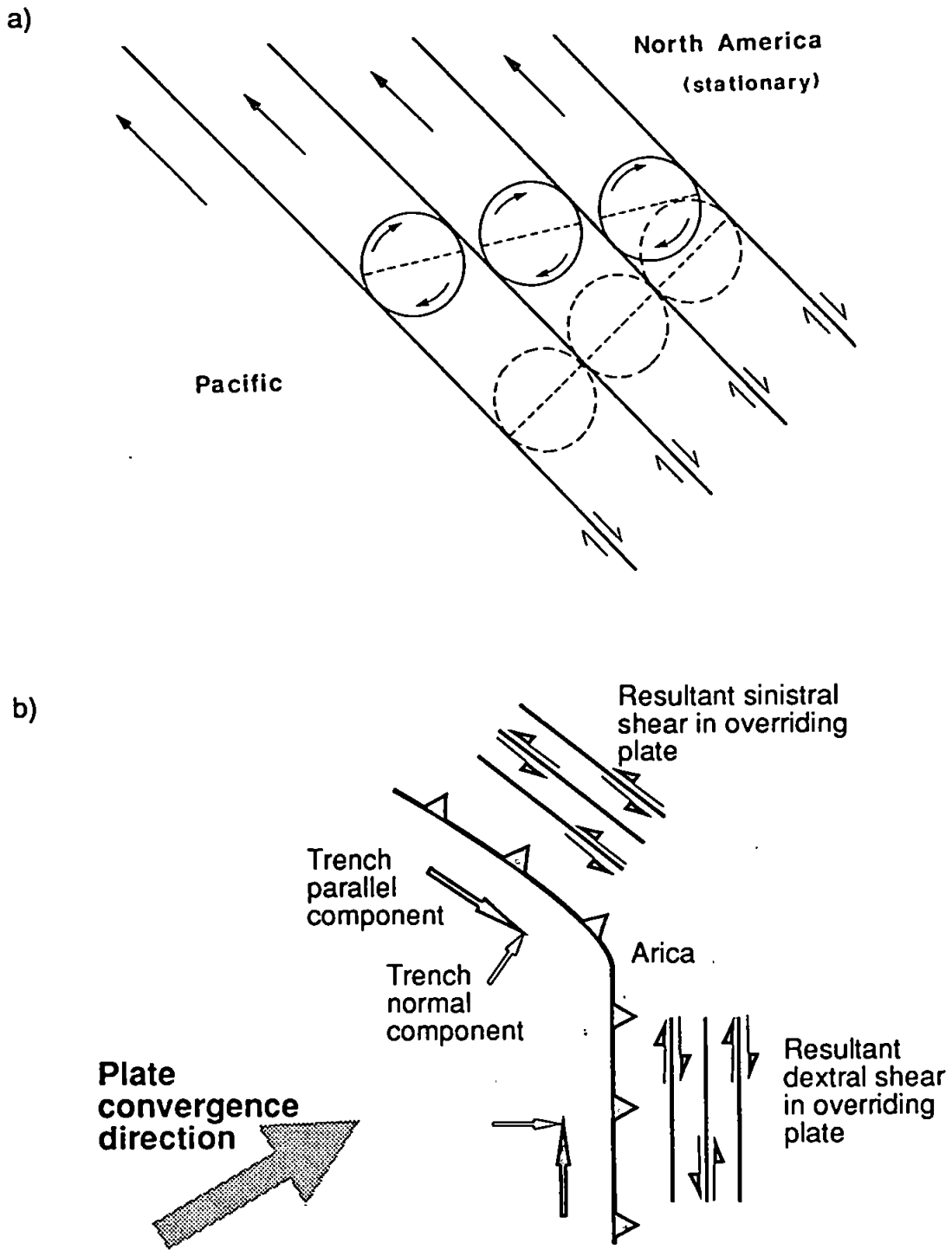


Figure 4.10 a) Ball-bearing model (from Beck, 1976, figure 4). Circular blocks rotate clockwise in response to dextral shear. Heavy lines represent strike-slip faults. b) In South America, oblique NE directed plate convergence is decomposed into a trench normal component, responsible for pure shear, and a trench parallel component which causes dextral shear in Chile and sinistral shear in Peru. (Modified from Beck, 1988, figure 7).

pure shear, and a trench-parallel component which drives the rotations (Figure 4.10b). Motion is controlled by the margin-parallel strike-slip faults only, and the blocks do not have bounding faults, therefore the block size is not defined within the fault system. To generate the clockwise rotations reported by Beck (1988) in the Chilean part of the Andean margin, the model requires a northward directed trench-parallel component in northern Chile to generate distributed dextral shear and clockwise rotations. The model is simplistic in that it regards the margin-parallel faults as planar features with only simple shear motion, the model cannot therefore account for the extensional and compressional structures which are commonly seen in strike-slip fault systems.

Slat, domino and bookshelf models. Most of the discrete models take the form shown in Figure 4.9, a set of parallel block-bounding faults between two system-bounding faults. When the rotation occurs, all of the blocks rotate together in the horizontal plane, hence there is no dip-slip motion on the block-bounding faults and the deformation zone extends parallel to the system-bounding faults. The rigid rotating blocks therefore resemble a set of rotating *dominoes* (e.g., Forsythe and Chisholm, 1994) or *slats* (e.g., McKenzie and Jackson, 1983; 1986). This type of rotation has also been called the *bookshelf* rotation model (Mandl, 1987) and has been demonstrated in both geological examples (e.g., Nicholson *et al.*, 1986; Luyendyk, 1989; Vickery and Lamb, 1995) and in experimental models (Shreurs, 1994). The model of Forsythe and Chisholm (1994) is based on work carried out in the Atacama Fault System in northern Chile, approximately 3° of latitude north of the study area covered in this thesis. This model is therefore discussed in more detail in Chapter 7.

McKenzie and Jackson (1983; 1986) propose a model which is similar to the domino model, but differs in that there is no movement of material and therefore no extension or contraction parallel to the system-bounding faults. Instead, the surface area is only affected by motion across the deformation zone accommodated on the block-bounding

faults (Figure 4.11). The slip on the block-bounding faults is therefore oblique and approximately normal to the system-bounding faults. The model as presented was for a transtensional regime, in which there is a component of extensional dip-slip motion on the block-bounding faults to preserve the block shape and avoid sphenochasms. The blocks therefore rotate around both vertical and horizontal axis. The rotation of the blocks is driven by the relative movement of the system-bounding faults, with the blocks and their bounding faults rotating passively during deformation. In this model, the deformation zone is treated as a shear zone and block-bounding faults have the opposite sense of displacement to the shear zone, dextral shear therefore generates sinistral block-bounding faults and clockwise rotation.

Domain rotation. Theoretical models of block rotation within *fault domains* have been developed by Ron *et al.* (1984) and Garfunkel (1989). These models consider rotation of faults within domains in an overall strike-slip fault system, but the system-bounding faults are not considered. One domain has faults with sinistral displacement and clockwise rotation, while the other domain has dextral faults and anticlockwise rotation (Figure 4.12). All of the deformation within both domains is by simple shear, and as there is no dip-slip motion on the block-bounding faults, the domain dimensions change during rotation to preserve area. Ron *et al.* (1984) carried out detailed structural studies as well as palaeomagnetic sampling and show that, in ideal circumstances, the amount of rotation recorded by the palaeomagnetic technique can be predicted from knowing the amount of displacement on the block-bounding faults and the size of the rotating blocks. The main criticism of this model is the lack of consideration of the system-bounding faults and hence does not explain the driving force for the rotation within the domain. In addition, the model implies that the region has pre-formed fault domains before the rotation, while in reality it is more likely that the fault development and rotation will be synchronous.

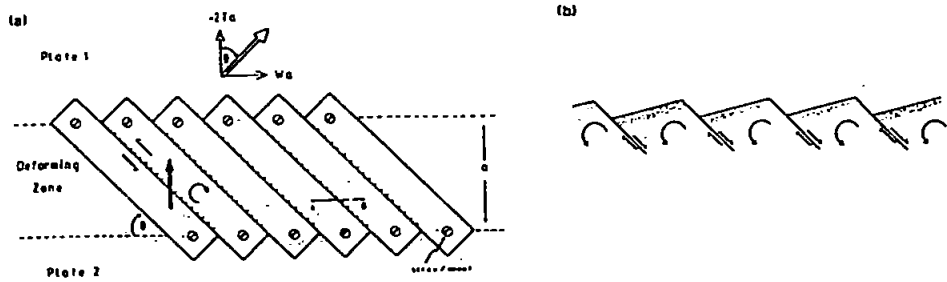


Figure 4.11. The slat model (from McKenzie and Jackson, 1989, figure 3). a) Plan view. b) In section. The large white arrow shows the relative motion across the deforming zone. The model requires the zone to take up some normal motion, which is achieved by oblique slip on the block bounding faults in the direction of the black arrow. The blocks will therefore rotate around both vertical and horizontal axes.

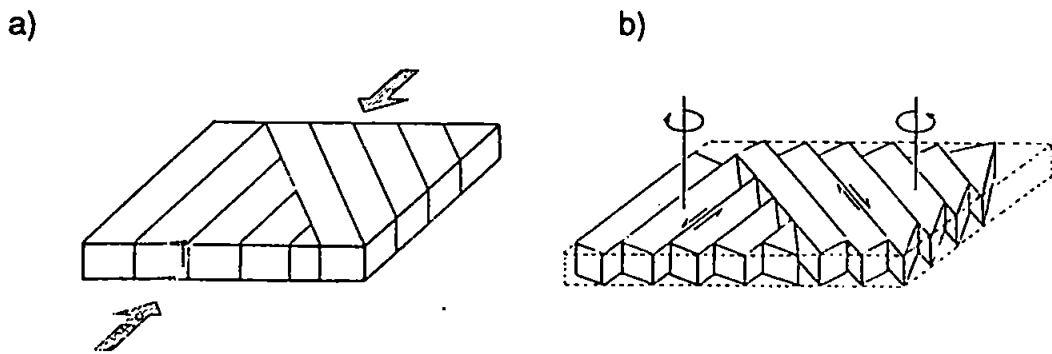


Figure 4.12. The two domain model (from Ron *et al.*, 1984, figure 1). (a) The initial fault geometry. (b) After deformation. Blocks bounded by sinistral faults rotate clockwise, those bounded by dextral faults rotate anticlockwise.

Problems with discrete models. All of the discrete models discussed in this section treat the rotating blocks as rigid or *hard*, indeed, the rotation calculations of Ron *et al.* (1984) require that the deforming blocks are rigid. Rotating rigid blocks causes a space problem as the blocks will form triangular 'holes' or 'sphenochasms' between the block and the system-bounding fault or the domain boundaries (Figure 4.12; Sylvester, 1988). If the blocks are indeed rigid, these holes may become sedimentary basins which will fill and subside with increased rotation (Luyendyk *et al.*, 1980). Alternatively the spaces may be filled by igneous plutons, again increasing in size as rotation occurs (Tikoff and Teyssier, 1992).

An alternative approach which is more geologically plausible is to consider the rotating block as being deformable, or *soft*, instead of rigid. In this case, the block-bounding faults will die out as they approach the system-bounding fault (Dibblee, 1977) and the block will deform internally as it rotates (Figure 4.13). This internal deformation may be achieved by a number of methods (Figure 4.14), the first mechanism works by having deformable edges to the block, in this case most of the deformation is concentrated into small areas at the corners of the block. The stress in the corners can be accommodated by zones of extension and contraction (Figure 4.14a) or by small conjugate strike-slip fault sets at the contacts between the blocks and the system-bounding faults or domain boundaries (Figure 4.14b). The second mechanism is to treat the block as completely deformable, in this case the deformation will be distributed throughout the block accommodated on minor faults or cleavage (Figure 4.14c, d). Dip-slip motion on the block-bounding faults themselves provides another mechanism for block deformation, in this case dip-slip motion allows the block to fill the gaps as it rotates (McKenzie and Jackson, 1986; Shreurs, 1994). It is likely that any deformation of the blocks or the associated faults will be a combination of the above mechanism and these will, in part, be controlled by variations in lithology and pre-existing structures.

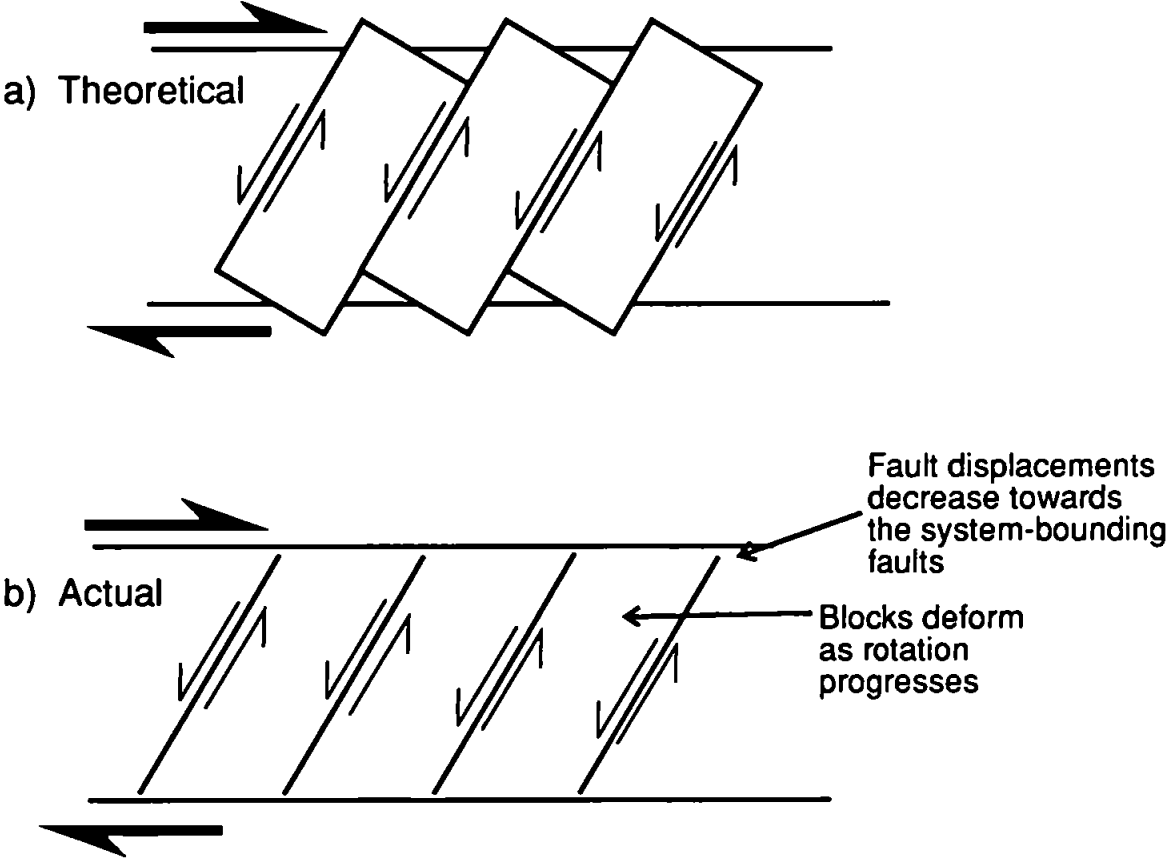


Figure 4.13. The 'soft' block model, redrawn from Dibblee (1977). The blocks deform and the faults die out towards the system-bounding faults. This means that there is no space problem at the block edges.

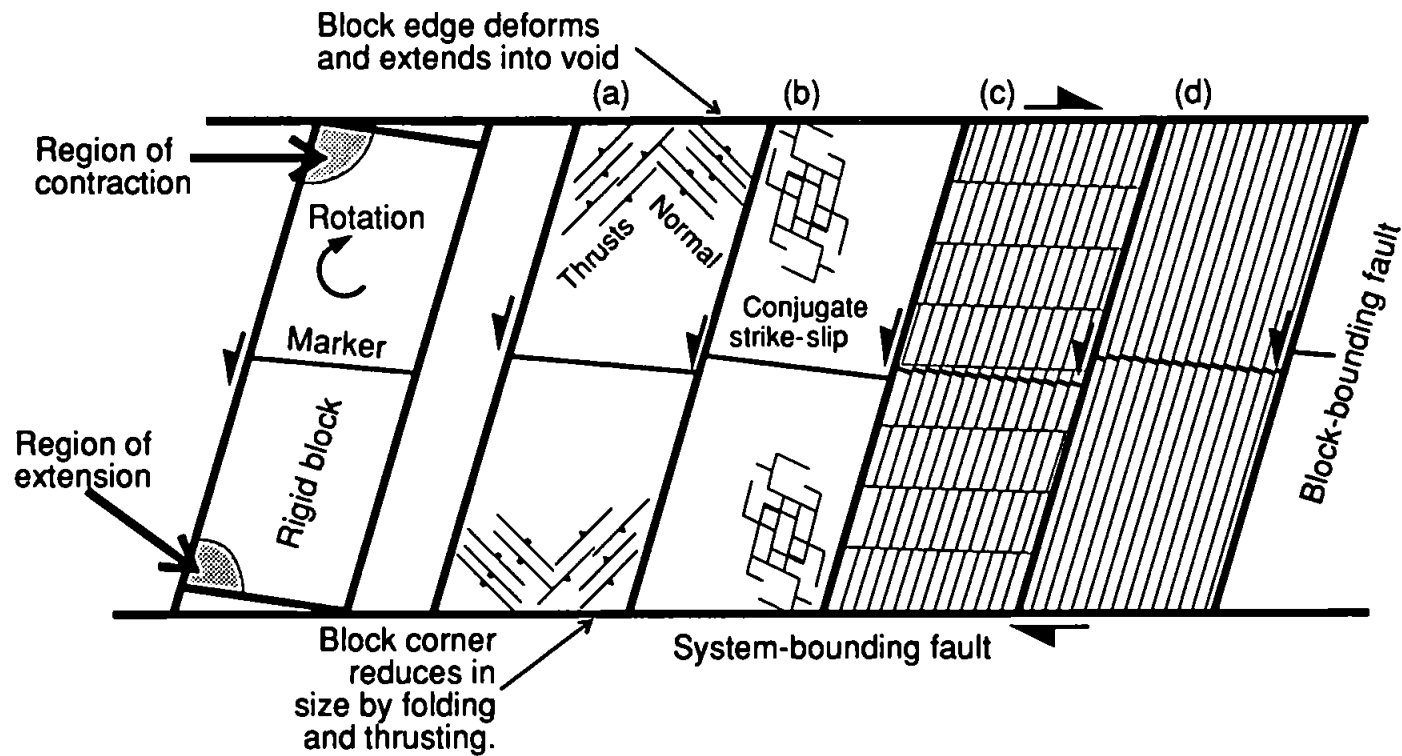


Figure 4.14. Solving the space problem caused by rigid blocks. a) By allowing the edges of the block to deform by formation of extensional and compressional structures. b) Developing strike-slip faults in the corners of the blocks allowing them to deform. c) and d) Pervasive deformation throughout the whole block accommodated on cleavage, small faults etc. (Modified from Peacock *et al.*, in prep.)

4.3.5 *In situ* rotation on thrust sheets

Another mechanism by which *in situ* rotation can occur is on thrust sheets (MacDonald, 1980; Hartley *et al.*, 1992a; Vickery and Lamb, 1995). As shortening increases across a deforming zone, the thrust sheets will be initiated and propagate. If the amount of slip is variable along the thrust plane, or if the fault becomes fixed (pinned) at one end, the sheet will rotate. Hartley *et al.* (1992a) suggest that this type of model may explain some of the rotations they identified in northern Chile, where palaeomagnetic rotations can be linked to thrust sheets operating in a thin-skinned tectonic setting.

4.4 Mechanisms and models for large-scale *in situ* vertical axis rotation

In contrast to the oroclinal bending/differential shortening models which require bending of the Andean margin, and the small-scale *in situ* block rotation models in which rotation is related to motion on strike-slip faults, some models have been presented which relate *in situ* rotation with large-scale tectonic processes.

Hartley *et al.* (1988) suggest that rotation can be caused by extension in the forearc as a result of a *retreating subduction boundary* (Royden, 1993). The extension is a result of transtension generated by a combination of oblique convergence and a reduction in plate convergence rate (Figure 4.15). The reduced plate convergence rate causes *subduction roll-back*. This roll-back imparts extensional stresses in the over-riding continental crust so the forearc extends. In the model, the forearc extends and rotates away from a trench-linked strike-slip fault. The main problem with the model of Hartley *et al.* (1988) is that the model can only account for rotations within the forearc and not inboard of the trench-linked strike-slip fault.

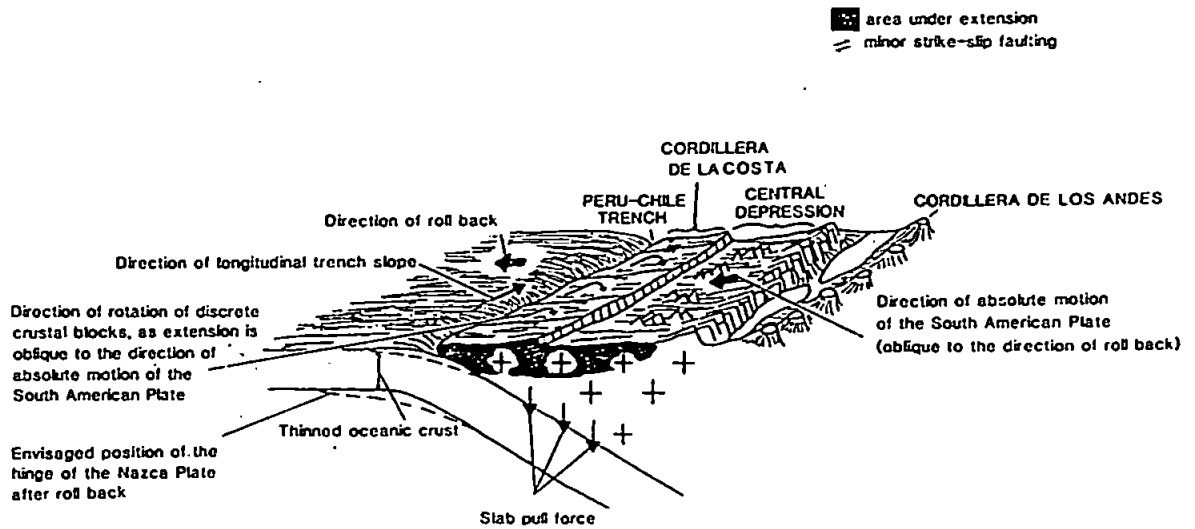


Figure 4.15. Transtension model (from Hartley *et al.*, 1988, figure 5b) for the Andean forearc in northern Chile. The extension of the South American plate is oblique to its direction of absolute motion. This causes rotation of the forearc.

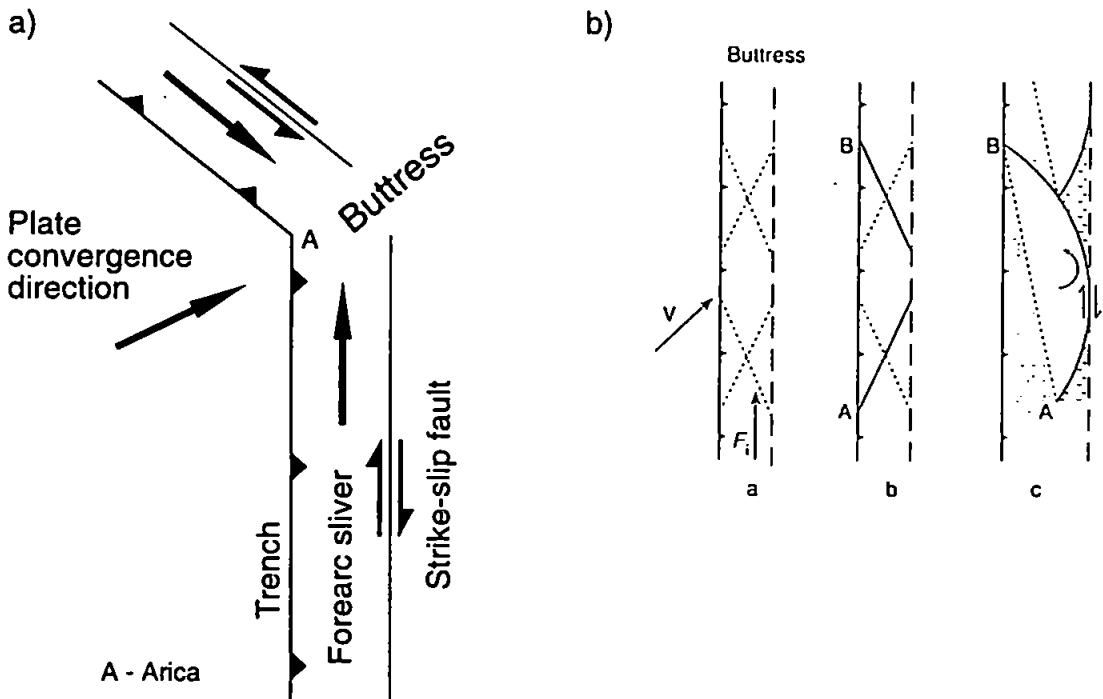


Figure 4.16. a) The plate convergence vector is oblique to the forearc both north and south of the deflection. Although both are detached and free to move they are restricted by a buttress at Arica. b) Overcoming the buttress by extension across the sliver. a. Sliver is pushed northward by a force F_1 by oblique subduction, V , but is prevented from moving by a buttress. This results in conjugate fractures (dotted lines) in the forearc, which is bounded by the trench and a major strike-slip fault (dashed line). b. Half-lens shaped blocks develop in the forearc. c. Blocks move northwards by rotating and overlapping and the sliver widens. Dotted pattern and wiggly pattern indicate areas of extension and contraction respectively. (Taken from Beck *et al.*, 1993, figure 8).

Beck (1986) and Beck *et al.* (1993) propose that large-scale rotation could be the result of restricting margin parallel motion of the forearc sliver by *buttressing*. Beck *et al.* (1993) used the Liquiñe-Ofqui fault zone in southern Chile as an example of this type of rotation. Although Beck *et al.* (1993) do not suggest that this model can explain the rotations around the Arica Deflection, they use the deflection as an example of a major tectonic buttress. If the model were to be applied to the Arica Deflection, this would require NE directed plate motion along the edge of the Chilean margin to develop a crustal scale dextral strike-slip fault and a detached forearc sliver (Figure 4.16a). The northward directed simple shear component will then drive the forearc sliver northwards along the strike-slip fault (Figure 4.16a). The opposite direction of movement will occur on a sinistral strike-slip fault in Peru. The movement will be restricted by a buttressing effect at the Arica Bend due to collision of the two forearcs. To continue strike-slip motion, and overcome the buttress, there must be either thickening of the crust, or extension of the forearc normal to the slip direction. This extension, suggest Beck *et al.* (1993), is achieved by breaking the forearc into arcuate blocks which overlap and rotate (Figure 4.16b). Beck *et al.* (1993) suggest that arcuate fault systems, as are often observed in continental settings, may be due to this type of rotation.

This buttressing model is very simplistic in its approach to the behaviour of fault zones and crustal blocks. The model suggests that the rotation of curved blocks bounded by faults would lead to the development of curved fault systems, this is not really the case. As is demonstrated by their own model, the major fault zone (dotted line, Figure 4.16b) still has a straight N-S orientation, and the block-bounding faults behave as subsidiary faults within a wider fault system. The major fault zone is not therefore curved. As with the model of Hartley *et al.* (1988), this model cannot explain rotation inboard of the trench-linked strike-slip fault.

4.5 Conclusions

In this chapter a number of models operating at a variety of scales and with a variety of rotation mechanisms have been discussed. The diversity of the models demonstrates the complex way in which fault systems and other tectonic processes operate. In the next two chapters results from this study are presented. The applicability of the models discussed here to both the new data in this thesis and the general pattern of rotation in the Andean margin is considered in Chapter 7.

Chapter 5

THE COASTAL CORDILLERA AND THE ATACAMA FAULT SYSTEM

5.1 Introduction

The first sampling region is in the Coastal Cordillera of northern Chile between 25°S-27°S, and principally to the west of the Atacama Fault Zone (AFZ) at approximately 70°W (Figure 5.1). This area lies within the Coastal Cordillera and the Jurassic-Early Cretaceous arc, as discussed in Chapter 1. The major structures are the (AFZ) and a set of subsidiary faults dominantly to the west of the AFZ. The aim of the study was to identify and quantify any rotation in this part of the Coastal Cordillera and to try and relate this to the fault pattern observed. To this end, units were targeted across the area, between the coast and the Atacama Fault Zone, and also from the east of the fault zone, hopefully to constrain the rotation should the AFZ prove to be the bounding fault to the system. Samples were collected from the La Negra Formation which had been shown previously to provide reliable palaeomagnetic results elsewhere (Hartley *et al.*, 1988), and a series of dyke swarms which intrude the magmatic arc plutons. The dykes were collected from the Vetado, Flamenco, Las Animas, Las Tazas plutons west of the AFZ, and the Remolino pluton just to the east of the main strands of the AFZ. As will be discussed, the dyke swarms are spatially and temporally restricted to their host pluton. They are therefore considered separately in the palaeomagnetic analysis.

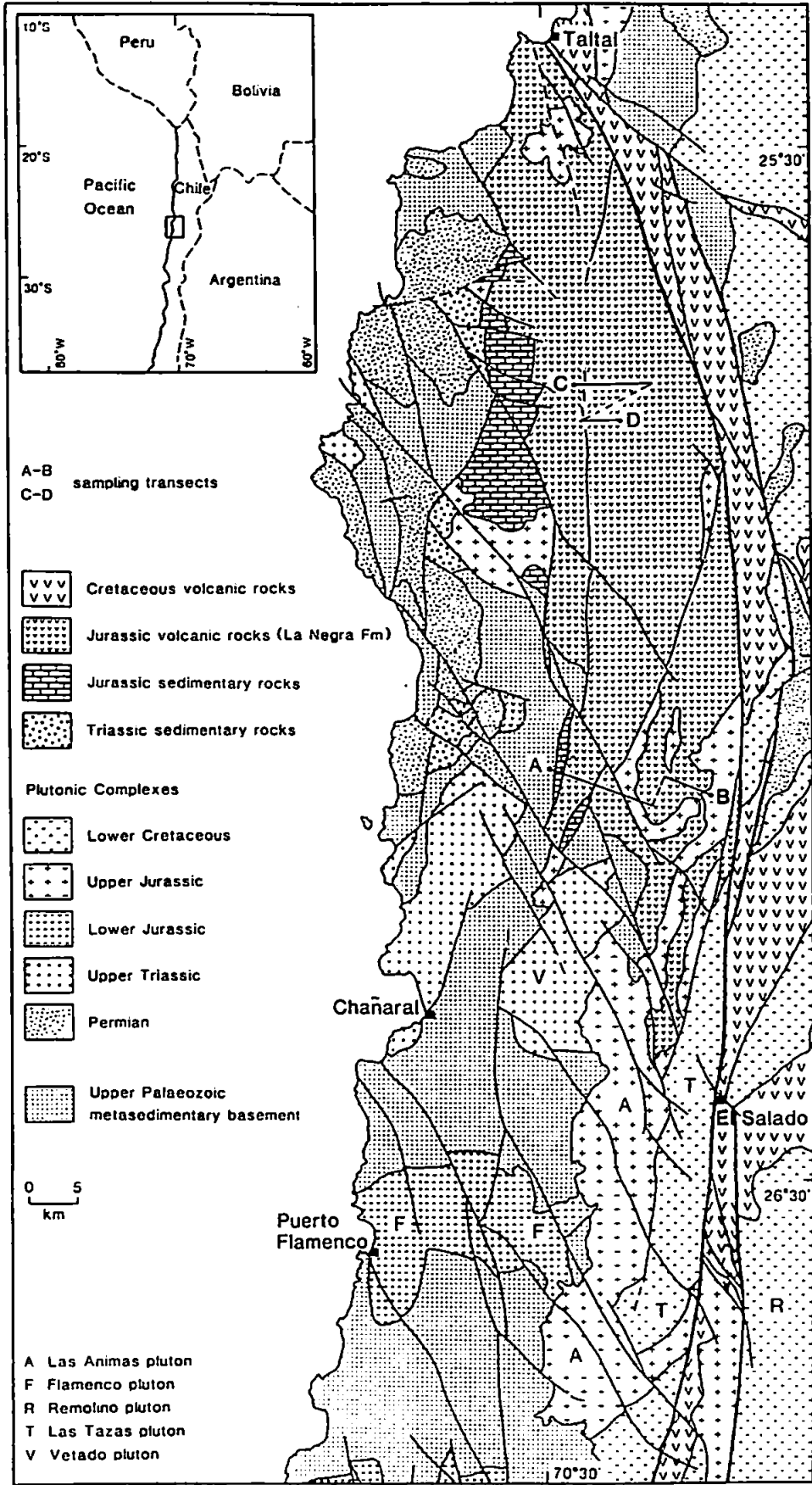


Figure 5.1. Geological map of the study area in the Coastal Cordillera. (Map prepared by Stella Bignold, Kingston University).

5.2 The geology of the Coastal Cordillera and the Atacama Fault System

5.2.1 Geology and petrology

A simplified geological map of the area is shown in Figure 5.1. The oldest lithology exposed in this part of the Coastal Cordillera is the late Palaeozoic basement comprising Carboniferous meta-sediments intruded by the Permian to early Triassic magmatic arc plutons. Intruded into, and lying stratigraphically above this basement are the rocks of what is usually termed the Jurassic-Early Cretaceous magmatic arc. The oldest sediments in this part of the Coastal Cordillera are, however, Late Triassic in age and are interpreted as having been deposited in an active rift basin. This suggests that the first stages of arc development began prior to the earlier Jurassic in this area. The stratigraphy and the ages of fault motions for the area are shown in Figure 5.2.

In the northern part of the study area, the Palaeozoic basement is overlain by sedimentary and volcanic sequences (Naranjo, 1978; Naranjo and Puig, 1984; Brown *et al.*, 1993; Grocott *et al.*, 1994; Dallmeyer *et al.*, 1996). At the base of the sequence, and separated from the basement by a major extensional fault system, are sediments of Triassic age. These Triassic rocks are known to outcrop in several places in northern Chile (Bell and Suárez, 1991) and the dominant unit in the Coastal Cordillera is the Cifuncho Formation (Bell and Suárez, 1991; Suárez and Bell, 1994). This formation is characterised by laterally variable conglomerates, sandstones and mudstones with some intercalated shallow marine limestones. Bell and Suárez (1991) suggest that the formation was deposited in a coastal environment, possible in a rift basin setting controlled by an extensional fault at the base of the formation. Lying conformably above the Cifuncho Formation is the Early Jurassic (Hettangian-Sinemurian) limestone sequence of the Pan de Azúcar Formation (Naranjo, 1978). These are highly fossiliferous shallow marine limestones with minor intercalated fine sandstones. In the north of the sampling region the

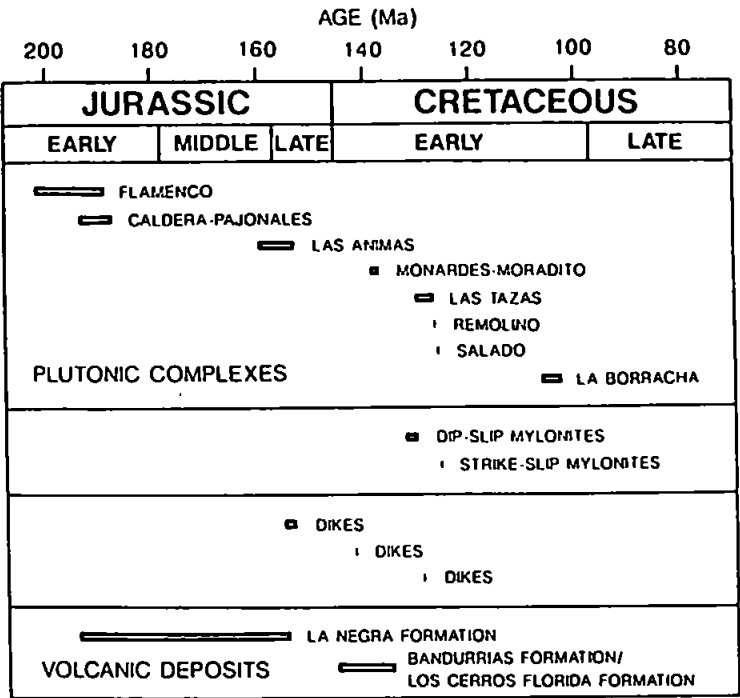


Figure 5.2. The timing of Jurassic and Cretaceous events in the Coastal Cordillera of northern Chile (taken from Dallmeyer *et al.*, 1996, figure 9). The Vetado pluton is probably Late Triassic in age, and is therefore not shown on this diagram. Diagram uses the timescale of Harland *et al.*, 1989.

Pan de Azúcar Formation is overlain by the coarse conglomerate of the Posada de los Hidalgo Formation, also dated as Sinemurian (Naranjo and Puig, 1984). In the study area however, the Posada de los Hidalgo Formation is absent and the Pan de Azúcar Formation is apparently conformably overlain by the La Negra Formation (Garcia, 1967), the main volcanic sequence exposed in the region.

The La Negra Formation is dated as Early Sinemurian to Kimmeridgian on palaeontological evidence (Garcia, 1967; Naranjo, 1978). The formation comprises a sequence of dominantly basaltic-andesitic lavas with minor intercalated volcanoclastic sediments and breccias. Thin section analysis (Appendix 1) has also identified rhyolitic lavas and devitrified ignimbrites within the sequence. The depositional setting for the formation is marginal or shallow marine in the west to subaerial in the east (Naranjo, 1978), however, as the formation dips mainly eastward this may be a temporal change due to younging representing emergence, rather than a strictly spatial change. The thickness of the formation is estimated to be 10 km (Garcia, 1967), however, the formation has been affected by extensional faulting and this may have exaggerated the thickness.

Based on the chemical composition of the rocks, Rogers and Hawkesworth (1989) suggested that the La Negra Formation represented ensialic back-arc basin deposits. Lucassen and Franz (1994) note however that sediments comprise only a small part of what is otherwise a totally subaerially deposited volcanic succession, this indicates that deposition of the lavas and subsidence of the crust were well balanced. This led Lucassen and Franz (1994) to suggest that there was insufficient extension to develop a back-arc basin.

As suggested above, the La Negra and underlying formations have been tilted by east-side-down fault bound blocks. In addition, evidence from the north-west of the sampling region suggests that these formations are also deformed by NW-SE trending, low

amplitude, very shallowly plunging open folds. Although not identified within the sampling region, the more widespread presence of these folds is suspected.

Lying to the east of the La Negra Formation and the Atacama Fault Zone is another sequence of intercalated volcanic and sedimentary rocks. This sequence has previously been sub-divided into three formations, the Bandurrias Formation (Mercado, 1978), the Los Cerros Florida Formation (Segerstrom, 1960; Naranjo, 1978), apart of the same volcanic sequence, but they are poorly dated and correlation between them is uncertain. The sequence is differentiated from the La Negra Formation by the presence of conspicuous shallow marine limestones, although the spatial and stratigraphic relations of the sequence to the La Negra Formation are uncertain. Fossils from these limestones suggests that the units may have been deposited over a long time period, possibly Middle Jurassic to Early Cretaceous (Naranjo, 1978). The depositional setting of the sequence is subaerial (dominantly) to shallow marine, there is also evidence of syn-sedimentary growth faulting. The sequence has been deformed and folded and vertical isoclinal fold have been identified to the east of the sampling region (Naranjo, 1978).

In the southern part of the sampling area, the sediments and volcanic rocks are absent and the Mesozoic magmatic arc is defined by Late Triassic to Early Cretaceous plutons which may have shared a common mantle source (e.g., Berg and Breitzkreuz, 1983; Brown, 1988; Lucassen and Franz, 1994). These Mesozoic arc plutons are separated from the Palaeozoic basement by a large extensional fault (Taylor *et al.*, in prep.). Some of the plutons have been dated using a number of methods (Berg and Breitzkreuz, 1983; Dallmeyer *et al.*, 1996) and, in most cases, these yield identical ages within error limits. Table 5.1 gives a summary of the ages obtained for the plutons within the sampling area, and those immediately to the east. The plutons, their associated mylonitic wall rocks, brittle fault systems and the sedimentary and volcanic sequences all show a systematic eastward

Pluton	Dating method	Age (Ma)	Reference
<i>Early Jurassic</i>			
Flamenco	U-Pb (Zircon)	190.1±1.9	1
	Rb-Sr (Biotite)	186.3±3.3	1
	Rb-Sr (Whole rock)	202±4	2
	⁴⁰ Ar/ ³⁹ Ar (Hornblende)	188.7±0.7	3
		198.2±0.6	3
<i>Late Jurassic</i>			
Las Animas	U-Pb (Zircon)	159.7±1.6	1
	Rb-Sr (Biotite)	157.6±2.6	1
	⁴⁰ Ar/ ³⁹ Ar (Hornblende)	153.0±0.8	3
	⁴⁰ Ar/ ³⁹ Ar (Muscovite)	~157	3
<i>Early Cretaceous</i>			
Las Tazas	U-Pb (Zircon)	130.3±1.3	1
	Rb-Sr (Biotite)	128.7±2.0	1
	⁴⁰ Ar/ ³⁹ Ar (Hornblende)	126.9±0.9	3
Remolino	U-Pb	126.8±1.3	1
	Rb-Sr (Biotite)	123.7±2.7	1
	⁴⁰ Ar/ ³⁹ Ar (Hornblende)	126.8±0.5	3
Salado	Rb-Sr (Whole rock)	126±2	2
La Borracha	Rb-Sr (Whole rock)	103±2	2
	⁴⁰ Ar/ ³⁹ Ar (Hornblende)	106.3±0.7	3
<i>Mylonite wall-rocks</i>			
Las Tazas	⁴⁰ Ar/ ³⁹ Ar (Hornblende)	130.2±0.6	3
		132.2±0.7	3
Remolino	⁴⁰ Ar/ ³⁹ Ar (Hornblende)	125.7±0.6	3

Table 5.1. Reported geochronological ages for plutons in the Mesozoic arc of the Coastal Cordillera. 1 = Berg and Breitzkreuz (1983); 2 = Brook *et al.* (1986), referenced in Dallmeyer *et al.* (1996); 3 = Dallmeyer *et al.* (1996).

younging within the arc (Figure 5.2; Table 5.1; Naranjo, 1978; Grocott *et al.*, 1994; Dallmeyer *et al.*, 1996).

The Middle Jurassic to Early Cretaceous plutons within the sampling area, namely Las Animas, Las Tazas and Remolino, are notably elongate in shape with their long axes parallel to the magmatic arc and the subduction margin. Geobarometry using the Al-in-hornblende method indicates shallow emplacement depths for the plutons. This, combined with the consistency of the different dating techniques, indicates that these plutons were emplaced at high crustal levels and cooled rapidly (Dallmeyer *et al.*, 1996). The Jurassic to Early Cretaceous plutons were emplaced at jogs within a developing extensional fault system linked to the Atacama Fault Zone (Grocott *et al.*, 1994). The consistency in the ages of the Las Tazas and Remolino plutons with the mylonites from their respective wall-rocks indicates coeval fault motion and intrusion. It is likely that the plutons were providing heat for the development of the mylonites at shallow crustal levels.

Each of the Late Triassic to Early Cretaceous plutons is intruded by a dense dyke swarm (Plate 5.1) which does not appear to extend far into the basement, or neighbouring plutons (Mercado, 1978). Dykes in four plutons were dated using the $^{40}\text{Ar}/^{39}\text{Ar}$ technique on whole rock samples (Dallmeyer *et al.*, 1996). The spatial and temporal relationships of the dykes with their host pluton suggest that they represent a final phase of emplacement of the pluton itself (Dallmeyer *et al.*, 1996). For example, dykes which intrude the Las Animas pluton have ages of *c.* 154 Ma, close to the age of the Las Animas pluton. One dyke from the Las Tazas pluton yields an age of *c.* 129 Ma, again within the 132-127 Ma spread of dates obtained from the host pluton (Table 5.1). The dykes in the Flamenco are dated as *c.* 154 Ma and, although they do not extend into the Las Animas pluton, were probably emplaced during the same intrusive phase. The dyke swarm in the Vetado pluton is truncated and structurally distinct from the Las Animas pluton, its age is therefore bracketed between pre-Late Jurassic (the age of the Las Animas pluton) and Late Triassic (the age of



Plate 5.1. Cross-cutting basalt-andesite dykes intruding the Vetado pluton.

intrusion of the Vetado pluton). It is possible that these dykes were feeders for the volcanic rocks of the La Negra Formation during the Middle Jurassic. Although there are no dates from dykes in the Remolino pluton, there is no reason to suggest that they too were not intruded soon after emplacement.

The petrology of the dykes from all of the swarms is very similar. Thin section analysis of 14 samples from dykes in Vetado, Las Animas, Las Tazas and Remolino plutons shows that they are dominantly fine-medium grained and of basic-intermediate composition (Appendix 1). Two dykes with dacitic composition were also identified, one in the Las Tazas and the other in the Remolino pluton. All of the dykes appear to have been emplaced with a near vertical attitude and they cross-cut at high angles. There seems to be no relationship between orientation and age defined by simple cross-cutting relationships. Structural analysis was also undertaken to assess whether the dykes have undergone any post-emplacement tilting, the results are discussed in Section 5.3.

All of the rock units studied for palaeomagnetic analysis from the Coastal Cordillera show varying degrees of low temperature alteration, particularly in proximity to faults. This alteration is characterised by epidote pseudomorph replacement of ferromagnesian minerals, sericitisation of feldspars and, in some cases, oxidation resulting in secondary haematization (Plate 5.2 and 5.3; see also Appendix 1). The cause of this alteration is not clear, as at least three contributing factors may be responsible. Firstly, deuteritic alteration, as a result of slow cooling in the presence of water, especially in the case of the volcanic rocks of the La Negra Formation, where the intercalated marine sedimentary horizons would have retained fluids and the subsequent extrusion of further lavas would have provided heat for the alteration. Deuteritic alteration may also have affected the dykes, particularly if the host plutons were still warm during dyke emplacement. The second type of alteration affecting some of these rocks may be the result of action by low temperature hydrothermal fluids, the presence of which is evidenced by the large amount of mineralisation observed in the region (e.g.,

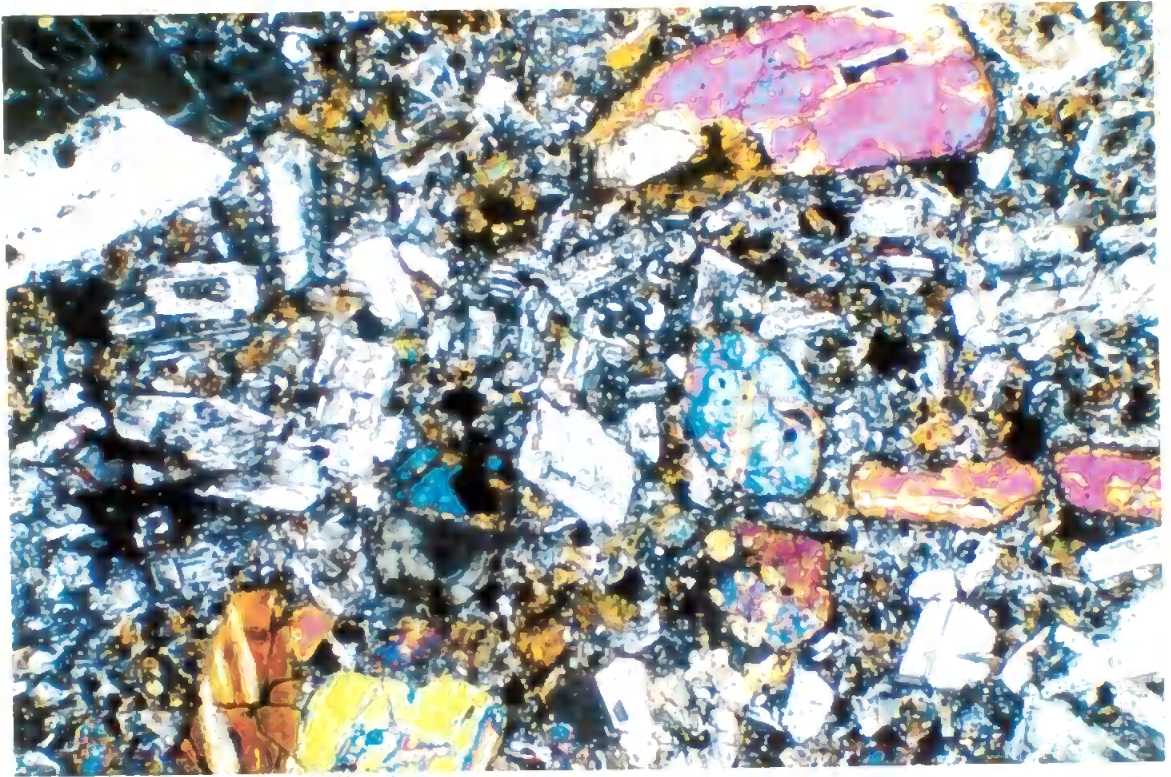


Plate 5.2. Thin section photograph of an altered porphyritic lava from the La Negra Formation. Phenocrysts of pyroxene and plagioclase can be seen in a fine groundmass. Alteration of the plagioclase to sericite can be seen. Secondary epidote is present in the groundmass. Field of view 3.3 mm, crossed polars.

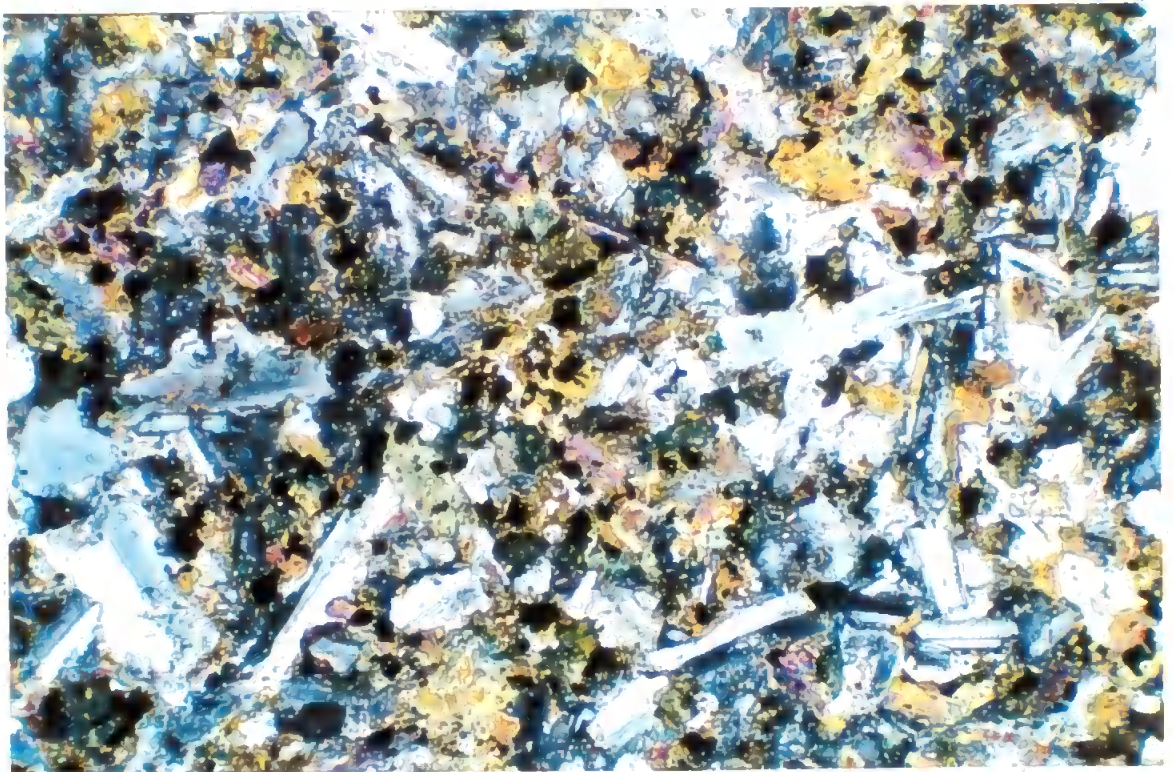


Plate 5.3. Thin section photograph of a dyke sample from the Vetado pluton. Plagioclase dominates and all of the ferromagnesian minerals are altered to epidote. Field of view is 3.3 mm, crossed polars.

Palacios *et al.*, 1992; Cornejo *et al.*, 1993; Skewes and Stern, 1994). These hydrothermal fluids are normally associated with the fault systems or in some cases with the plutons. Wherever possible sampling was conducted in areas which were not obviously affected by such mineralisation. Thirdly, the area may have been subjected to low grade metamorphism. Lucassen and Franz (1994) recognise a pervasive greenschist facies metamorphic mineral assemblage from the La Negra Formation to the north of this sampling area. Additionally, Aguirre *et al.* (1989) identified low temperature sub-greenschist facies metamorphism from comparable volcanic suites to the south of this study area. This metamorphism is thought to be the result of burial, probably occurring rapidly after extrusion or emplacement. Lucassen and Franz (1994) note that the pervasive alteration only affects the volcanic rocks, the plutons only showing alteration around joints and faults.

Overall, the tectonic setting for the emplacement of the Jurassic-Early Cretaceous magmatic arc is one of a retreating subduction margin (Royden, 1993). This means that the overall rate of convergence is lower than the rate of subduction, the deformation in the overriding plate is therefore characterised by extension at this time.

5.2.2 Structural geology and the Atacama Fault System

In the Coastal Cordillera, a series of major fault systems were active throughout the Mesozoic and in part controlled sedimentation (Bell and Suárez, 1991) and pluton emplacement within the arc (Grocott *et al.*, 1994). Like the plutonic complexes and the sediments, the fault systems also young sequentially eastwards (Dallmeyer *et al.*, 1996), the oldest being the extensional fault separating the Palaeozoic basement from the units of the Mesozoic arc (Taylor *et al.*, in prep.). This fault was succeeded to the east by the Atacama Fault Zone (AFZ), the major tectonic feature in this area (Figure 5.3).

As stated in Chapter 1, the sampling area is located in the northern part of the El Salado segment of the AFZ (Naranjo, 1987). Here the fault zone is defined by a series of

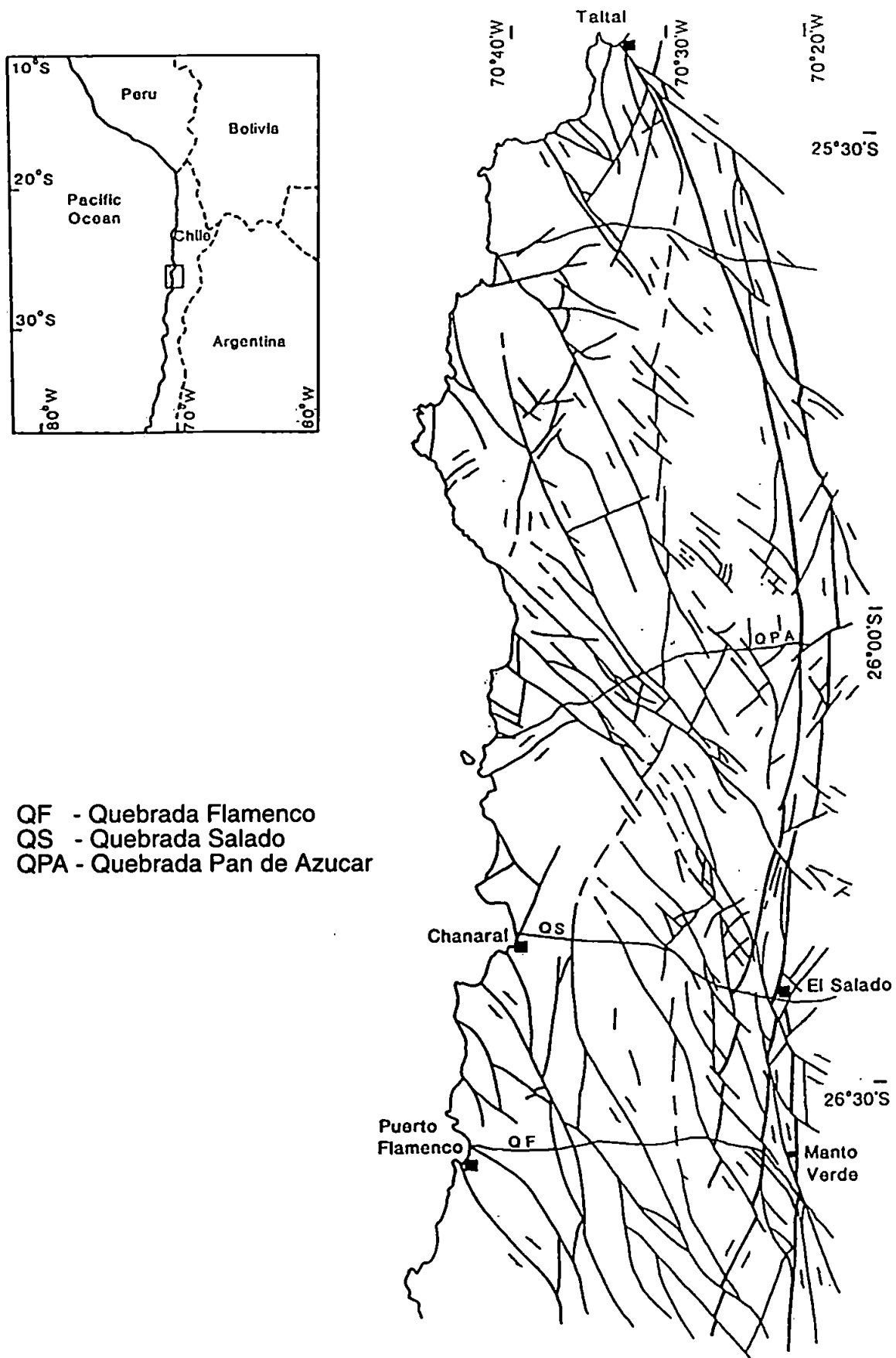


Figure 5.3. Map of the Atacama Fault Zone and the NW trending faults to the west. Taken from Taylor *et al.* (in prep).

ductile and brittle, sub-parallel and en-echelon north-south curvilinear faults. The AFZ may have been initiated in the Triassic as part of an extensional fault system (Grocott *et al.*, 1994; Dallmeyer *et al.*, 1996; Taylor *et al.*, in prep.). Subsequently, a series of margin parallel extensional faults developed which reached a low angle detachment at shallow depth, and these faults controlled emplacement of the Late Jurassic to Early Cretaceous plutons (Grocott *et al.*, 1994). The major phase of motion of the AFZ was as a sinistral strike-slip fault, at least for the El Salado and Paposos segments (Hervé, 1987; Scheuber and Andriessen, 1990; Grocott *et al.*, 1994). The principal ductile sinistral movements in the El Salado segment of the fault are dated as Early Cretaceous in age (c. 132-126 Ma; Dallmeyer *et al.*, 1996), this was then succeeded by a phase of brittle cataclastic sinistral strike-slip motion. The mylonitic and cataclastic motions were part of a single deformational event, with the heat for the mylonite formation being provided by the granitic plutons (Brown *et al.*, 1993; Grocott *et al.*, 1994). At this time, this part of the AFZ was a trench-linked strike-slip fault, and part of a much larger fault system which defined the forearc sliver from La Serena (30°S) to at least Taltal (26°S) during the Mesozoic.

A major feature of the region is a series of NW-SE trending, steeply dipping, oblique-slip sinistral strike-slip faults most clearly recognised to the west of the AFZ (Figures 5.1 and 5.3). The NW trending faults were initiated as a result of the strike-slip displacement on the AFZ, but later, with increased shortening across the arc, some of the larger of these faults continued to propagate eastwards and cut through the AFZ reactivating and displacing it (Figure 5.4). These faults have offset the AFZ by up to 70 km (Brown *et al.*, 1993). The faults which cut the AFZ can be traced to the eastern margin of the Coastal Cordillera (Arevalo, 1994; 1995) where they sole out into the Central Valley Shear Zone (CVSZ), a major N-S trending fault system which separates the Coastal Cordillera from the Central Valley (Taylor *et al.*, in prep.). The CVSZ and the NW trending faults together form the Atacama Fault System (AFS).

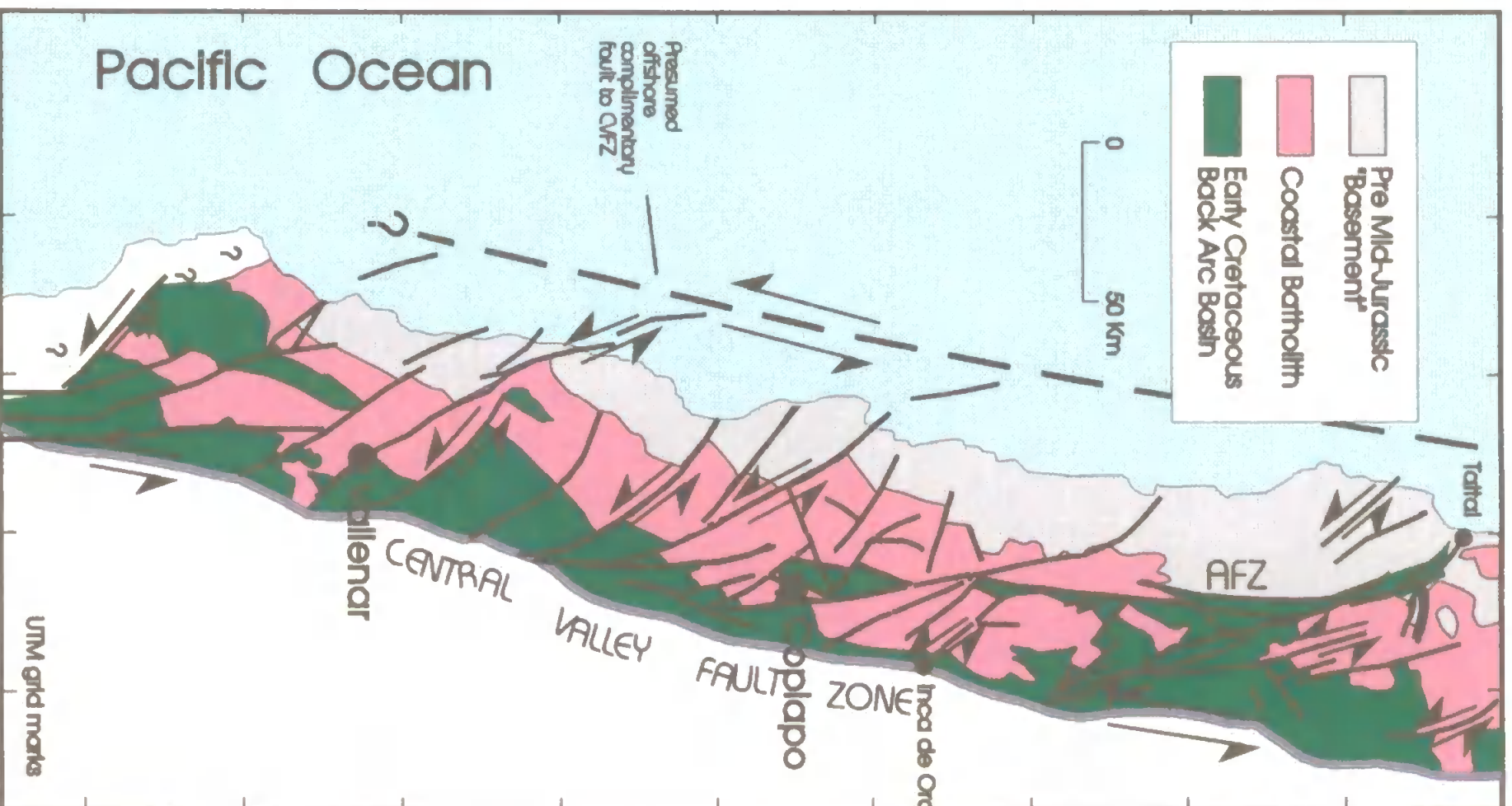


Figure 5.4. The AFS and its dissection of the Coastal Cordillera. Larger NW trending faults are seen to cut and displace the older AFZ. These faults appear to sole out into the Central Valley Fault Zone in the east (Taylor et al. In prep).

The youngest plutons in the study area are dated as 106-103 Ma (Table 5.1) and represent the final phase of magmatic activity in the region. At about this time (c. 100 Ma) the locus of magmatic activity migrated eastward to form the mid-Cretaceous magmatic arc east of the Central Valley Shear Zone (Scheuber and Reutter, 1992). In the Copiapo area, the NW trending faults of the AFS are post-dated by the Aptian to Albian Cerillos Formation (Arevalo, 1995), this suggests a minimum age constraint for the fault activity and is contemporaneous with the age of arc abandonment suggested by the intrusions. The eastward migration and abandonment of the Jurassic to Early Cretaceous arc in the Coastal Cordillera correlates with the first major phase of Andean compressional deformation, the Peruvian Orogeny (Coira *et al.*, 1982). In the Coastal Cordillera this deformation phase is expressed as a change from transtensional strike-slip tectonics on the AFZ to transpressional strike-slip tectonics on the AFS (Taylor *et al.*, in prep.). This marked change in tectonic and magmatic activity is interpreted as the consequence of the margin becoming an advancing type of subduction boundary (Royden, 1993), where the overall convergence rate is greater than the rate of subduction and deformation in the overriding plate is characterised by contraction.

Subsequent to the mid-Cretaceous deformation phase the Coastal Cordillera has not played a significant role in the tectonics of the northern Chile. During the Miocene the Coastal Cordillera was uplifted and the AFS and AFZ were reactivated and underwent minor extensional, east side down, and dextral strike-slip movement (St. Amand and Allen, 1960; Arabasz, 1971; Hervé, 1987). These motions have generated a number of neotectonic features, particularly fault scarps. The fault system is still active and known to offset and disrupt drainage systems (Buddin *et al.*, 1993).

5.3 Structural and palaeostress analysis of the dykes

One of the problems with using dykes for palaeomagnetic analysis is that any post-emplacement tilting is difficult to identify. If the dykes are part of a sheeted dyke intrusion it is usually assumed that they were near vertical when emplaced, and it is normal practice to correct the remanence directions from dyke samples to a palaeo-vertical. If the dykes do not form a sheeted intrusion identifying tilting is more difficult. As dykes were used for palaeomagnetic analysis in this study, an investigation of the structural relations and palaeostress orientations was made from dykes in three of the plutons, Vetado, Las Animas and Las Tazas. Dykes in these three plutons were chosen as they have the best three-dimensional outcrop, thus allowing structural measurements. It is generally accepted that most dyke swarms are intruded with a near vertical attitude, indicating that the stress field was close to horizontal during emplacement. Therefore if the plunge of the extension direction does not lie close to horizontal this may indicate post-emplacement tilting of the dykes.

5.3.1 Dyke emplacement and orientation

Dykes are rapidly intruded sheet-like structures of magma which cut across bedding or older foliations at high angles (Jaeger, 1959; Delaney and Pollard, 1982; Spence and Turcotte, 1985; Emerman and Marrett, 1990). If there is no regional lateral extension, emplacement is into hydraulic fractures generated by magma pressure. In this case magma pressure exceeds the compressive stress across the dyke plane and a magma-driven fracture develops ahead of the dyke tip (Spence and Turcotte, 1985; Delaney *et al.*, 1986; Renshaw and Pollard, 1994). The maximum volume of dyke material that can be injected in this way is less than 1% of the country rock (Price and Cosgrove, 1990), therefore if a dyke

swarm has a larger volume than this it indicates that there was a regional tensile stress during emplacement.

It is more common for dyke swarms to be emplaced under conditions of regional tensile stress, in this case a dyke can be emplaced into either newly developed hydraulic fractures, or into pre-existing fractures already present in the host rock. In an unfractured, isotropic medium under regional tensile stress all dykes will have a similar orientation as they form by propagation of hydraulic fractures normal to σ_3 , the least principal stress direction (Pollard *et al.*, 1982; Spence and Turcotte, 1985; Emmerman and Marrett, 1990). Any cross-cutting dykes which result from hydraulic hybrid fracturization must have interfracture angles less than 45° , in addition, these dykes will tend to be inclined, or form *en echelon* sets (Price and Cosgrove, 1990). If the magma follows along pre-existing fractures in the host rock, the dyke orientations will be the same as the fractures, so horizontal stress may also give rise to inclined dykes. Whether a particular pre-existing fracture can dilate is controlled by the stress ratio (defined from magma pressure and stress orientation) and the orientation of the fracture with respect to σ_3 (Delaney *et al.*, 1986). Above a certain stress ratio, fractures of any orientation can be dilated, this allows dykes of identical age to cross-cut and have large interfracture angles controlled only by the orientations of the pre-existing fractures.

As stated in section 5.2.1, the dyke swarms which cut the Vetado, Las Animas and Las Tazas plutons are structurally distinct and predominantly confined to the pluton. Within each swarm there is a range of orientations and there is no simple relationship between orientation and cross-cutting hierarchy, indicating that within each swarm, the dykes of all orientations are the same age. Angles larger than 45° are seen between cross-cutting dykes (Plate 5.1) and this has led previous workers to call the dykes 'conjugate' (Grocott *et al.*, 1994), implying that the dykes were intruded into conjugate fractures

developing by hydraulic fracturing as a result of extension. This term is inappropriate as extension cannot occur in two directions in the horizontal plane during a single extensional event, therefore conjugate fractures cannot develop. It seems more likely therefore that the dominant control on dyke emplacement and orientation is pre-existing fractures in the host plutons.

5.3.2 Palaeostress analysis

When extension occurs across a region with pre-existing fractures in a range of orientations some will be orientated obliquely to the direction of extension. The dykes observed in the plutons of the Coastal Cordillera display many features related to their opening, some controlled by the orientations of the original fractures and others as a result of hydraulic fracturing (Figure 5.5a). Dykes which follow fractures opening obliquely to the tensile direction will side-step causing the dyke trend to offset, or bridges to develop (Figure 5.5b). Bussell (1989) and Kretz (1991) showed that these offsets can be used to find the true dilation direction of the dyke swarm.

For analysis of the dykes in this study, the graphical method of Bussell (1989) was employed. The features of a side-stepping dyke are shown in Figure 5.6a; these are the dyke wall, the offset plane and the apparent dilation direction. In the field, the orientation of the offset edge is measured, or this can be constructed from measurements of the dyke wall and offset plane orientations. Also measured is the apparent dilation direction, this is the orientation of a line which joins matching corners of the offset. The dilation plane for the offset is found by stereographic construction of a plane which contains the apparent dilation direction and the orientation of the offset edge (Figure 5.6b). This dilation plane must contain the true dilation direction, and measurement of enough dilation planes in a range of orientations allows a best fit dilation direction to be obtained for the dyke swarm.

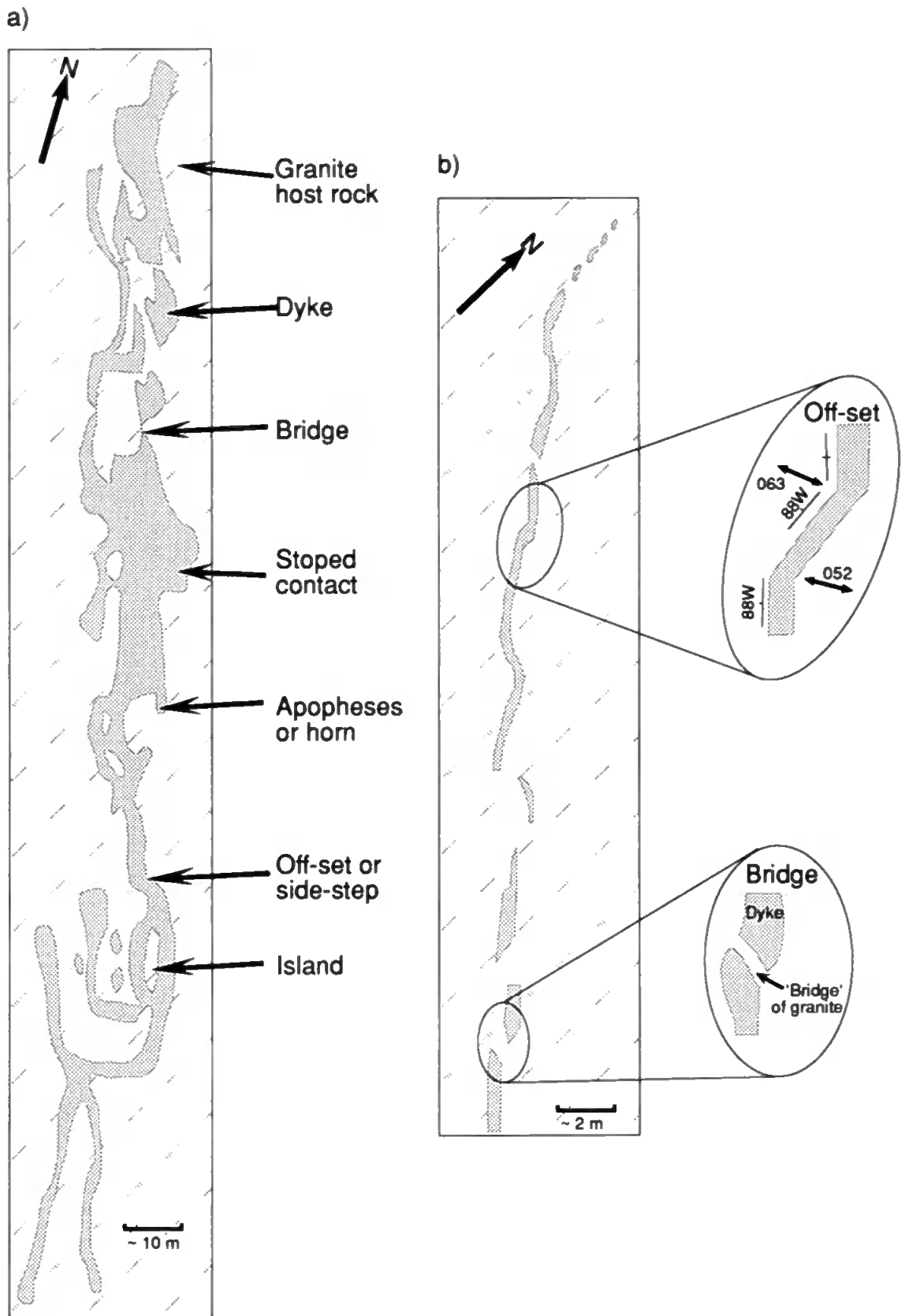


Figure 5.5. Examples of features seen within dykes which intrude a) the Vetado and b) the Las Animas plutons.

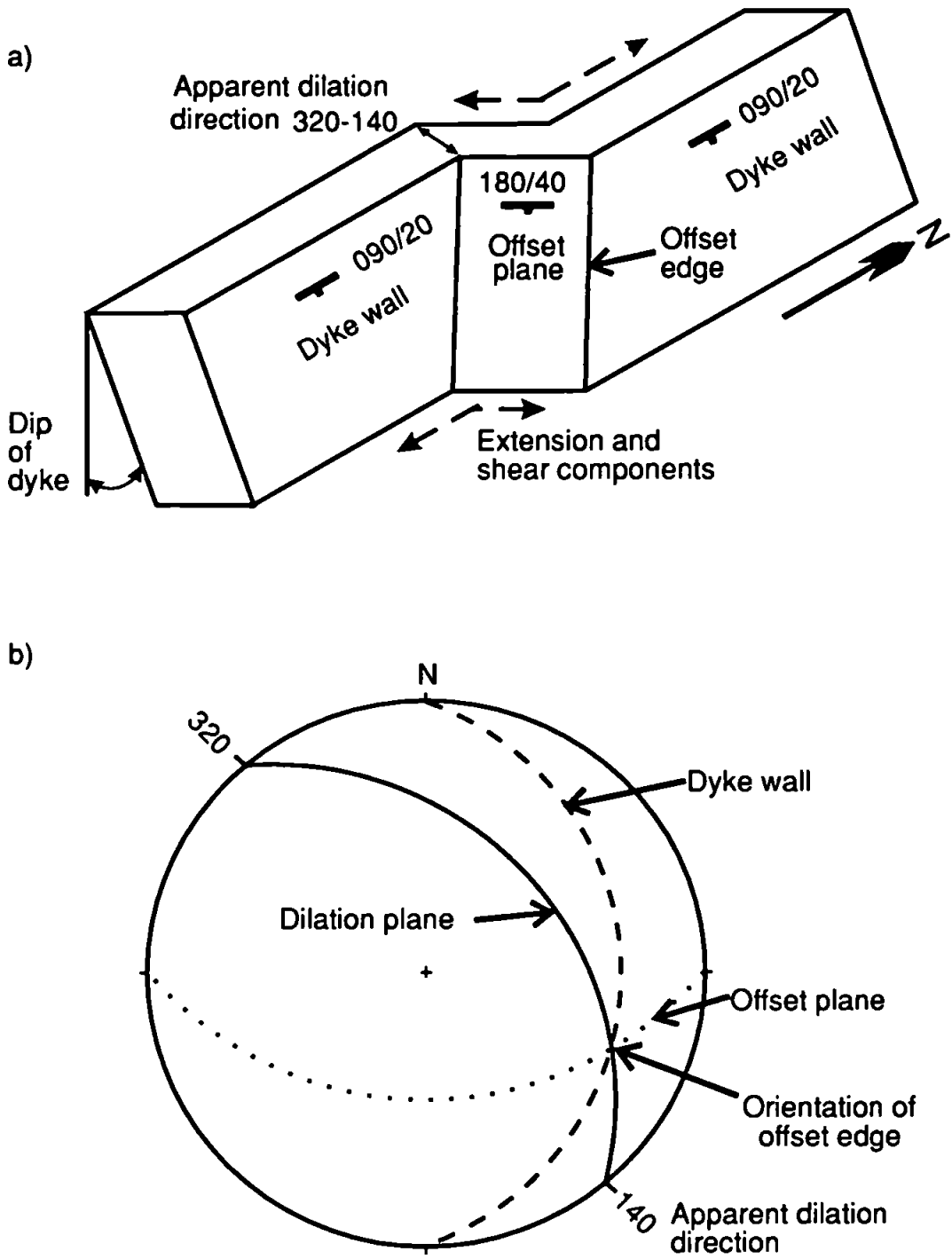


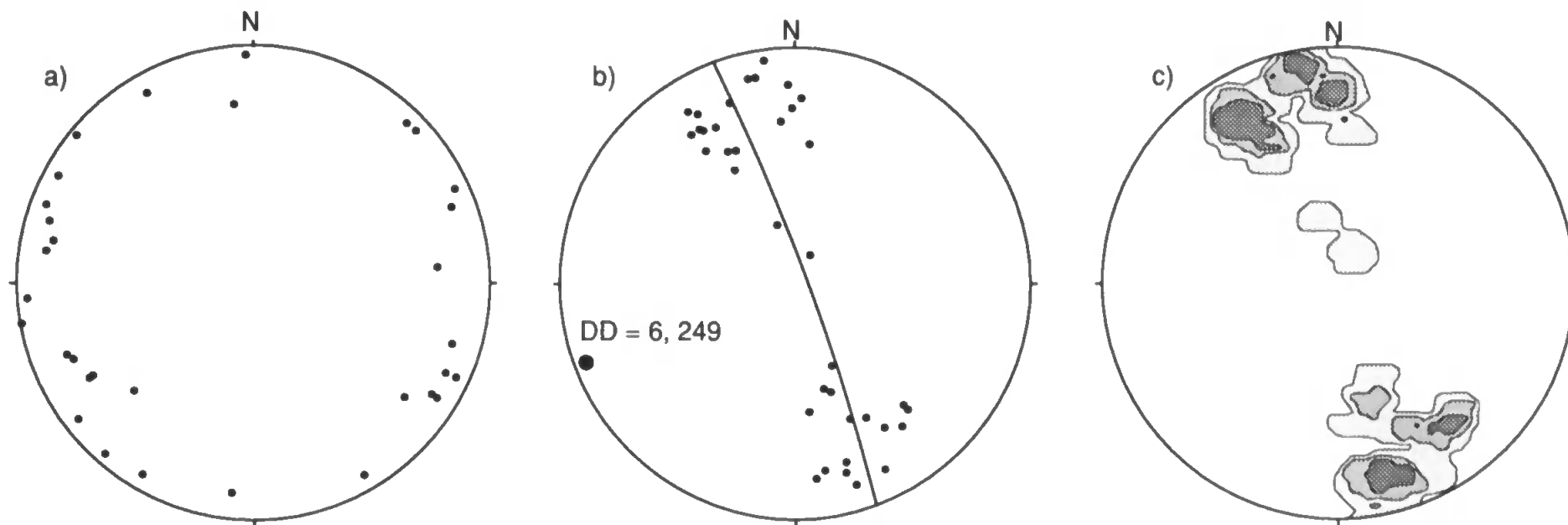
Figure 5.6. a) Diagram showing the features of a side-stepping dyke. b) The construction of the dilation plane following the method of Bussell (1989).

A total of 125 measurements were taken of dyke segment orientations in addition to 132 offset orientations from dykes which intrude the Vetado, Las Animas and Las Tazas plutons. The orientations of the dyke segments, the dilation planes and directions, and density plots of the data are shown in Figure 5.7. Dykes in the Vetado pluton are generally close to vertical and, although they have a wide range of strike directions, they show a dominant approximately N-S trend. The dykes in the Las Animas pluton have a wider range of dips, although again, in most cases, this is within 20° of vertical. The strikes of the dykes are better grouped than those in the Vetado pluton and show an approximately NW-SE trend. In the Las Tazas pluton the dyke orientations are much better grouped and all of the measured dyke segments dip steeply towards the SW.

The dilation directions demonstrate variation between the three swarms. As suggested by the dyke segment orientations, the dykes in the Vetado pluton show a dilation direction close to E-W, the finite direction is at 6° , 249° . In the Las Animas pluton the dilation direction is at 1° , 232° , and in the Las Tazas pluton at 7° , 205° . The data show a general clockwise rotation of the dilation direction with increasing dyke age. In all cases the plunge of the dilation is low indicating that a presumed near horizontal stress field existed during emplacement.

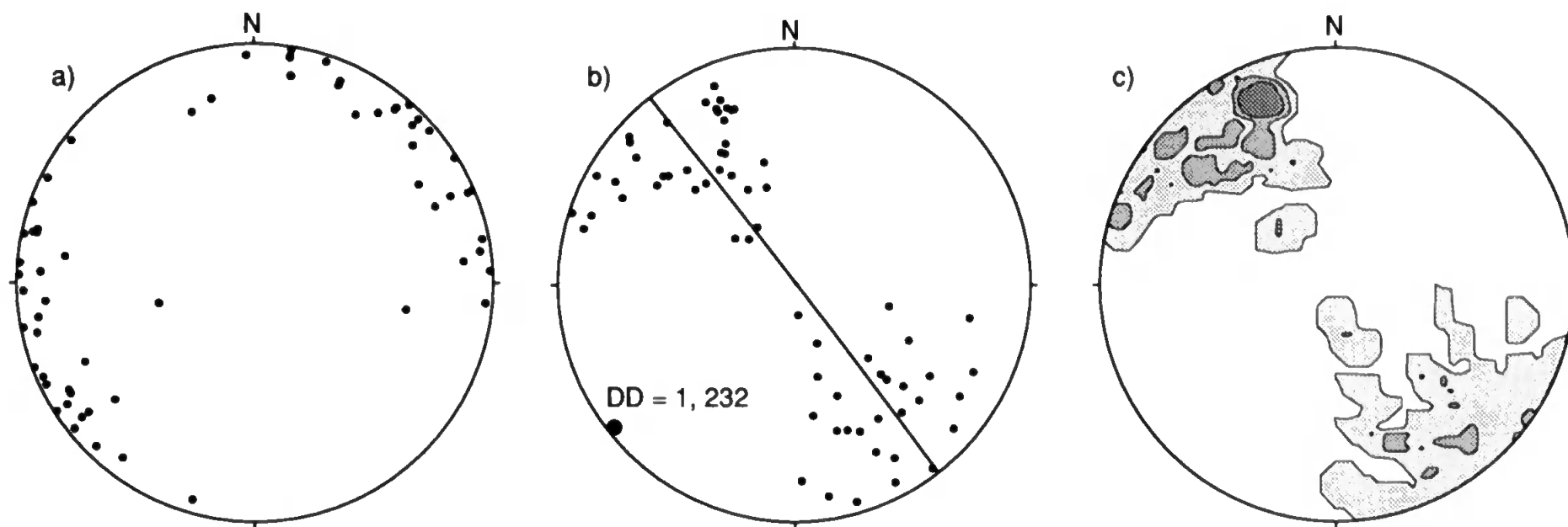
5.3.3 Discussion of the palaeostress analysis results

The differences in the range of dyke strikes within each of the plutons may be due to a number of reasons. Firstly, as the Vetado pluton is older it may have had a greater range of pre-existing fracture orientations which could be dilated during extension. A second possibility is the dykes in the Las Animas or Las Tazas plutons may have been emplaced under a lower stress ratio (Delaney *et al.*, 1986). This would have restricted the range of fracture orientations that could be dilated during the extension. Thirdly, the ages



Vetado n = 37

Figure 5.7. Equal area projection of a) poles to dyke orientations; b) Best fit dilation plane and direction from the dyke offsets in the plutons. DD is the plunge and trend of the dilation direction. c) Density plots of dilation data. Divisions are at 10, 40 and 70 %.



Las Animas n = 66

Figure 5.7. Continued.

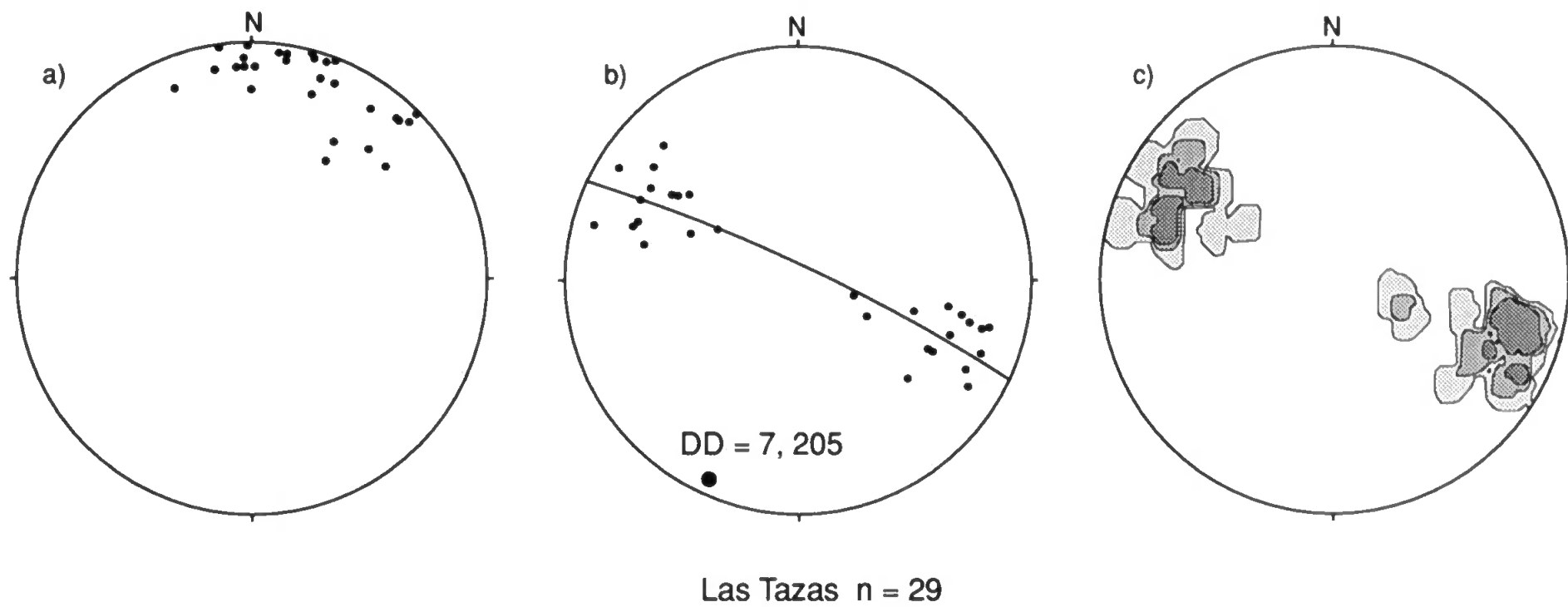


Figure 5.7. Continued.

of the dyke swarms in the younger plutons suggest that they were emplaced soon after the plutons themselves, and probably while the plutons were still hot. The dykes in the Vetado pluton may, however, be significantly younger than the age of the pluton and would have been intruded into cold, brittle rock. Although Spence and Turcotte (1985) demonstrated that fracture resistance could be neglected when considering a magma driven crack in an elastic medium, intrusion into a warmer, and presumably weaker host rock may have aided propagation of dykes normal to σ_3 , and therefore in a smaller range of orientations. The grouping of dyke orientations in the Las Tazas pluton may indicate that a smaller range of fractures were present or capable of being dilated in the host rock. The consistent NE dip of the dykes may indicate a consistent original dip to the fractures, or possibly a component of vertical shear during dyke emplacement.

The near vertical field attitude of the dykes and the palaeostress analysis indicates that the extension direction was close to horizontal during emplacement of all three of the dyke swarms. It is likely that when considering an extending margin on a regional scale, the stress conditions under which the dykes were emplaced was close to horizontal, if this is the case, then the data indicate that the dykes have undergone no significant post-emplacement tilting. Any inclined dykes that are sampled are probably in their original orientation and their palaeomagnetic remanence directions do not need to be corrected back to vertical.

The declinations of the best fit dilation directions seem to show that the stress field was rotating from WSW-ENE, in the Early Jurassic when the Vetado dykes were intruded to more SSW-NNE in the Early Cretaceous. These directions do not take into account any vertical axis rotation of the dyke swarms since emplacement.

5.4 Palaeomagnetic results

5.4.1 La Negra Formation

i) Palaeomagnetic sampling localities

Sites for palaeomagnetic analysis were collected along two W-E transects. Twelve sites, AT69-AT80, were collected in 1992 along the more southerly transect and a further 9 sites, AT81-AT89 were collected in 1993. All sites were collected as oriented hand samples. Figure 5.8 shows the sampling locations along the transects. Structural data for palaeohorizontal control was taken from igneous features and where possible, from the rare sedimentary horizons within the formation. In some places it was difficult to establish the palaeohorizontal and several measurements were taken to obtain a mean for the outcrop.

ii) Magnetic mineralogy

Samples from eight sites were subjected to IRM acquisition and three-axis demagnetisation as described in section 2.6.1. Samples were selected which reflected the range of demagnetisation behaviour observed. Results from four of the samples are shown in Figure 5.9a-d. Sample AT87-2-2b (Figure 5.9a) acquires IRM rapidly up to ~300 mT and then saturates. Demagnetisation of the IRMs is completed at 550°C-580°C and show a dominance of the lowest coercivity component, only a small amount of the IRM is carried by grains with high coercivities. NRM demagnetisation shows a rapid reduction with AF and a steady decrease in intensity with thermal demagnetisation up to a maximum of 60 mT and 580°C respectively. These experiments indicate a magnetite and/or titanomagnetite carrier for both the NRM and IRM, probably with a range of grain sizes present. The dominance of the low coercivity component suggests a significant multi-domain component.

Sample AT76-4-3 (Figure 5.9b) again shows a dominance of low and intermediate coercivity carriers for the IRM. The low and intermediate coercivity IRMs do not

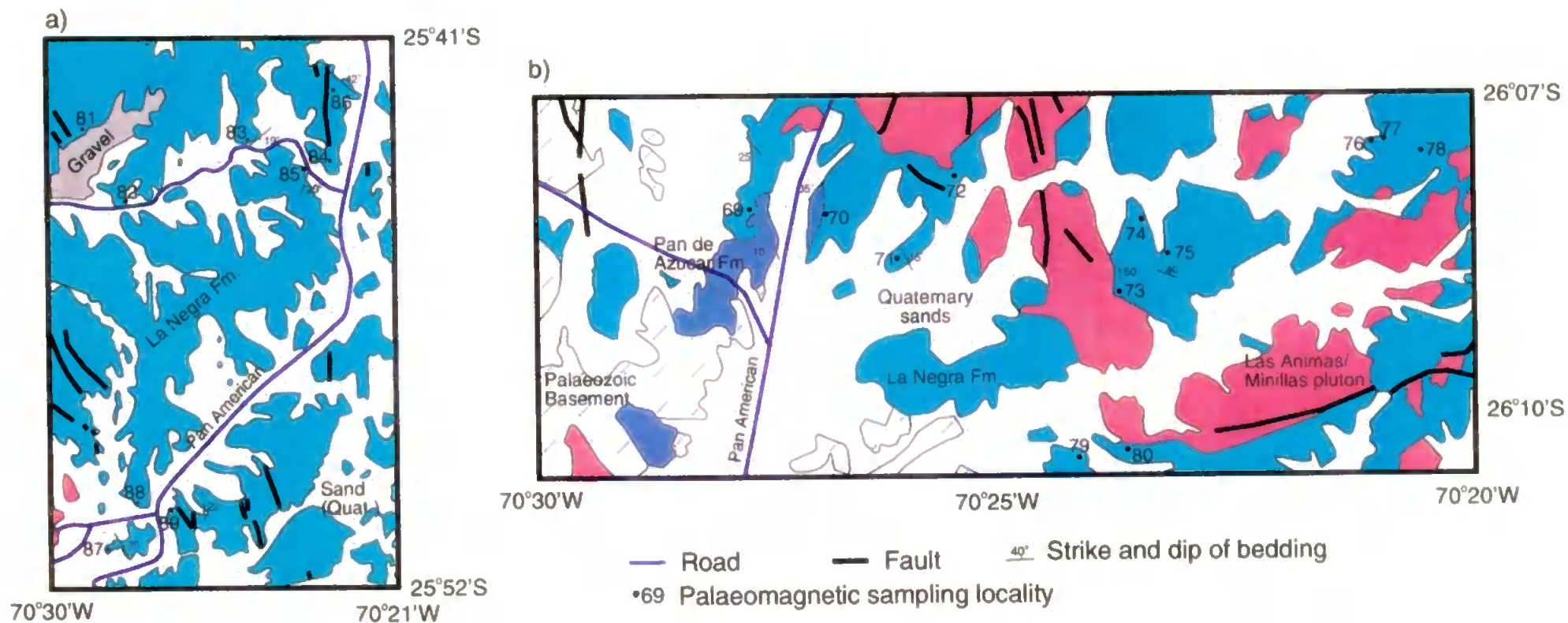


Figure 5.8. Map of palaeomagnetic sampling localities from a) the northern and b) the southern transects through the La Negra Formation. The northern section is redrawn from the 1: 250 000 scale map (1 cm = 2.5 km) of Naranjo and Puig (1984), the southern section is from the 1: 100 000 scale map (1 cm = 1 km) of Naranjo (1978).

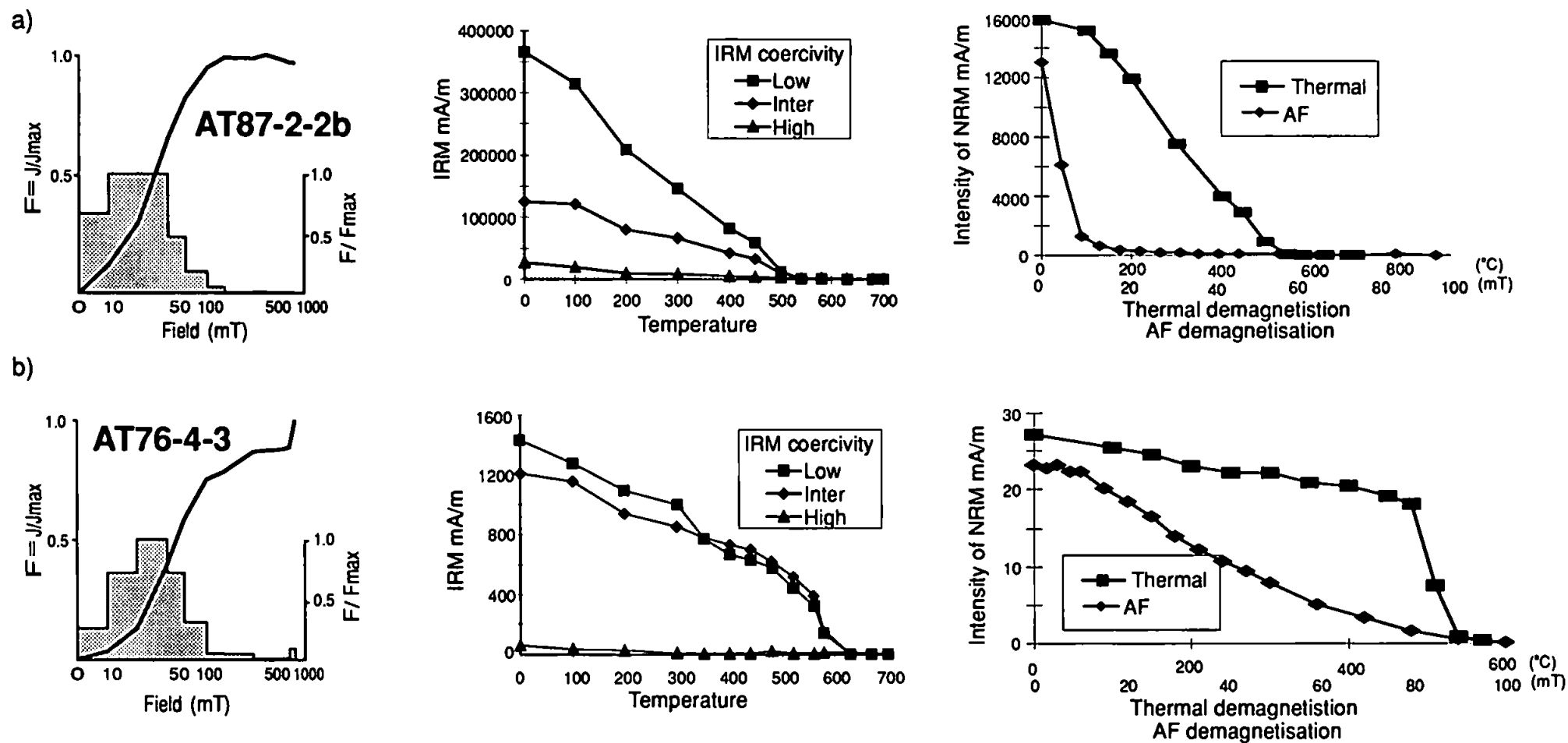


Figure 5.9 a, b. Rock magnetic experiments from samples of the La Negra Formation. Graphs show acquisition of IRM, demagnetisation of 3-axis IRMs and demagnetisation of remanence.

completely demagnetise until 630°C, while the NRM was demagnetised at ~540°C. This discrepancy may be due to a problem with the oven failing to attain its true temperature setting during the IRM demagnetisation experiments rather than being a true measure of unblocking temperature. Noticeably different to sample AT87-2-2b is the drop in the IRM of the low coercivity component at ~300°C-400°C. This may be due to the presence of some maghemite in the sample. Maghemite has a saturation magnetisation comparable to that of magnetite and would show similar IRM acquisition characteristics. Maghemite however changes to haematite at approximately 300°C-350°C and this would result in a fall of intensity in the low coercivity IRM component. However, the same intensity drop is not observed in the NRM, suggesting that if maghemite is present, it may not have been a contributor to the NRM. This sample is interpreted as being dominated by a mixture of magnetite and titanomagnetite, again probably in a range of grain sizes. In addition, there may also be some maghemite present. These two types of rock magnetic behaviour are representative of most of the samples from the La Negra Formation.

The IRM acquisition of sample AT71-2-R, shown in Figure 5.9c, indicates the presence of a high coercivity component in addition to a more significant contribution from low coercivity grains. This is confirmed by demagnetisation of the IRMs which show that the low coercivity component is demagnetised by 580°C while the high coercivity component remains stable up to 670°C, this indicates a mix of haematite and magnetite or titanomagnetite. The demagnetisation of the NRM is complete at 570°C or 30 mT, this suggests that while haematite is present in the sample it is not a significant carrier of NRM. As in sample AT71-2-R, there is a significant drop in the IRM of the low coercivity component at approximately 300°C-350°C, although in this sample the drop is also observed in the demagnetisation of NRM. Following the discussion above, this may indicate the presence of maghemite in this sample. Sample AT70-1-4, shown in Figure 5.9d, has an IRM and NRM carried by high coercivity grains unaffected by AF

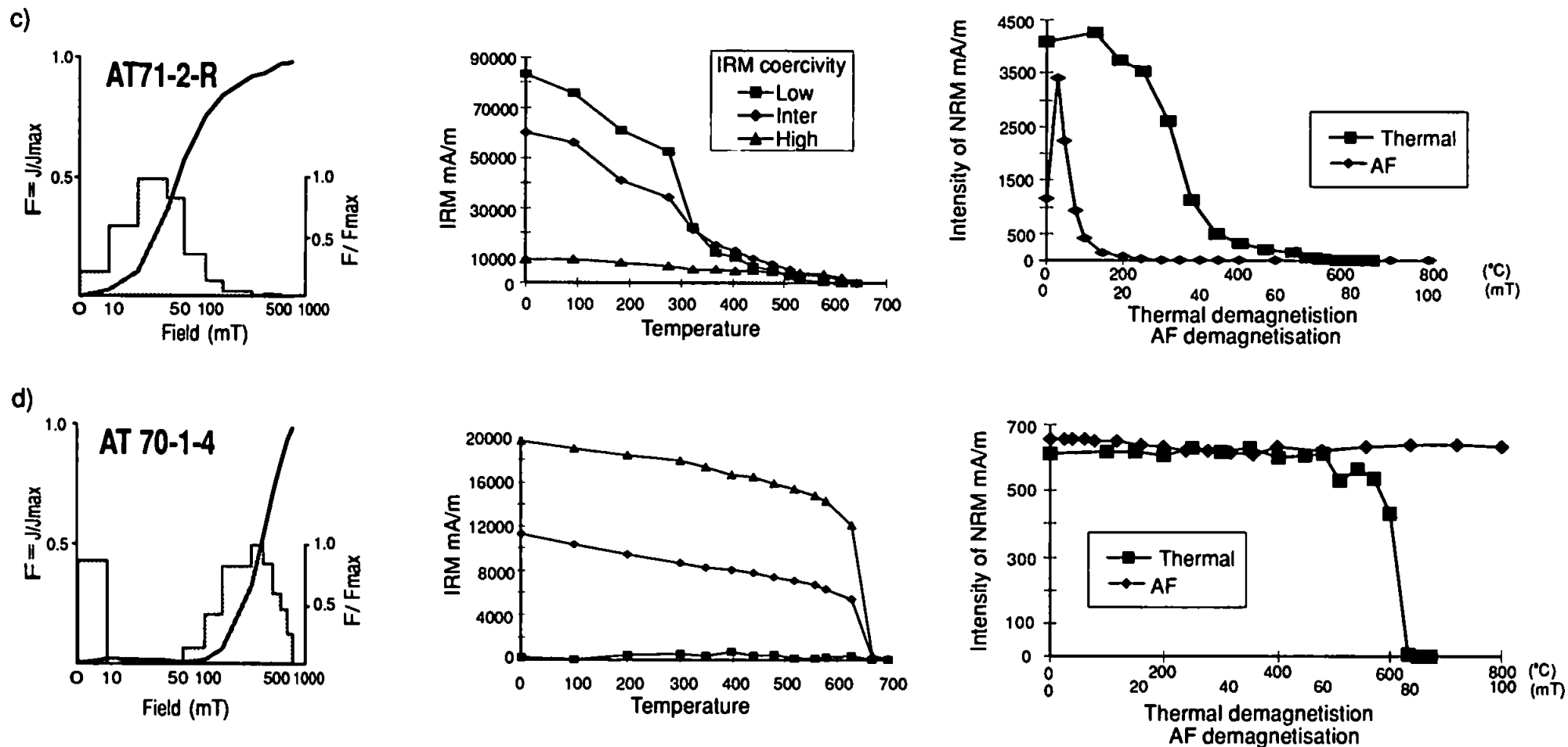


Figure 5.9 c, d. Rock magnetic experiments from samples of the La Negra Formation. Graphs show acquisition of IRM, demagnetisation of 3-axis IRMs and demagnetisation of remanence.

demagnetisation, which have an unblocking temperature of 670°C. In this sample the only carrier was haematite.

Thin section studies of samples collected for palaeomagnetic analysis recognised a large amount of opaque minerals within the formation, some specifically associated with secondary veins and infilling of vesicles. Petrological studies by Lucassen and Franz (1994) on the La Negra Formation near to Antofagasta (approximately 250 km north of this sampling region) recognised a dominance of titanomagnetite and titanomaghemite in their samples, with minor ilmenite. They interpreted the presence of the titanomagnetite as evidence for low temperature hydrothermal alteration. Hartley *et al.* (1988) sampled the formation from near to Antofagasta for palaeomagnetic study. They identified discrete magnetite and haematite in their samples, as well a large amount of secondary haematite associated with veins. The petrological evidence from this study and those from further north suggests that there may be several phases of magnetic mineral growth within these rocks, some of which may be localised in secondary features. Overall, the petrological and rock magnetic data indicate a complex range of carriers in the La Negra Formation which may have been acquired over a significant time period.

iii) Anisotropy of magnetic susceptibility

The anisotropy of magnetic susceptibility (AMS) of samples from the sites in the northern transect was measured (sites AT81-AT89), and results are given in Table 5.2. Figure 5.10 shows the variation in shape parameter, T , with corrected anisotropy degree, P_j . The parameter T is given by

$$T = \left(\frac{2 \ln(k_2 / k_3)}{\ln(k_1 / k_3)} \right) - 1$$

Sample (AT)	Maximum		Intermediate		Minimum		Susceptibility					
	Dec.	Inc.	Dec.	Inc.	Dec.	Inc.	k1	k2	k3	kgeom	PJ	T
81-1-1	112.7	38.2	312.7	50.0	210.7	9.9	4114.3	4104.4	4088.5	4102.4	1.0064	0.2341
81-1-2A	121.1	19.8	329.6	67.8	214.7	9.8	4167.9	4157.3	4138.9	4154.7	1.0071	0.2706
81-1-2B	117.7	29.4	295.1	60.6	27.1	1.0	4326.7	4318.5	4296.5	4313.9	1.0073	0.4583
81-2-1	81.3	9.8	33.5	60.4	176.5	27.6	19914.4	19861.7	19789.0	19854.9	1.0064	0.1609
81-2-2	189.7	30.2	81.9	27.7	317.9	46.8	18918.4	18842.4	18785.3	18848.6	1.0071	-0.1405
81-2-3	232.4	67.9	69.4	21.3	337.1	5.9	25170.6	25025.4	24986.1	25060.5	1.0078	-0.5727
82-1-1	319.7	6.2	64.2	66.7	227.2	22.5	24115.3	33717.9	33368.8	33732.6	1.0224	-0.0593
82-1-2	321.7	11.0	66.5	52.7	223.8	35.1	32853.0	32473.3	32259.8	32527.7	1.0186	-0.2759
82-1-3	317.8	8.8	65.0	62.3	223.6	26.0	34894.4	34471.4	34197.2	34519.8	1.0205	-0.2086
82-2-1	34.0	31.7	152.7	37.9	227.2	36.0	38534.3	38283.7	38010.1	38275.3	1.0138	0.0475
82-2-2	35.0	29.3	153.1	40.0	280.9	36.1	31891.2	31572.4	31333.5	31598.1	1.0179	-0.1389
82-2-3	35.5	29.8	163.9	47.3	288.1	27.5	33918.2	33646.2	33328.5	33630.0	1.0177	0.0820
83-1-1	4.0	8.9	101.2	38.4	263.1	50.2	32079.0	31818.5	31642.5	31846.1	1.0139	-0.1903
83-1-2	10.8	20.0	118.7	40.3	261.0	43.0	33513.9	33335.9	32829.9	33225.2	1.0216	0.4833
83-1-3	5.2	20.0	107.4	30.2	246.9	52.5	36567.8	36258.7	35973.3	36265.7	1.0165	-0.0356
83-2-1	322.0	23.5	212.8	37.2	76.5	43.7	35640.6	35319.2	35100.7	35352.7	1.0155	-0.1870
83-2-2	337.6	21.5	223.1	46.5	84.0	35.6	38021.1	37633.7	37493.8	37715.4	1.0146	-0.4667
83-2-3	336.2	31.5	244.8	2.2	151.2	58.4	35375.8	35020.7	34897.4	35097.3	1.0142	-0.4819
84-1-1	166.0	68.6	10.0	19.7	277.1	8.0	684.3	679.7	677.7	680.6	1.0100	-0.3919
84-1-2	27.0	60.4	193.8	28.9	287.0	5.7	694.9	693.6	690.4	693.0	1.0067	0.4237
84-1-3	57.9	74.8	187.4	9.8	279.9	11.5	686.2	684.9	678.6	683.2	1.0120	0.6595
84-2-1	36.1	39.8	188.2	46.7	293.9	14.2	763.7	761.5	756.4	760.5	1.0099	0.3993
84-2-2	31.1	43.0	185.6	43.2	298.2	13.1	771.7	769.7	764.6	768.7	1.0096	0.4386
84-2-3	36.7	60.1	202.4	29.2	295.9	6.2	788.3	783.8	780.0	784.0	1.0107	-0.0816
85-1-1	237.8	23.5	212.5	53.1	80.5	26.7	21899.9	20902.5	20811.2	21198.8	1.0582	-0.8283
85-1-2	340.5	23.0	227.0	43.3	89.7	37.9	18096.7	17272.3	17189.4	17514.7	1.0585	-0.8129
85-1-3	341.0	23.1	220.2	50.2	85.5	30.4	20110.2	19186.1	19097.8	19459.3	1.0588	-0.8214
85-1-4	338.6	30.3	200.4	52.1	81.3	20.7	18060.8	17220.0	17099.0	17454.7	1.0613	-0.7423
85-2-1	138.8	12.7	145.5	13.7	9.9	71.1	44624.8	43682.6	43214.0	43836.4	1.0332	-0.3286
85-2-2	229.6	8.2	138.3	8.7	2.3	78.1	47069.4	46100.1	45001.5	46049.1	1.0460	0.0737

Table 5.2

Continued...

Sample (AT)	Maximum		Intermediate		Minimum		Susceptibility					
	Dec.	Inc.	Dec.	Inc.	Dec.	Inc.	k1	k2	k3	kgeom	PJ	T
86-1-3	267.8	56.9	175.8	1.3	85.0	33.1	9060.5	8915.1	8783.4	8918.9	1.0316	-0.0417
86-2-1	280.0	72.3	135.5	14.5	43.0	9.8	17785.1	17435.5	17091.3	17434.9	1.0406	0.0022
86-2-2	223.6	76.6	317.4	0.9	47.6	13.4	16439.5	16164.3	15864.4	16154.3	1.0363	0.0518
86-2-3	246.4	77.8	146.1	2.2	55.6	11.9	16617.2	16317.7	16001.0	16310.0	1.0385	0.0373
87-1-1A	100.2	66.6	231.6	16.1	326.6	16.6	51352.0	51320.5	50765.9	51145.3	1.0130	0.8929
87-1-1B	210.2	57.6	46.2	31.4	311.7	7.2	53827.7	53467.6	53098.4	53463.6	1.0137	0.0161
87-2-1	310.4	27.9	179.3	50.9	54.6	24.8	50625.2	50236.8	50082.1	50314.1	1.0112	-0.4282
87-2-2	305.9	27.9	157.5	58.1	43.5	14.2	57223.2	56404.5	56351.5	56658.2	1.0174	-0.8775
87-2-3A	301.3	27.9	191.0	33.1	62.0	44.0	60056.4	59580.9	59353.1	59662.6	1.0121	-0.3495
87-2-3B	305.1	24.5	202.1	26.2	71.8	52.6	51480.7	51022.9	50839.3	51113.5	1.0130	-0.4249
88-1-1	123.0	38.9	30.6	2.9	297.0	50.9	10658.3	10488.3	10412.4	10519.1	1.0242	-0.3777
88-1-2	122.5	44.5	230.2	17.2	335.3	40.5	10247.8	10065.8	10033.1	10115.1	1.0231	-0.6926
88-1-3	111.3	37.4	343.9	38.4	227.2	29.6	10020.3	9858.2	9826.9	9901.4	1.0211	-0.6736
88-2-1	203.3	43.1	69.4	36.6	319.2	24.9	1966.2	1938.4	1915.8	1940.0	1.0263	-0.0967
88-2-2	206.4	34.6	64.3	48.8	310.5	19.5	2002.5	1975.3	1950.7	1976.1	1.0266	-0.0437
88-2-3	209.0	37.0	58.7	49.1	310.7	15.1	1892.9	1865.5	1844.9	1867.7	1.0261	-0.1354
89-1-1A	169.0	29.6	3.1	59.7	262.5	6.1	20632.6	20342.7	20132.2	20368.1	1.0250	-0.1527
89-1-1B	83.9	6.3	286.6	83.1	174.2	2.6	29062.0	28597.7	28484.8	28713.7	1.0215	-0.6057
89-1-2	166.3	33.7	347.6	56.3	256.7	0.6	21928.3	21715.8	21473.3	21704.9	1.0212	0.0711
89-1-3	167.9	26.8	7.4	61.8	262.0	8.1	22964.7	22678.2	22437.6	22692.4	1.0235	-0.0813
89-2-1	77.8	0.2	347.1	74.6	167.9	15.5	29902.9	29578.9	29332.1	29603.6	1.0195	-0.1305
89-2-2	74.7	5.0	329.6	71.4	166.3	17.9	30613.9	30290.2	30025.5	30308.8	1.0196	-0.0995

Table 5.2. Anisotropy data from the northern transect through the La Negra Formation. Dec. and Inc. are tilt corrected declination and inclination of susceptibility axes; k1, k2 and k3 are the maximum, intermediate and minor axis susceptibilities; kgeom is the geometric average susceptibility; PJ is corrected anisotropy degree; T is the shape parameter (Jelinek, 1981).

where k_1 is the maximum susceptibility, k_2 is the intermediate susceptibility and k_3 is the minimum susceptibility. The corrected anisotropy degree, P_J , is given by

$$P_J = \exp \sqrt{2(\eta_1 - \eta_m)^2 + (\eta_2 - \eta_m)^2 + (\eta_3 - \eta_m)^2}$$

where $\eta_1 = \ln k_1$ $\eta_2 = \ln k_2$ $\eta_3 = \ln k_3$

and $\eta_m = \sqrt[3]{\eta_1 \times \eta_2 \times \eta_3}$

The results indicate that most samples have less than 4% corrected anisotropy degree. For most samples the shape parameter (T) is close to 0, indicating the presence of triaxial AMS ellipsoids. Only four of samples display significant AMS, these are from site AT85 and are prolate with P_J approximately 6%.

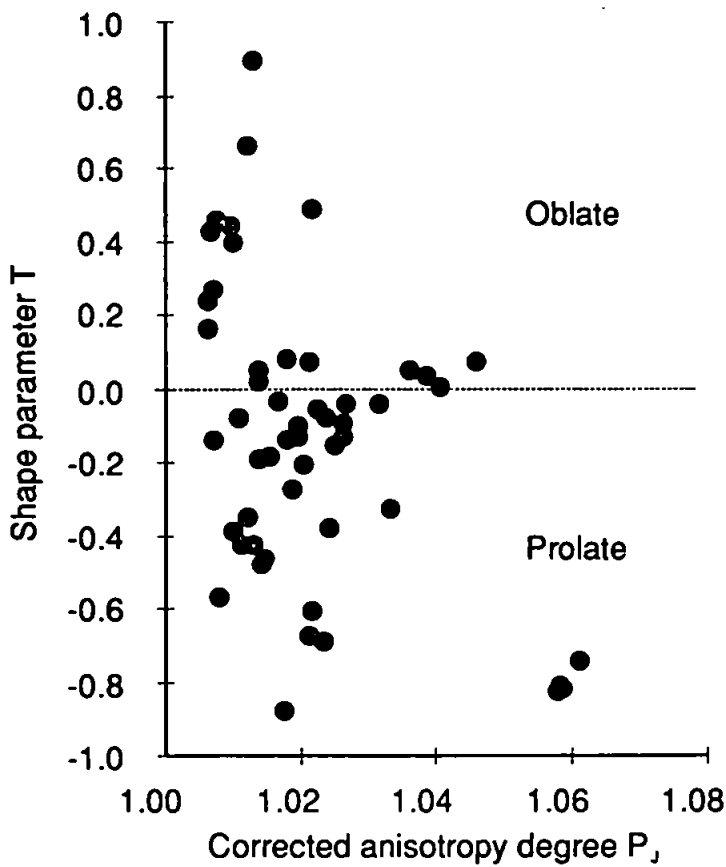


Figure 5.10. Shape parameters of anisotropy, La Negra Formation.

Figure 5.11 shows the directions of the principle susceptibility axes. For most sites there is no pattern and the axes are either widely scattered, or grouped within each hand sample block. At sites AT83 and AT86 the maximum axes are well-grouped while the intermediate and minimum axes form poorly defined great circle distributions. Site AT84 has well-grouped minimum axes with the maximum and intermediate axes forming a great circle girdle, indicating a near vertical oblate fabric. At sites AT87 and AT89 some of the maximum and minimum axes of different samples have the same orientation. This may result from the presence of a mixture of multi- and single domain magnetite grains in the samples. In the samples dominated by single domain grains the maximum susceptibility lies perpendicular to the easy axis of the grain, while in multi-domain grains, the maximum susceptibility axis lies along the easy direction. This is because with low field susceptibility there is insufficient energy to re-align the susceptibility of single domain grains, while the domain structure of multi-domain grains allows re-alignment of the maximum susceptibility along the easy axis of the fabric (Stephenson *et al.*, 1986).

The AMS results show that in most cases samples from the northern transect of the La Negra Formation have low anisotropy. The AMS present is likely to be due to flow within the lava, with variations due to the samples being collected from different position within the flows. Samples from close to the sides of a flow are more likely to have oblate ellipses as a result of flow by layer shearing, while those from within the lava flow will have prolate ellipses related to faster magma flow. The data from the La Negra Formation indicates that the amount of AMS measured in these samples is unlikely to affect the direction of palaeomagnetic remanence in any of the sites.

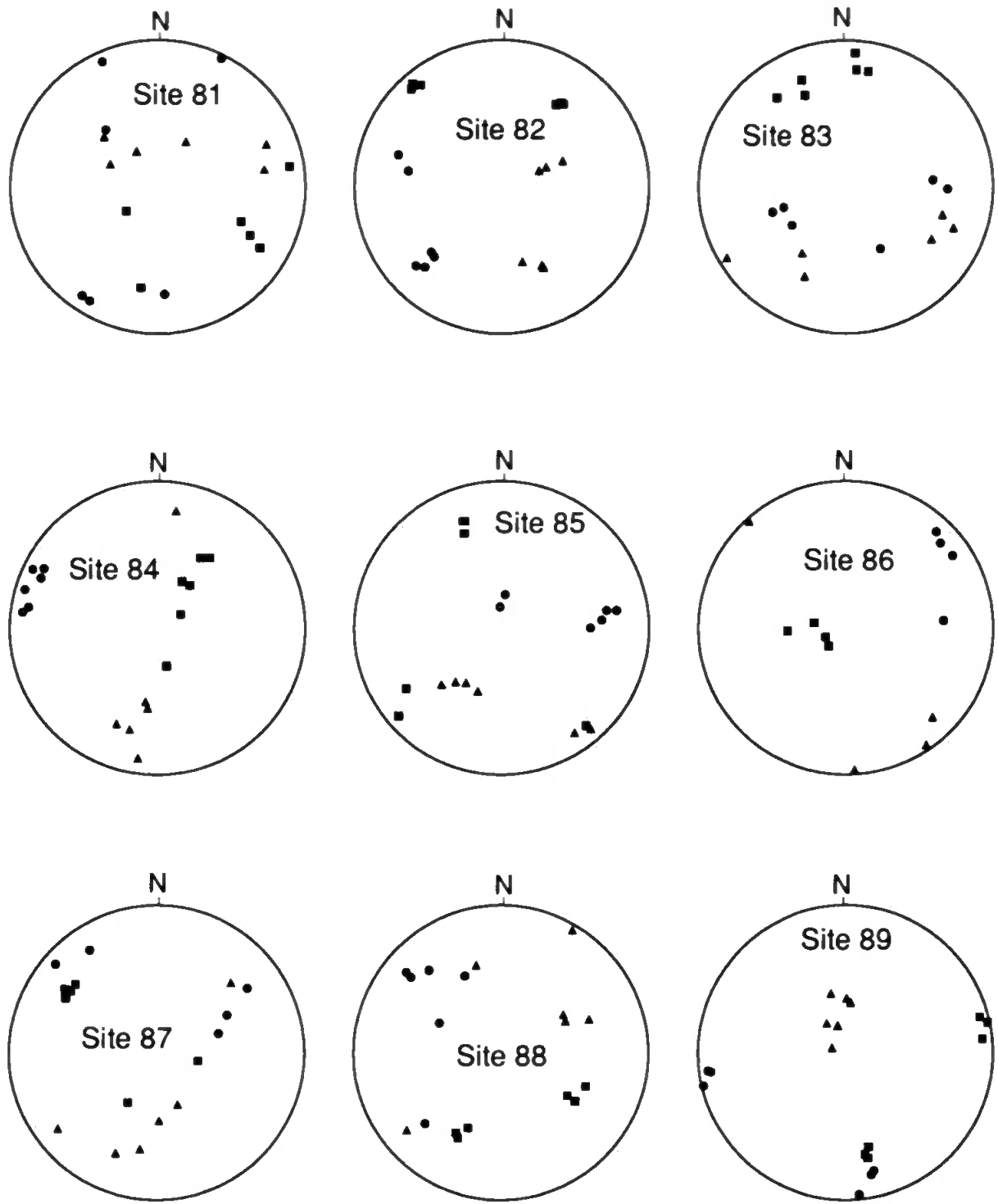


Figure 5.11. Equal area stereographic projections of principle susceptibility axes. Squares are k_{\max} ; triangles are k_{int} ; circles k_{\min} .

iv) Palaeomagnetic remanence measurements

A total of 21 sites were collected from the La Negra Formation from a number of lithologies (Table 5.3). Many of the samples exhibit multi-component behaviour which was found to be extremely variable, even within each site. For this reason, a range of demagnetisation levels at which the characteristic remanent magnetisation (ChRM) was recovered for is recorded for some sites. The directions of palaeomagnetic remanence are given in Table 5.4. Although the demagnetisation was complex, most sites yielded a stable remanence direction and the ChRM was isolated at the highest demagnetisation level in 20 of 21 sites.

A stereographic projection of the low coercivity or unblocking temperature components is shown in Figure 5.12. Most sites exhibited a single low coercivity or unblocking temperature component which was removed by 25 mT or 250°C. Some sites also contained an intermediate component, typically in the 200-450°C or 20-35 mT range, although they are less well defined during AF demagnetisation. It is obvious from Figure 5.12 that in most cases the directions do not form a well defined group, even within site. After applying a tilt correction the pattern is not significantly different. The low components from some sites do show diffuse grouping or linear trends, for example sites AT74, AT79 and AT86. The samples from site AT78 are notably different as they do form a coherent group at approximately 30° clockwise of north with a -30° inclination. The demagnetisation plots from two samples from this site are shown in Figure 5.13, on the stereographic projections the directions plot as a great circle path suggesting that there two components of magnetisation, in this case probably the ChRM and a time averaged present-day component. The poor within site grouping of the low and intermediate coercivity and unblocking temperature components indicates that the majority were most likely acquired after the samples were removed from the host rock, and therefore represent viscous remanences acquired as sampling or laboratory induced components.

Site	Sampling site		Lithology	Tilt correction	°C Min.	ChRM isolation		mT Max.
	Long. W	Lat. S				Max.	Min	
* AT69	70°28'00"	26°08'30"	Ignimbrite	254/21	480	570	10	100
AT70	70°27'30"	26°08'15"	Basaltic/andesitic lava	224/40	510	670	None	
AT71	70°26'00"	26°08'30"	Andesitic lava	324/36	150	630	3→5	100
* AT72	70°25'37"	26°08'20"	Basaltic/andesitic lava	338/24	450	550	3	100
AT74	70°23'15"	26°08'15"	Andesitic lava	155/10	200	600	7.5	80
* AT75	70°23'03"	26°08'40"	Andesitic lava	358/32	510	600	3→20	100
* AT76	70°21'45"	26°07'30"	Rhyolite lava	206/52	480	570	25	100
AT77	70°21'45"	26°07'30"	Basaltic/andesitic lava	233/13	400	570	3→15	100
* AT78	70°21'18"	26°07'30"	Basaltic lava	251/16	100-	540	3	25
* AT79	70°24'00"	26°10'20"	Andesitic lava	220/09	300	600	5→20	100
* AT80	70°23'30"	26°10'30"	Basaltic lava	192/23	NRM→400	600	5→15	35→60
AT81	70°37'00"	25°44'00"	Brecciated lava	332/60	100→300	600	10	35
* AT82	70°36'00"	25°45'00"	Andesitic lava	352/30	NRM	480	3	20→45
* AT83	70°35'00"	25°44'00"	Andesitic lava	320/30	100→300	600	3	45
* AT84	70°35'00"	25°45'00"	Andesitic lava	356/44	NRM	650	NRM	100
* AT85	70°35'00"	25°45'00"	Andesitic lava	017/57	400	630	3	20
* AT86	70°35'00"	25°43'50"	Basaltic/andesitic lava	328/42	200	450	15	70
AT87	70°36'00"	25°47'00"	Basaltic/andesitic lava	350/17	NRM	580	10	100
* AT88	70°36'00"	25°47'00"	Andesitic lava	358/28	400	680	10	100
* AT89	70°36'00"	25°47'00"	Andesitic lava	356/22	150	540	20	100

Table 5.3. Sampling and demagnetisation data from sites in the La Negra Formation. Tilt correction is given in right-hand-rule format. ChRM isolation is demagnetisation level at which ChRM is isolated in the site, a range with an arrow indicates a within site variation.

Site	n/No	Uncorrected		Corrected		k	α_{95}
		Dec.	Inc.	Dec.	Inc.		
* AT69	11/11	26.0	-41.7	44.8	-55.1	70.6	5.5
AT70	6/8	152.6	63.6	294.9	69.3	73.9	7.8
AT71	6/9	291.1	-4.9	293.8	14.4	188.4	4.9
* AT72	8/9	234.4	7.1	227.7	30.6	40.0	8.9
AT74	9/11	171.1	7.5	169.6	10.2	171.9	3.9
* AT75	5/9	40.6	9.6	40.1	-12.2	13.3	21.8
* AT76	9/18	2.2	-48.3	60.9	-42.2	17.0	12.9
AT77	5/7	277.1	-48.0	265.6	-57.8	77.4	8.8
* AT78	12/19	33.4	-37.2	45.5	-45.6	38.0	7.1
* AT79	19/19	211.4	43.2	221.2	43.3	74.7	3.9
* AT80	8/11	54.1	-42.2	31.6	-54.3	38.8	9.0
AT81	7/7	24.4	-60.0	270.9	-50.9	32.6	10.7
* AT82	8/9	241.1	1.5	237.9	29.3	43.9	8.6
* AT83	7/9	225.5	18.8	223.5	48.7	22.3	13.6
* AT84	6/7	25.9	-5.0	15.0	-24.0	17.2	16.9
* AT85	7/7	231.7	-23.6	236.4	12.7	85.2	6.7
* AT86	4/6	25.6	16.5	25.3	-18.8	59.1	23.2
AT87	7/7	286.7	15.4	290.2	30.3	133	5.3
* AT88	7/7	50.7	4.3	48.2	-18.1	34.6	10.4
* AT89	7/7	43.4	-38.2	25.8	-52.2	76.2	7.3
Mean	14/20	40.2	-17.0			8.1	14.9
				42.0	-35.5	17.9	9.6

Table 5.4. Remanence data from the La Negra Formation. n/No. is number of samples included in site mean/ number of samples demagnetised; dec. and inc. are declination and inclination of remanence vector; k is Fisherian precision parameter; α_{95} is size of 95% cone of confidence. Sites marked * are included in formation mean.

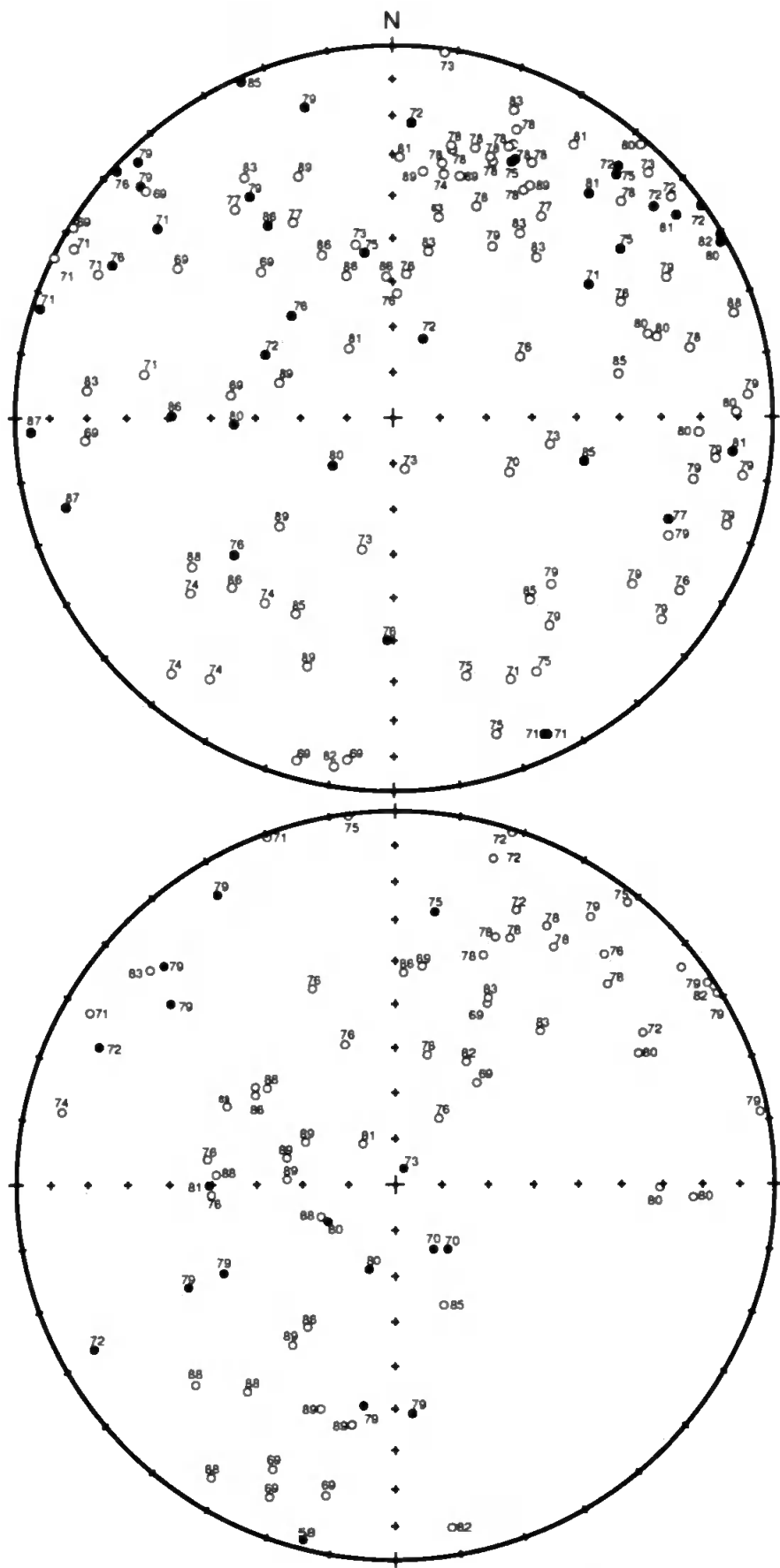


Figure 5.12. Equal area stereographic projection of low and intermediate coercivity and unblocking temperature components from the La Negra Formation. a) Components up to 25 mT and 250 °C. b) Intermediate components greater than 25 mT and 250 °C, but not ChRM. Directions are *in situ*, numbers are site numbers. Open (filled) points on the stereonet are upper (lower) hemisphere projections.

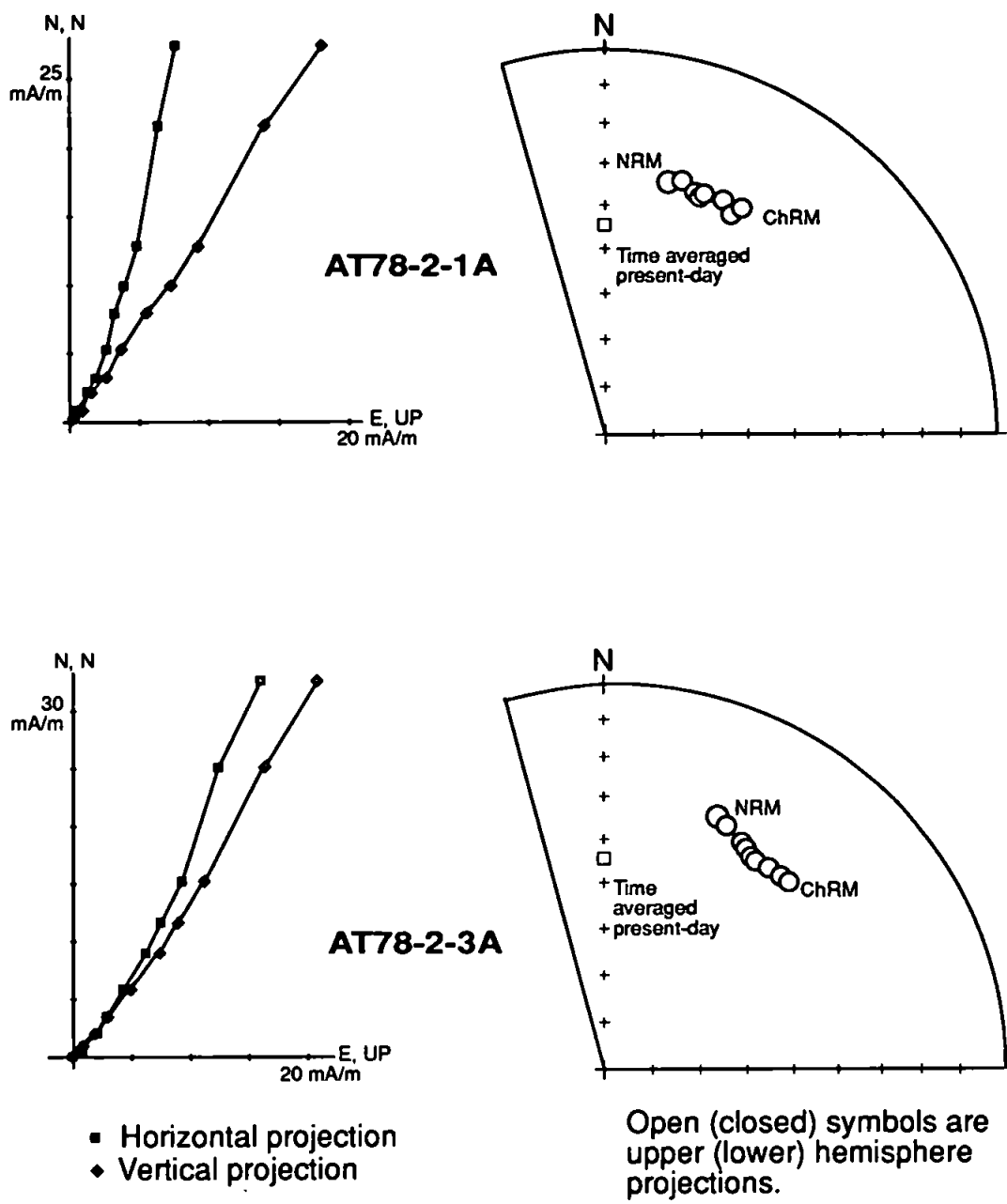


Figure 5.13. Zijderveld and equal area stereographic projections of two samples from site AT78 in the La Negra Formation. All plots are *in situ* coordinates, this is because the secondary component is likely to be post-folding. In addition, the tilt correction for this site is small, and causes only a small change in the direction of magnetisation.

After tectonic correction the ChRM from 14 sites give results with close agreement (Table 5.4, Figure 5.14). Of the six sites rejected five are from lava flows (AT70, AT71, AT74, AT77, AT87) and gave site mean directions unrelated to the formation mean, some of these also have small α_{95} confidence limits. Site AT70 is also unusual in that it has an exclusively haematite magnetic carrier. Site AT81 is from a brecciated lava and although its tilt corrected ChRM direction lies away from the main group its *in situ* direction is close to the tilt corrected formation mean direction.

The demagnetisation behaviour of the 14 sites included in the mean is variable and many have two or more components of magnetisation, which in some cases are overlapping. Examples of the demagnetisation are shown in Figure 5.15a-h. Three sites have single component demagnetisation similar to Figures 5.15 a and b. The majority of sites have two or more components of magnetisation and some sites have components with overlapping coercivities or unblocking temperatures. Examples of these are shown in Figures 5.15 c-h. In some sites the ChRM is only defined by high temperature/coercivity end points or remagnetisation circles.

The formation mean direction is given in Table 5.4 and shown in Figure 5.14 along with the site mean directions. Five of the sites have reversed polarity and there is no correlation between reversed sites and lithology or type of demagnetisation behaviour. The improvement in the precision parameter k on tilt correction ($k_1/k_2 = 2.21$, is greater than the statistically significant value of 1.94 at 95 % confidence level) passes the fold test of McElhinny (1964). The tilt corrected directions pass the reversal test of McFadden and McElhinny (1990) with a C classification at 95% confidence.

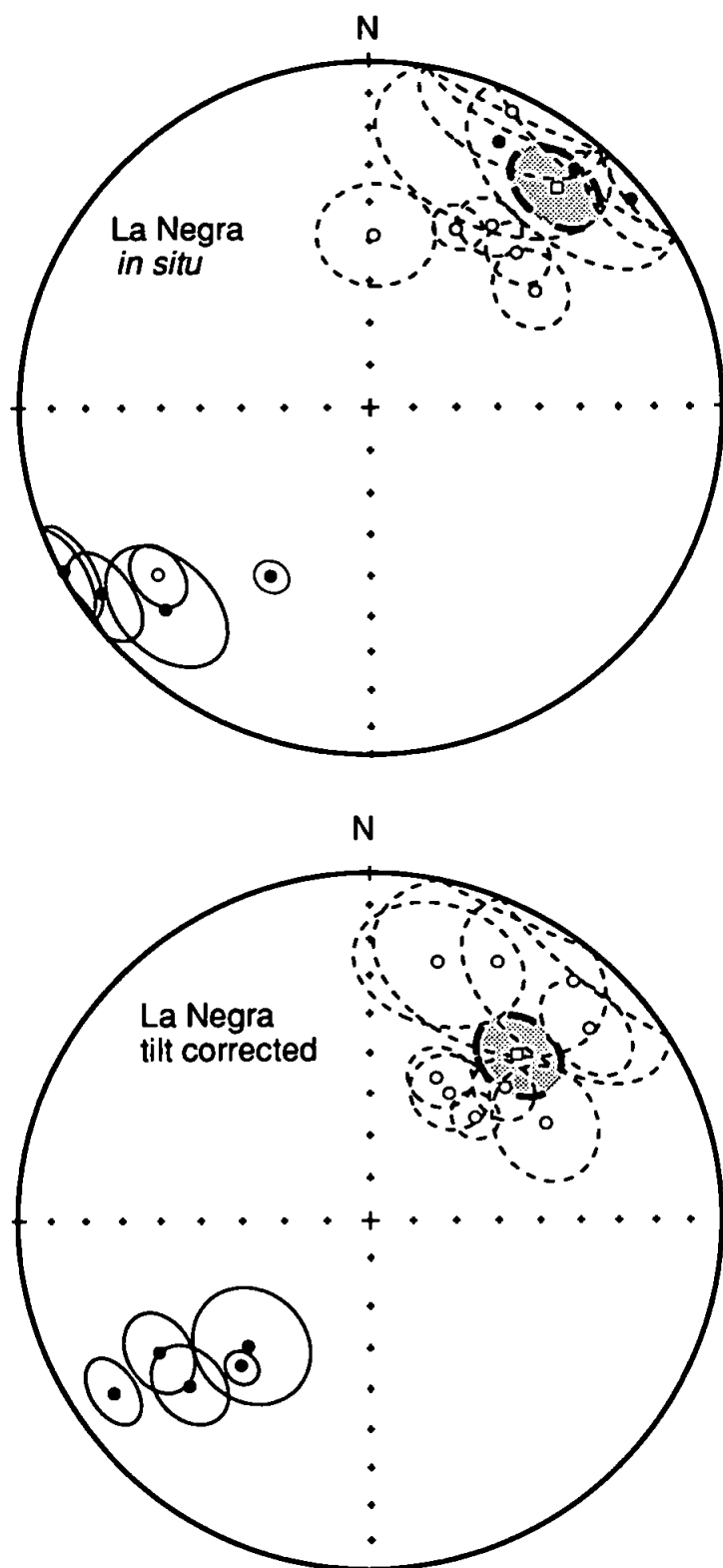


Figure 5.14. Stereographic projection of site mean directions from the La Negra Formation (circles) and the formation mean directions (square). Errors are α_{95} cones of confidence. Open (closed) symbols are upper (lower) hemisphere projections.

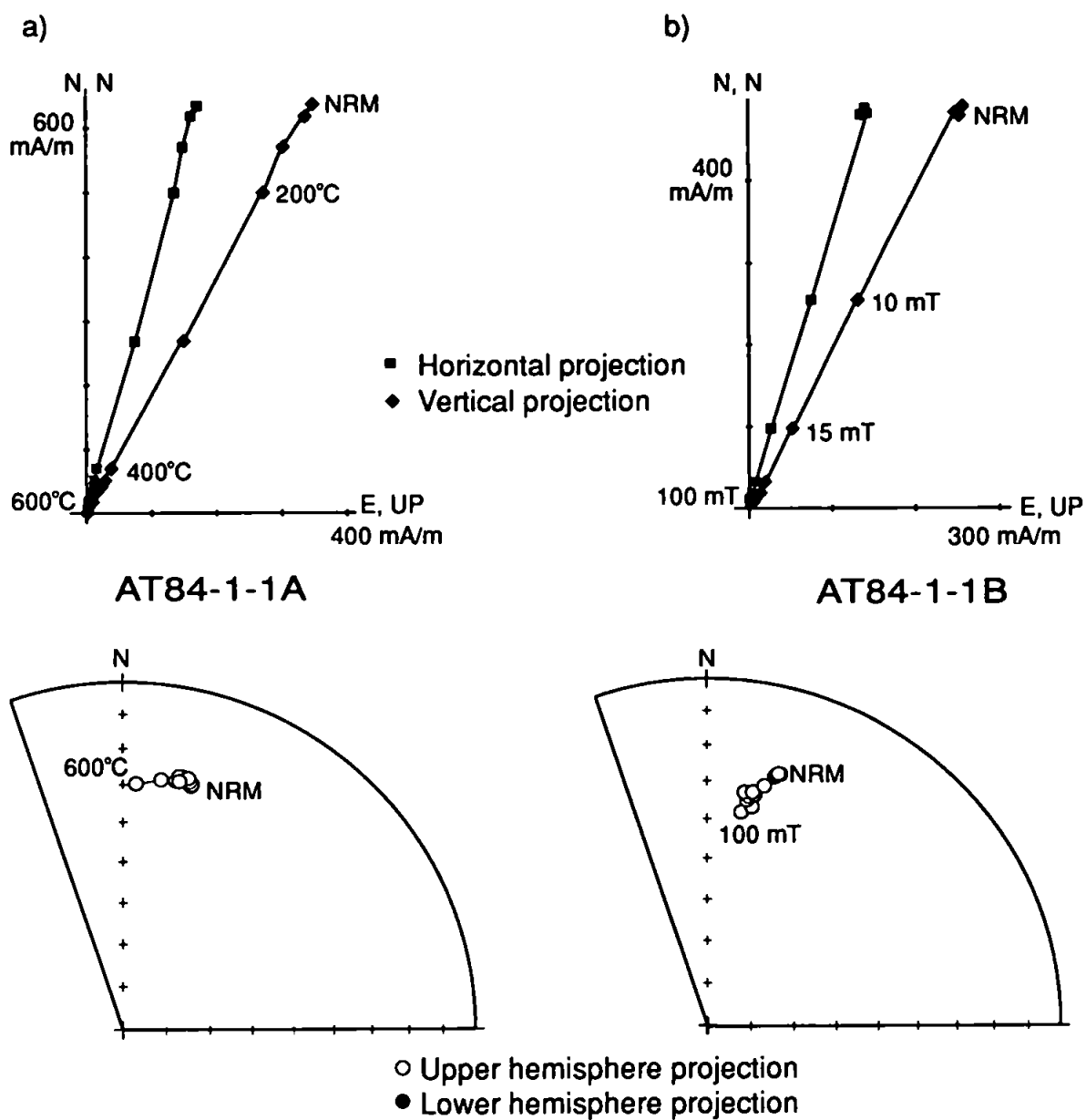


Figure 5.15a b. Examples of demagnetisation behaviour in samples from the La Negra Formation. Both plots show tilt corrected data

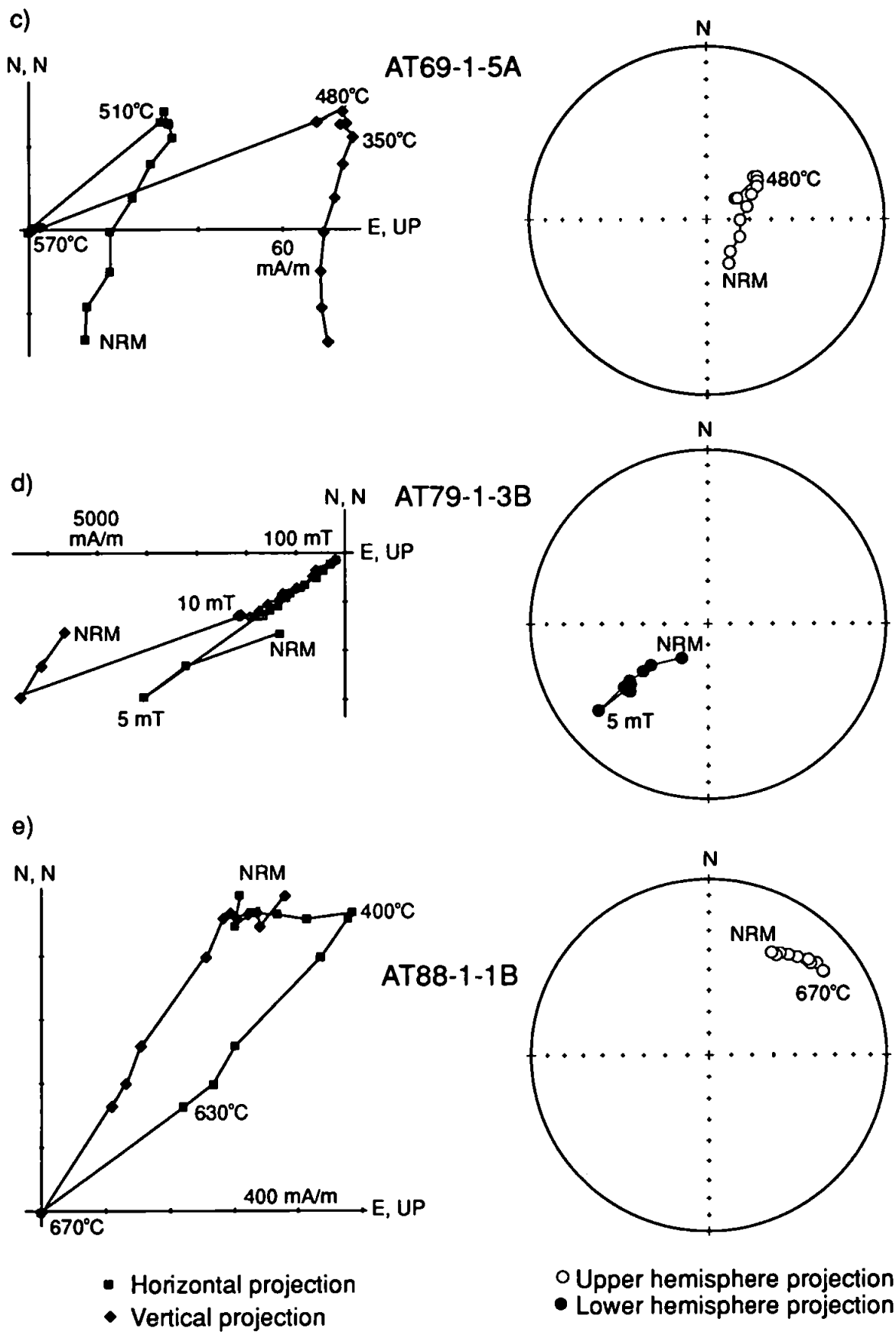


Figure 5.15c, d, e. Examples of demagnetisation behaviour in samples from the La Negra Formation. All plots show tilt corrected data.

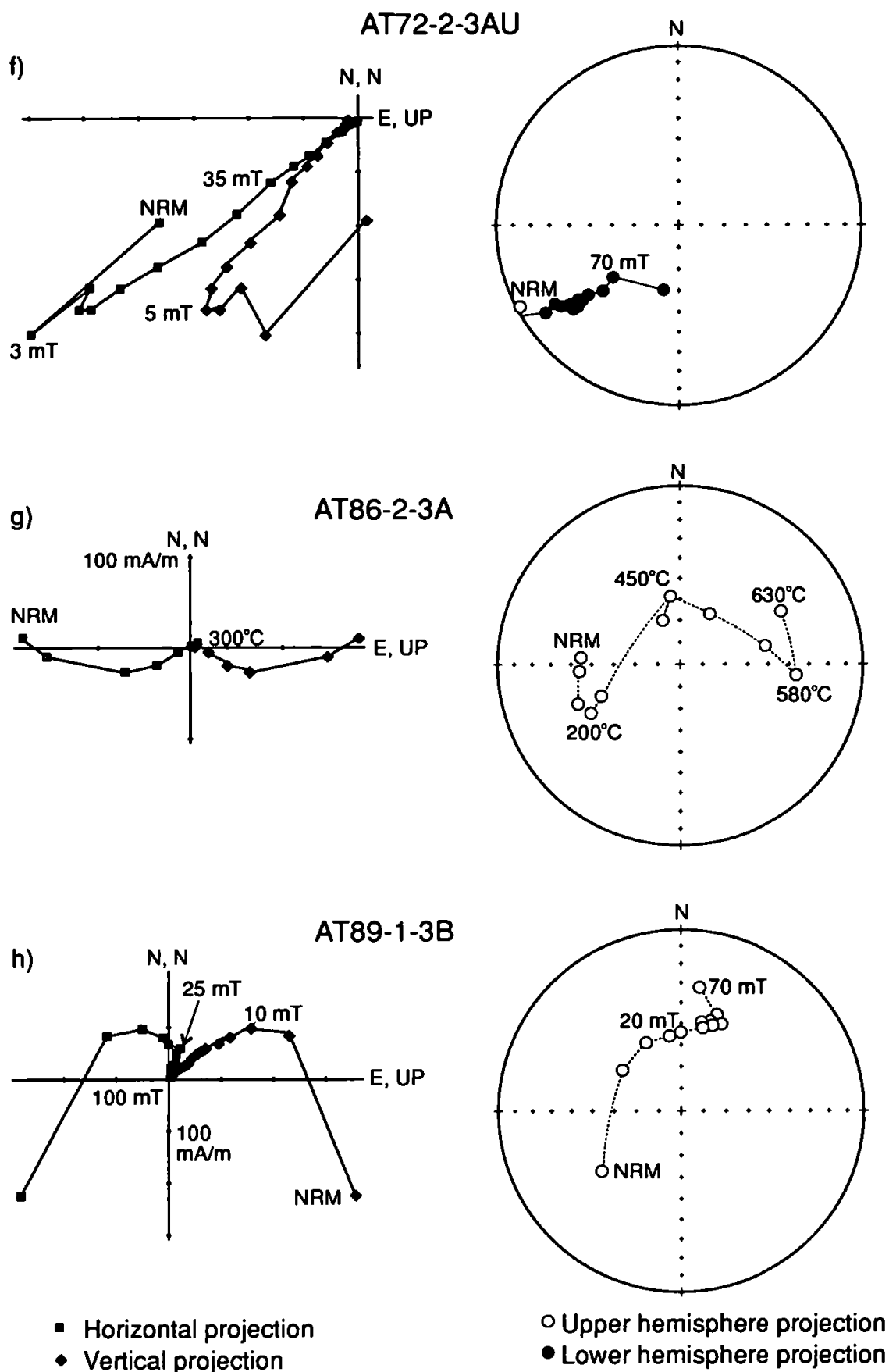


Figure 5.15f, g, h. Examples of demagnetisation behaviour in samples from the La Negra Formation. All plots show tilt corrected data.

v) Discussion of results

The mineralogical and rock magnetic studies indicate a complex mineralogy for the La Negra Formation, with the possibility of several types and generations of magnetic carriers. The formation has suffered alteration by hydrothermal fluids and/or low grade metamorphism and this has given rise to complex magnetisations in many of the samples. A ChRM can however, be extracted from the majority of samples. One of the excluded sites, AT81 has a tilt corrected ChRM direction which lies away from the main group, although its *in situ* direction is close to the tilt corrected formation mean direction. This would suggest a post-folding remagnetisation for this site. This is inconsistent with the positive fold test from the other sites in the formation. Site AT81 was collected from brecciated lava, and it is possible that the site has been preferentially remagnetised due to its higher permeability.

The presence of reversed sites and a positive reversal and fold test suggests that the ChRM is primary or certainly pre-folding in origin. Although the fold test is positive it is only just so. As stated in section 5.2.1 the La Negra Formation may have been folded as well as being tilted around horizontal axes on fault blocks. The low k_1/k_2 value may indicate a problem with simply tilt correcting the palaeomagnetic vectors by restoring the dips around a line of strike in this region. The restoration of the site mean vectors to the palaeohorizontal does, however, change the formation mean inclination from -17.0° to -35.5° , which is much closer to the inclination that would be expected at this site for any time since the Jurassic (see Chapter 3). This again indicates that the remanences are pre-tilting in origin.

The complex magnetisations and evidence for secondary magnetic minerals led Hartley *et al.* (1988) to suggest that the La Negra Formation had been remagnetised. They suggest that the remanence may be as young as Early Cretaceous, but is unlikely to be more recent. As the timing of the folding and tilting is not known this cannot be disproved

unequivocally by the positive fold test in this study area. The data presented here would, however, suggest that the remanence was acquired soon after deposition or extrusion. The formation mean direction is therefore compared with the Middle Jurassic reference direction and this indicates that the La Negra Formation has undergone a clockwise rotation of $40.0 \pm 11.5^\circ$, with a latitudinal displacement of $7.5 \pm 9.1^\circ$ northwards. This is a larger rotation than was recorded by Hartley *et al.* (1988) from the La Negra Formation near Antofagasta at approximately 24°S . Their rotation was $27.3 \pm 14.8^\circ$, when compared to the Middle Jurassic reference direction from Chapter 3.

5.4.2 Magnetic mineralogy of dyke samples

Although the magnetic mineralogy of the dyke samples is variable, they display common groups of behaviour. For this reason the magnetic mineralogy of all of the dyke swarms are considered together. A total of 20 representative samples, four from each swarm, have been submitted to IRM acquisition and demagnetisation. The behaviour generally falls into one of six groups represented by samples shown in Figure 5.16a-f. Sample AT20-1-1 (Figure 5.16a) shows a rapid rise in IRM but identifying saturation is difficult due to noise in the measurements. This noise is only observed with samples of very high intensity where the fluxgate magnetometer is set to its least sensitive setting and therefore appears to be due to instrument error rather than sample instability. The IRM demagnetisation of sample AT20-1-1 shows a dominance of the low and intermediate coercivity components with unblocking temperatures in the range $100\text{--}540^\circ\text{C}$. Demagnetisation of the NRM is completed at 90 mT and 400°C with AF and thermal treatment respectively, although the remanence is much more stable to AF demagnetisation. The fairly rapid fall of both IRM and NRM during demagnetisation may be due to either a range of magnetite grain sizes being present, or a combined magnetite

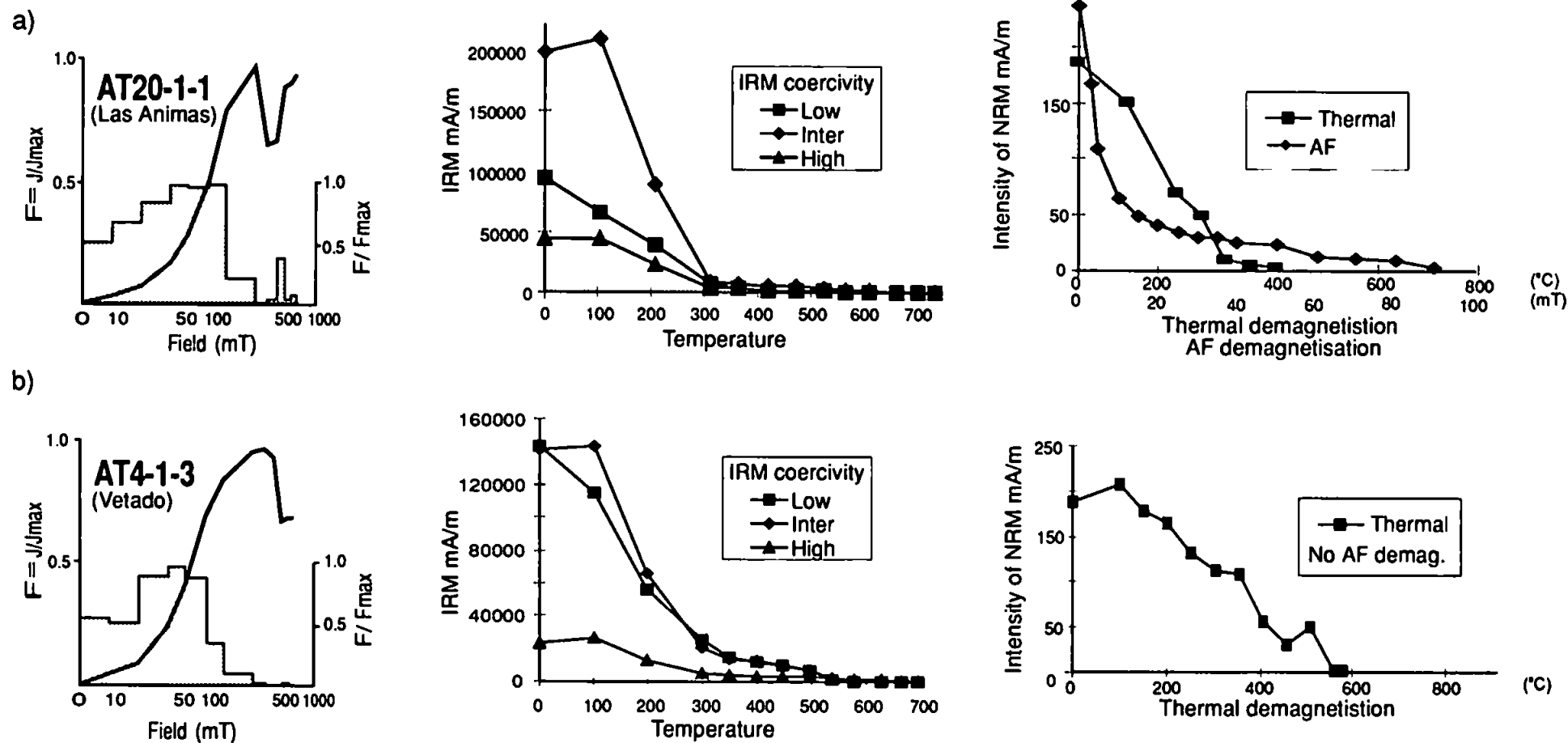


Figure 5.16a, b. Rock magnetic experiments on dyke samples. Graphs show acquisition of IRM, demagnetisation of three-axis IRMs and demagnetisation of NRM.

and titanomagnetite carrier. Typically, if a range of magnetite grain sizes is present, the demagnetisation trends in the IRM and NRM will be different, this is because the large multi-domain magnetite grains will carry an IRM but often not a significant component of NRM. As the demagnetisation of the IRM and NRM is similar in this sample, a mix of magnetite and titanomagnetite is most likely to be the carrier.

Most of the dykes fall into one of two categories, represented by samples AT4-1-3 and AT67-2-3 (Figures 5.16b, c). IRM acquisition rises rapidly and saturates at approximately 300 mT; again there are problems with instrument instability at high intensities in sample AT4-1-3. The IRM demagnetisation is dominated by the low and intermediate coercivity components, and both the IRM and NRM have unblocking temperatures in the range 100-580°C. This indicates a magnetite carrier for both the NRM and IRM. Comparisons of the IRM and NRM demagnetisation suggests that there may be a range of grain sizes and the presence of titanomagnetite in these samples.

During IRM acquisition, sample AT29-1-1 (Figure 5.16d) does not saturate in the 800 mT applied field. Although dominated by the intermediate coercivity IRM component there is also a significant high coercivity component present. The low and intermediate coercivity components are demagnetised in the range 100-580°C, dominantly 500-580°C while the high coercivity component is stable to 670°C. This suggests a mixture of both magnetite and/or titanomagnetite, and haematite are present in the sample. The demagnetisation of the NRM is incomplete, despite the sample being demagnetised to high levels. At high demagnetisation levels the magnetisation direction became unstable without a significant loss in intensity. This is most likely to be due to a significant viscous component in the sample.

Examples AT61-1-3 and AT46-1-3 showed more unusual behaviour which is difficult to explain. The NRM of sample AT61-1-3 (Figure 5.16e) is rapidly reduced by

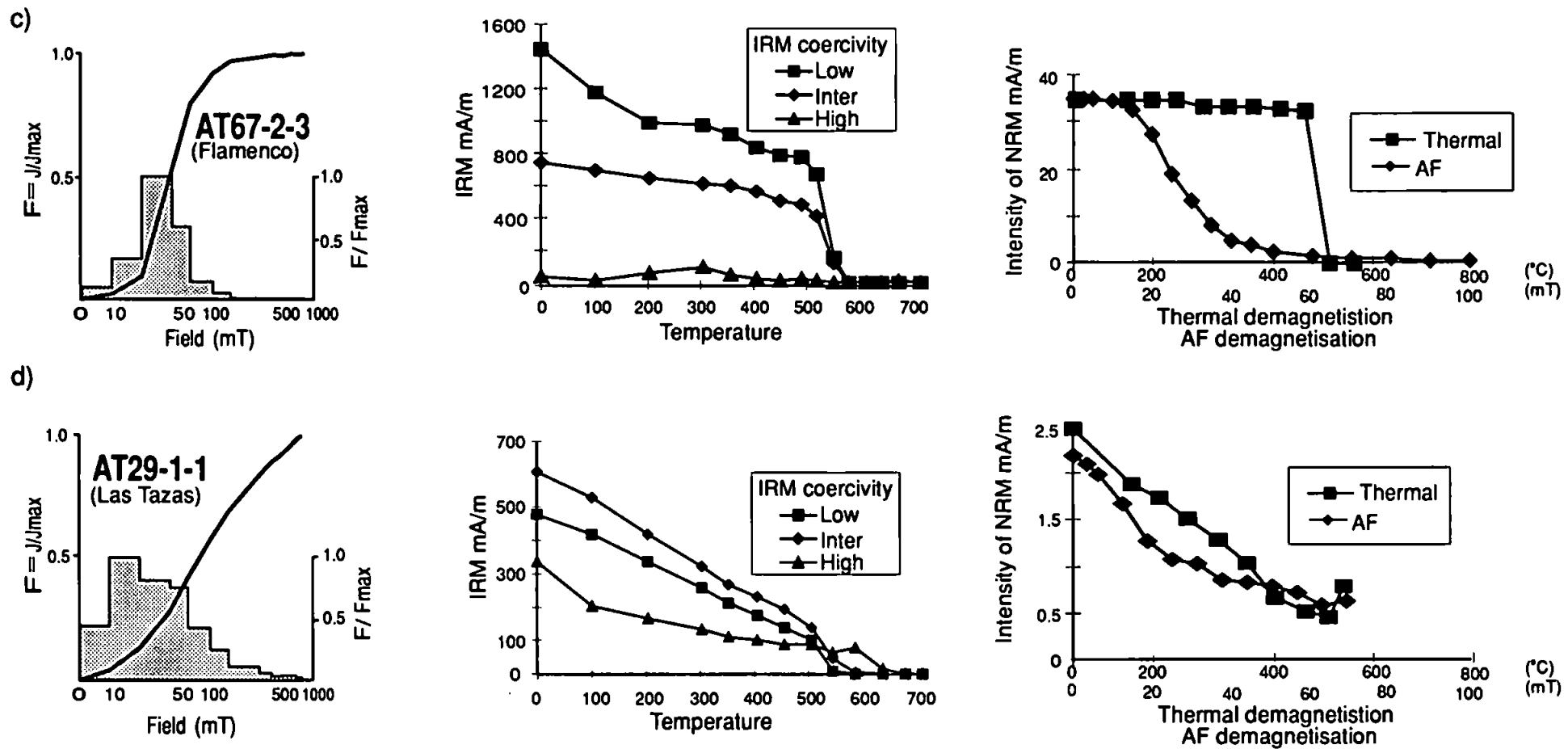


Figure 5.16c, d. Rock magnetic experiments on dyke samples. Graphs show acquisition of IRM, demagnetisation of three-axis IRMs and demagnetisation of NRM.

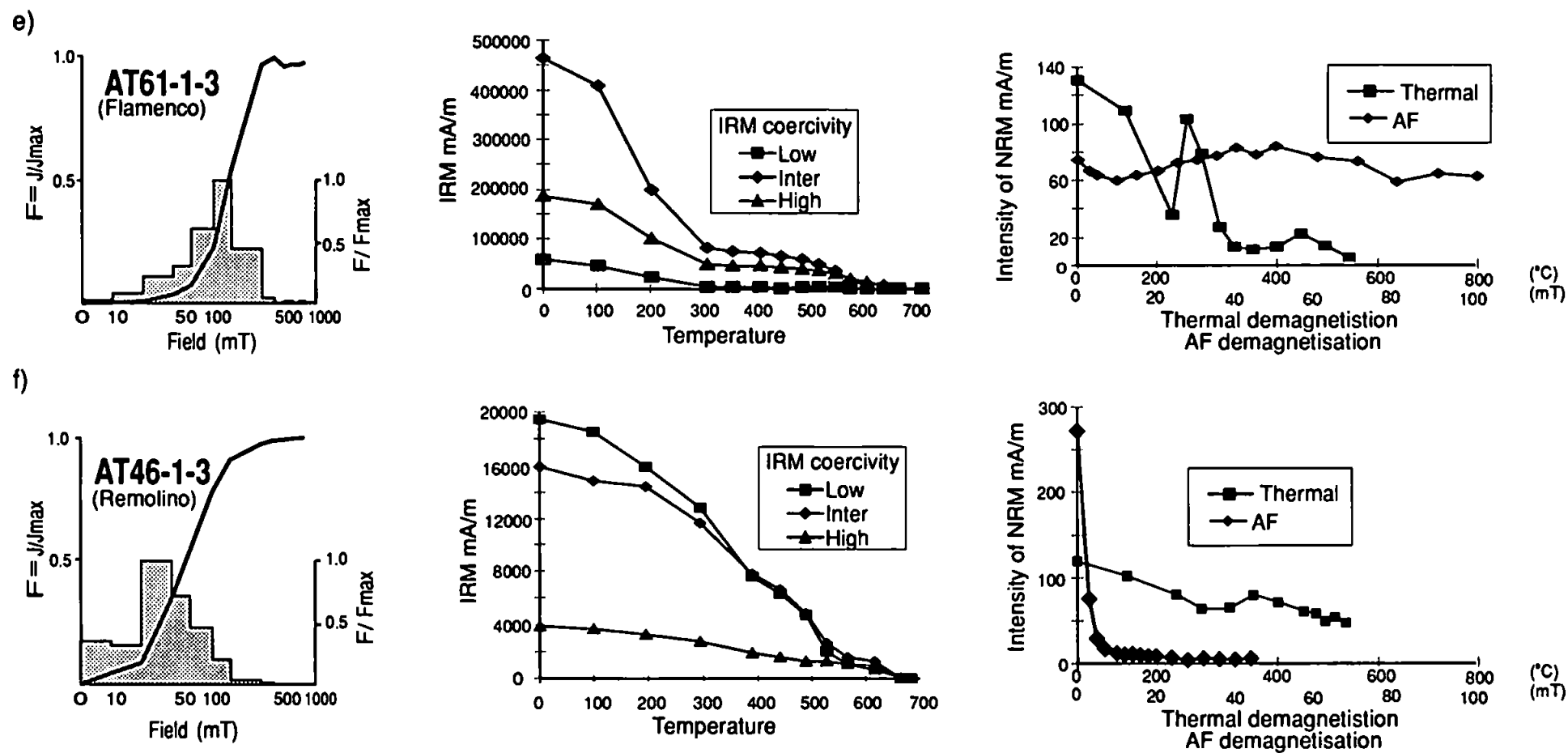


Figure 5.16e, f. Rock magnetic experiments on dyke samples. Graphs show acquisition of IRM, demagnetisation of three-axis IRMs and demagnetisation of NRM.

thermal demagnetisation to $\sim 400^{\circ}\text{C}$ whilst being unaffected by AF treatment. IRM acquisition rises fairly slowly and seems to plateau at ~ 300 mT, although it is noisy. The three IRMs are dominated by the intermediate and high coercivity components which show large intensity drops at $100\text{--}350^{\circ}\text{C}$ and $500\text{--}670^{\circ}\text{C}$. The inability to AF demagnetise the NRM, and the demagnetisation of IRM suggests a dominant high coercivity carrier, however, the IRM acquisition appears to indicate a significant low coercivity component. The cause of this behaviour is uncertain, but may be indicating the presence of maghemite or pyrrhotite (maximum coercivity 0.5-1 T, unblocking temperature 320°C). The IRM demagnetisation certainly indicates haematite, although this was not apparent in the NRM and the reason why the IRM acquisition seems to saturate at 300 mT cannot be explained.

The IRM acquisition of sample AT64-1-3 (Figure 5.16f) shows a fairly rapid rise in intensity which does not saturate in the 800 mT applied field. The demagnetisation behaviours of the IRM and NRM are extremely different. The IRM is dominated by the low and intermediate coercivity components which show significant intensity drops at 350°C , $500\text{--}570^{\circ}\text{C}$ and full demagnetisation at 670°C . This may indicate a combination of possible pyrrhotite, maghemite, magnetite and haematite in this sample. The thermal and AF demagnetisation of the NRM was carried out on two sub-samples from the same core, in one sub-sample the NRM is rapidly reduced to the noise level by AF treatment to 45 mT, typical of multi-domain magnetite, while the thermally demagnetised sub-sample loses only 50 % of its initial intensity up to 580°C before behaving erratically, suggesting that there may be a significant unstable haematite carrier in this sample. These NRM and IRM results may indicate complex magnetic mineralogy in these samples with large variations even within the same core.

The magnetic mineralogy experiments and demagnetisation of NRMs indicates a varied range of magnetic carriers, and probably a range of grain sizes in the dyke samples.

All of the dyke swarms show variation, and it is not possible to differentiate between the swarms on magnetic mineralogy. In most cases, a magnetite/titanomagnetite mix seems to dominate the samples, and samples also exhibit behaviour consistent with a range of grain sizes being present. This assemblage may be primary or a result of later secondary mineral growth. Evidence for secondary mineral growth is found in thin section where large opaque minerals are seen associated with small veins. Although the experiments suggest that pyrrhotite, haematite and maghemite are present, they rarely contribute significantly to the NRM. These minerals may also be secondary, possibly related to the hydrothermal activity and alteration in the rocks. Lucassen and Franz (1994) recognised low grade metamorphic assemblages from dykes which intrude plutons north of this sampling region, they note however that the metamorphism is not penetrative and is confined to areas around joints or faults.

5.4.3 Low and intermediate coercivity/unblocking temperature components in the dyke samples

In addition to the ChRM, samples from most sites collected from the dykes exhibit low and intermediate coercivity and unblocking temperature components. Although the directions of these components vary within both individual sites and the swarms overall, they generally fall into two categories. Firstly, some sites show within site scattering of the low components, indicating that they were gained after extraction from the host block and therefore represent a laboratory induced viscous remanence. Secondly, some sites have well grouped component directions which have negative inclination and lie in the northern part of the stereoplot. These most probably represent a VRM acquired in the present-day field direction prior to sampling. In some sites both of these components are observed in addition to the ChRM.

5.4.4 Dykes in the Vetado pluton

i) Palaeomagnetic sampling localities

A total of 16 sites were collected from dykes in the Vetado pluton (Figure 5.17). Most sites were collected from exposures in the area around the junction between the Pan American Highway and Quebrada del Salado and two sites (AT15 and AT16) were collected from further north at Portezuelo Blanco. Sites are numbered AT1-AT16 and all but the first three sites were collected as magnetically orientated hand samples. Sites AT1-AT3 were collected by drill core and orientated by magnetic compass.

ii) Palaeomagnetic remanence measurements

Of the 16 sites collected, ten have been demagnetised, all using the thermal technique. Details of sampling localities and remanence data are given in Table 5.5. All sites have low NRM intensities and show multi-component, often complex behaviour with the ChRM only being isolated in a narrow demagnetisation range (Table 5.5). Despite this, nine of the ten sites demagnetised have a stable remanence direction, site AT2 being excluded due to its high α_{95} .

A stereographic projection of the low unblocking temperature components is shown in Figure 5.18. Many of the sites appear to have both low and intermediate unblocking temperature components, however, in some cases the intermediate component is an artefact resulting from demagnetisation of two components with overlapping blocking spectra.

Of the nine sites which yield a stable direction, six have been used to calculate the formation mean (Table 5.5, Figure 5.19). The three rejected sites (AT1, AT5 and AT6) all have declinations $>20^\circ$ less than the formation mean, additionally, two of these are also characterised with high within site dispersion while the other has a very small α_{95} . The

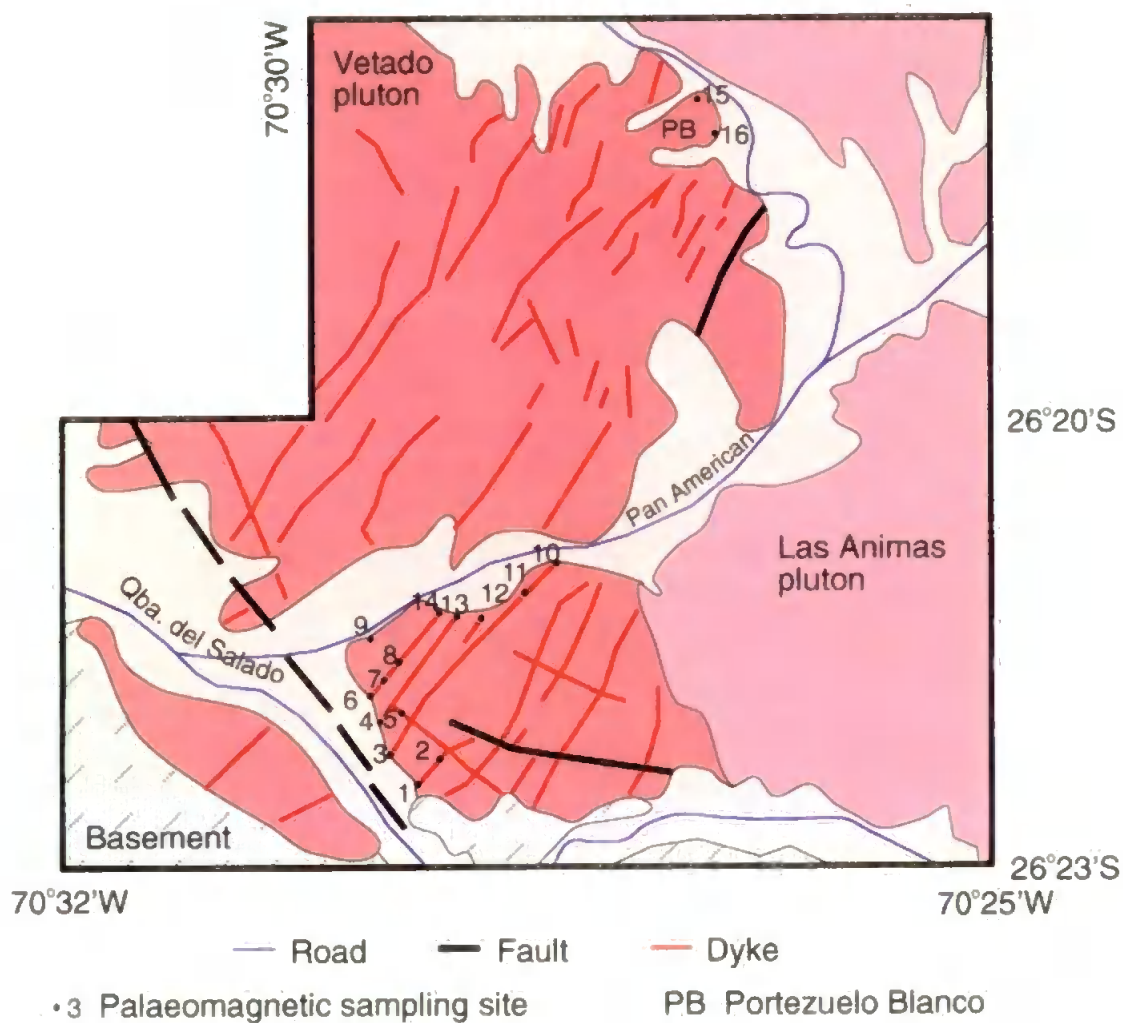


Figure 5.17. Palaeomagnetic sampling localities from dykes in the Vetado pluton. Redrawn from Mercado (1978) and Naranjo (1978).

Site	Sampling site		n/No.	Dec.	Inc.	k	α_{95}	ChRM isolation °C	
	Long. W	Lat. S						Minimum	Maximum
AT1	70°29'30"	26°22'30"	4/6	18.0	-34.7	24.2	19.0	100	450→510
AT2	70°29'30"	26°22'30"	4/6	56.5	-45.8	11.7	29.6	200 or 510	400 570
* AT3	70°29'40"	26°21'35"	5/6	58.0	-52.8	69.0	9.3	~200	400
* AT4	70°29'45"	26°21'45"	6/6	42.4	-31.3	12.7	20.8	300	500
AT5	70°29'45"	26°21'45"	4/6	12.4	-58.2	834.4	3.4	150	630
AT6	70°30'00"	26°21'50"	6/6	18.2	-41.2	13.6	18.8	300	350→500
* AT7	70°30'00"	26°21'50"	5/6	247.6	60.6	585.6	4.6	100 or 350	350 510
* AT8	70°30'00"	26°21'50"	6/6	54.8	-49.9	37.0	12.4	150	400
* AT10	70°29'00"	26°21'45"	6/6	26.5	-60.2	37.4	11.9	400	570
* AT11	70°29'00"	26°21'45"	6/6	226.4	39.0	32.9	12.3	100→400	540
Mean			6/10	48.9	-49.6	31.9	12.1		

Table 5.5. Sampling and demagnetisation data from dykes in the Vetado pluton. n/No. is number of samples included in site mean/number of samples demagnetised; dec. and inc. are declination and inclination of remanence vector; k is Fisherian precision parameter; α_{95} is semi-angle of 95% cone of confidence. ChRM isolation is demagnetisation level at which the ChRM is isolated in the site, a range with an arrow indicates a within site variation. Sites marked * are included in formation mean.

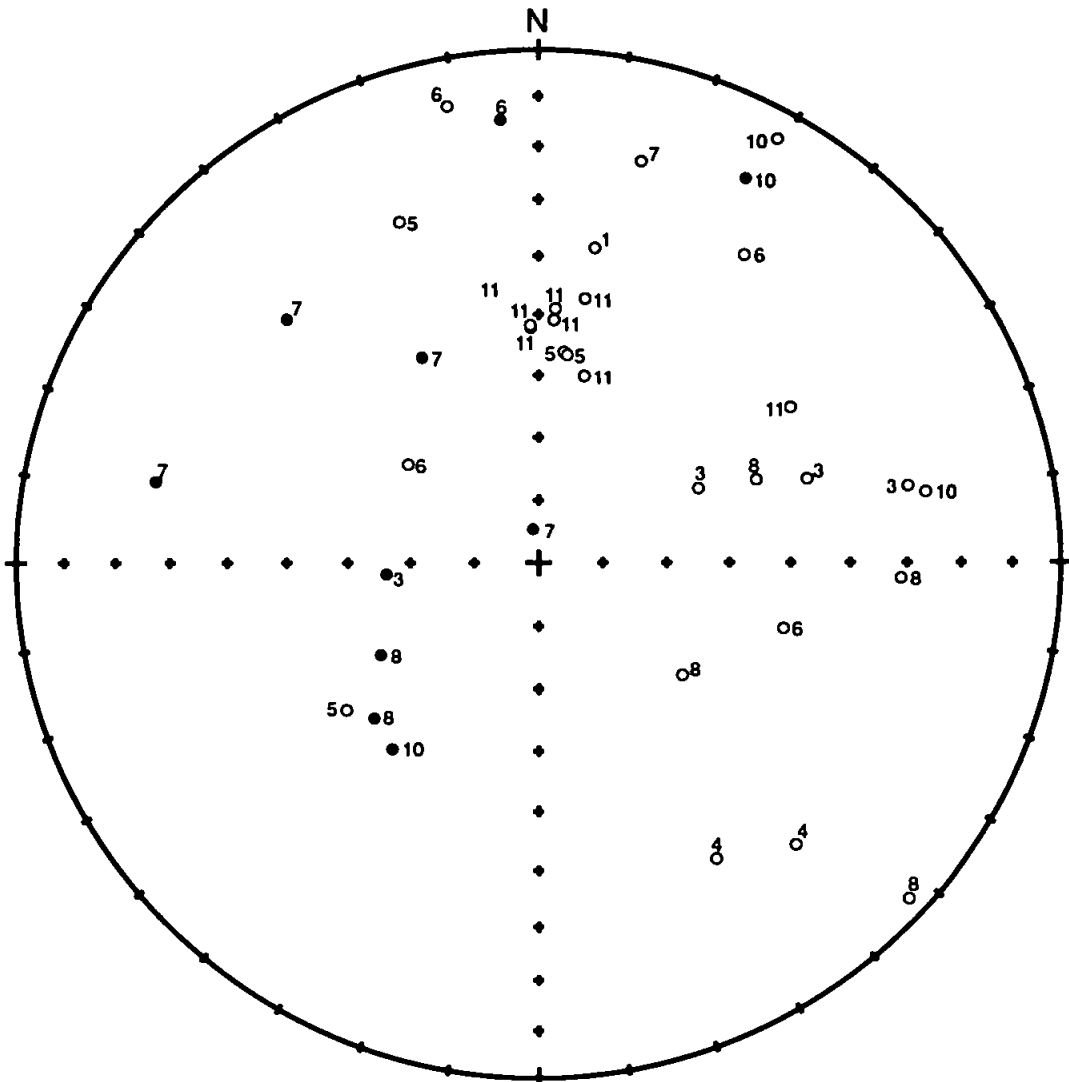


Figure 5.18. Equal area stereographic projection of low unblocking temperature components from dykes in the Vetado pluton. Open (closed) points are upper (lower) hemisphere projections. Directions are *in situ* and there are no tilt corrections for the dykes. Numbers are site numbers.

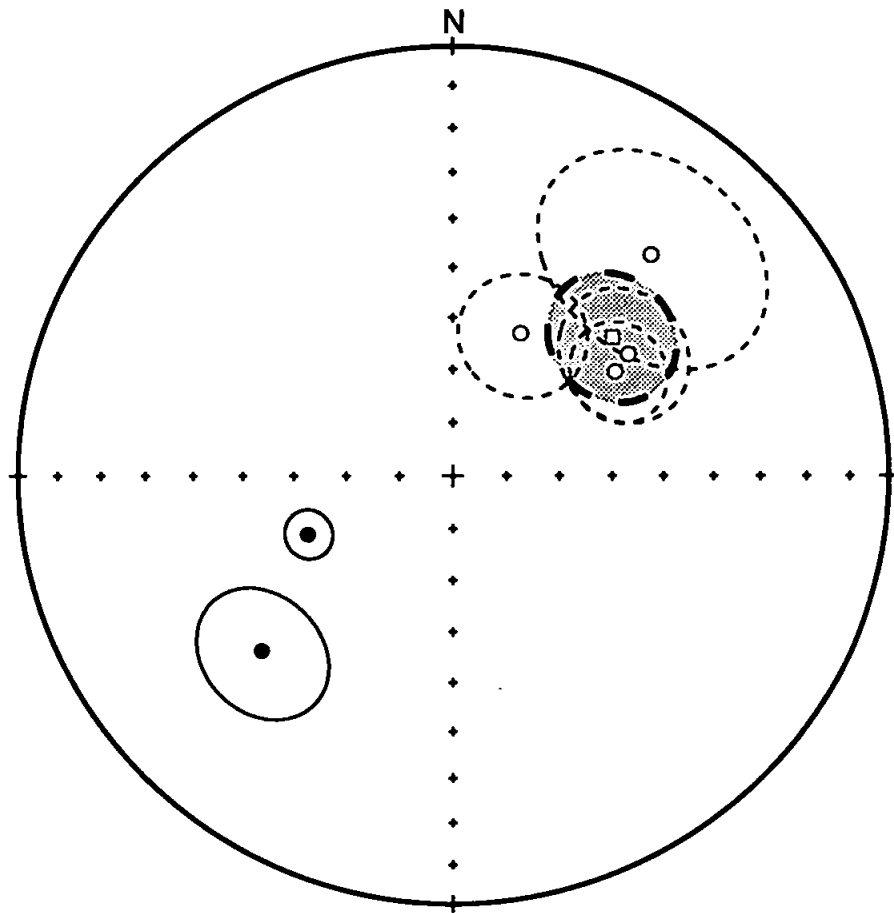


Figure 5.19. Equal area stereographic projection of site mean directions from dykes in the Vetado pluton (circles) and the formation mean directions (square). Error ellipses are 95% confidence. Open (closed) symbols are upper (lower) hemisphere projections

demagnetisation behaviour of these sites is generally single component and therefore less complicated than the other sites demagnetised from these dykes.

Examples of the demagnetisation behaviour observed in the six sites included in the mean are shown in Figure 5.20a-d. Most of the samples exhibit multiple component magnetisations (e.g., Figures 5.20a, b, d), and in some cases the ChRM is defined by end points and remagnetisation circles. Samples from some sites seem to have both normal and reversed polarity within the same sample. If present, the reversed component is only characterised by a great circle track of the last two or three data points (Figure 5.20d).

The formation mean direction is given in Table 5.5 and shown in Figure 5.19, along with the site mean directions. Two sites (AT7 and AT11) have reversed polarity, although some samples from these sites have both polarities present. If the reversed component is observed, it is always the highest unblocking temperature component

iii) Discussion of results

The poor within site grouping of the low unblocking temperature components suggests that laboratory induced viscous remanences are present in these samples. The low unblocking temperature components from sites AT1, AT11 and some from AT5 probably represent a present-day directed VRM.

The results show that although the magnetisation of the samples is complex, a stable ChRM is obtained from the majority of sites. Three sites are rejected due to there anomalously low declination. These sites lie close to a fault (Figure 5.17) and also close to a large, cross-cutting dyke which is not typical of the others in this part of the pluton, it is brown, and has an anomalous NW trend. These sites may have therefore been remagnetised by fluid flow during fault motion, or later dyke emplacement. The reason why other sites from the same area do not show the remagnetisation is unknown, but it

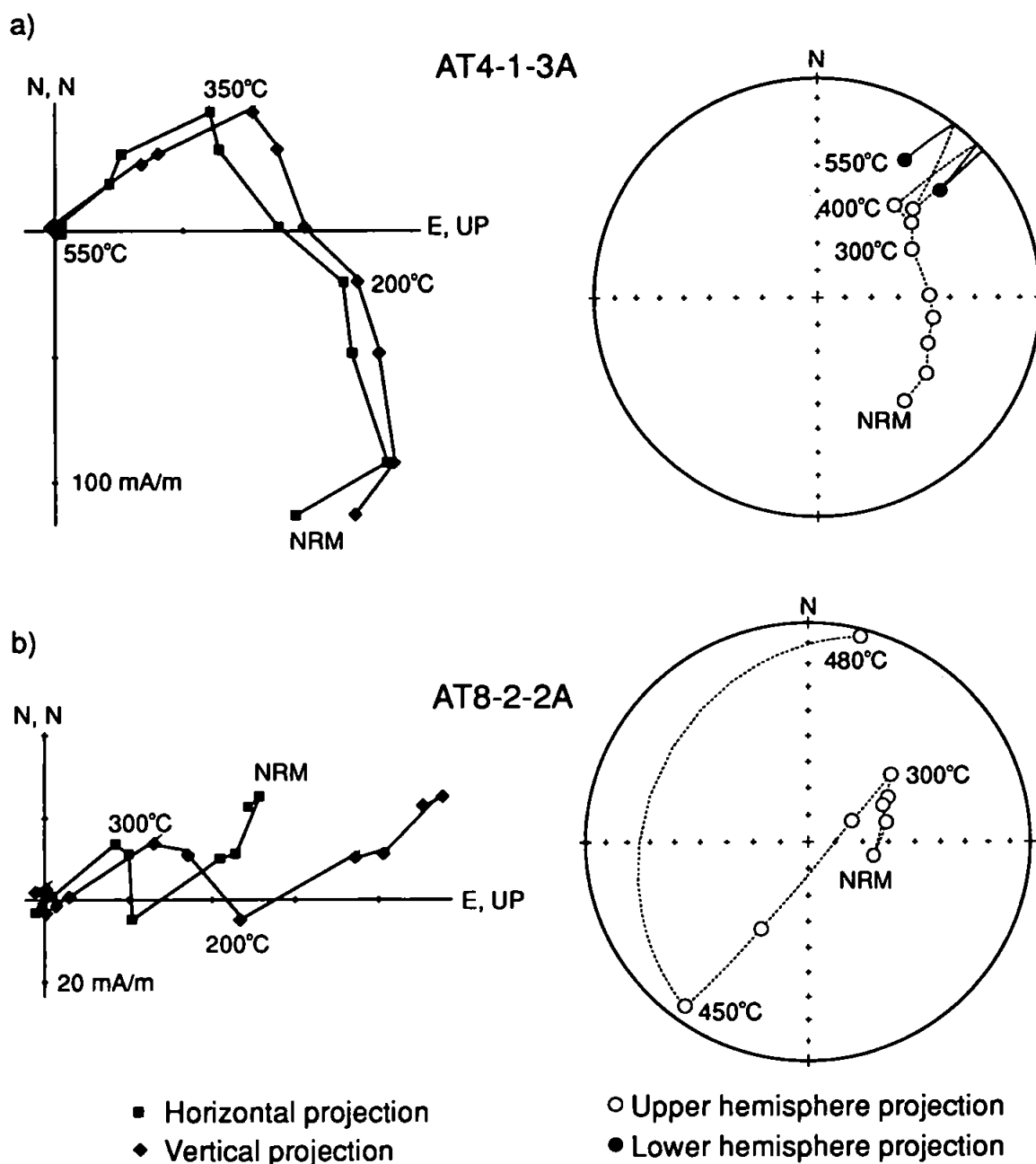


Figure 5.20a, b. Examples of demagnetisation behaviour in dyke samples from the Vetado pluton.

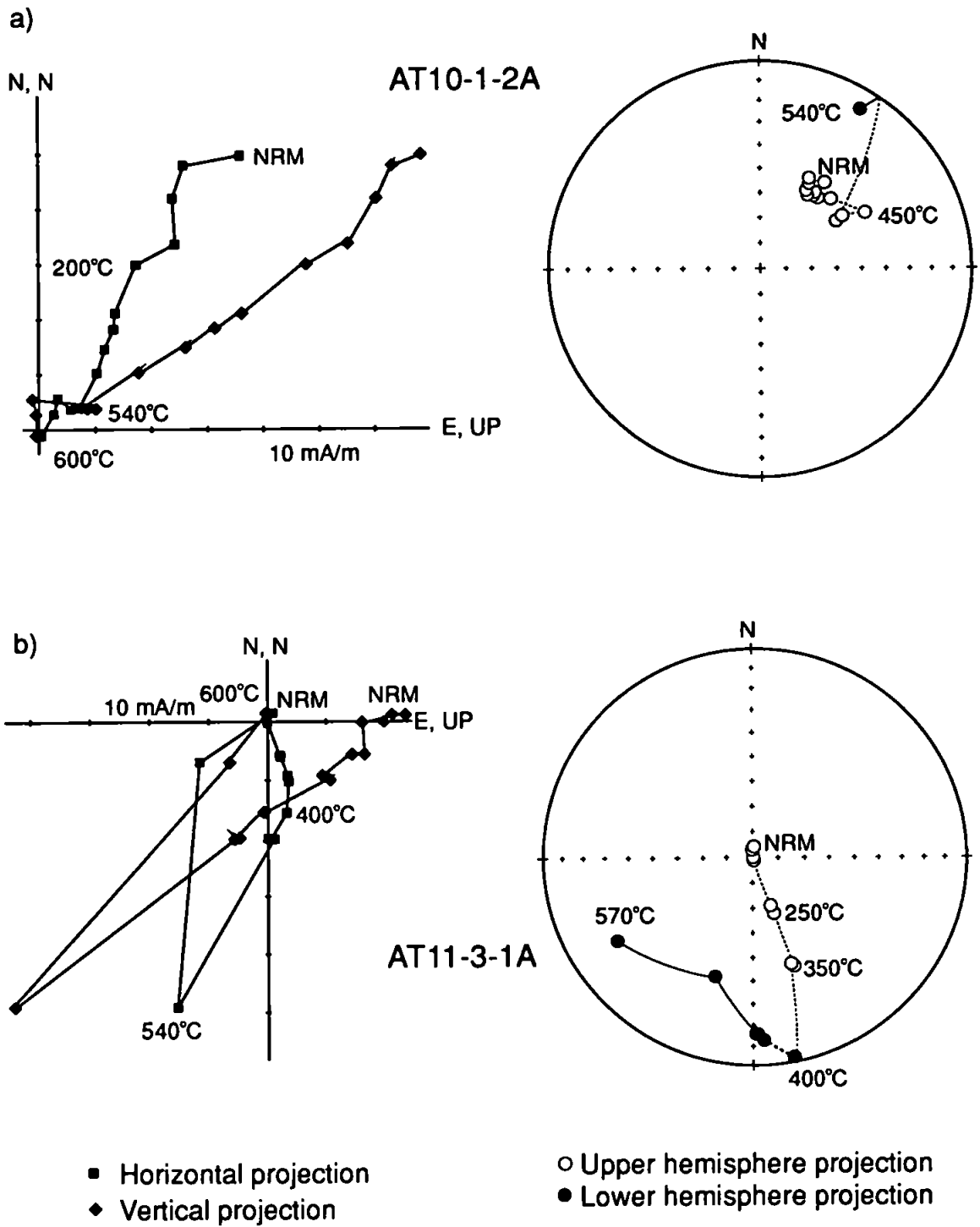


Figure 5.20c, d. Examples demagnetisation behaviour in dyke samples from the Vetado pluton.

may be related to the samples mineralogy, or the dykes may have been more jointed, aiding more pervasive remagnetisation. The presence of reversed samples is evidence that extensive and rapid remagnetisation of the dyke swarm as a whole is unlikely, and that the ChRM is an ancient remanence. The samples which exhibit antiparallel components seem to be characterised by magnetite or titanomagnetite carriers and the change in direction occurs in the range $\sim 480\text{--}570^\circ\text{C}$. Given the mineralogy and the temperature range, self reversal, particularly as a result of a pyrrhotite magnetic carrier seems unlikely. The data are consistent with the samples having cooled through a reversing magnetic field and this is further evidence that the remanence is ancient, and probably primary.

As discussed in Section 5.2.1, the dykes in the Vetado pluton are probably Early Jurassic in age. Comparison of the mean direction with the reference direction indicates a clockwise rotation of $46.9 \pm 16.5^\circ$ with southward translation of $6.6 \pm 10.8^\circ$.

5.4.5 Dykes from the Flamenco pluton

i) Palaeomagnetic sampling localities

Eight sites were collected from dykes within a small area of the Flamenco pluton, just south of Quebrada Flamenco as shown in Figure 5.21. All of the sites were collected as orientated hand samples. Site AT62 was collected from a dyke which had been dated as $155.5 \pm 0.6 \text{ Ma}$ ($^{39}\text{Ar}/^{40}\text{Ar}$; Dallmeyer *et al.*, 1996).

ii) Palaeomagnetic remanence measurements

Six sites of the eight collected have been demagnetised and the data are given in Table 5.6. Although all samples exhibit multi-component behaviour, the demagnetisation plots are generally less complex than those observed from the other plutons. All of the sites yielded a stable mean direction.

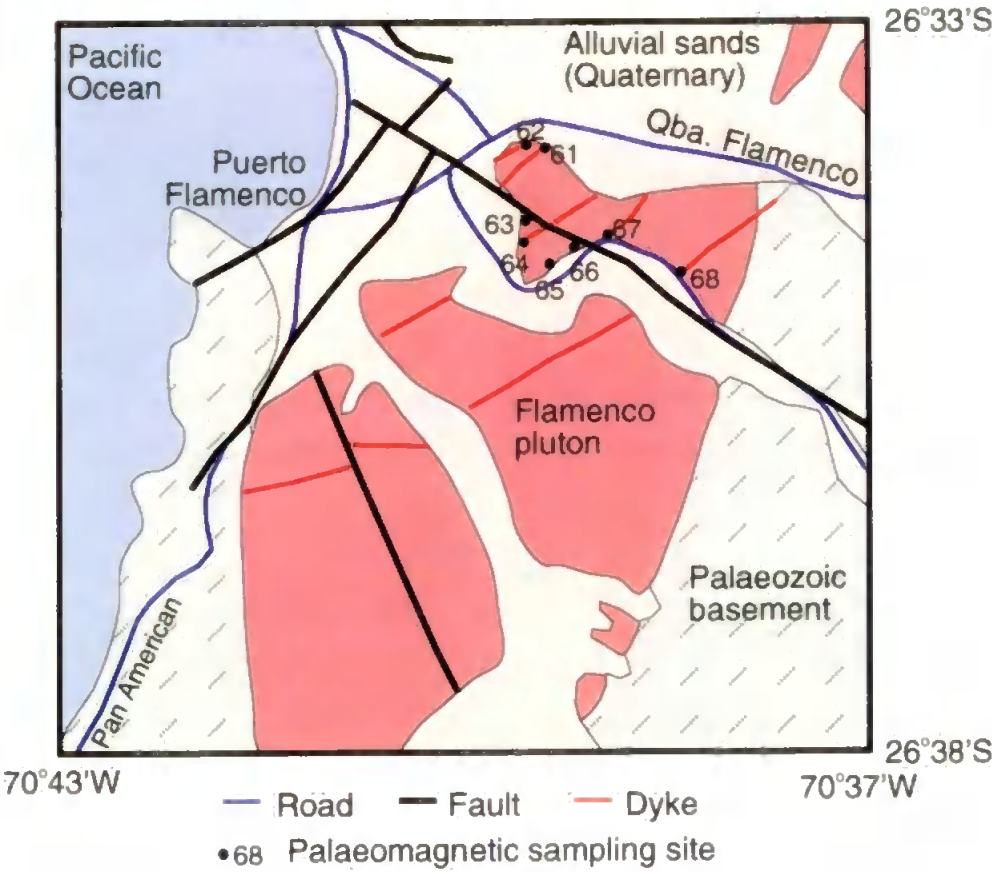


Figure 5.21. Sampling localities from dykes in the Flamenco pluton. Redrawn from Mercado (1978).

Site	Sampling site		n/No.	Dec.	Inc.	k	α_{95}	°C Min.	ChRM isolation		mT Max.
	Long. W	Lat. S							Max.	Min.	
* AT61	70°39'10"	26°33'50"	7/7	233.6	39.1	35.9	10.2	270	370→570	None	
* AT62	70°39'10"	26°33'50"	7/7	232.5	47.9	23.9	12.7	420	570	60	100
AT63	70°39'45"	26°34'10"	7/7	350.4	-67.8	39.5	9.8	100	540→600	10	25
* AT64	70°39'45"	26°34'15"	7/7	233.9	35.9	30.4	11.1	250	600	40	90
* AT66	70°39'00"	26°34'10"	7/7	29.0	-50.6	68.4	7.4	300	580	15	100
* AT67	70°38'45"	26°34'05"	7/7	46.8	-40.2	67.6	7.4	100→400	500	NRM	70
Mean			5/6	45.6	-43.0	76.3	8.8				

Table 5.6. Sampling and demagnetisation data from dykes in the Flamenco pluton. n/No. is number of samples included in site mean/number of samples demagnetised; dec. and inc. are declination and inclination of remanence vector; k is Fisherian precision parameter; α_{95} is semi-angle of 95% cone of confidence. ChRM isolation is demagnetisation level at which the ChRM is isolated in the site, a range with an arrow indicates a within site variation. Sites marked * are included in formation mean.

A plot of the low unblocking temperature and low coercivity components is shown in Figure 5.22, many demonstrate reasonable within site grouping. Some samples have low and intermediate components which are antipodal which, where present, are both removed by demagnetisation to 400°C or 40 mT.

Five of the six sites are used to calculate the formation mean (Table 5.6, Figure 5.23). The rejected site, AT63, is characterised by a single component of magnetisation, the mean having an anomalously steep inclination, while its declination lies away from the formation mean and closer to the present-day field direction. It may therefore represent a present-day overprint. Examples of the demagnetisation behaviour observed from the five sites included in the mean are shown in Figures 5.24a-d. Many sites have two components of magnetisation with an abrupt change in direction at 260°C-300°C or 25mT. In some cases the two components are antipodal (Figure 5.24a and d). Two sites, AT64 and AT66 have both normally and reversely magnetised samples, and in some of the sites the components of magnetisation appear to be overlapping. The change in direction between the two components is typically in the range 450°C-520°C or between the NRM and 20mT. An example of this behaviour is given in Figure 5.24c.

The formation mean direction is given in Table 5.6 and shown in Figure 5.23. It can be seen that three of the sites have reversed polarity, in most cases both polarities are present in these sites, but the reversed component dominates.

iii) Discussion of results

The low coercivity and unblocking temperature components in these sites represent present-day VRMs. The presence of the reversed samples, and particularly those which show within sample reversal may be evidence that the remanence was acquired soon after emplacement of the dyke. The magnetic mineralogy of the dykes from the Flamenco

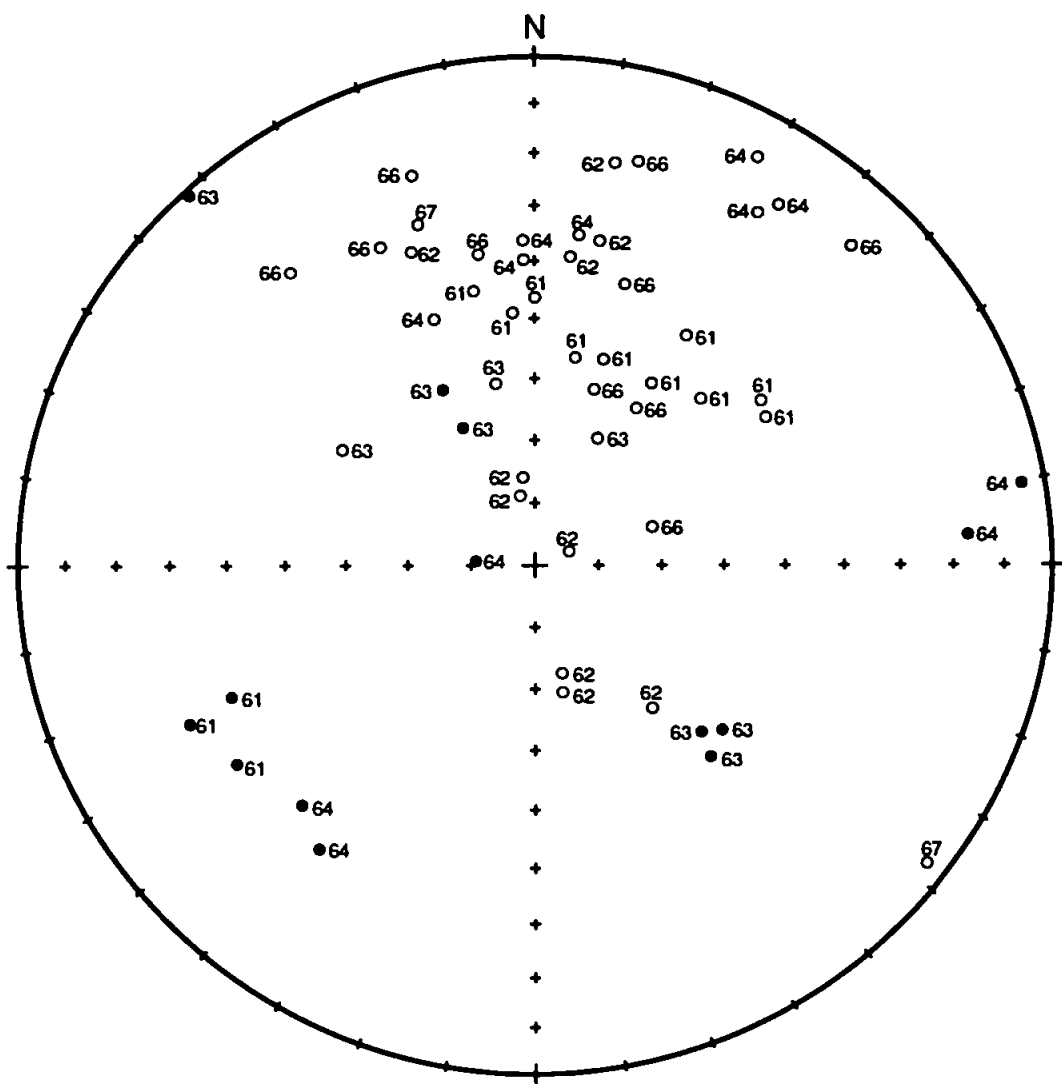


Figure 5.22. Equal area stereographic projection of low coercivity and unblocking temperature components from dykes in the Flamenco pluton. Open (closed) symbols are upper (lower) hemisphere projections. Directions are *in situ*, numbers are site numbers.

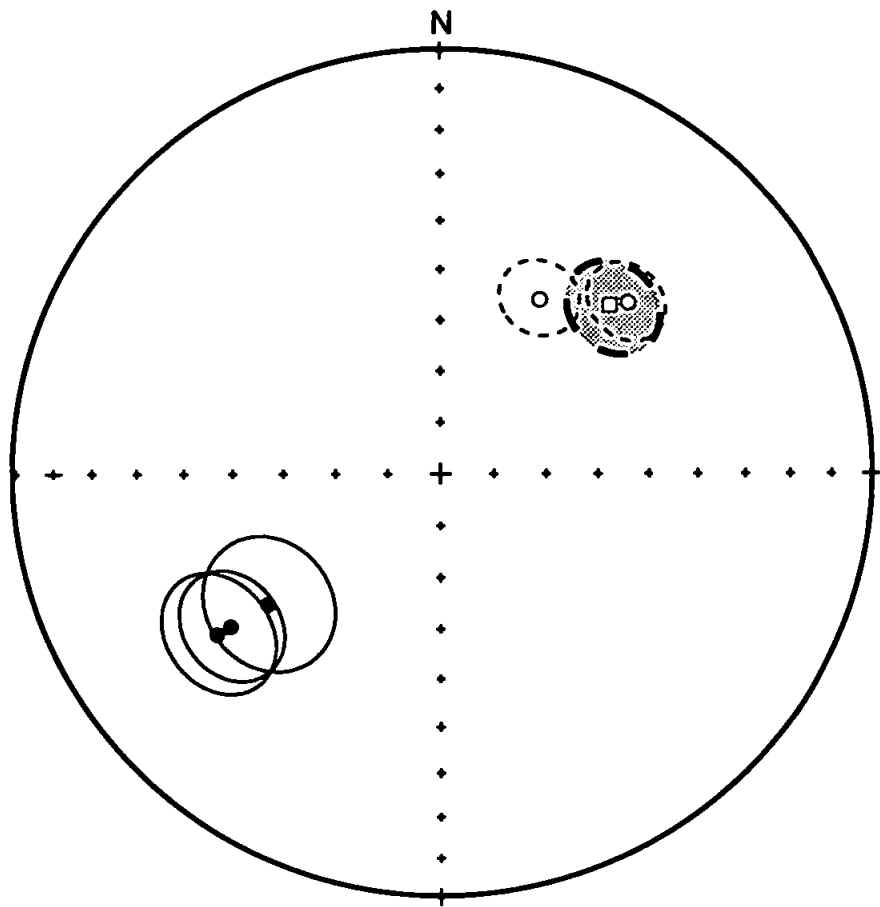


Figure 5.23. Equal area stereographic projection of site mean directions from dykes in the Flamenco pluton (circles) and the formation mean directions (square). Error ellipses are $\alpha 95$ cone of confidence. Open (closed) symbols are upper (lower) hemisphere projections.

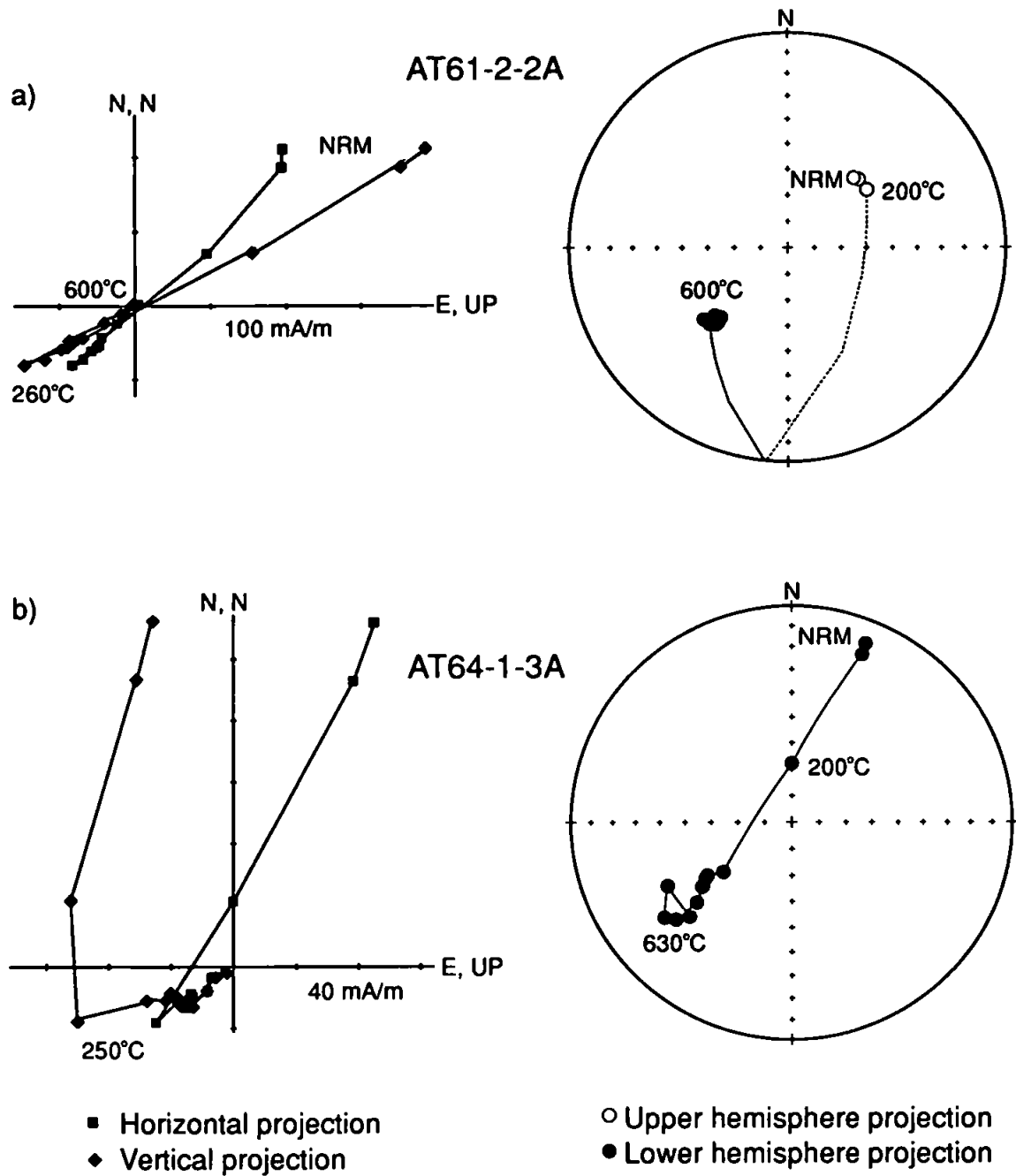


Figure 5.24a, b. Examples of demagnetisation behaviour in dyke samples from the Flamenco pluton.

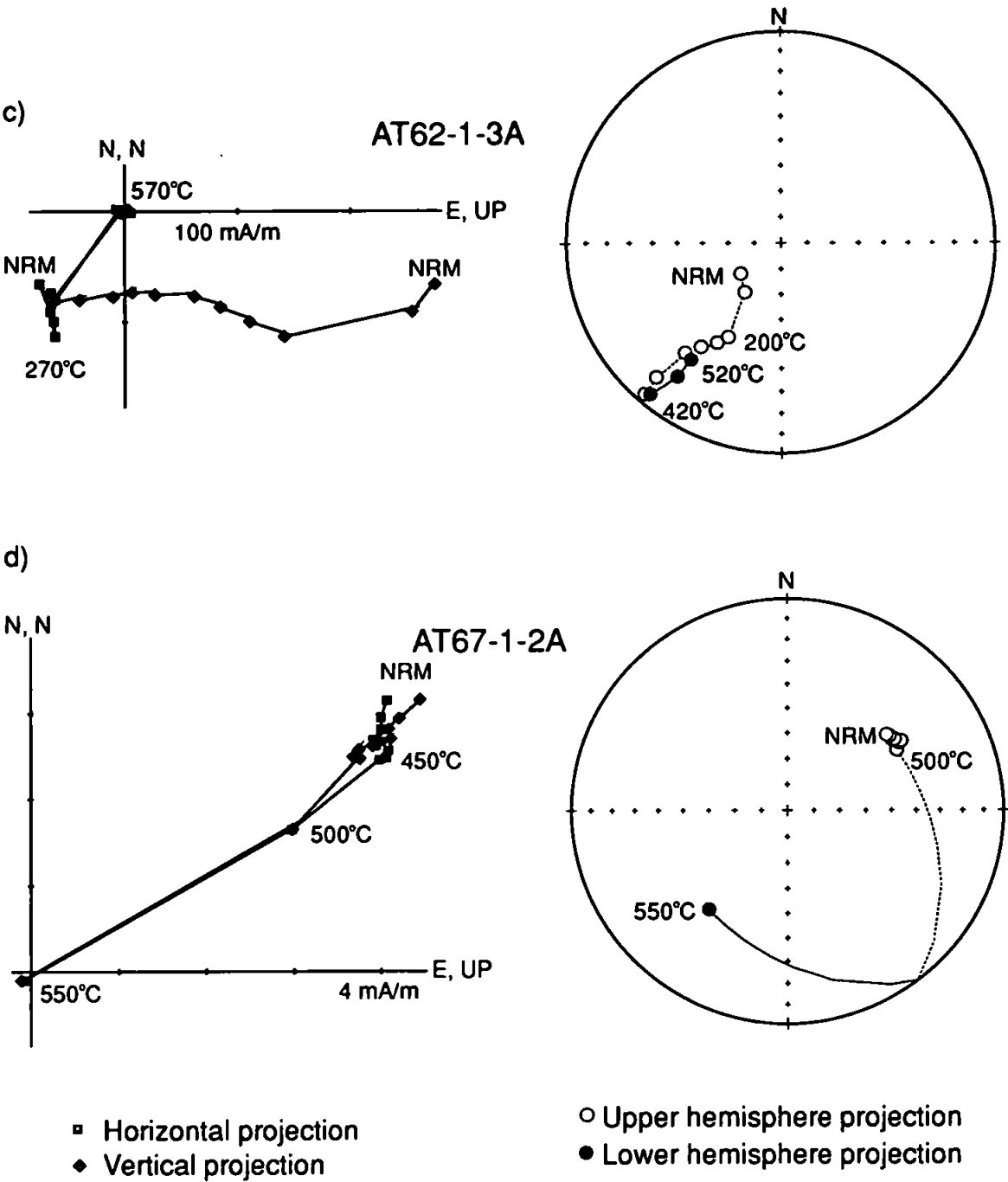


Figure 5.24c, d. Examples of demagnetisation behaviour in dyke samples from the Flamenco pluton.

pluton is dominantly magnetite or titanomagnetite, although haematite is more common than in any of the other dyke swarms. As shown by IRM experiments (Section 5.4.2) pyrrhotite may also be present in these dyke samples, and this could lead to self reversal of samples. If this were occurring, the reversal of the sample's direction should occur at about 320°C. The change in polarity in these samples tends to occur either in a range 250°C-300°C or above 450°C. This is interpreted as being more likely the result of the sample having cooled through a reversal of the Earth's magnetic field rather by self reversal of pyrrhotite.

The age date available for the dykes in the Flamenco pluton suggest that they are Late Jurassic in age. As no reliable reference direction is available for this period (see discussion in Chapter 3.4.1iii), the Middle Jurassic reference is used. Comparison of the mean direction from the five sites with the reference indicates a clockwise rotation of $43.6 \pm 11.7^\circ$, with no latitudinal transport, $0.0 \pm 8.5^\circ$.

5.4.6 Dykes from the Las Animas pluton

i) Palaeomagnetic sampling localities

Ten sites were collected from dykes in the Las Animas pluton as shown in Figure 5.25. Six of the sites (AT17-AT22) are from the northern part of the outcrop near the Pan American highway, the others were from the southern part of the same part of the pluton near Quebrada del Salado. All sites were collected as orientated hand samples.

ii) Palaeomagnetic remanence measurements

Of the ten sites collected six, those from the northern part of the exposure, have been demagnetised. A summary of the data from these sites is given in Table 5.7. All of the sites show multi-component behaviour and there is often substantial within site

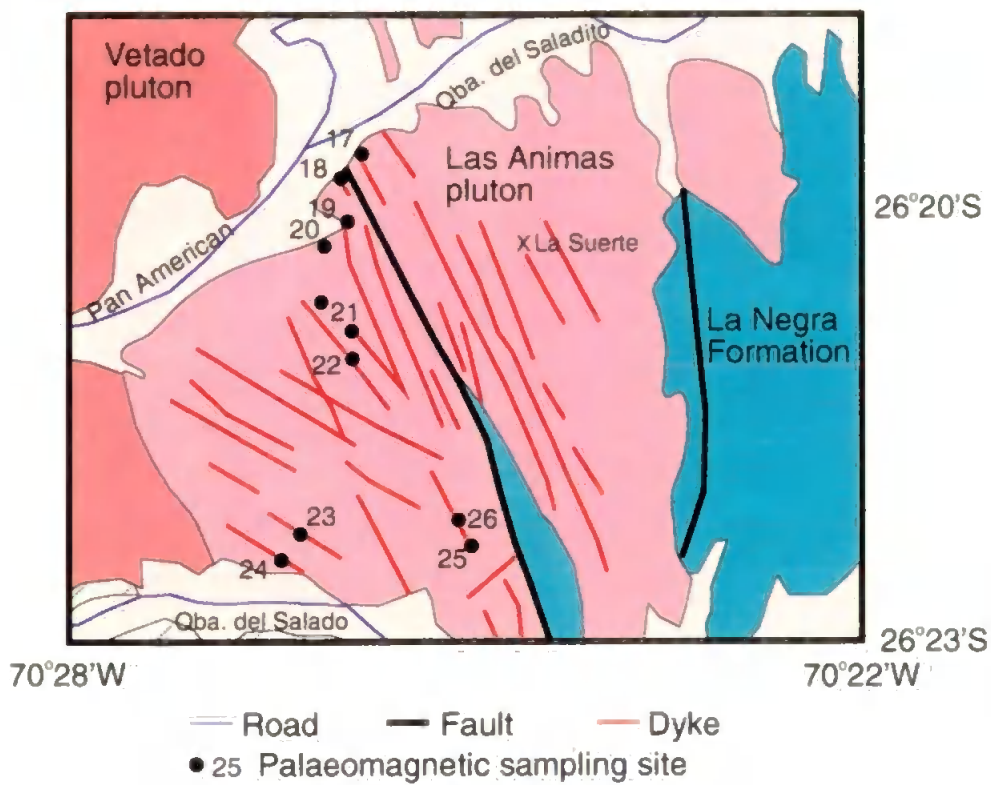


Figure 5.25. Sampling sites from dykes in the Las Animas pluton. Redrawn from Mercado (1978) and Naranjo (1978).

Site	Sampling site		n/No.	Dec.	Inc.	k	α_{95}	°C Min.	ChRM	isolation	mT Max.
	Long. W	Lat. S							Max.	Min.	
AT17	70°25'50"	26°19'50"	3/9	229.6	38.0	29.3	23.2	150	500	5	35
* AT18	70°25'50"	26°19'50"	4/4	237.9	40.9	130.6	8.6	500	530	20	45
* AT19	70°26'00"	26°20'00"	7/9	57.1	-41.7	25.4	12.2	470	580	Unstable	
* AT20	70°26'00"	26°20'35"	7/7	21.8	-55.1	22.1	13.3	300	400	30	70
* AT21	70°25'50"	26°21'00"	7/7	36.3	-50.8	9.5	20.7	350	400→500	50	60
* AT22	70°26'00"	26°21'10"	7/8	39.4	-50.6	11.5	18.7	350	470	20	60
Mean			5/6	44.0	-48.6	47.2	11.2				

Table 5.7. Sampling and demagnetisation data from dykes in the Las Animas pluton. n/No. is number of samples included in site mean/ number of samples demagnetised; dec. and inc. are declination and inclination of remanence vector; k is Fisherian precision parameter; α_{95} is semi-angle of 95% cone of confidence. ChRM isolation is demagnetisation level at which the ChRM is isolated in the site, a range with an arrow indicates a within site variation. Sites marked * are included in formation mean.

variation. NRM intensity values, sometimes within sites, are variable and range between 0.3 mAm^{-1} and 300 mAm^{-1} . Some samples were unstable to demagnetisation, with the NRM intensity rapidly reduced by both thermal and AF treatment. In all sites the ChRM is isolated at lower demagnetisation levels than any of the other dyke sets, typically around $350\text{-}500^\circ\text{C}$ or $20\text{-}60 \text{ mT}$. Despite this the ChRM was isolated from all sites, although only five are used to calculate the formation mean (Table 5.7 and Figure 5.26). Site AT17 was rejected as it displayed extreme within site variability and its site mean direction is poorly constrained.

Figure 5.27 shows the low coercivity and unblocking temperature components from the samples. In most of the sites (excluding AT17) some of the low coercivity and unblocking temperature components are well grouped, dominantly in a northerly direction with moderate negative inclination.

The demagnetisation behaviour of the Las Animas samples is extremely variable, examples are shown in Figure 5.28a-d. In all cases the NRM comprises at least two components of magnetisation which are often overlapping. The ChRM is usually only recognised at the highest demagnetisation levels before the sample becomes unstable. Often the ChRM is identified by combining remagnetisation circles and stable end point vectors.

The formation mean direction is given in Table 5.7 and shown in Figure 5.26, along with the site mean directions. Site AT18 has reversed polarity, site AT19 contains samples with both polarities, but normal polarity dominates.

iii) Discussion of results

The low temperature and AF demagnetisation fields suggests that multi-domain magnetite, or titanomagnetite is the main remanence carrier in these rocks. The variation

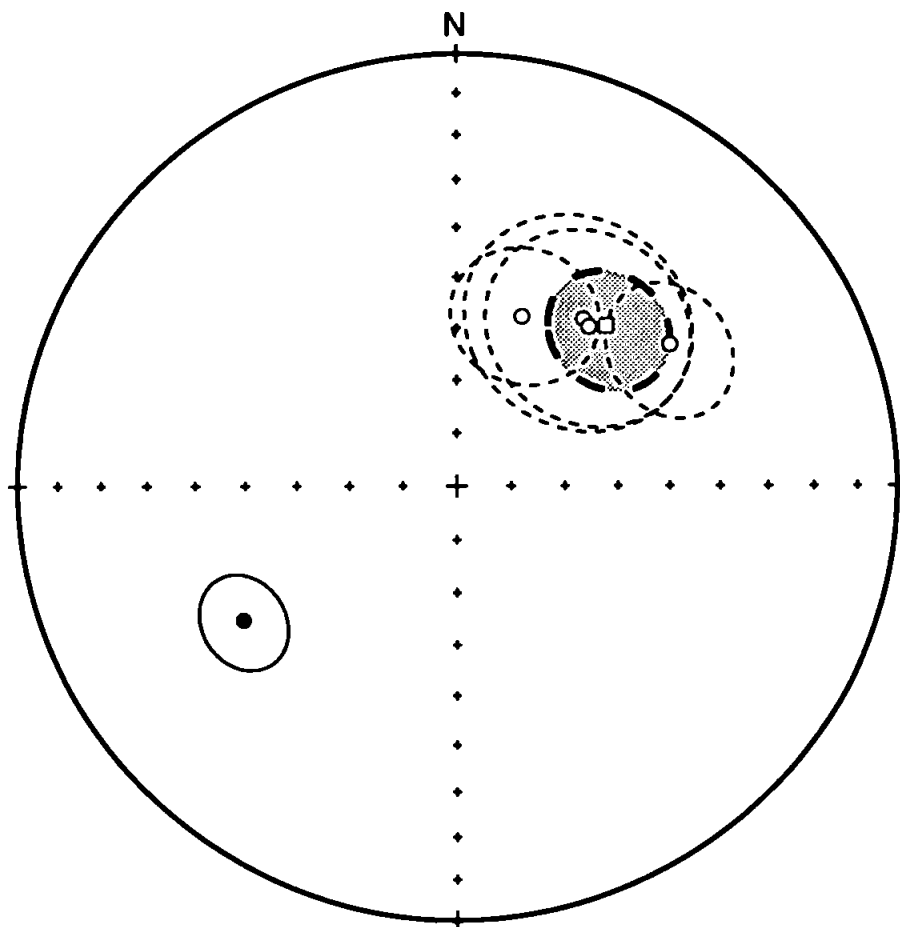


Figure 5.26. Equal area stereographic projection of site mean directions from dykes in the Las Animas pluton (circles) and the formation mean directions (square). Error ellipses are 95% confidence. Open (closed) symbols are upper (lower) hemisphere projections.

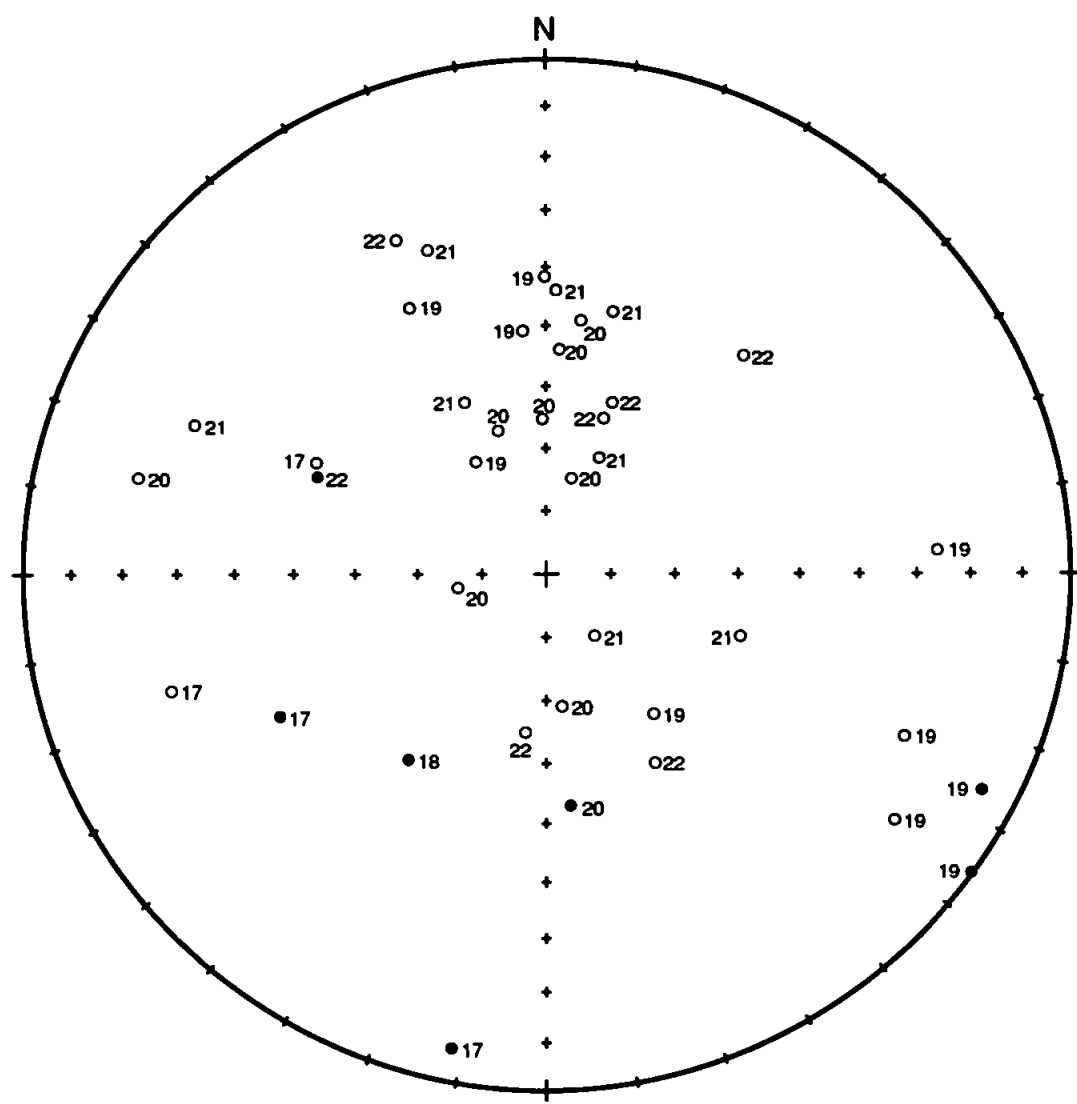


Figure 5.27. Equal area stereographic projection of low coercivity and unblocking temperature components from dykes in the Las Animas pluton. Open (closed) symbols are upper (lower) hemisphere projections. Directions are *in situ*, numbers are site numbers.

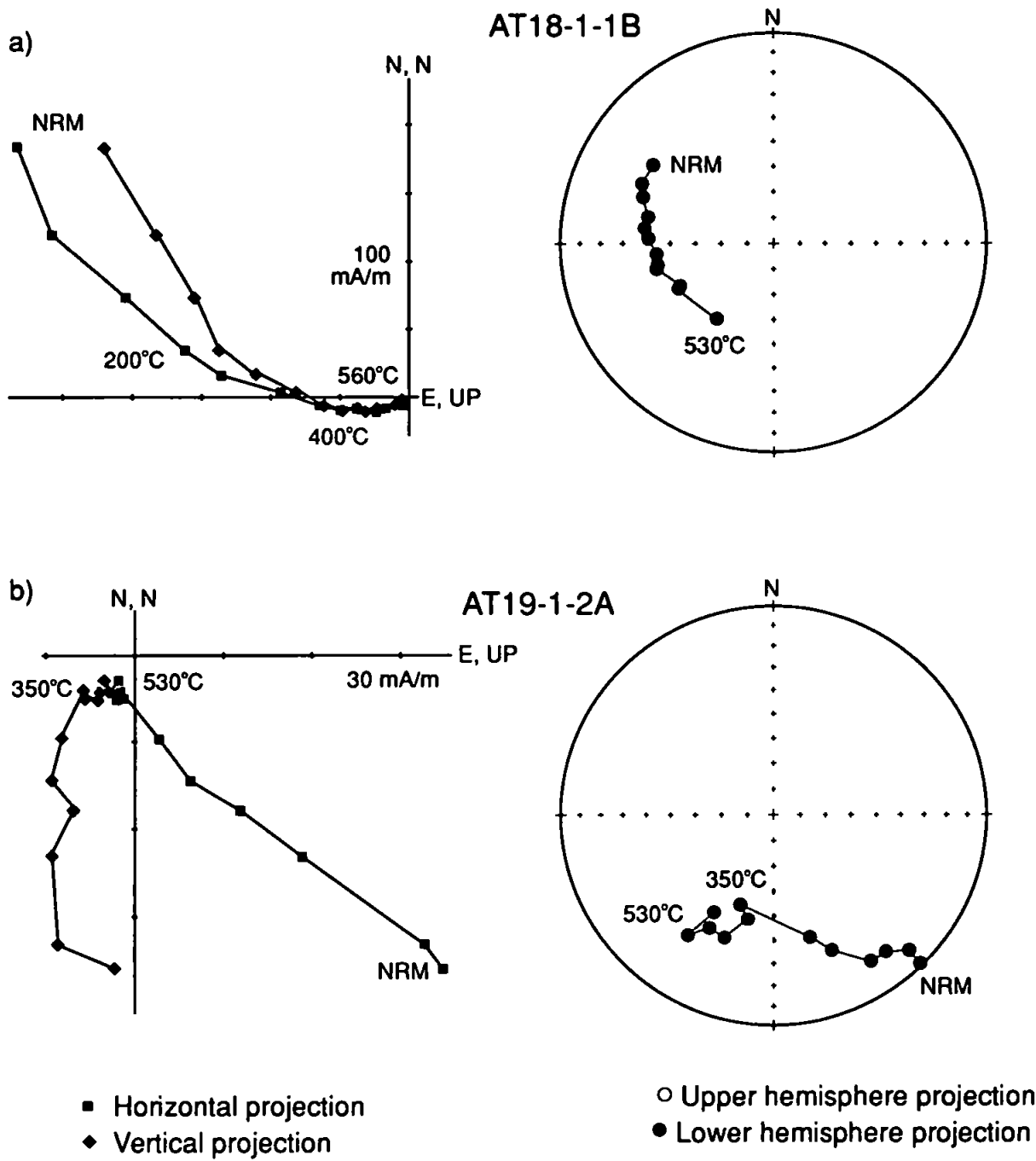


Figure 5.28a, b. Examples of demagnetisation behaviour in dyke samples from the Las Animas pluton.

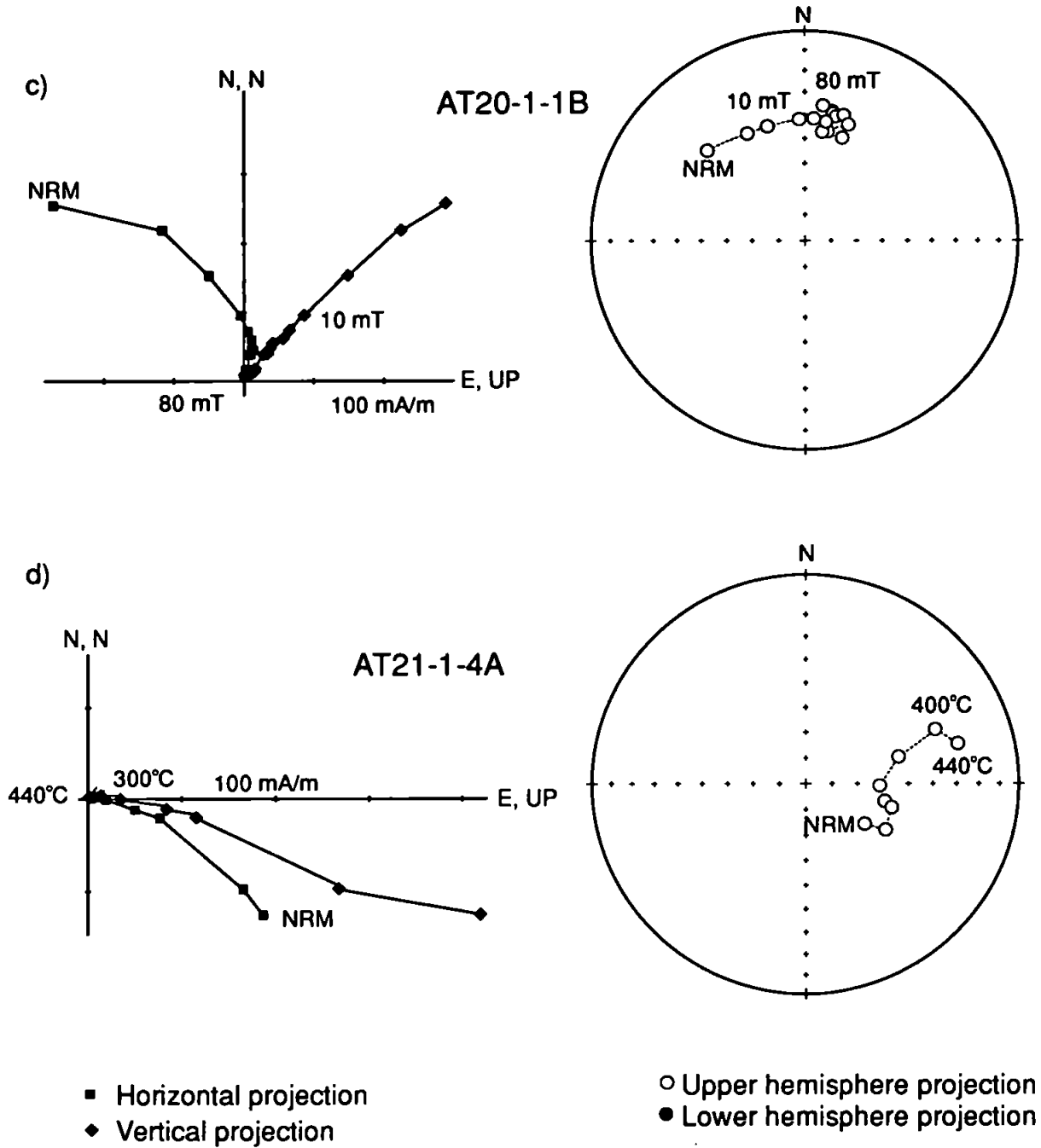


Figure 5.28c, d. Examples of demagnetisation behaviour in dyke samples from the Las Animas pluton.

in within site stability, particularly in the low coercivity and unblocking temperature components may be a result of variations in grain size or magnetic mineralogy. This may also cause the variation in NRM intensities observed in the sites.

Although the magnetisation in these samples is complicated and several components are present, a stable ChRM is identifiable in all of the sites. The ChRM is only recognised at the highest demagnetisation levels before the sample becomes unstable, although the ChRM isolation levels tend to be much lower than in any of the other dyke swarms. This is likely to be a result of multi-domain magnetite and/or titanomagnetite in these samples. The presence of samples with reversed polarity may be indicative of a primary or early remanence in these samples.

The dyke swarm in the Las Animas pluton is dated as Late Jurassic, however, as there is no well defined Late Jurassic reference direction (see discussion in Chapter 3.4.1iii), the mean is compared to the Middle Jurassic reference. The mean direction indicates a clockwise rotation of $42.0 \pm 15.2^\circ$ with a southward latitudinal translation of 5.6 ± 10.2 .

5.4.7 Dykes from the Las Tazas pluton

i) Palaeomagnetic sampling localities

A total of 12 sites were collected from dykes throughout the Las Tazas pluton as shown in Figure 5.29. Four sites (AT27-AT30) were collected near the northern end of the pluton just north of the Quebrada del Salado road. Four more sites (AT31-AT34) were collected from a small area south of Quebrada de Las Animas, a further two (AT35 and AT36) were collected on the south side of this area of exposure near to Quebrada de Guamanga. The last two sites are from the southernmost exposure of the pluton, site AT38

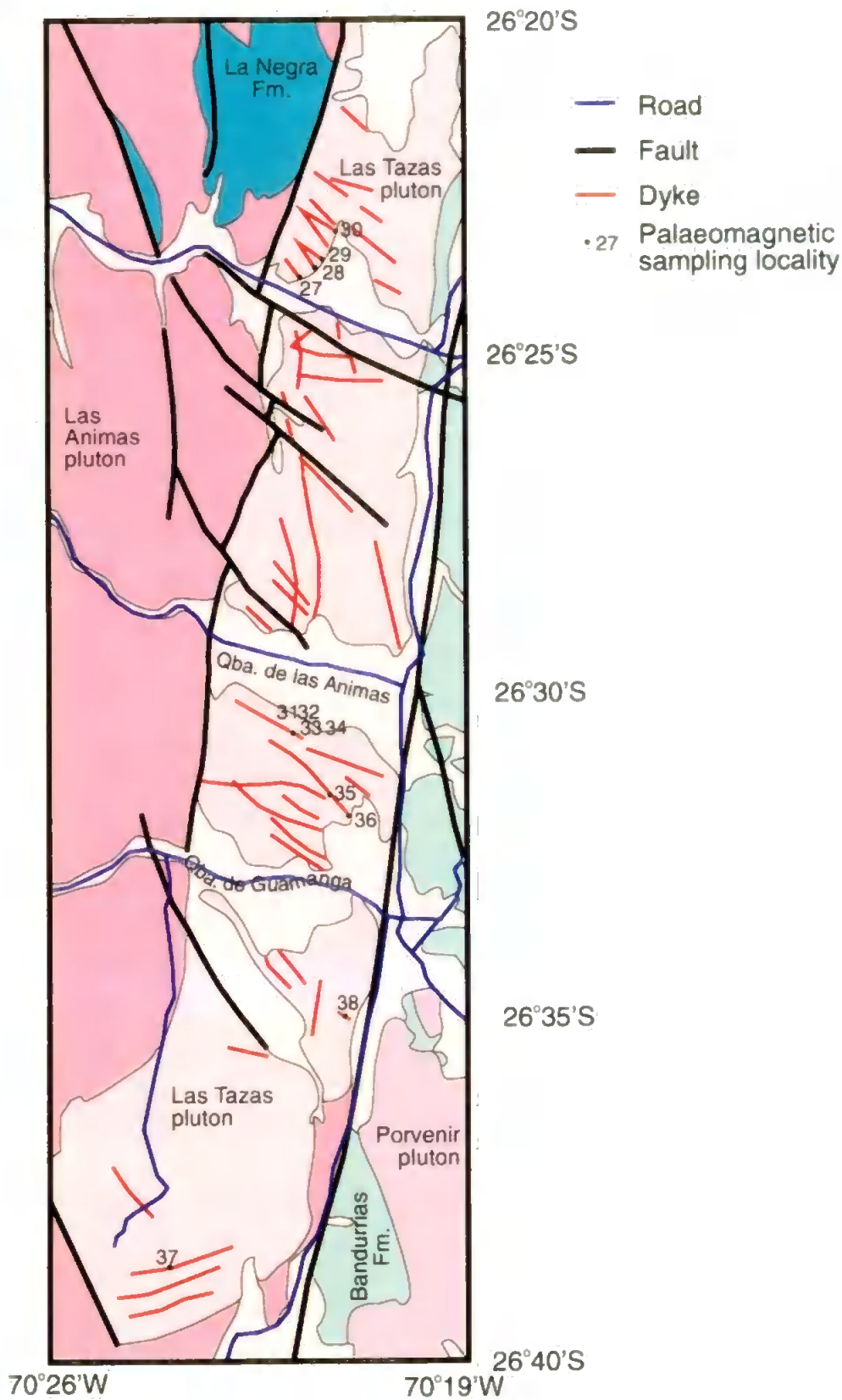


Figure 5.29. Palaeomagnetic sampling sites from dykes in the Las Tazas pluton. Redrawn from Mercado (1978).

is from the south-east portion close to the Atacama Fault Zone, while AT37 is from a dyke close to the southern margin of the intrusion. All sites were collected as hand samples.

ii) Palaeomagnetic remanence measurements

Ten of the twelve sites collected have been demagnetised and their remanence measured. The results from these ten sites are given in Table 5.8. All sites show multi-component behaviour and in most cases the ChRM is only recognised from the last few points before the sample becomes unstable, or from remagnetisation circles. There is often a range of behaviour and NRM intensities within sites, sometimes not all of the samples in a site display the ChRM direction identified at the highest demagnetisation levels in the site. In some samples after demagnetisation to high levels, there remains a significant remanence intensity although the direction becomes unstable. For this reason it is not certain whether the ChRM has truly been isolated, therefore some of the ChRM isolation levels quoted in Table 5.8 are questionable and are marked as such.

It was possible to isolate the ChRM in nine of the ten sites, excluding AT31 (Table 5.8 and Figure 5.30). Although the mean direction from site AT31 seems to be well constrained, a few of the samples seem to show a second component at the highest demagnetisation levels, but this component could not be reliably extracted. For this reason it seems that the site mean direction is that of a stable secondary overprint and the site is excluded. Two other sites (AT27 and AT37) are also excluded from the formation mean calculation. Site AT27 is unusual in having a single, very stable component of magnetisation, the direction of which is significantly different from the ChRM in the majority of samples. Site AT37 has two components with overlapping blocking spectra. The ChRM of the site is well defined in terms of angular error, but typically based on only

Site	Sampling site		n/No.	Dec.	Inc.	k	α_{95}	°C Min.	ChRM isolation		mT Max.
	Long. W	Lat. S							Max.	Min.	
AT27	70°21'30"	26°24'00"	7/7	193.0	4.7	279.3	3.6	100	570	3	45→60
* AT28	70°21'30"	26°24'00"	6/8	43.9	-43.8	18.4	16.6	150	400→440	ChRM not isolated	
* AT29	70°21'10"	26°23'30"	7/7	39.8	-46.5	75.5	7.0	100→300	440	4	40
* AT30	70°21'00"	26°23'10"	5/7	43.0	-15.8	51.7	11.5	400	540	ChRM not isolated	
AT31	70°21'35"	26°30'45"	6/6	154.8	28.5	21.9	10.5	ChRM not isolated		Not done	
* AT32	70°21'35"	26°30'45"	6/8	20.4	-47.0	155.9	6.0	400	510	35	60
* AT33	70°21'30"	26°31'00"	6/6	220.9	62.1	17.3	17.7	~400	510	Not done	
* AT34	70°21'30"	26°31'00"	6/6	212.7	32.5	17.8	19.2	~450	570	Not done	
AT37	70°23'40"	26°39'00"	6/6	155.8	44.7	333.7	3.7	570 ?		Not done	
* AT38	70°21'00"	26°35'00"	5/6	48.9	-40.2	34.5	13.6	400 ?		Not done	
Mean			7/10	38.7	-41.5	26.4	12.0				

Table 5.8. Sampling and demagnetisation data from dykes in the Las Tazas pluton. n/No. is number of samples included in site mean/ number of samples demagnetised; dec. and inc. are declination and inclination of remanence vector; k is Fisherian precision parameter, α_{95} is semi-angle of 95% cone of confidence. ChRM isolation is demagnetisation level at which the ChRM is isolated in the site, a range with an arrow indicates a within site variation. Sites marked * are included in formation mean.

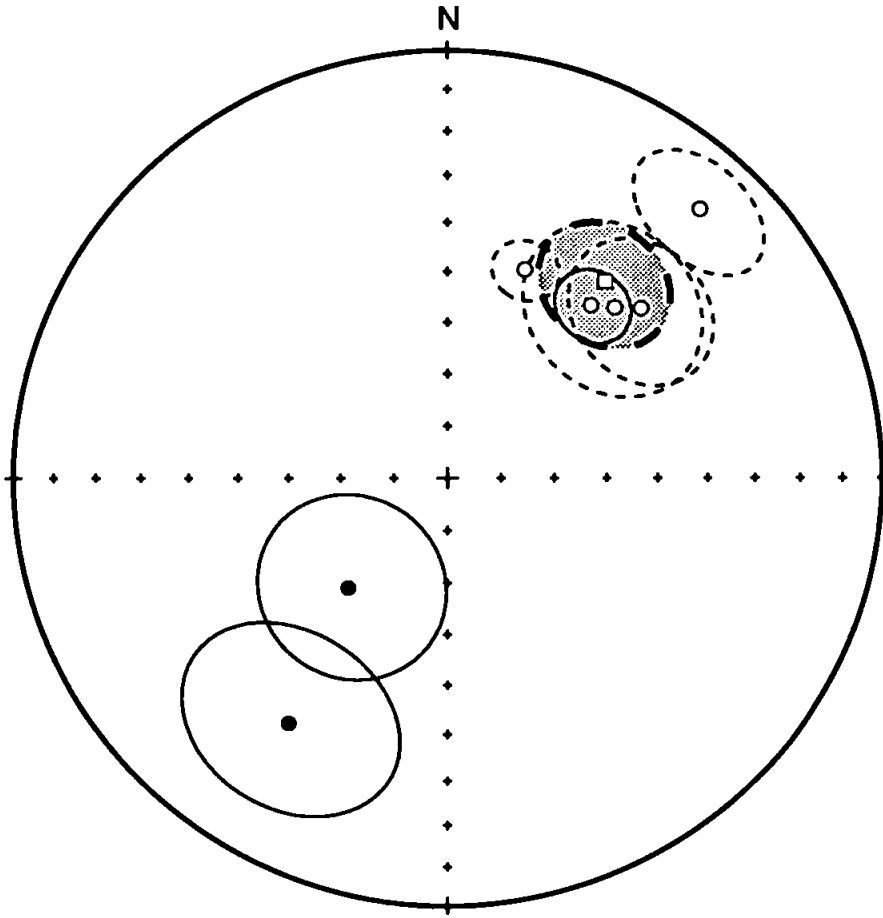


Figure 5.30. Equal area stereographic projection of site mean directions from dykes in the Las Tazas pluton (circles) and the formation mean directions (square). Error ellipses are 95% confidence. Open (closed) symbols are upper (lower) hemisphere projections.

a single end point. Its direction is also significantly different from that of the formation mean and for these reasons it is not included in the formation mean calculation.

Figure 5.31 shows the low unblocking temperature and coercivity components seen in the samples. In many of the sites the low components are fairly well grouped, at least within individual sampling blocks. Notably absent, compared with low coercivity and unblocking temperature components from the other dyke swarms, is any grouping close to the position of the present-day field, or a group antipodal to the formation mean. Instead the low coercivity and unblocking temperature components in the Las Tazas pluton are dominated by directions with low to moderate inclinations grouped towards the south and north-north-west of the stereoplot. The cause of these directions is unclear.

As with the other dyke swarms from the Coastal Cordillera the demagnetisation behaviour of samples from the Las Tazas pluton is extremely variable, even within site. Examples of the demagnetisation are shown in Figure 5.32a-d. It can be seen that in most cases the ChRM is only identified at the highest demagnetisation levels after removal of at least one secondary component. In some of the samples the demagnetisation plots show a curved trace, interpreted as overlapping unblocking or coercivity spectra.

The formation mean direction is given in Table 5.8 and shown on Figure 5.30 along with the included site mean directions. Two sites, AT33 and AT34, have reversed polarity. Both sites with reversed polarity have large α_{95} confidence limits, this is because they are based on remagnetisation circles only, and they may not be entirely free of the influence of secondary components.

iii) Discussion of results

The most striking feature of the Las Tazas dyke samples is the variability of the demagnetisation behaviour, particularly within individual sites. The low coercivity and

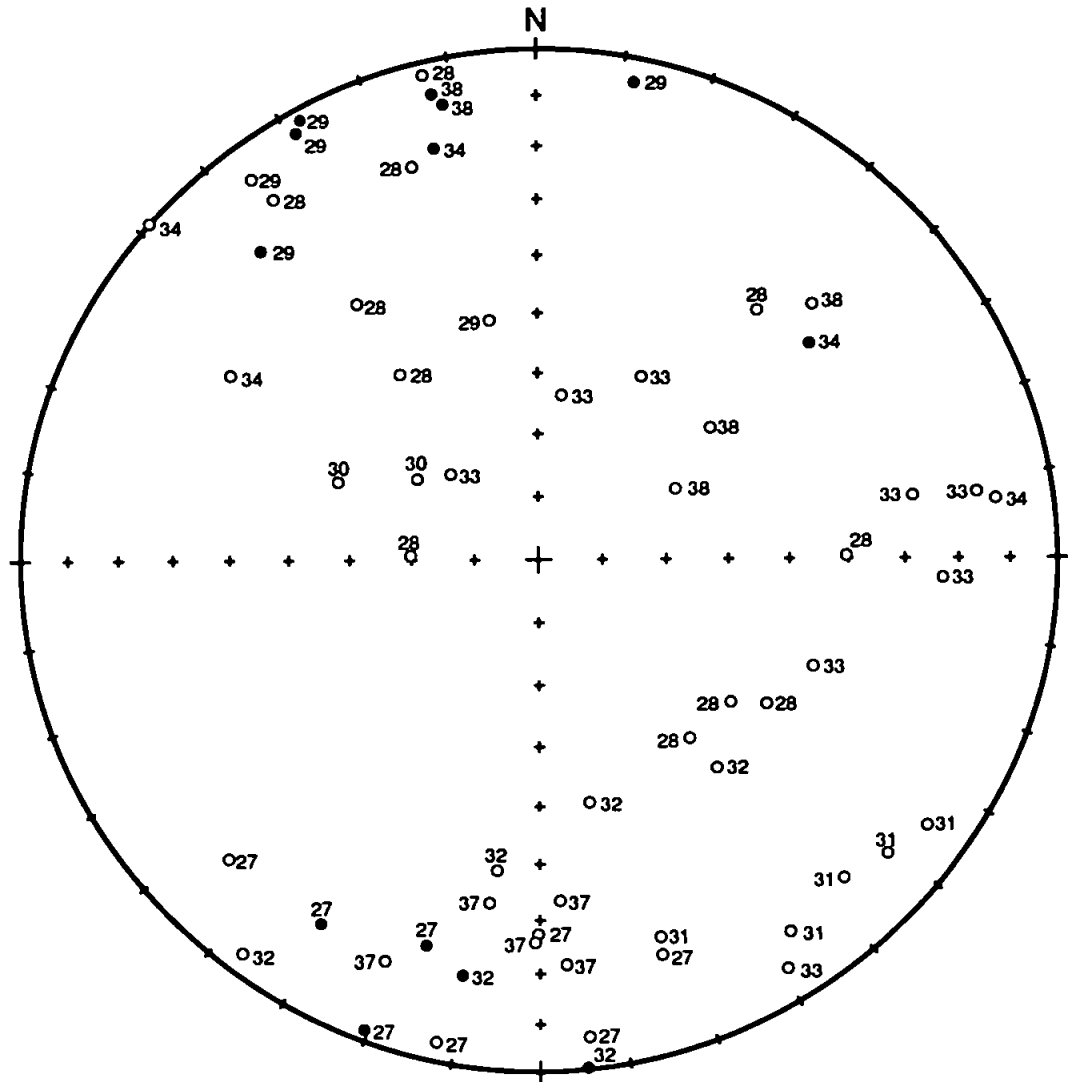


Figure 5.31. Equal area stereographic projection of low coercivity and unblocking temperature components from dykes in the Las Tazas pluton. Open (closed) symbols are upper (lower) hemisphere projections. Directions are *in situ*, numbers are site numbers.

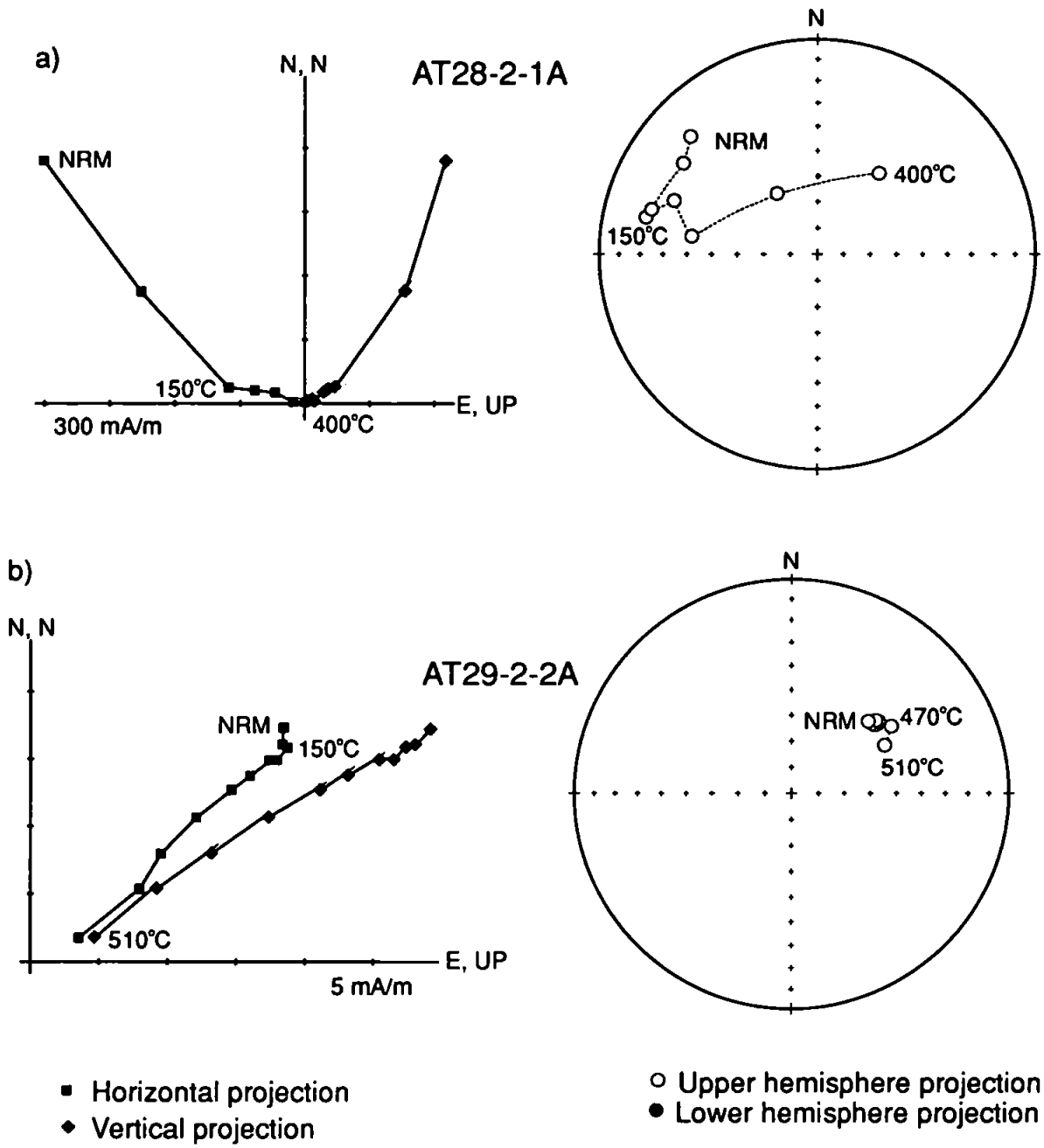


Figure 5.32a, b. Examples of demagnetisation behaviour in dyke samples from the Las Tazas pluton.

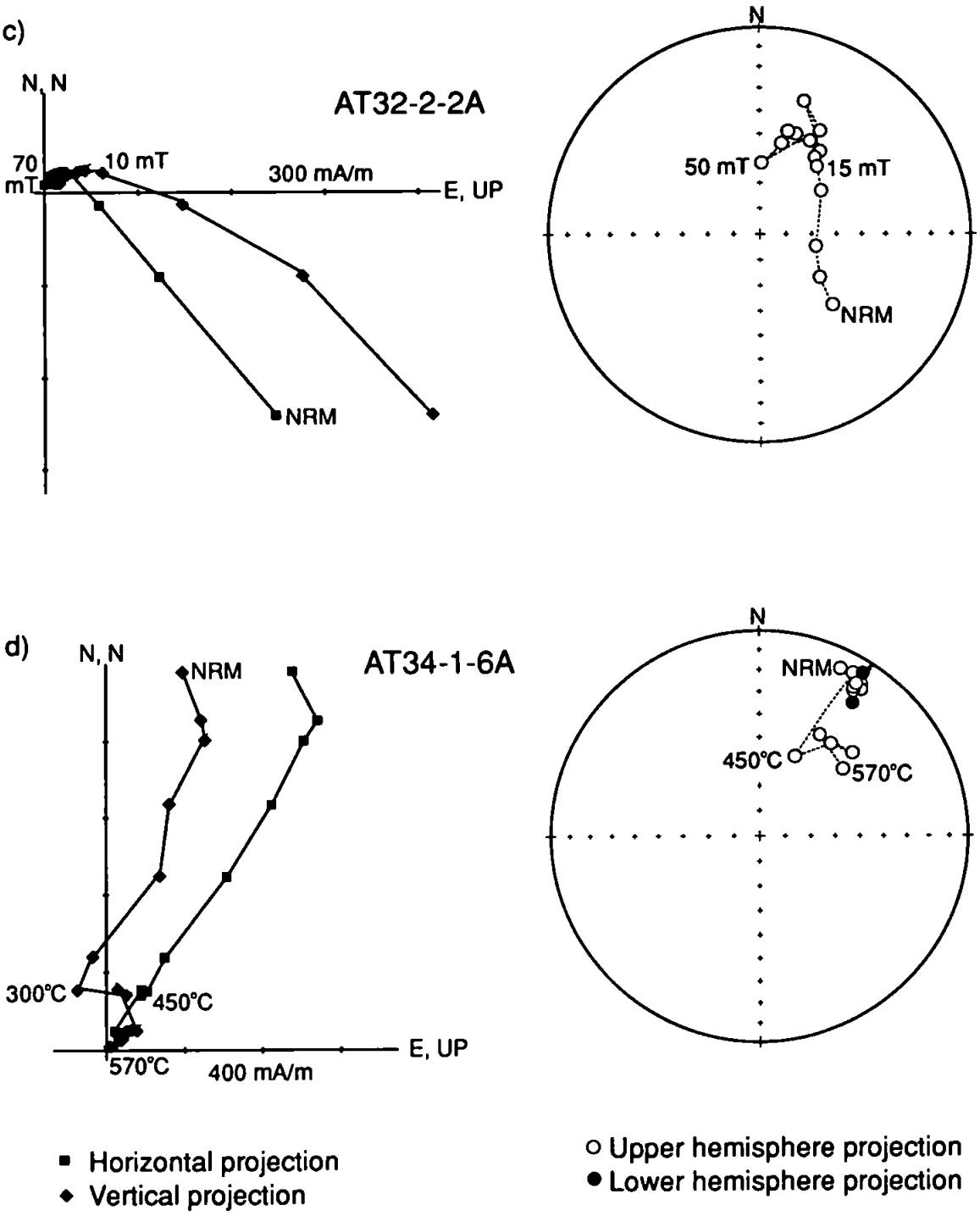


Figure 5.32c, d. Examples of demagnetisation behaviour in dyke samples from the Las Tazas pluton.

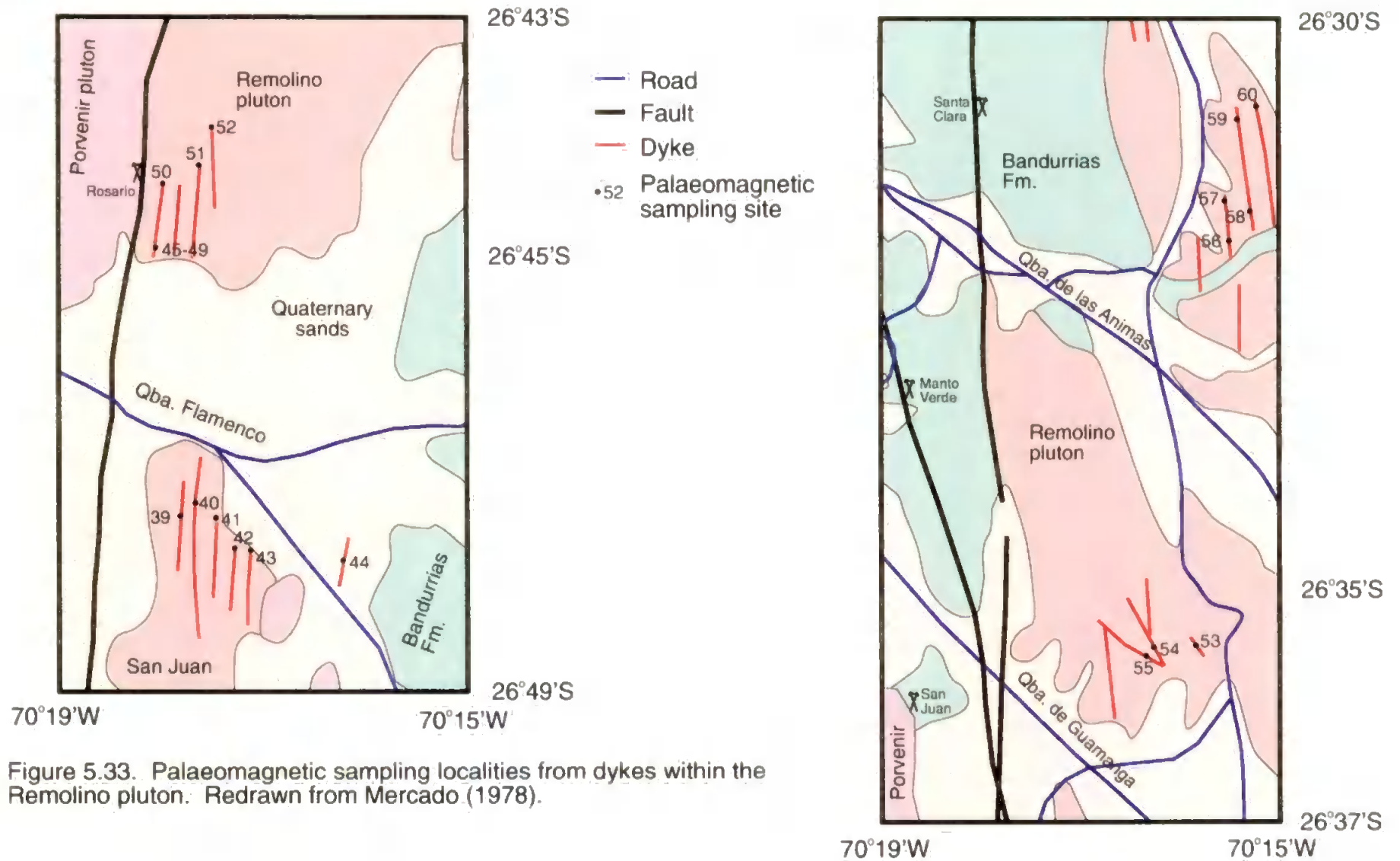


Figure 5.33. Palaeomagnetic sampling localities from dykes within the Remolino pluton. Redrawn from Mercado (1978).

unblocking temperature components do, however, form reasonably coherent groups. This variability may be indicating more intense, but localised alteration and overprinting of the magnetisation than has been observed in the dyke swarms from the other plutons. This may be due to the proximity of the sampling sites to the AFZ. Hydrothermal fluids have been preferentially concentrated close to the AFZ and its immediate subsidiary faults. The dykes in the Las Tazas pluton may have therefore been affected by several generations of mild heating and fluid flow to cause alteration. Thin section analysis (Appendix 1) indicates that samples from these dykes have undergone extensive alteration, including the possible introduction of later magnetic minerals.

Considering the amount of alteration seen in these samples, identifying the ChRM as primary is difficult. The two sites which show reversed directions are poorly defined; recognised by remagnetisation circles only. The best evidence that the remanence is at least ancient, if not primary, is that the formation mean direction is consistent with those from the other adjacent dyke swarms.

Dated samples from dykes in the Las Tazas pluton suggest a middle Cretaceous age. Comparison of the mean direction with the middle Cretaceous reference direction indicates a clockwise rotation of $39.7 \pm 13.8^\circ$, with a northward latitudinal shift of $6.5 \pm 10.1^\circ$.

5.4.8 Dykes from the Remolino pluton

i) Palaeomagnetic sampling localities

Twenty-two sites were collected as oriented hand samples from two areas within the Remolino pluton to the east of the AFZ. Figure 5.33 shows the location of the sampling sites. Eight sites (AT53-AT60) were collected from the northerly sampling locality at approximately $26^\circ 33'S$. The other fourteen sites, AT39-AT52, were collected

from the more southern locality at approximately 26°45'S near Quebrada Flamenco. Six of these sites AT39-AT44 were collected from San Juan, south of Quebrada Flamenco. Although most of the Remolino pluton is granodioritic, San Juan is marked on the map of Mercado (1978) as tonalite. This tonalite is regarded as being of similar age to the rest of the Remolino pluton and as such is part of the same plutonic complex. For this reason the outcrop south of Quebrada Flamenco is marked in the same colour as the Remolino pluton in Figure 5.33. The dykes from this outcrop are therefore regarded as being the same age as those in the rest of the Remolino pluton and are not considered separately.

ii) Palaeomagnetic remanence measurements

Seventeen sites, twelve from the southern sampling area and five from the northern have been demagnetised, the results are given in Table 5.9 and shown in Figure 5.34. Most sites demonstrate multi-component NRM's although a ChRM is recognised in most sites either from end points or remagnetisation circles. Some sites (five) display a stable ChRM component identified from several demagnetisation points. The demagnetisation behaviour can be variable within site, even within a single core sample. An example of this within core variation is shown in Figure 5.35 where three specimens from core AT45-2-3 have different intensities and demagnetisation behaviour. Some sites, or occasionally one hand sample from a site, are also characterised by very high NRM intensities, in some cases up to 20 Am⁻¹. These components are easily demagnetised by AF treatment, and often record directions unrelated to the ChRM identified from the rest of the samples in the site. As a result, such samples have been excluded from the site means and this results in a small number of samples included in some of the calculations (Table 5.9).

Figure 5.36 shows the low and intermediate unblocking temperature and coercivity components isolated. The low components are typically removed by demagnetisation to

Site	Sampling site		n/No.	Dec.	Inc.	k	α_{95}	°C		ChRM isolation		mT	
	Long. W	Lat. S						Min.	Max.	Max.	Min.	Max.	Max.
* AT39	70°18'00"	26°47'30"	4/7	4.9	-18.5	57.8	12.2	500	570		35	100	
* AT40	70°18'00"	26°47'30"	6/7	30.0	-23.3	17.8	16.3	540	585		90	100 ?	
* AT41	70°17'50"	26°47'30"	7/7	36.3	-25.5	17.9	14.7	500→540	585		90	100 ?	
* AT42	70°17'50"	26°47'30"	6/7	59.5	-49.6	40.6	10.6	400	570		10	100	
* AT43	70°17'45"	26°47'30"	7/7	29.8	-51.5	347.5	3.2	450→540	585		10	100	
AT44	70°16'00"	26°47'32"	4/7	260.0	-28.1	999.9	1.8	300	585 ¹		45	100	
* AT45	70°17'30"	26°44'45"	8/18	33.7	-30.6	17.2	14.0	540	570		12	50 ?	
* AT46	70°17'30"	26°44'45"	9/17	34.5	-36.0	8.2	19.2	~410	540		ChRM not isolated		
* AT47	70°17'30"	26°44'45"	10/10	47.3	-57.3	268.2	3.0	410	540		10→40	85	
* AT48	70°17'30"	26°44'45"	15/17	42.3	-41.6	9.0	13.5	200→410	510		15	20	
* AT49	70°17'30"	26°44'45"	14/14	6.2	-64.0	26.5	7.9	100	510		55	90	
AT50	70°17'30"	26°44'45"	15/15	119.2	27.8	107.9	3.7	150	570		5	50	
* AT53	70°16'10"	26°35'45"	5/7	86.8	-32.6	49.1	11.0	~350	500		ChRM not isolated		
AT54	70°16'10"	26°35'45"	7/7	232.3	-22.8	49.0	8.7	200→350	570		4	100	
* AT55	70°16'10"	26°35'45"	3/7	31.5	-18.3	88.2	13.2	~200	450		ChRM not isolated		
* AT56	70°15'50"	26°31'40"	4/6	43.4	-47.8	45.2	13.8	540	585		20	80	
AT57	70°15'50"	26°31'40"	3/7	48.3	-30.0	23.7	25.7	150	300 ?		65	85 ?	
Mean			13/17	37.2	-39.3	13.8	11.6						

Table 5.9. Sampling and demagnetisation data from dykes in the Remolino pluton. n/No. is number of samples included in site mean/number of samples demagnetised; dec. and inc. are declination and inclination of remanence vector; k is Fisherian precision parameter; α_{95} is semi-angle of 95% cone of confidence. ChRM isolation is demagnetisation level at which the ChRM is isolated in the site, a range with an arrow indicates a within site variation. Sites marked * are included in formation mean.

¹ May not be isolating the ChRM, some samples may have a higher temperature component but it is indistinct.

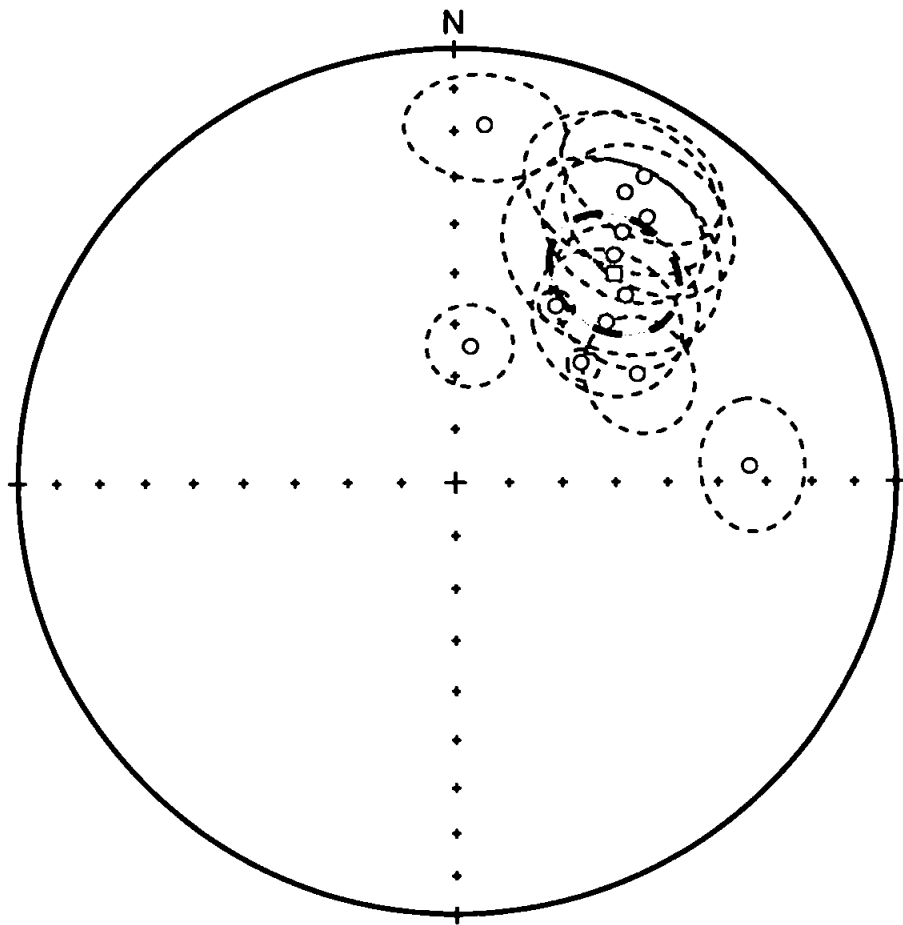


Figure 5.34. Equal area stereographic projection of site mean directions from dykes in the Remolino pluton (circles) and the formation mean directions (square). Error ellipses are 95% confidence. Open (closed) symbols are upper (lower) hemisphere projections.

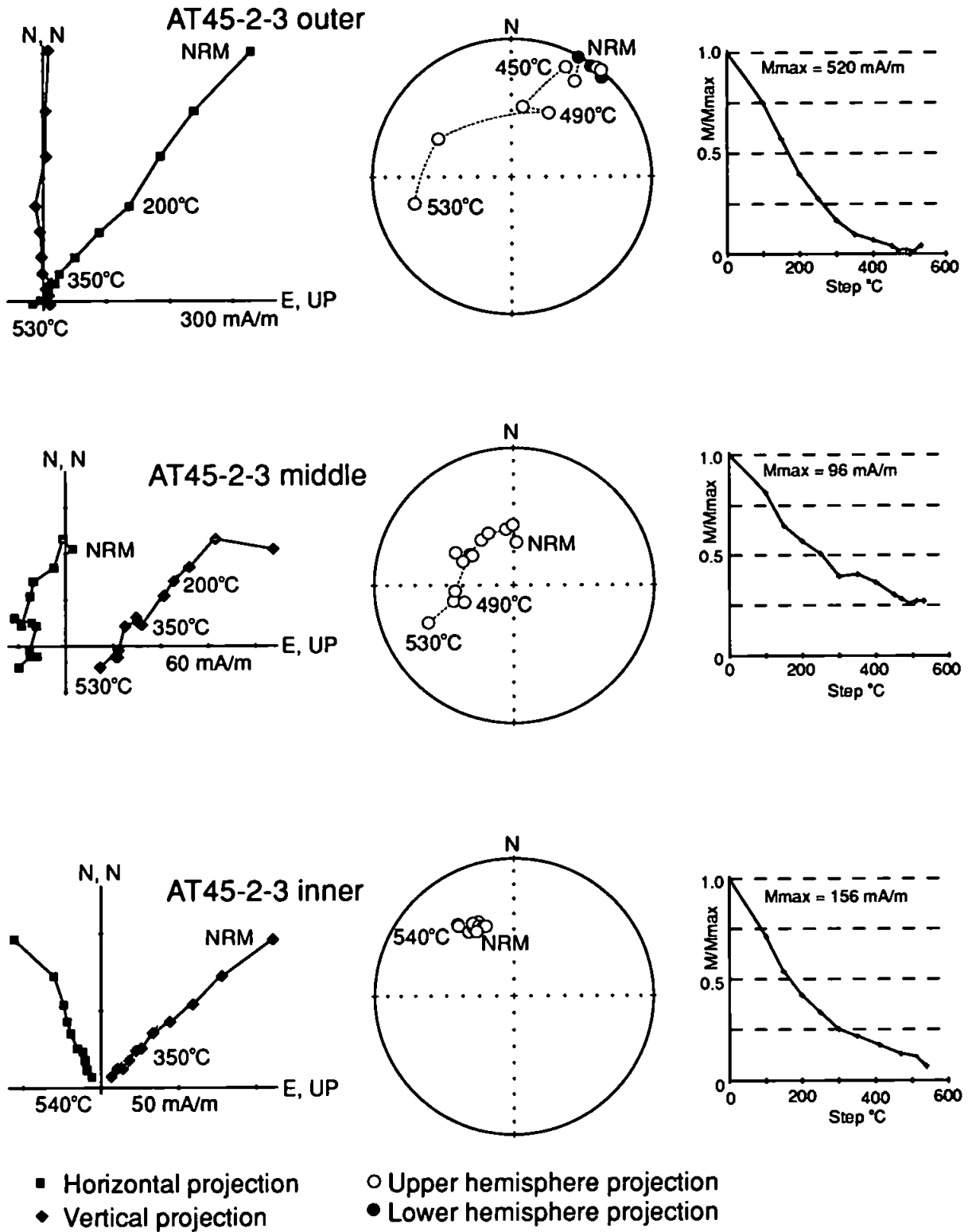


Figure 5.35. Demagnetisation plots from a single core sample collected from a dyke in the Remolino pluton. The outer specimen is from the part of the core closest to the weathered surface.

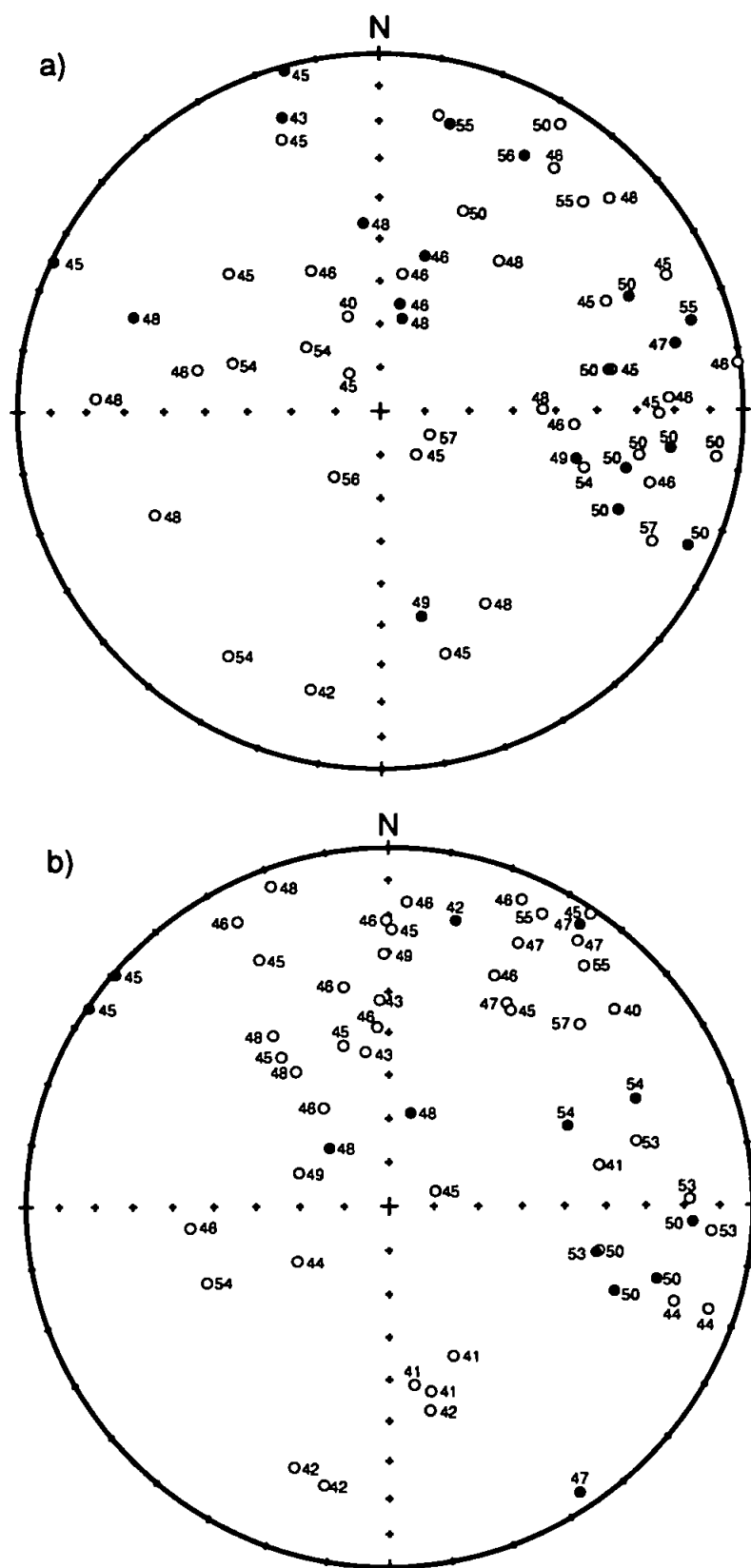


Figure 5.36. Equal area stereographic projection of low coercivity and unblocking temperature components from dykes in the Remolino pluton.
 a) Unblocking temperatures or coercivity below $100^{\circ}\text{C}/10\text{ mT}$,
 b) Unblocking temperatures above $100^{\circ}\text{C}/10\text{ mT}$, but below ChRM.
 Open (closed) symbols are upper (lower) hemisphere projections.
 Directions are *in situ*, numbers are site numbers.

100°C or 10 mT, while the intermediate components are recovered between 100°C/10 mT and the lowest level at which the ChRM is isolated. The lowest components tend not to form groups in most sites, but there is a grouping of several samples with eastward directed low to moderate inclinations.

A stable ChRM was isolated from all sites except AT57, where the site mean direction is poorly constrained and based on data from only three samples. Three other sites (AT44, AT50 and AT54) were also excluded from the formation mean calculation as they have directions apparently unrelated to the ChRM. All three sites have very high total NRM intensities, site AT44 has a multi-component NRM with overlapping components of magnetisation, while sites AT50 and AT54 have a single component of magnetisation. These sites are probably recording a post-emplacement overprint, and the most likely source for the high intensity is an IRM as a result of a lightning strike.

Examples of the demagnetisation behaviour of the remaining 13 sites are shown in Figure 5.37a-f. There is much within site variation, and in some cases the ChRM is not recovered from all of the samples in the site. In these cases, the ChRM is usually identified from stable end points (Figure 5.37a) or remagnetisation circles (Figure 5.37b). AF demagnetisation rapidly reduces the NRM intensity and samples become directionally unstable at approximately 20 mT, the ChRM is not usually recovered by this treatment. Other sites do display stable vector components of magnetisation. Figures 5.37c and d show examples of two component demagnetisation where the ChRM is recovered at ~400°C-580°C or up to 100 mT. The softer component is typically the intermediate component discussed previously which represents a present-day overprint. Two sites are characterised by a single component remanence, examples of which are shown in Figure 5.37e and f.

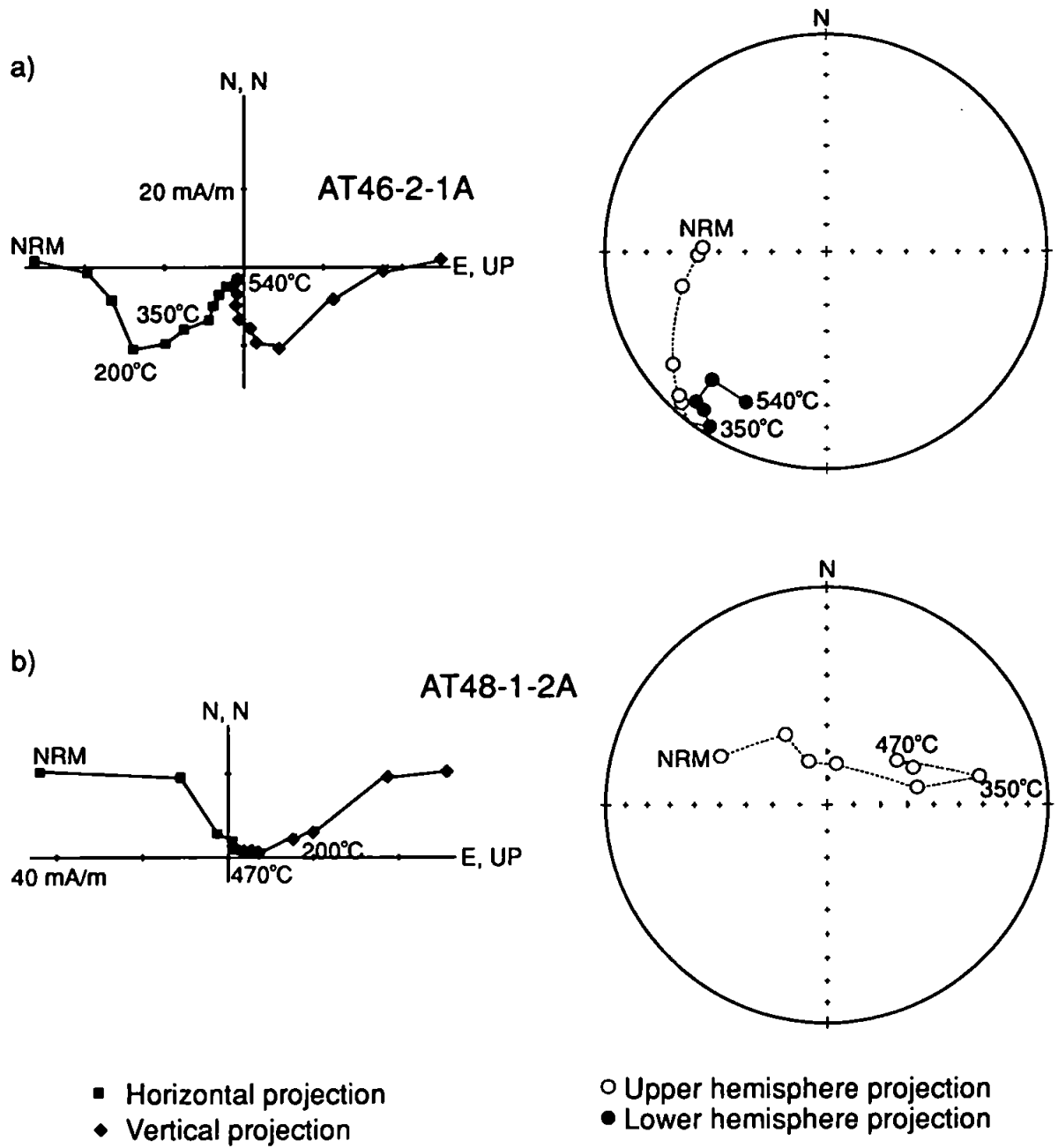


Figure 5.37a, b. Examples of demagnetisation behaviour in dyke samples from the Remolino pluton.

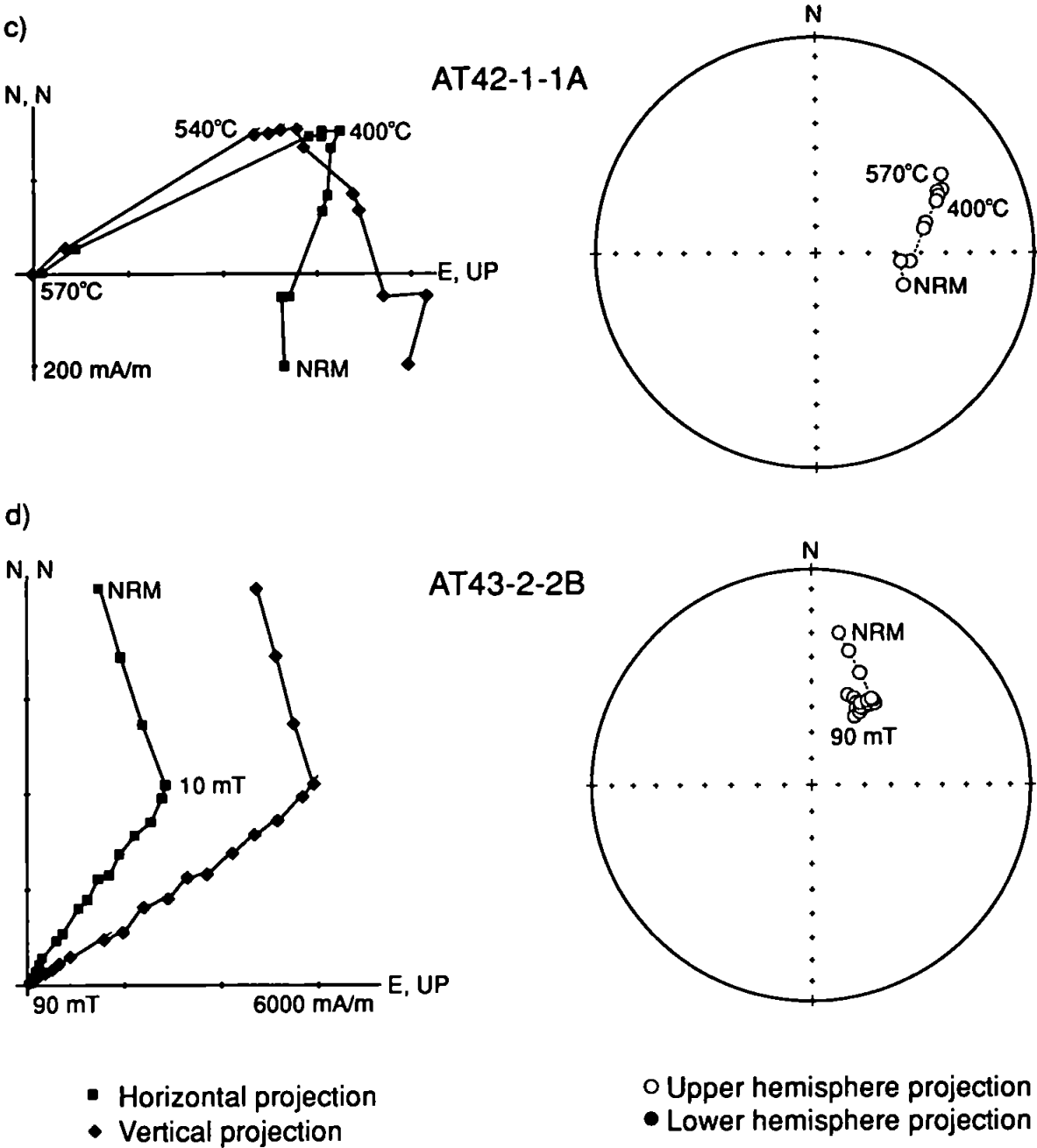


Figure 5.37c, d. Examples of demagnetisation behaviour in dyke samples from the Remolino pluton.

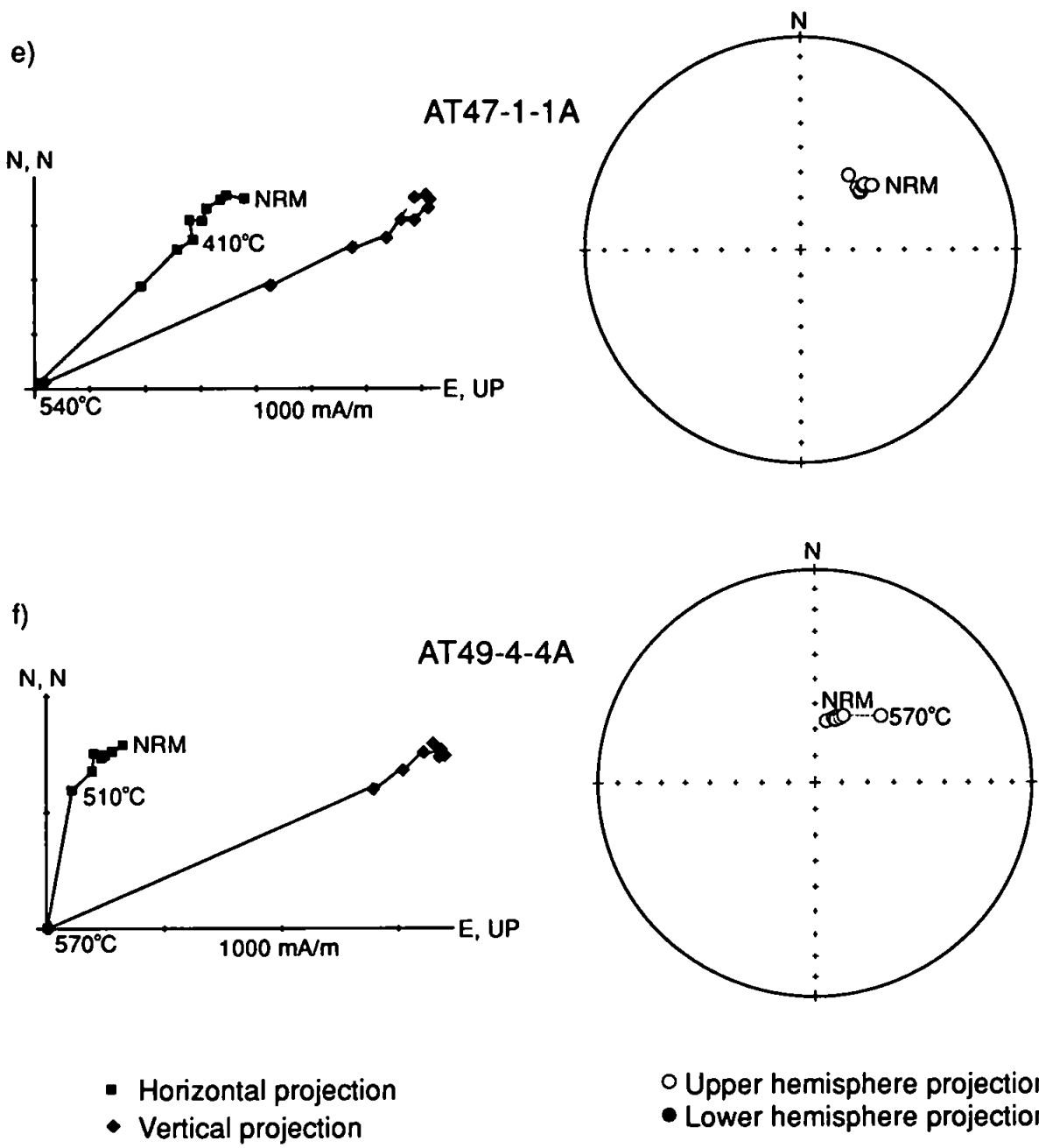


Figure 5.37e, f. Examples of demagnetisation behaviour in dyke samples from the Remolino pluton.

The formation mean direction is given in Table 5.9 and shown in Figure 5.34, all sites have normal polarity, although samples in some sites do seem to contain a reversed polarity component at lower demagnetisation levels than those of the accepted ChRM.

iii) Discussion of Results

One of the most obvious features of the samples from the dykes in the Remolino pluton is the down core variation in intensity and direction of magnetic vectors. There may be several reasons for this, although none can be established unequivocally as the cause. It is possible that the variation may be due to changes in the magnetic mineralogy through the hand sample. This may be a result of sampling through a chilled margin, or a result of variations in the amount of secondary alteration through the block. Lucassen and Franz (1994) noted that the alteration in intrusive rocks to the north of the study area tended to be concentrated along the joints and fractures, the weathered surface may therefore have been more affected by fluid alteration. The high intensities observed in some samples are probably the result of IRMs induced by lightening strikes, this may also cause variation in the intensities and direction down an individual core.

The lowest unblocking temperature and low coercivity components represent laboratory induced VRMs, while the more stable intermediate components represent present-day VRMs.

The demagnetisation behaviour and IRM experiments suggest that magnetite, dominantly multi-domain, is probably the main remanence carrier of the NRM. This NRM is fairly unstable and rapidly demagnetised by AF treatment. Thin section analysis shows coarse grained opaque minerals as a common accessory phase typically in late stage veins. These secondary minerals may be carrying the later, soft remanence whereas the ChRM is carried by more stable, primary magnetic grains.

Although some individual samples seem to contain a reversed polarity component, sites all have normal polarity. This therefore offers no evidence as to whether the remanence is of a primary origin, but could be seen to be consistent with the dykes having acquired their remanence during the mid-Cretaceous long normal polarity period (i.e., post ~117 Ma).

Although there is no date for the dykes in the Remolino pluton there is no reason to indicate that they do not have a similar age to the host pluton, as observed in the Las Animas and Las Tazas plutons. The dykes are therefore likely to be mid-Cretaceous in age and the formation mean direction is compared to this reference direction. The mean direction indicates a clockwise rotation of $38.2 \pm 13.0^\circ$, with southward latitudinal displacement of $8.7 \pm 9.8^\circ$.

5.5 Discussion and conclusions

The palaeostress analysis from dykes in three of the plutons indicates that the dykes have undergone no significant post-emplacement tilting. The dilation direction from the dykes suggest that the stress field rotated, from WSW-ENE to SSW-NNE, during the period Early Jurassic to Early Cretaceous. These directions do not take account of any vertical axis rotations which have occurred since dyke emplacement.

Demagnetisation behaviour and rock magnetic studies show that the magnetic mineralogy of the samples is variable. Some samples probably contain several phases of magnetic mineral growth and as a result several components of magnetic remanence. This has lead to complex NRM in most of the samples demagnetised, both in the La Negra Formation and the five dyke sets. Despite this a ChRM has been identified in each of the

formations which is regarded as being primary or at least acquired soon after deposition or intrusion. The evidence for this is:

- positive fold and reversal tests in the La Negra Formation,
- the presence of reversed sites in four of the five dykes swarms,
- consistency of the ChRM directions obtained from the six sampled formations across a wide sampling area suggests that the direction is stable and representative of the region,
- the ChRM does not correspond with any younger reference direction (see Chapter 3).

The formation mean directions, and the amount of rotation and flattening are shown in Table 5.10. With the exclusion of the direction from the La Negra Formation, the results suggest a possible east-west variation in the amount of rotation. This may be related to the spatial or temporal distribution of the sampling sites. The errors on the rotations do, however overlap, and it is not possible to differentiate between the amounts of rotation in the different sampling units. The results are therefore interpreted as indicating a consistent clockwise rotation of the whole region by approximately 42° . The latitudinal displacement displayed by the formations is inconsistent and all are within their associated errors. This suggests that latitudinal translation has not occurred in the Coastal Cordillera and the rotation has occurred *in situ*.

Formation name	Age of Formation and presumed age of magnetisation	Formation mean			Reference used	Rotation ±error	Flattening ±error (°)
		Dec.	Inc.	α_{95}			
La Negra Formation	Middle Jurassic	42.0°	-35.5°	9.6°	Middle Jurassic	40.0±11.5°	-7.5±9.1
Vetado dykes	? Middle Jurassic	48.9°	-49.6°	12.1°	Middle Jurassic	46.9±16.5°	6.6±10.8
Flamenco dykes	c. 154 Ma	45.6°	-43.0°	8.8°	Middle Jurassic	43.6±11.7°	0.0±8.5
Las Animas dykes	c. 154 Ma	44.0°	-48.6°	11.2°	Middle Jurassic	42.0±15.2°	5.6±10.2
Las Tazas dykes	c. 127 Ma	38.7°	-41.5°	12.0°	mid-Cretaceous	39.7±13.8°	-6.5±10.1
Remolino dykes	< 127 Ma	37.2°	-39.3°	11.6°	mid-Cretaceous	38.2±13.0°	-8.7±9.8

Table 5.10. Amount of rotation and flattening indicated by comparison of formation mean directions with stable reference directions. Rotation and flattening and associated errors calculated as described in section 2.7.1. Dec. and Inc. are, respectively, the declination and inclination of the formation palaeomagnetic mean direction; α_{95} is the semi-angle of the 95% confidence limit. In the rotation column, a negative (positive) value indicates anticlockwise (clockwise) rotation. In the flattening column, a negative (positive) value indicates northward (southward) latitudinal transport.

Chapter 6

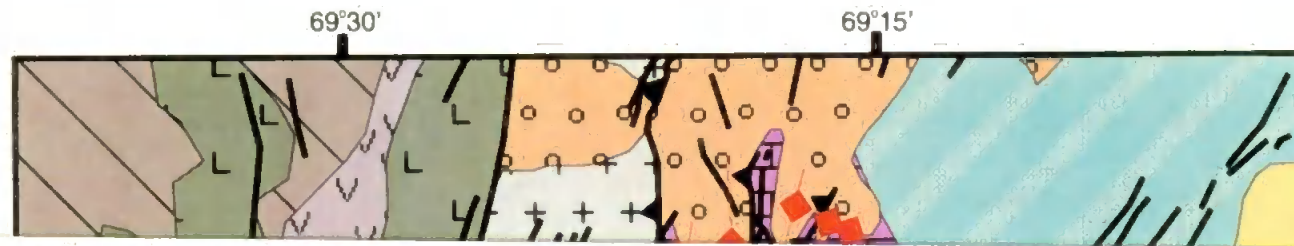
THE PRE-CORDILLERA AND THE DOMEYKO FAULT SYSTEM

6.1 Introduction


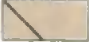


The eastern of the two sampling areas lies between 26°S and 27°S, and 60°15' and 69°40'W, east of the major mining district of El Salvador in the in the Cordillera de Domeyko. This region is part of the Andean pre-Cordillera and lies to the west of the active volcanic zone of the central Andes. The area has not, however, undergone any volcanic activity since the Quaternary (Baker *et al.*, 1987). This part of northern Chile has recently been re-mapped and extensive petrographic analyses have been carried by the Servicio Nacional de Geología y Minería. The report written to accompany the maps (Cornejo *et al.*, 1993) is the most detailed account of the geology and structure of this area. Much of the geology section is therefore based on information contained in this report. Sampling was carried out after extensive reconnaissance in the area with P. Cornejo and A. Tomlinson from SERNAGEOMIN.





The pre-Cordillera was the location of the Late Cretaceous to Palaeogene magmatic arc (Figure 1.4). The major structures are the Domeyko Fault Zone (DFZ) and a set of subsidiary faults to the east of the DFZ (Figure 6.1). Together the subsidiary faults and DFZ define the Domeyko Fault System (DFS). The subsidiary faults to the east form two distinct, but slightly overlapping domains; a fold-and-thrust belt in the north, and a zone of NW trending sinistral strike-slip faults in the south. The aim of the study was to identify and quantify rotations within the subsidiary fault domains. Samples were collected from Late Jurassic and Palaeocene volcanic rocks and Early Cretaceous sandstones from east of the DFZ. The sandstones, the Quebrada Monardes Formation, had previously been shown

Figure 6.1 (over page). Simplified geological map of the study area in the Cordillera de Domeyko. This map was compiled from the preliminary 1:50 000 maps of the Servicio Nacional de Geología y Minería.



West of the Sierra Castillo-Agua Amarga Fault










-  Undifferentiated Tertiary volcanics
-  Sierra Mantos Gruesos sequence
-  Llanta Fm.
-  Sierra Fraga Fm.

-  Unit contact
-  Fault
-  Thrust
-  Fold

0 5 10 15 20 km



East of the Sierra Castillo-Agua Amarga Fault

-  Undifferentiated Eocene-Oligocene volcanics and intrusives
-  Cerro Valiente Volcanics
-  L. Cret.-Palaeocene Volcanics
-  Quebrada Monardes Fm.
-  Pedernales Fm.
-  Quebrada Vicunita Fm.
-  Asientos Fm.
-  Montandon Fm.
-  Quebrada del Salitre and El Mono Fm.

Palaeozoic igneous basement

to carry a stable magnetic remanence (Riley *et al.*, 1993). Sites were also collected from the Sierra Fraga Formation west of the DFZ, above the Agua Amarga Thrust.

6.2 The geology and structure of the Cordillera de Domeyko and the Domeyko Fault System

The rocks in this part of the pre-Cordillera are the result of two distinct phases of volcanic and tectonic activity in the Chilean margin. During the Late Triassic to Early Cretaceous the magmatic arc (the La Negra arc) was in the Coastal Cordillera (Figure 1.4). At this time the pre-Cordillera was part of an extensive back-arc basin system known as the Tarapacá Basin (Mpodozis and Ramos, 1989). Deposited in the basin were a series of limestones, sandstones and volcanic rocks, all of which are exposed in the study area.

In the middle Cretaceous, a major tectonic reorganisation occurred throughout the region resulting in cessation of volcanic activity in the La Negra arc. Uplift and tectonic inversion of the Tarapacá Basin generated a topographic high and ended sedimentation. The area then became the source rock for the Purilactis Sandstone Formation to the east of the study area (Mpodozis and Ramos, 1989; Hartley *et al.*, 1992a).

After abandonment of the La Negra arc and regional uplift, the active volcanic centre migrated eastwards. The pre-Cordillera then became part of the Late Cretaceous to Palaeogene magmatic arc (Hammerschmidt *et al.*, 1992; Scheuber and Reutter, 1992). This active arc is represented by a series of volcanic and intrusive rocks. After the Palaeogene the locus of magmatic activity migrated to its present position in the Andean Cordillera.

6.2.1 Geology and petrology of lithologies in the study area

The major tectonic feature of the area is the north-south trending Domeyko Fault Zone (DFZ), which divides the region into two geologically distinct regions. A simplified geological map of the study area is shown in Figure 6.1, while the stratigraphy on either side of the fault zone is shown in Figure 6.2.

To the western side of the DFZ are a sequence of Jurassic-Cretaceous volcanic rocks dominated by the Jurassic-Early Cretaceous Sierra Fraga Formation (Sepúlveda and Naranjo, 1982). Although the base of this formation was not seen in the field, it is known to lie unconformably on Triassic sediments to the south of this area. This formation is a ~3000 m thick sequence of mainly lavas intercalated with limestones, terrigenous sandstones, volcaniclastic sandstones and breccias (Mpodozis and Allmendinger, 1992). Thin section analysis of two lava samples shows that they are vesicular and basalt-andesite in composition (Appendix 1). Both samples are porphyritic containing phenocrysts of plagioclase feldspar, some of which contain early opaque minerals, and clino-pyroxene in a fine, sometimes glassy, groundmass which also contains opaque minerals. The rocks have been pervasively altered, probably by hydrothermal fluids and there is a large amount of epidote, sericite and chlorite present.

During the course of this work, the Sierra Fraga Formation was sampled in the south-west of the study area, just above the Agua Amarga Thrust. At the base of the outcrop is an intercalated limestone bed containing fossils of Bajocian age. The volcanic rocks sampled from this locality are therefore probably Middle or Late Jurassic in age.

Deposited upon the Sierra Fraga Formation is the Llanta Formation. The contact between the formations is a 50-60° westward dipping, angular unconformity, the cause of which is uncertain as no major pre-middle Cretaceous deformation events are recognised elsewhere in this part of the margin. The Llanta Formation is poorly dated and loosely referred to as Early Cretaceous in the literature. The formation comprises a series of

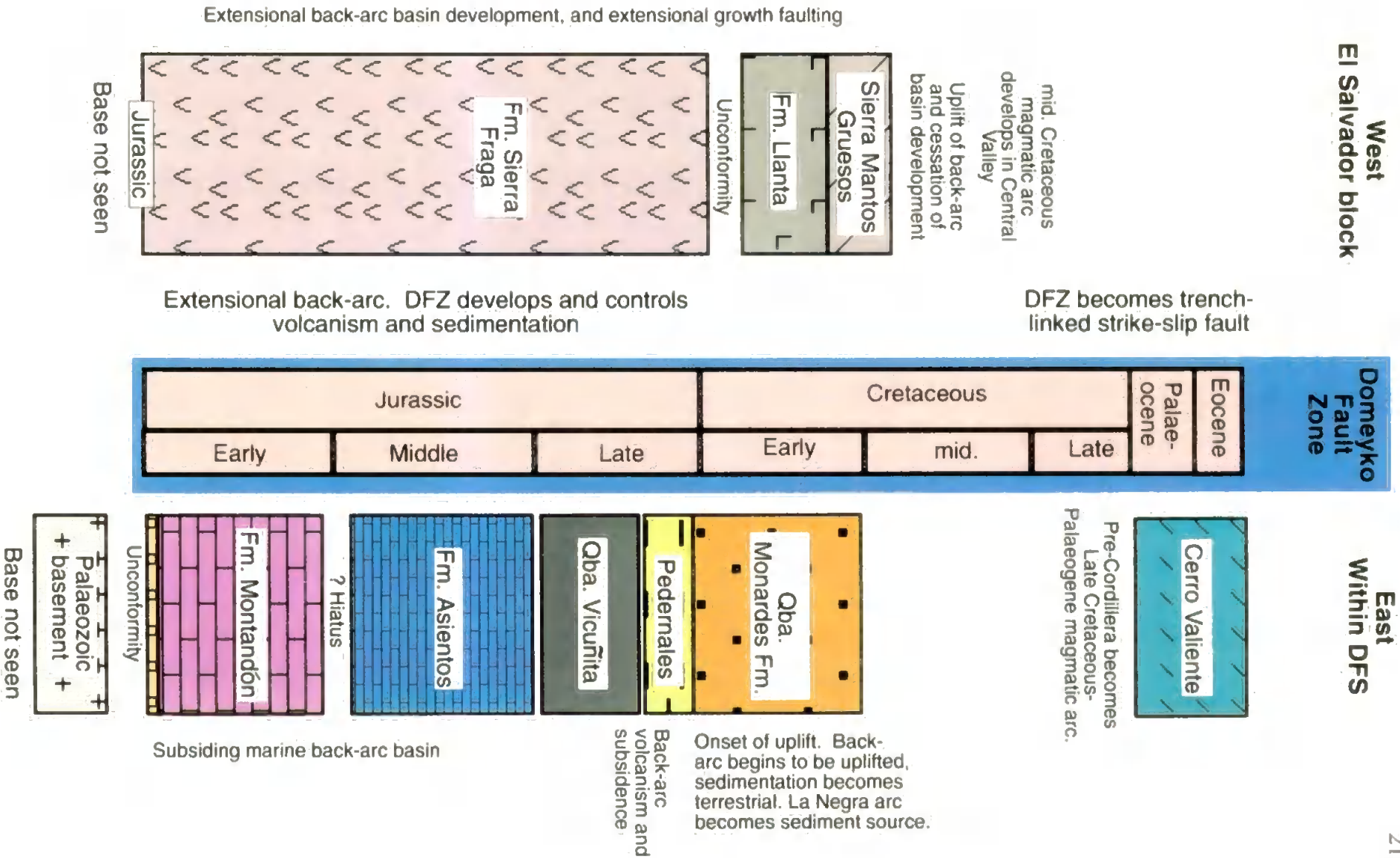


Figure 6.2. Stratigraphy on either side of the Domeyko Fault Zone. (Compiled from Cornejo *et al.*, 1993).

andesitic lavas and breccias intercalated with grey and green sandstones and conglomerates which may be laterally equivalent to the Cerillos Formation farther west.

At the top of the sequence, west of the DFZ, is the Sierra Mantos Gruesos Sequence. This series of andesitic-basaltic lavas with associated sandstones and pyroclastic flow deposits form outcrop only in the NW corner of the study area. A contact with the Llanta Formation is difficult to identify and the sequence may be a localised temporal variation in the Llanta Formation.

The geology east of the DFZ is characterised by a sequence of Mesozoic to Pliocene sediments and volcanic rocks. At the base of the sequence are the Early-Middle Jurassic limestones of the Montandón and Asientos Formations (Plate 6.1a) (Harrington, 1961). The Montandón formation has a basal conglomerate and is in unconformable contact with the Palaeozoic granitic basement, elsewhere the formation is known to lie conformably on Triassic clastic sediments. The Montandón formation comprises a combination of intercalated marine limestones and sandstones, while the Asientos Formation is characterised by marine calc-arenites and green volcanic sandstone horizons. Palaeontological evidence indicates that there may have been an hiatus in deposition between the two limestone units, although its length has not been established.

A period of volcanism in the Late Jurassic resulted in deposition of the Quebrada Vicuña Formation (Plate 6.1a and b). The formation is dominated by a series of green andesitic lavas intercalated with thin horizons of limestones and calc-arenites. Thin sections of lava samples show that they are basaltic in composition (Appendix 1). All three lavas analysed were vesicular and porphyritic, containing phenocrysts of plagioclase feldspar and clino-pyroxene in a fine groundmass of feldspar, pyroxene and opaque minerals. Plate 6.2 shows the typical composition of the lavas. Like the Sierra Fraga Formation these samples show the effects of pervasive alteration, characterised by sericitisation of feldspars and the



Plate 6.1a. The major Jurassic units in Asientos Gulch. In the background are the limestone units of the Montandon and Asientos Formations, in the foreground are the lavas of the Quebrada Vicunita Formation.



Plate 6.1b. Asientos Gulch. The Quebrada Vicunita Formation at the base of the valley side, overlain by the limestones of the Pedernales Formation.

presence of quartz (often with fluid inclusions), epidote, chlorite and calcite. Vesicles are often filled with epidote and chlorite. The groundmass also contains secondary haematite. Plate 6.3 shows two cross-cutting veins which demonstrate the order of secondary mineralisation; epidote-chlorite-quartz-calcite. The age, composition and alteration of the formation suggests that it may be laterally equivalent to the Sierra Fraga Formation.

At the end of the Jurassic, sedimentation was resumed and continued through the Early Cretaceous. Stratigraphically above the Quebrada Vicuña Formation are a series of Late Jurassic shallow marine limestones with intercalated green volcanic horizons which constitute the Pedernales Formation (Plate 6.1b) (Harrington, 1961). The limestones are succeeded by the Quebrada Monardes Formation (Bell, 1991), also known as the Agua Helada Formation (Garcia, 1967). This is a sequence of aeolian and fluvial red arkosic sandstones with minor evaporite horizons which were deposited in a sabkha type environment as the result of marine regression in the Early Cretaceous (Suárez and Bell, 1985). This marine regression is linked to the early stages of uplift of the Coastal Cordillera and the La Negra arc, which became the source area for the Quebrada Monardes Formation. The major phase of uplift in northern Chile was middle Cretaceous in age, when the magmatic arc migrated eastwards from the Coastal Cordillera. This resulted in uplift and the cessation of deposition in the pre-Cordillera. Thin section analysis of samples from the Quebrada Monardes Formation shows the petrology to be dominantly fine to medium sand sized grains of altered feldspar (Plate 6.4). Also present in decreasing abundance are igneous lithic fragments, quartz, polycrystalline quartz and mica. The non-polycrystalline quartz often contains fluid inclusions indicative of a hydrothermal origin. The petrology of the lithic clasts indicate an igneous or low grade metamorphic source for the clasts, consistent with derivation from the magmatic arc to the west.

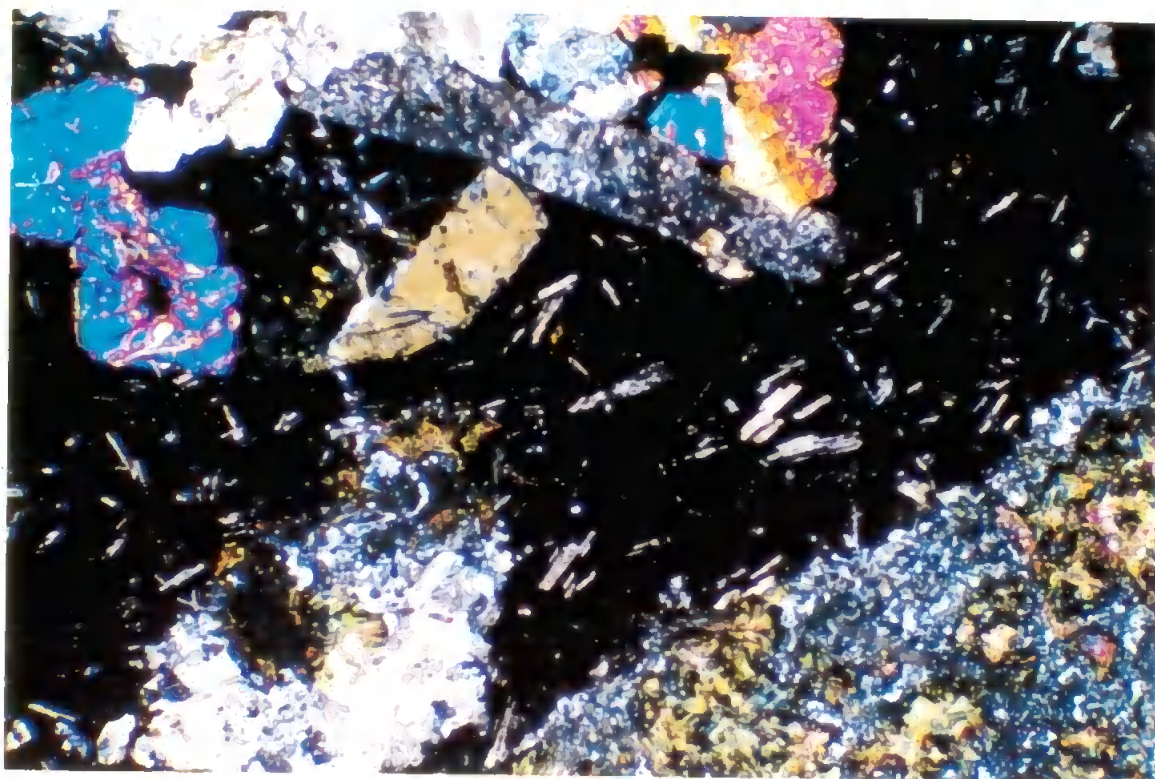


Plate 6.2. Thin section photograph of a lava from the Quebrada Vicunita Formation. Phenocrysts of clino-pyroxene and altered feldspar can be seen in a fine groundmass. Horizontal field of view 3.3 mm, crossed polars.

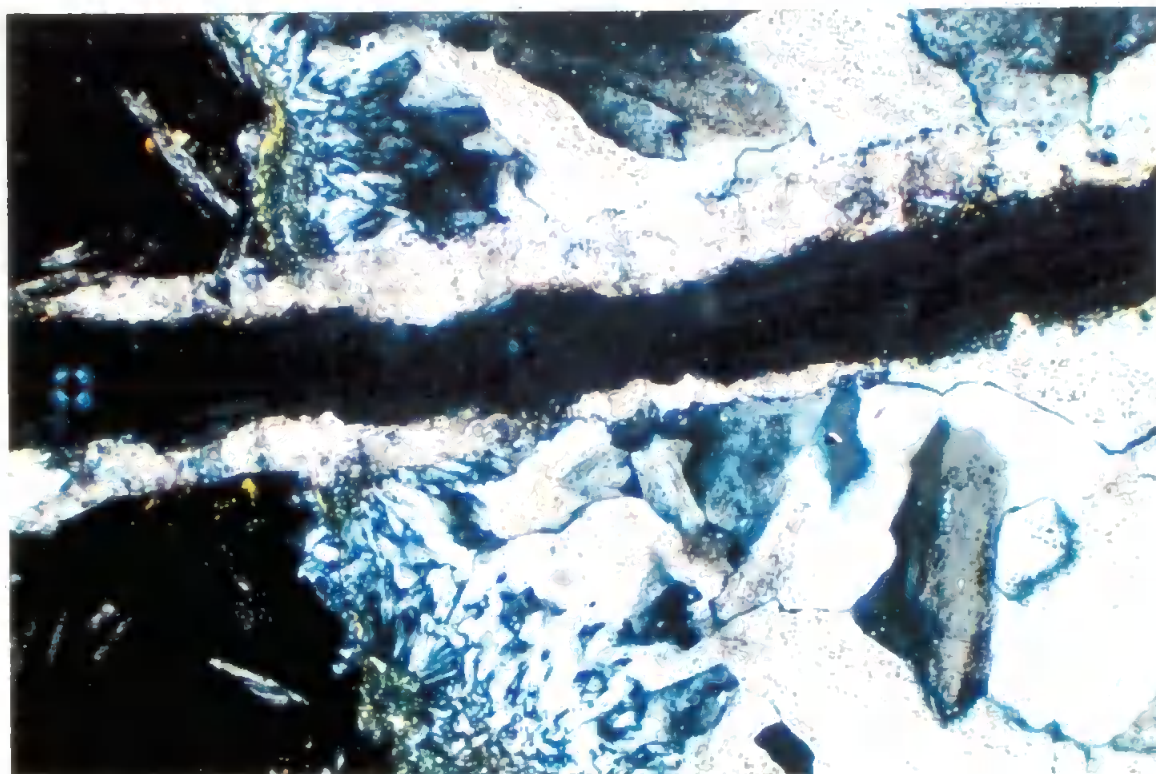


Plate 6.3. Thin section photograph of two cross-cutting veins from the Quebrada Vicunita Formation. The order of secondary mineralization is epidote, chlorite and quartz in the N-S vein, cut by a later E-W calcite filled vein. Horizontal field of view 1.29 mm, crossed polars.

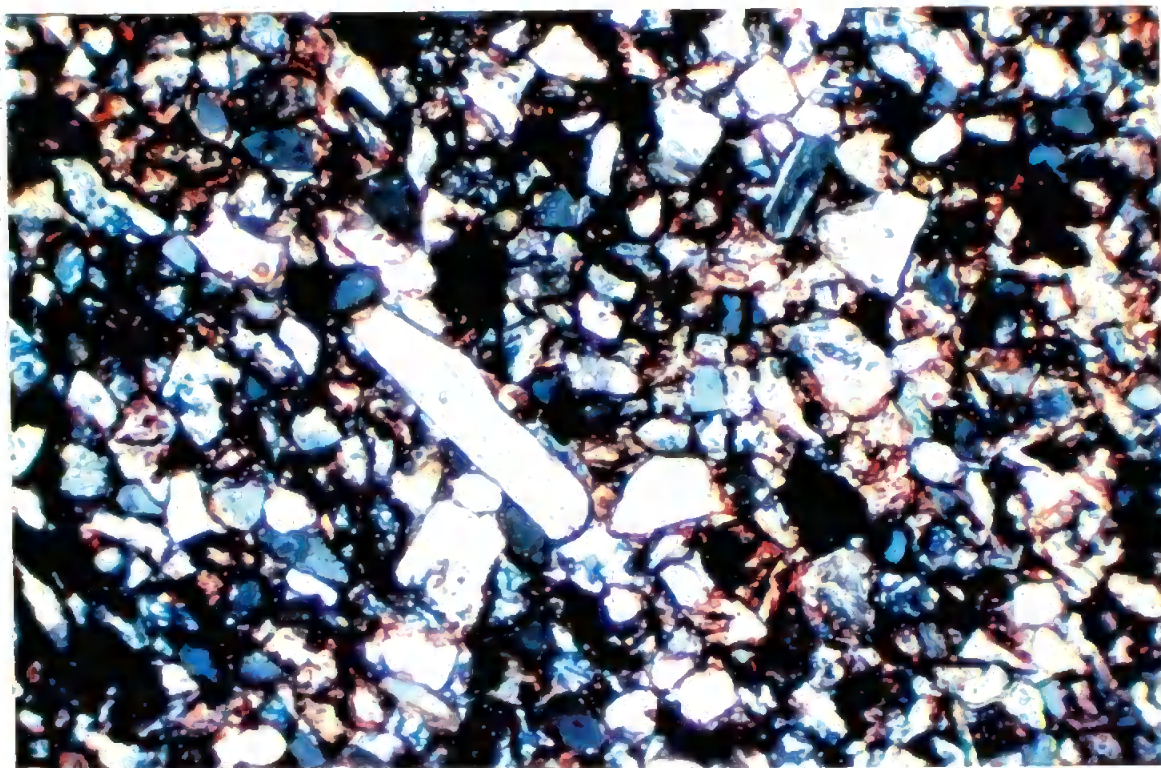


Plate 6.4. Thin section photograph of grains in the Quebrada Monardes Formation. Plagioclase dominates, but quartz and lithic fragments can also be seen. Horizontal field of view 1.29 mm, crossed polars.

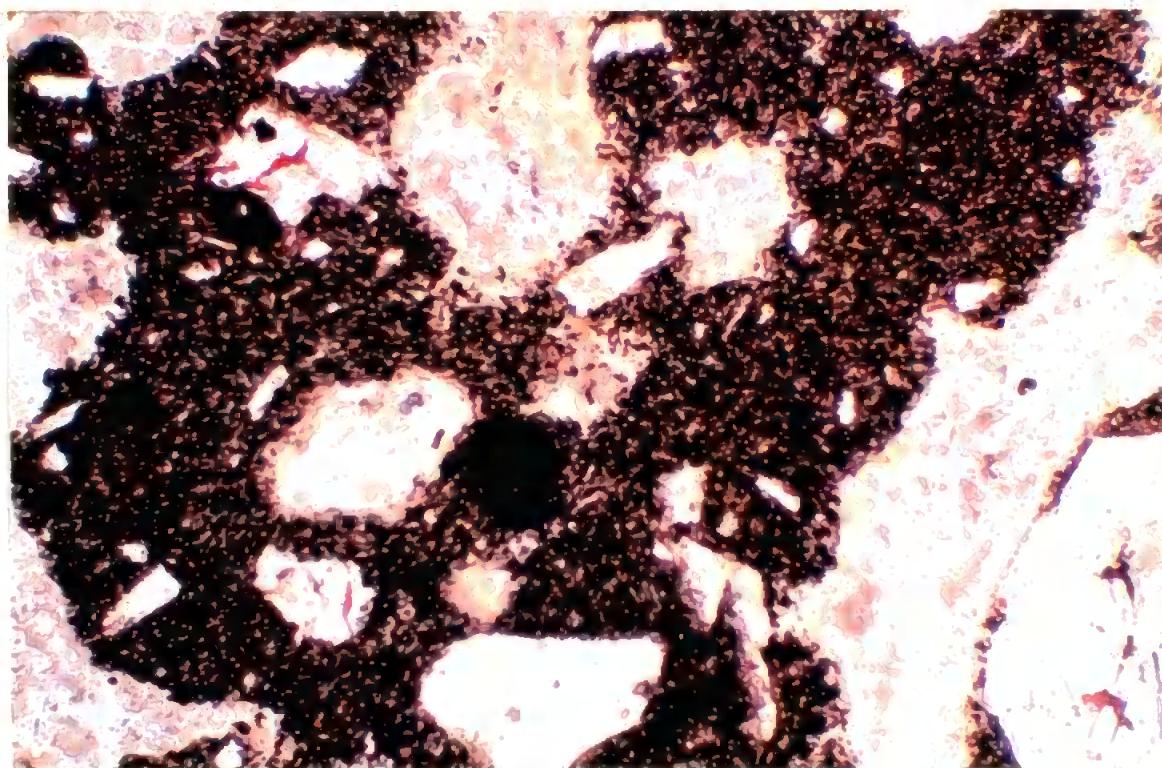


Plate 6.5. Thin section photograph of a Cerro Valiente lava. Plagioclase and olivine phenocrysts in a fine groundmass of opaque minerals and possibly glass. Secondary haematite is present. Horizontal field of view 3.3 mm, plane polarised light.

Although magmatic arc rocks of Late Cretaceous to Pliocene age outcrop in the pre-Cordillera, only the Palaeocene-Eocene rocks of the Cerro Valiente Sequence are exposed in the study area where they rest unconformably on the Mesozoic sediments. The petrology of this unit is highly variable and it is subdivided into three main sub-units. The basal unit comprises trachy-andesitic lavas and breccias, with minor rhyolitic flows; the middle unit is dominated by rhyolitic lavas with ignimbrites and trachy-andesitic lavas; and the upper unit is composed of both basaltic and rhyolitic flows. All three sub-units occur in the study area, with the basal unit being well exposed. Two thin sections have been studied from samples of the upper unit in the northern part of the study area. The rocks are highly altered porphyritic basalt lavas, having phenocrysts of both plagioclase feldspar and olivine. Some of the feldspars contain early formed opaque minerals. The groundmass is composed of opaque minerals and feldspar with some glassy patches (Plate 6.5). There is also a large amount of secondary haematite in the groundmass, particularly associated with veins.

6.2.2 Structural geology and the Domeyko Fault System

The major tectonic feature in the study area is the sub-vertical north-south trending Domeyko Fault Zone (DFZ) which forms the western boundary to the Cordillera de Domeyko. In the sampling region this fault zone is defined by the Sierra Castillo-Agua Amarga Fault System and the La Ternera Fault (Figure 6.3), although the DFZ also includes the West Fissure Fault to the north (Tomlinson *et al.*, 1993). The fault zone appears to have had a long history of activity, the distribution of rocks either side of the DFZ indicating that it affected volcanism in the Jurassic and was therefore active from this time. The main phase of fault motion was associated with the Late Cretaceous-Palaeogene magmatic arc, when the fault became a trench-linked strike-slip fault (Mpodozis and Ramos, 1989).

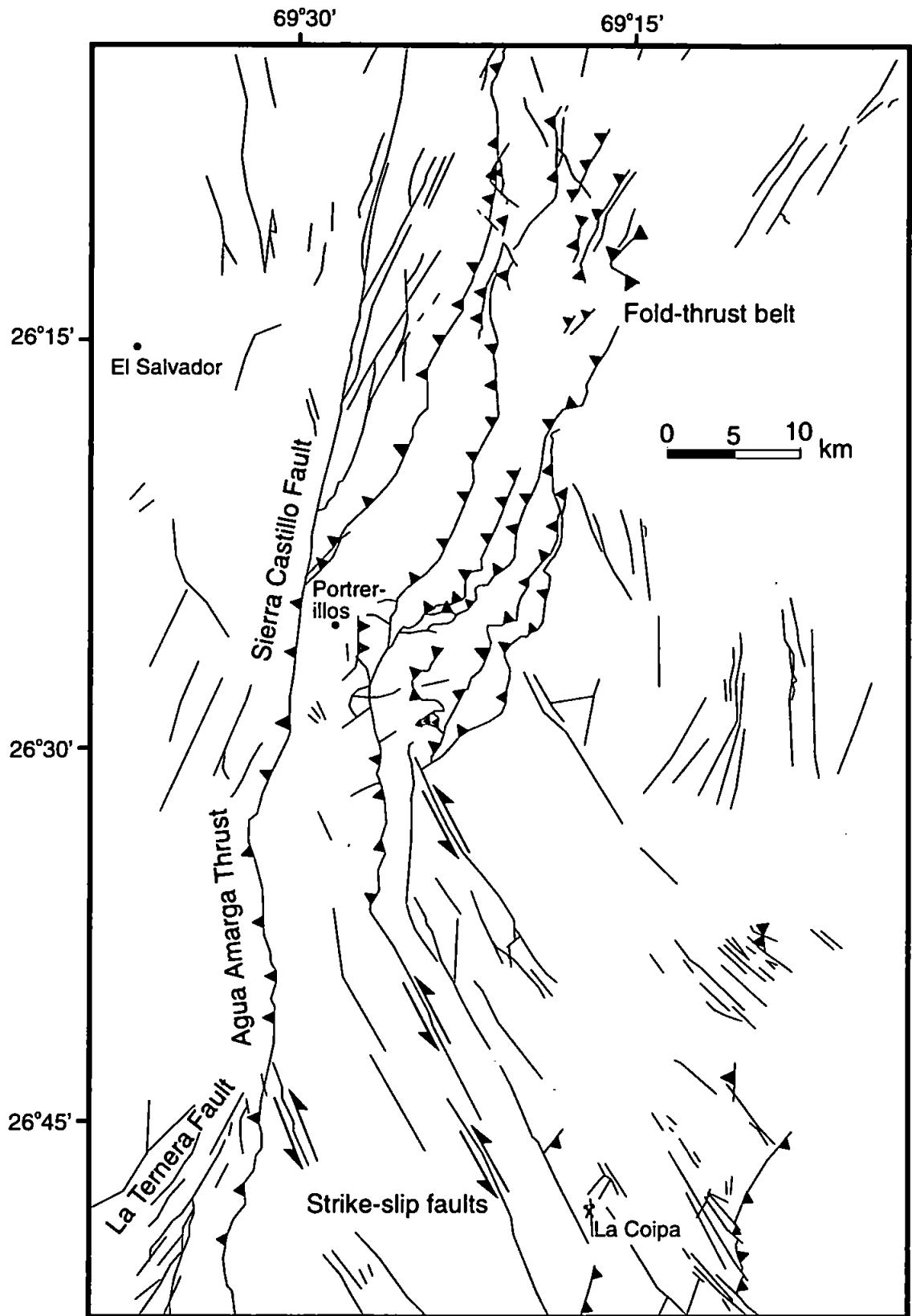


Figure 6.3. Map of the major fault which comprise the Domeyko Fault System in the study area. The Domeyko Fault Zone comprises the Sierra Castillo Fault and the Agua Amarga Thrust in this area. Map compiled from preliminary structural geology maps of the Servicio Nacional de Geología y Minería, Chile.

In the north, the Sierra Castillo Fault is a near vertical fault and displays a consistent sinistral strike-slip shear sense. The fault has also undergone a component of reverse, up to the east slip (Tomlinson *et al.*, 1993). The Sierra Castillo fault apparently changes into the Agua Amarga Thrust in the south, but the Agua Amarga Thrust may be an eastward directed thrust flap, a thin thrust sheet pushed over the top of the main strike-slip fault during transpression (Tomlinson *et al.*, 1993). The La Ternera Fault, a sinistral strike-slip fault in the hanging-wall of the Agua Amarga Thrust (Figure 6.3), may be the true southward continuation of the Sierra-Castillo Fault. If the Agua Amarga Thrust is a thrust flap its timing of emplacement over the Sierra Castillo-La Ternera strike-slip fault zone is uncertain. The La Ternera Fault is, however, less well defined than the Sierra Castillo Fault and does not show the same amount of displacement. This would imply that if the Agua Amarga Thrust is a thrust flap, it was emplaced after the major phase of strike-slip motion on the La Ternera Fault. This may indicate that the Agua Amarga Thrust was emplaced towards the end of the period of major tectonics, probably in the Eocene-Oligocene.

To the east of the DFZ are a series of subsidiary faults which can be divided into two distinct but slightly overlapping structural domains. In the north is a fold-and-thrust belt, and in the south a set of sinistral strike-slip faults (Figure 6.3). The structures in these domains do not extend westward beyond the DFZ indicating that the DFZ is a regional structural break. When considered with the DFZ the two domains define a wide deformation zone here called the Domeyko Fault System (DFS).

The fold-and-thrust belt, the northern domain, is approximately 14 km wide and has accommodated a minimum of 50% east-west shortening. The fold-and-thrust belt can itself be sub-divided into two smaller areas based on the structural style of the deformation. The eastern area is characterised by thin-skinned ramp-flat style folding and thrusting, while the western sub-division displays thick-skinned deformation involving thrusting of the

Palaeozoic basement. Copper porphyry deposits cut by the fold-and-thrust belt indicate that the deformation occurred during the Eocene-Oligocene (Olson, 1989).

The southern domain is dominated by NW trending sinistral strike-slip faults, although there are some high angle reverse faults with a NNE orientation. As in the fold-and-thrust belt there is an east-west variation in the deformation style. The major western set of strike-slip faults have a spacing of 2-3 km and a relatively large amount of displacement, while in the east the strike-slip faults are more closely spaced, typically 0.5-1 km, and show smaller displacements. Syntectonic Eocene intrusions (42-38 Ma) emplaced along the faults at an angle to the general trend of the magmatic arc indicate that the faults were active at this time. It is likely therefore that the major phase of activity on the strike-slip faults coincided with the Eocene-Oligocene development of the fold-and-thrust belt. In the eastern strike-slip fault set Oligocene to early Miocene (24-22 Ma) volcanic rocks in some places cover, and in other places are cut by the faults, indicating that these strike-slip faults also underwent a period of motion at this time.

The area to the west of the DFZ, the El Salvador Block, is not described in detail here as the area covered during this study only extends as far as the syncline in the hanging-wall of the Agua Amarga Thrust. Cornejo *et al.*, (1993) report that large scale folds and several faults sets have been identified within the block, most of which are associated with the development of the Las Amarillos-El Salvador caldera complex. Two sets of post-caldera faults have also been recognised, but these faults do not seem to form a distinct structural domain as is seen to the east in the DFS. Their relationship to the DFS is therefore not clear.

6.3 Palaeomagnetic results

6.3.1 Sierra Fraga Formation (Middle-Late Jurassic)

i) Palaeomagnetic sampling localities

Sites from the Sierra Fraga Formation were collected in the southern part of the study area only (Figure 6.4). Sites were collected from both limbs of an overturned syncline in the hangingwall of the Agua Amarga Thrust. Ten sites, ESP32-41, were sampled. Four sites, ESP32-34 and ESP40, were collected as drill cores, all other sites were collected as orientated hand samples. At this location the formation is composed of intercalated lavas and volcanoclastic sediments which could be used for good structural control.

ii) Magnetic mineralogy

IRM data for two of four investigated samples is shown in Figure 6.5. IRM acquisition is indicative of combined low and high coercivity carriers, dominated by the low coercivity fraction. This is confirmed by the demagnetisation of IRM which shows dominant intermediate and low coercivity components removed steadily up to 570-600°C. The highest coercivity component is demagnetised at 680°C. Demagnetisation of the NRM is completed at 80 mT in ESP37-2-3, and at 100 mT or 600°C in ESP40-3. Although some remanence remains in these samples above these demagnetisation levels, no consistent end point direction was obtained. This indicates that the haematite component does not hold a stable magnetic remanence in the NRM. The IRM and NRM data indicate a combined magnetite/titanomagnetite and haematite carrier, dominated in both cases by the low coercivity component.

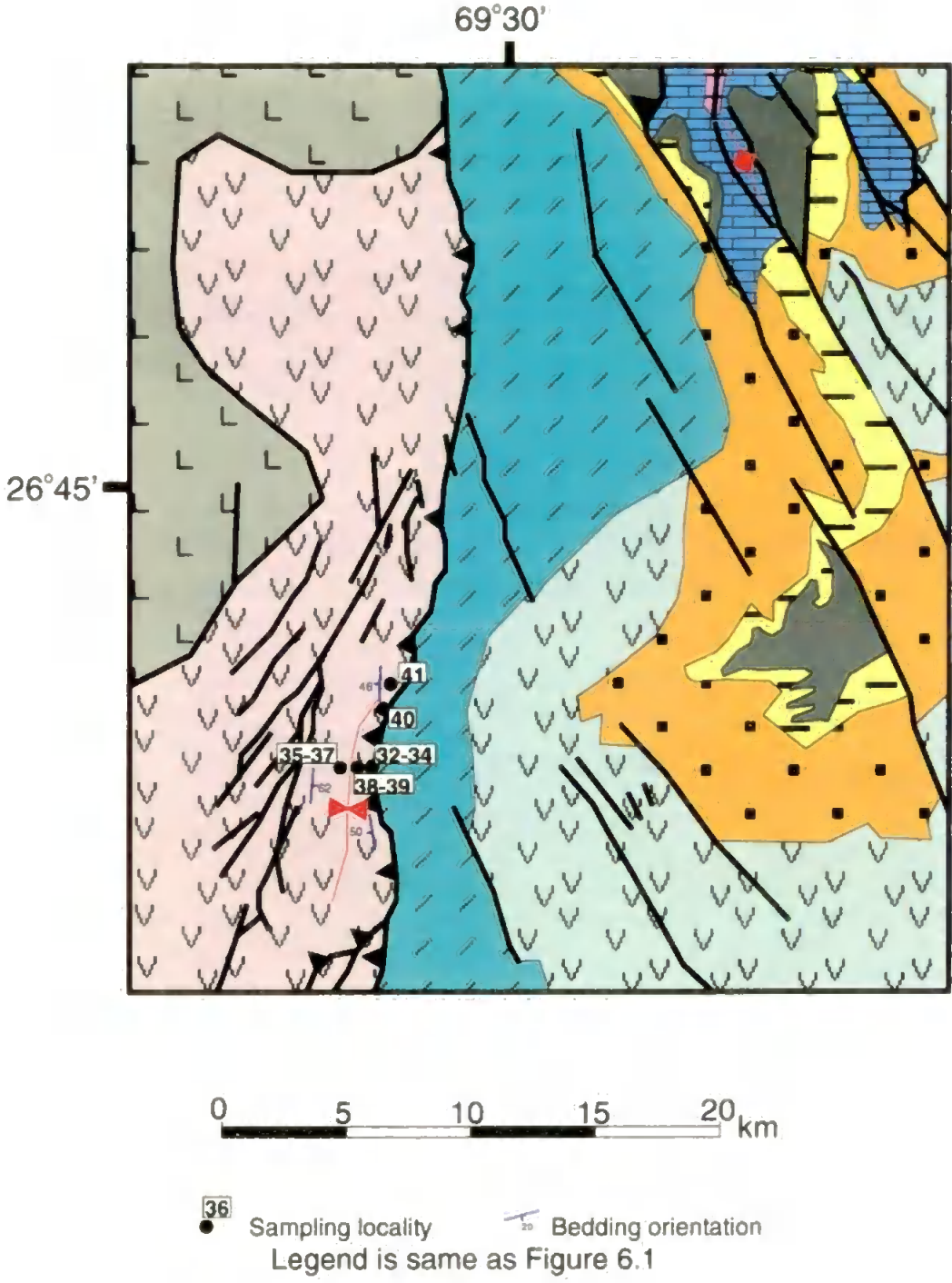


Figure 6.4. Sampling localities for the Sierra Fraga Formation, these were collected in the southern region of the study area only.

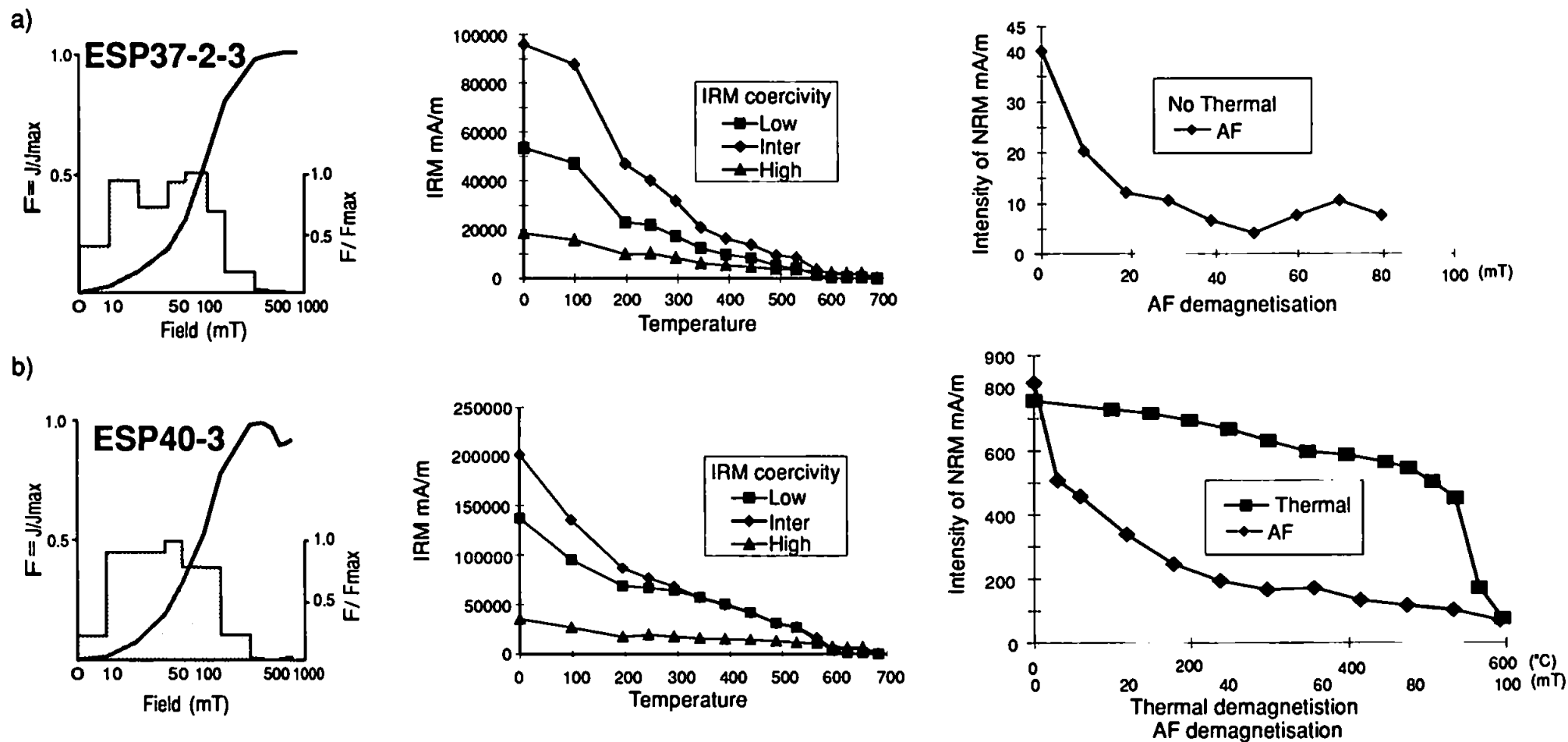


Figure 6.5a, b. Rock magnetic experiments from samples of the Sierra Fraga Formation. Graphs show acquisition of IRM, demagnetisation of three-axis IRMs and demagnetisation of remanence.

iii) Palaeomagnetic remanence measurements

All ten sites from the Sierra Fraga Formation have been demagnetised and the results are given in Tables 6.1 and 6.2. Samples display a large amount of within site variation. For this reason some of the site mean directions are based on only a few samples, additionally, the α_{95} confidence limits for many of the site mean directions are large. Table 6.1 shows that the characteristic direction within a site is often isolated across a range of demagnetisation levels, this is due to variation in the blocking temperature of the multiple components within the sites.

A plot of the low coercivity and unblocking temperature directions is shown in Figure 6.6. Generally the directions are scattered and the grouping does not improve on tilt correction. Notably absent is a present day field direction. In many of the sites collected as hand samples, low component directions tend to be well grouped within each block, samples drilled in the field do not form a coherent group. These results suggest that the low coercivity/unblocking temperature components were acquired after the cores or blocks were collected, and therefore represent a laboratory induced component.

Site mean directions are extremely variable, both *in situ* and after tilt correction, and identifying a formation ChRM is not possible. Demagnetisation behaviour is also variable both within and between sites, Figures 6.7a-d show examples of demagnetisation plots from the formation. Figure 6.7a shows a single component of magnetisation carried by both magnetite and haematite, some of the other samples from this site (ESP34) are less stable and show more complex demagnetisation trajectories. The demagnetisation plots shown in Figure 6.7b-d indicate multiple magnetisation components some with overlapping blocking and coercivity spectra. This type of demagnetisation is characteristic of most samples studied, although there is significant variation in the directions of the components.

Site	Sampling site		Tilt correction	°C Min.	ChRM isolation		mT Max.
	Long. W	Lat. S			Max.	Min.	
ESP32	69°33'	26°50'	180/50	NRM→450	610	20	80
ESP33	69°33'	26°50'	180/50	300	600	NRM→30	90
ESP34	69°33'	26°50'	180/50	NRM→400	680	10→30	90
ESP35	69°34'	26°50'	005/64	Not done		20	60→100
ESP36	69°34'	26°50'	005/62	Upto 630		10	100
ESP37	69°34'	26°50'	005/62	Not done		NRM→20	50→80
ESP38	69°34'	26°50'	190/56	500	590→700	10	100
ESP39	69°34'	26°50'	192/54	Upto 630→700		10→40	100
ESP40	69°33'	26°49'	182/46	400	680	10	100
ESP41	69°33'	26°49'	181/46	250	550	NRM→60	100

Table 6.1. Sampling and demagnetisation data from sites in the Sierra Fraga Formation. Tilt correction is given in right-hand-rule format, ChRM isolation is demagnetisation level at which ChRM is isolated in the site, a range with an arrow indicates a within site variation.

a)	Site	n/No	Uncorrected		Corrected		k	α_{95}
			Dec.	Inc.	Dec.	Inc.		
	Agua Amarga Region							
a b c	ESP32	7/7	177.9	71.5	246.2	38.2	27.2	11.8
	ESP33	Unstable no site mean direction						
c	ESP34	4/6	175.3	30.9	202.1	22.6	115.9	8.6
a b c	ESP35	6/6	137.1	47.3	122.3	-7.5	60.9	8.6
a b c	ESP36	6/6	75.6	55.6	84.2	-4.8	12.0	20.9
a b c	ESP37	5/6	299.1	-24.8	301.0	32.3	16.0	20.3
a b c	ESP38	5/6	104.5	79.2	278.8	44.8	13.2	24.6
a c	ESP39	3/6	314.0	51.5	301.2	2.1	62.7	15.7
	ESP40	6/6	232.2	3.4	224.0	-30.7	24.7	13.8
	ESP41	7/7	53.9	-10.1	49.4	26.2	10.9	19.3

b)	Visually identified groupings		No. sites	Dec.	Inc.	k	α_{95}
a	Best Mean	In situ	6/10	292.8	18.3	1.4	106.1
		Tilt corrected		283.7	23.0	8.3	24.7
b	Best Mean	In situ	5/10	120.2	59.4	8.7	27.5
		Tilt corrected		133.4	20.2	1.2	180.0
c	Best fit great circle pole	In situ	7/10	229.6	3.1	0	36.9
		Tilt corrected		52.8	56.5	0	29.4

Table 6.2. a) Remanence data from the Sierra Fraga Formation. n/No. is number of samples included in site mean/number of samples demagnetised; dec. and inc. are declination and inclination of remanence vector, k is Fisherian precision parameter, α_{95} is semi-angle of 95% cone of confidence. a b c in the first column indicates inclusion of the site within a formation mean calculation. b) Formation mean calculations for three visually identified groupings. Data are given *in situ* and tilt corrected although the groupings were identified in the co-ordinate system marked in bold.

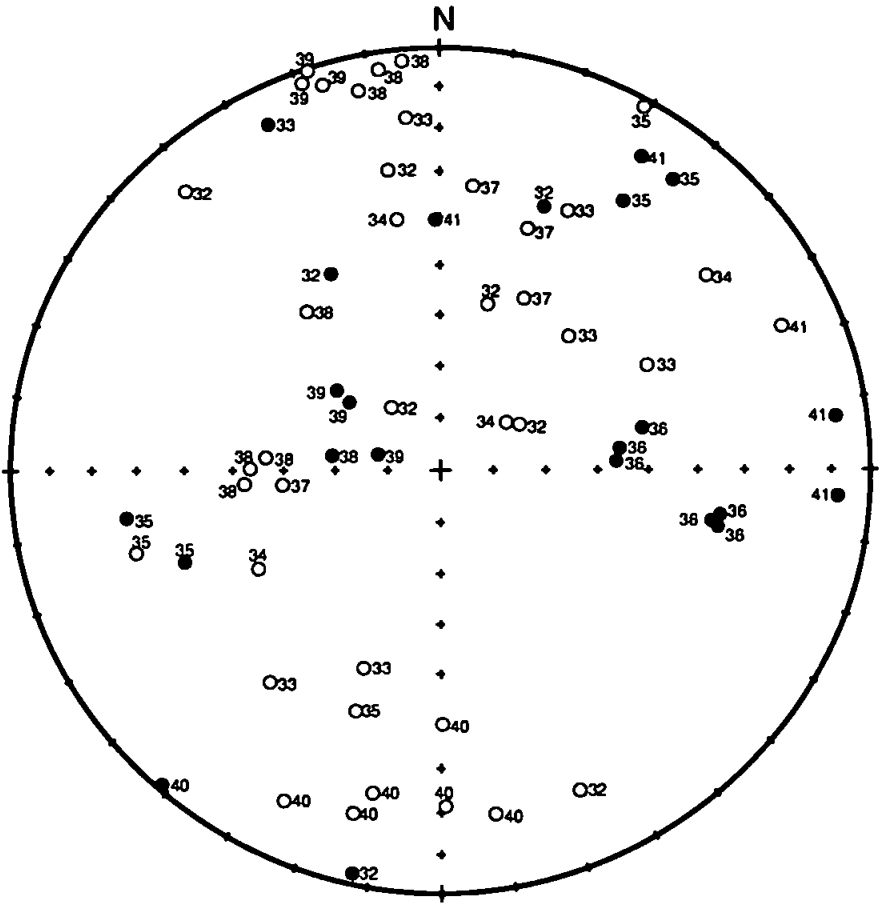


Figure 6.6. Equal area stereographic projection of low coercivity and unblocking temperature components from sites in the Sierra Fraga Formation. Open (closed) symbols are upper (lower) hemisphere projections. Directions are *in situ* numbers are site numbers.

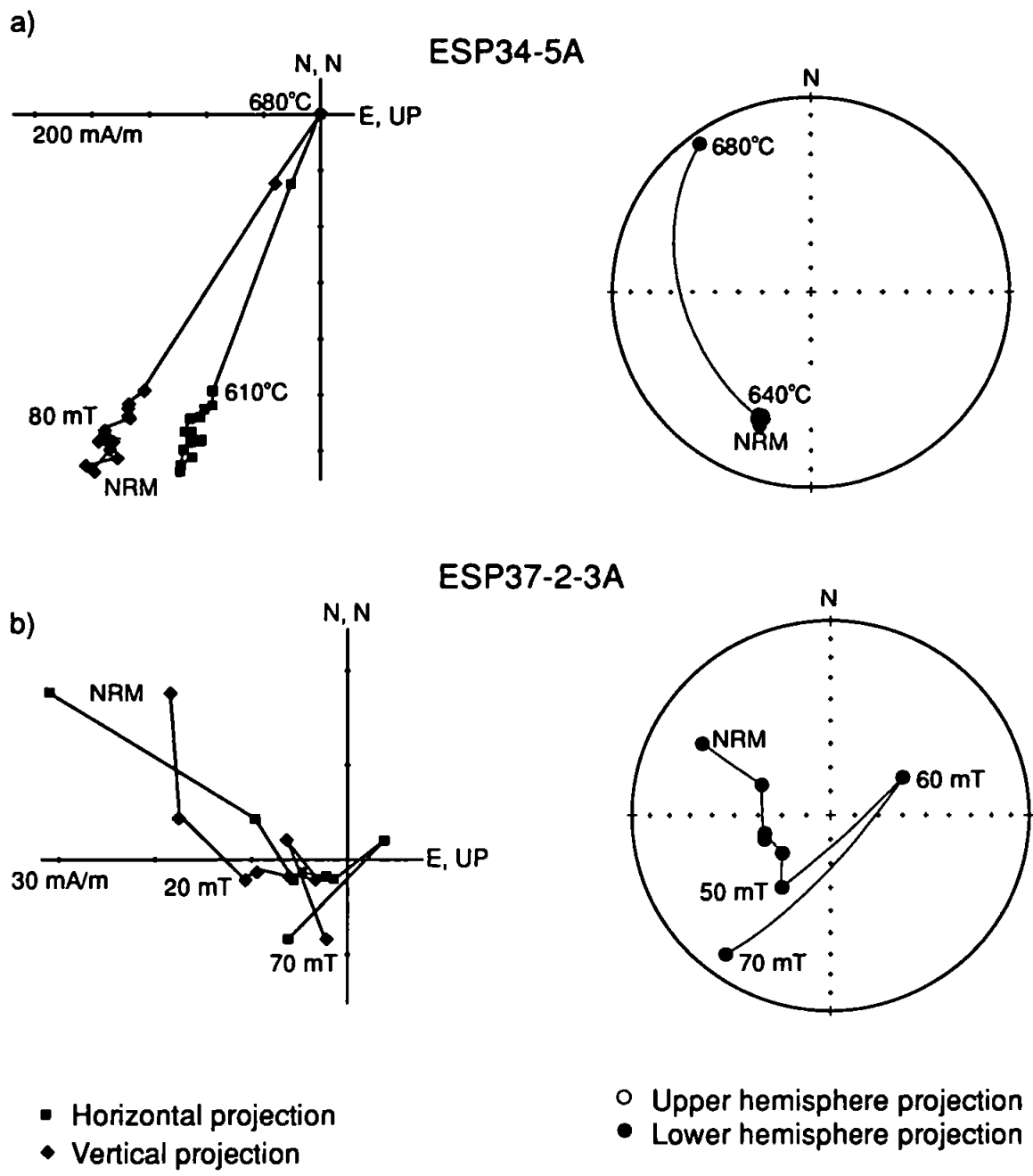


Figure 6.7a, b. Examples of demagnetisation behaviour in samples from the Sierra Fraga Formation. All plots are tilt corrected.

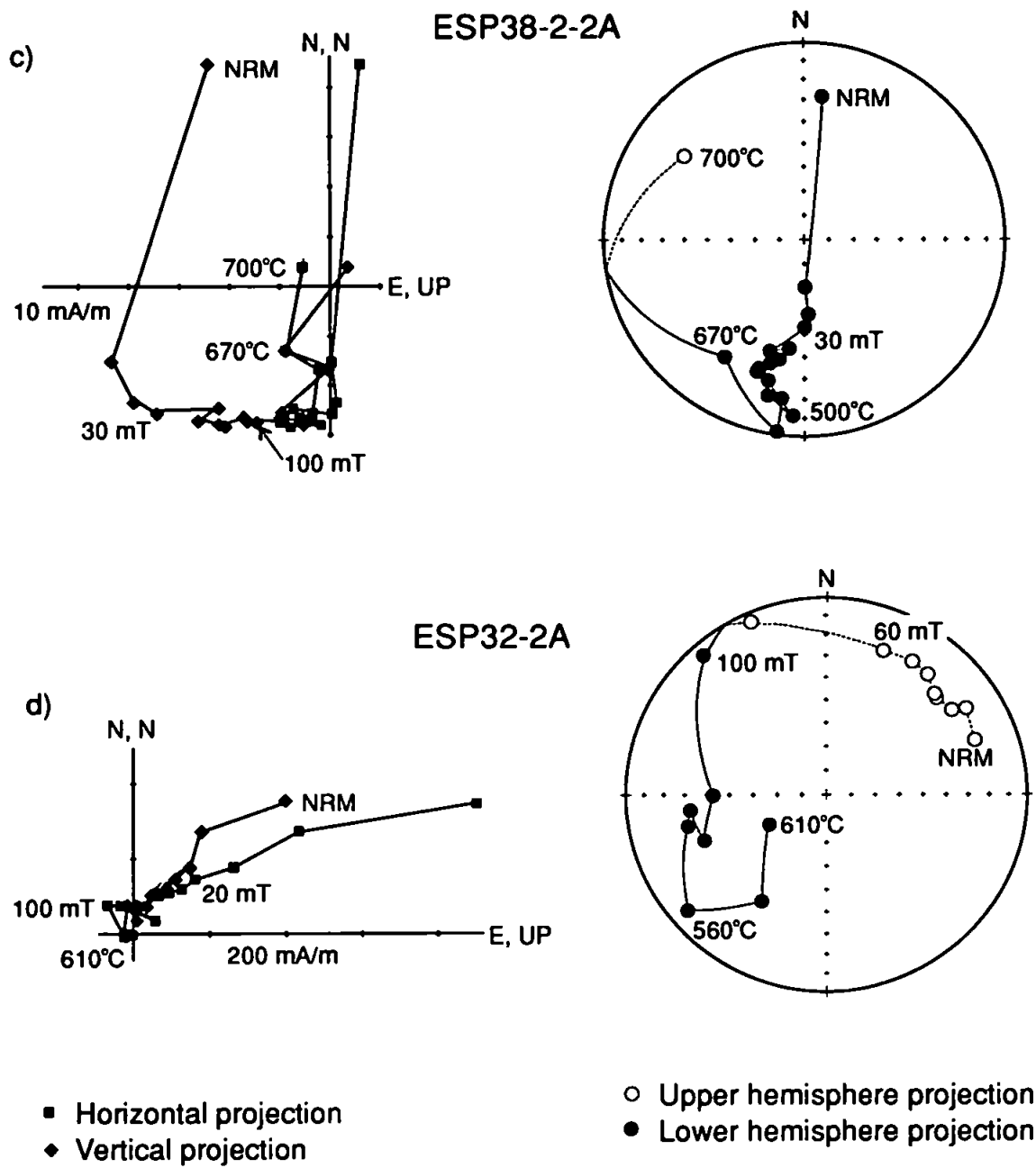


Figure 6.7c, d. Examples of demagnetisation behaviour in samples from the Sierra Fraga Formation. All plots are tilt corrected.

Three possible distributions of mean directions have been analysed based on visual assessment of the distribution of the data both *in situ* and after tilt correction (Table 6.2b; Figure 6.8). These distributions are all poorly constrained with large confidence limits. The three groupings are:

a) a tilt corrected mean direction based on six sites, four with reversed polarity. The improvement in k on tilt correction ($k_1/k_2 = 4.3$, greater than the statistically significant value of 2.98 at the 95 % confidence level) passes the fold test of McElhinny (1964). The inclination of the mean direction is too shallow for the sampling locality if it is to represent a geologically meaningful direction.

b) an *in situ* grouping based on five sites, four of which have reversed polarity. The increase in precision parameter, k , on tilt correction fails the fold test of McElhinny (1964) as $k_1/k_2 = 0.14$ which is less than the 95 % statistically significant value of 3.44.

c) a great circle path defined by seven sites after tilt correction. The positions of the sites before and after tilt correction are shown in Figure 6.9. Although a fold test cannot be performed on a great circle distribution, the α_{95} confidence limit on the mean is smaller when the data are considered in tilt corrected co-ordinates. Five of the site mean directions which are included in the great circle distribution also compose the *in situ* mean direction.

iv) Discussion of results

The three mean distributions identified from the site mean directions are very poorly constrained. The semi-angle of their confidence limits means that none of these mean groupings is statistically significant, as accepted in this work (i.e., $\alpha_{95} < 24^\circ$). In addition, the groupings do not have directions consistent with those interpreted from other units in

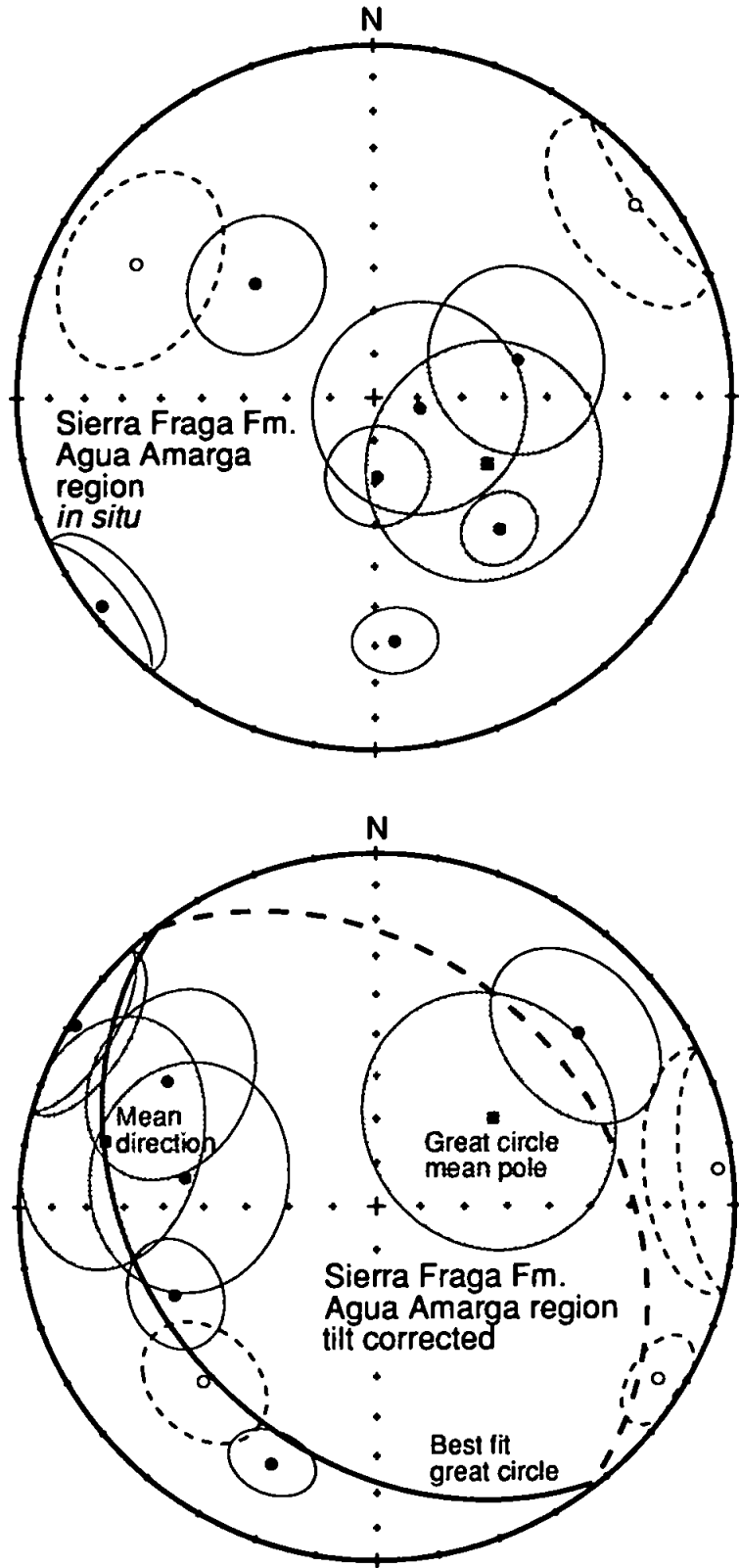


Figure 6.8. Equal area stereographic projection of site mean directions from the Sierra Fraga Formation (circles) from the Agua Amarga region. The three identified formation mean directions are also shown (squares). Error ellipses are 95% confidence. Open (closed) symbols are upper (lower) hemisphere projections.

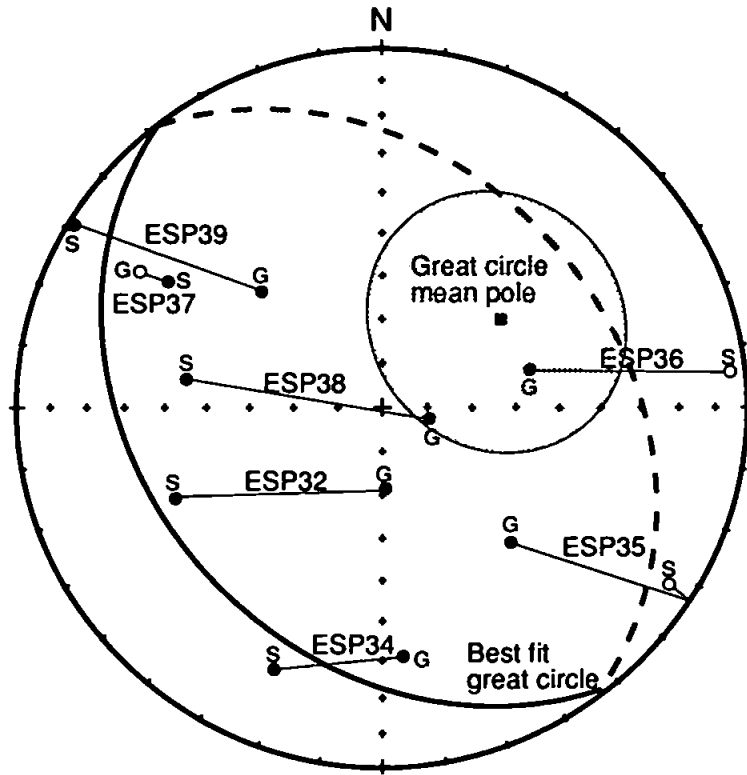


Figure 6.9. Equal area stereographic projection of site mean directions from the Sierra Fraga Formation used in calculation of the best fit great circle. G indicates the sites in situ position, and S its tilt corrected position. Open (closed) symbols are upper (lower) hemisphere projections.

the pre-Cordillera from this study, and therefore do not make geological sense. None of the three groupings are therefore considered further.

6.3.2 Quebrada Vicuña Formation (Late Jurassic)

i) Palaeomagnetic sampling localities

The Quebrada Vicuña Formation was sampled in both the northern and southern structural domains (Figures 6.10 and 6.11). A total of 28 sites were collected, 17 in the north (ESP43-59), and 11 in the south (ESP1-11). The northern sites were sampled through two NE-SW trending synclines, most were collected in Quebrada Asientos, a large E-W trending valley. All sites except ESP55 were collected as orientated hand samples. Figures 6.12 and 6.13 show cross-sections through the synclines where samples were taken. Structural control could be obtained from the limestone beds intercalated with or lying directly below the lavas.

Sites in the southern domain were collected as orientated hand samples from the core of a shallowly SW plunging syncline. Individual site dips were measured from primary lava flow surfaces and limestones of the Pedernales formation which lie above the lavas. The dips were variable due to minor folding on the limbs of the major structure.

ii) Magnetic mineralogy

Figure 6.14 shows the results of IRM experiments on two samples from the formation. Both samples show rather noisy IRM acquisition curves, due to instrument instability of the magnetometer when measuring very high intensities. The general trend of the graphs would seem to indicate a significant high coercivity component. This is not, however, supported by the IRM demagnetisation which shows only a small contribution of the high coercivity component to the IRM. This is particularly the case in ESP3-1-2 (Figure

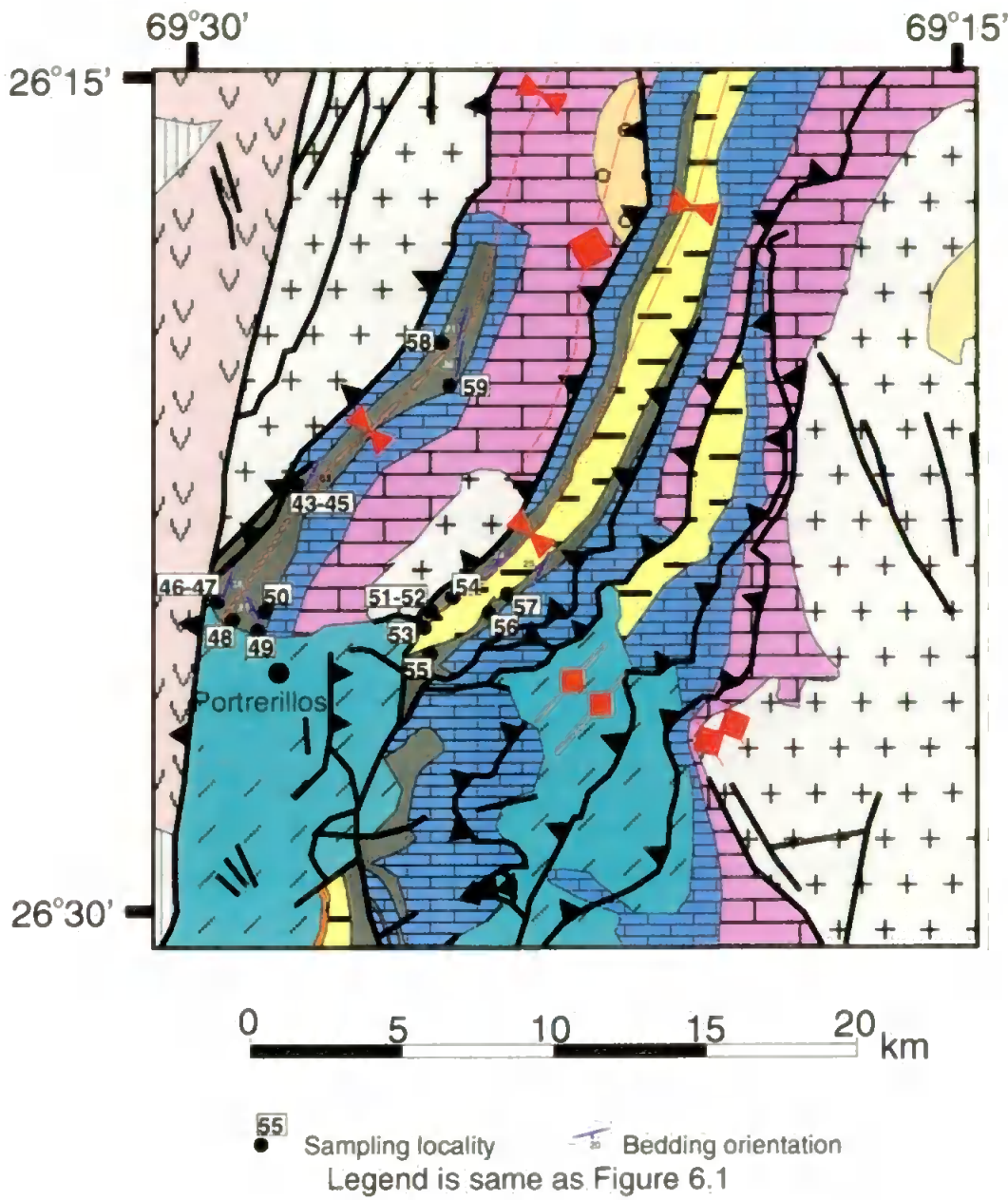


Figure 6.10. Sampling localities for the Quebrada Vicunita Formation in the northern region of the study area.

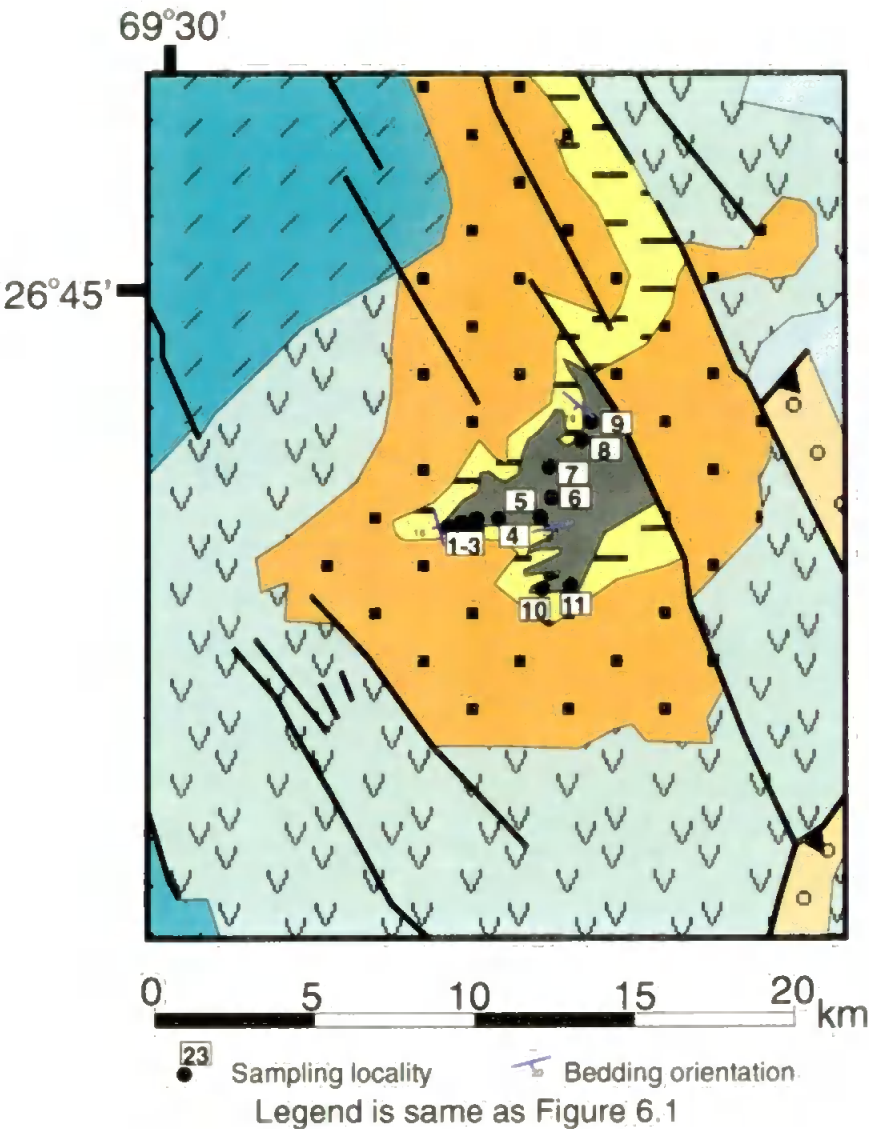


Figure 6.11. Sampling localities for the Quebrada Vicunita Formation in the southern region of the study area.

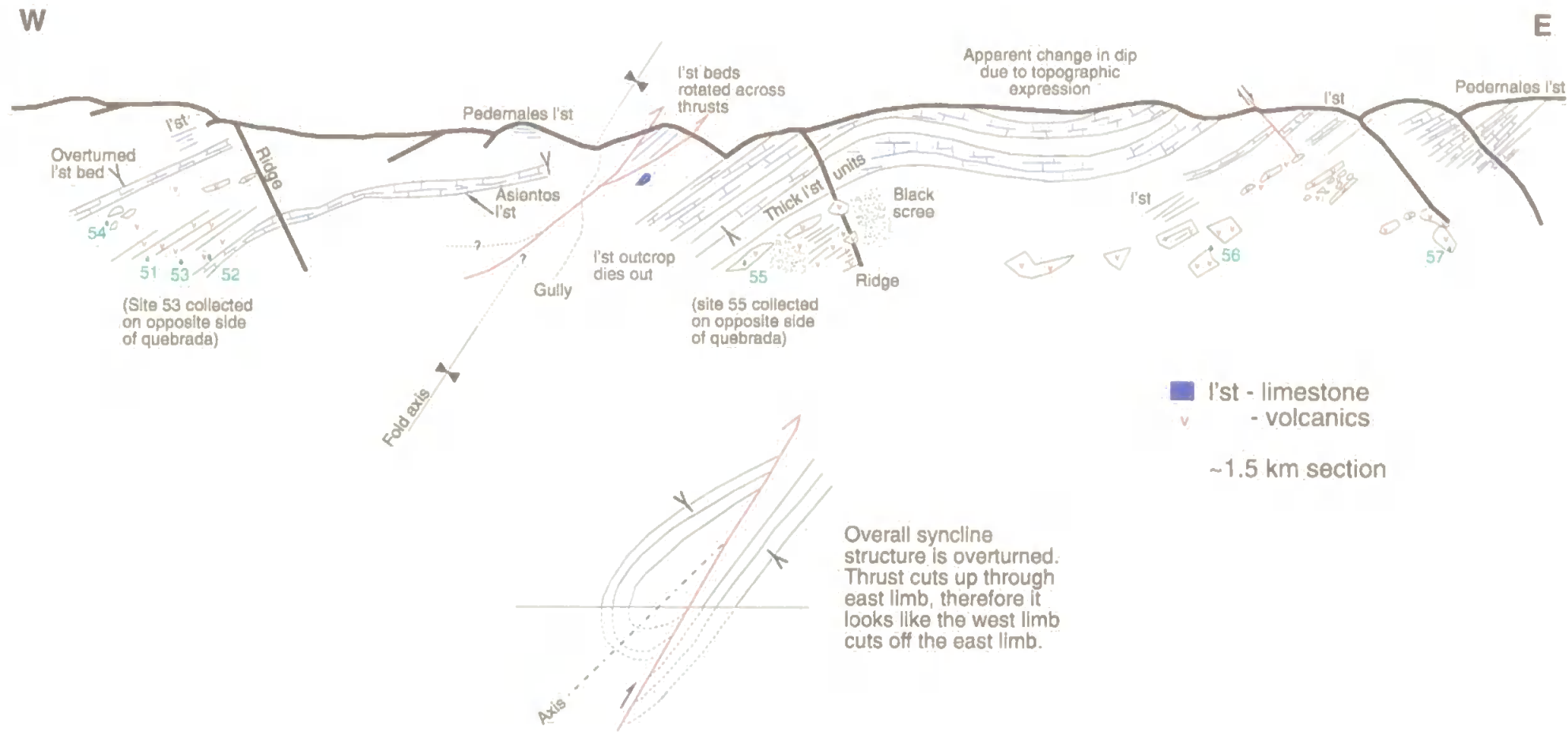


Figure 6.13. Positions of sampling sites for the Quebrada Vicunita Formation in the northern fold-and-thrust belt. Cross-section of the eastern syncline in Quebrada Asientos.

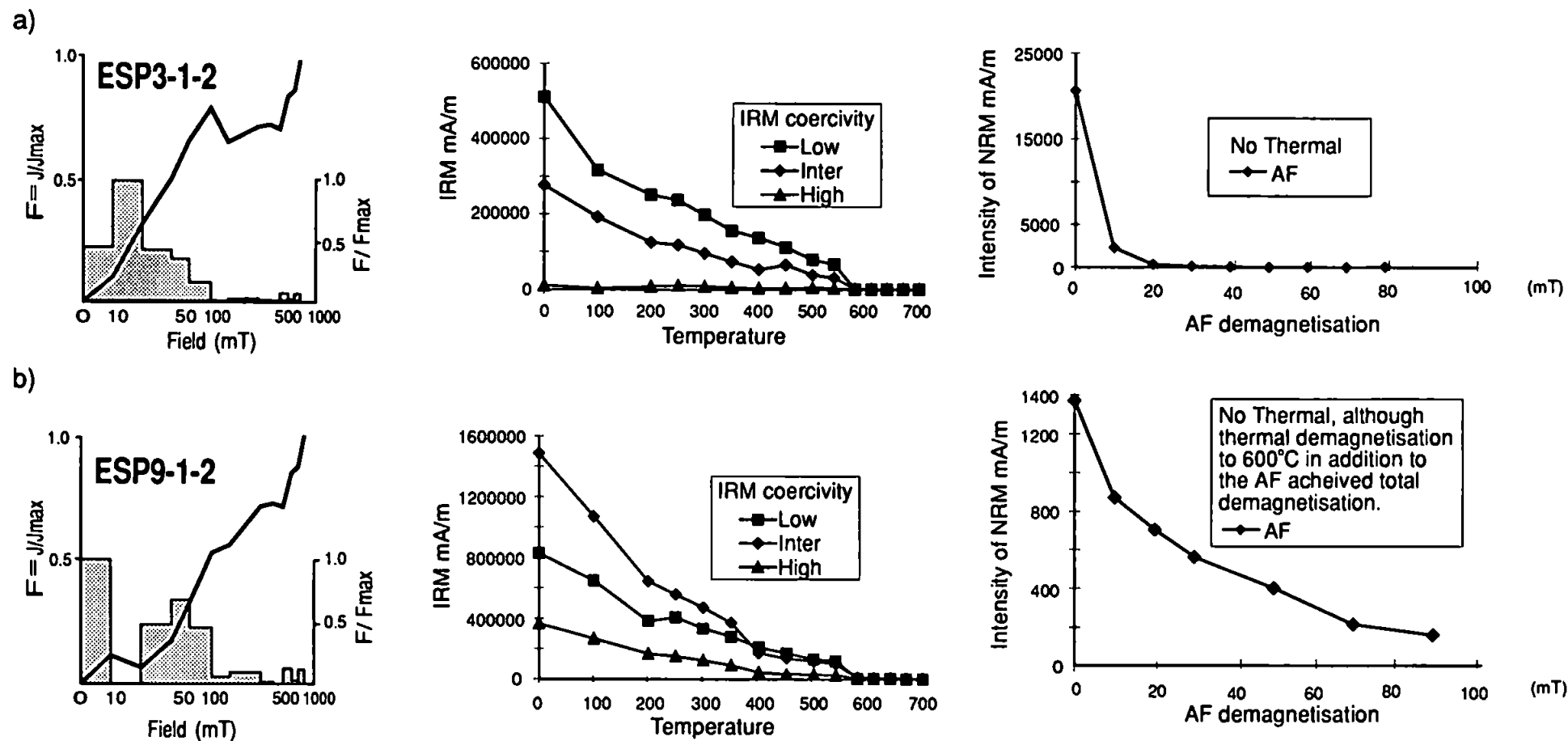


Figure 6.14a, b. Rock magnetic experiments on samples from the Quebrada Vicunita Formation. Graphs show acquisition of IRM, demagnetisation of three-axis IRMs and demagnetisation of NRM.

6.14a) where there is virtually no high coercivity component. A low coercivity carrier dominates and all three IRMs are fully demagnetised at 570°C, indicative of magnetite. The NRM in this sample is rapidly reduced by AF demagnetisation which is normally indicative of multi-domain magnetite.

ESP9-1-2 (Figure 6.14b) is dominated by the intermediate IRM coercivity component and demagnetisation is completed at 570°C, indicating magnetite as the dominant carrier. Near complete demagnetisation of the NRM at 90 mT is consistent with magnetite as the dominant carrier of the NRM. There is also an intensity drop in the intermediate IRM coercivity component at ~300-400°C, this may be the result of some pyrrhotite in the sample (pyrrhotite has a maximum unblocking temperature 320°C, maximum coercivity 0.5-1 T; Lowrie, 1990). The NRM remaining after 90 mT is easily demagnetised by thermal treatment to 600°C, consistent with the presence of a small component carried by pyrrhotite. The failure of the IRM acquisition to saturate in the 800 mT field may also be due to pyrrhotite.

Grain size analysis using RRM and ARM (Section 2.6.2) on two samples from the formation shows that the average grain size is variable but dominantly multi-domain or pseudo-single domain (Table 6.3).

VRM decay in samples ESP3-1-2 and ESP9-1-2 was examined as described in Section 2.6.3. The results show that VRMs are more prevalent after thermal demagnetisation, and ESP3-1-2 is particularly susceptible to short term application of magnetic fields (Table 6.4 and Figure 6.15). This most probably indicates significant chemical alteration of these samples on heating. The data indicate therefore that AF demagnetisation may be a better demagnetisation technique than thermal for these samples.

Sample	RRM mAm ⁻¹	ARM mAm ⁻¹	Effective field (Bg) μT	Particle size (d) μm
ESP3-1-2	586.6	5201.1	7.9	12.7
ESP55-3	1015.8	4441.5	16.0	6.2

Table 6.3. Magnetic grain size analysis in the Quebrada Vicuña Formation using RRM and ARM acquisition as described in section 2.6.2.

iii) Palaeomagnetic remanence measurements

Sixteen of the 28 sites collected from the Quebrada Vicuña Formation have been demagnetised, ten in the northern domain, and six in the southern domain. The demagnetisation and remanence data are given in Tables 6.5 and 6.6. Samples from all sites carry a stable magnetic remanence, the directions of which are well grouped with each site. In many sites, the mean directions from individual hand samples within a site are different. Where this is the case, the directions of both the individual sampling blocks and, where appropriate, the site means are given in Table 6.6.

The low coercivity and unblocking temperature component *in situ* directions are shown in Figure 6.16 and the directions become more scattered after tilt correction. For most sites in both the northern and southern sampling areas the low components are fairly well grouped, at least within each sampling block if not within site. Although there is some variability in the directions shown in both plots, the dominant direction is northward directed with an intermediate inclination. These low coercivity/unblocking temperature components are most likely to be a recent present-day secondary overprint.

Site mean directions, and indeed some hand sample mean directions, are extremely variable, particularly when viewed after tilt correction. Grouping of the site mean directions, and identification of the ChRM is best when directions are viewed *in situ*. The components of magnetisation identified in the samples are similar in all of the sites. Figure

Decay time (s)	<u>AF demagnetisation only</u>		<u>After thermal demag. to 700°C</u>	
	IRM (mA/m)	Normalised %	IRM (mA/m)	Normalised %
<u>3-1-2</u>				
7	23030	100.0	21453	100.0
20	22920	99.5	20770	96.8
30	22880	99.3	20551	95.8
40	22850	99.2	20374	95.0
50	22810	99.0	20236	94.3
60	22790	99.0	20122	93.8
80	22740	98.7	19930	92.9
100	22700	98.6	19816	92.4
120	22670	98.4	19704	91.8
240	22490	97.7	19241	89.7
480	22250	96.6	18727	87.3
720	22080	95.9	18366	85.6
1000	21940	95.3	18067	84.2
<u>9-1-2</u>				
7	51673	100.0	28902	100.0
20	51656	100.0	28477	98.5
30	51599	99.9	28345	98.1
40	51539	99.7	28267	97.8
50	51544	99.8	28185	97.5
60	51459	99.6	28121	97.3
80	51501	99.7	28043	97.0
100	51459	99.6	27957	96.7
120	51427	99.5	27904	96.5
240	51286	99.3	27588	95.5
480	51298	99.3	27178	94.0
720	51310	99.3	26853	92.9
1000	51447	99.6	26563	91.9

Table 6.4. Data for VRM experiments. Each sample was exposed to a 5 mT field to induce an IRM. The intensity of the IRM was measured at regular intervals over a period of 1000 s. Data is given as absolute measurement and normalised percentage of maximum intensity.

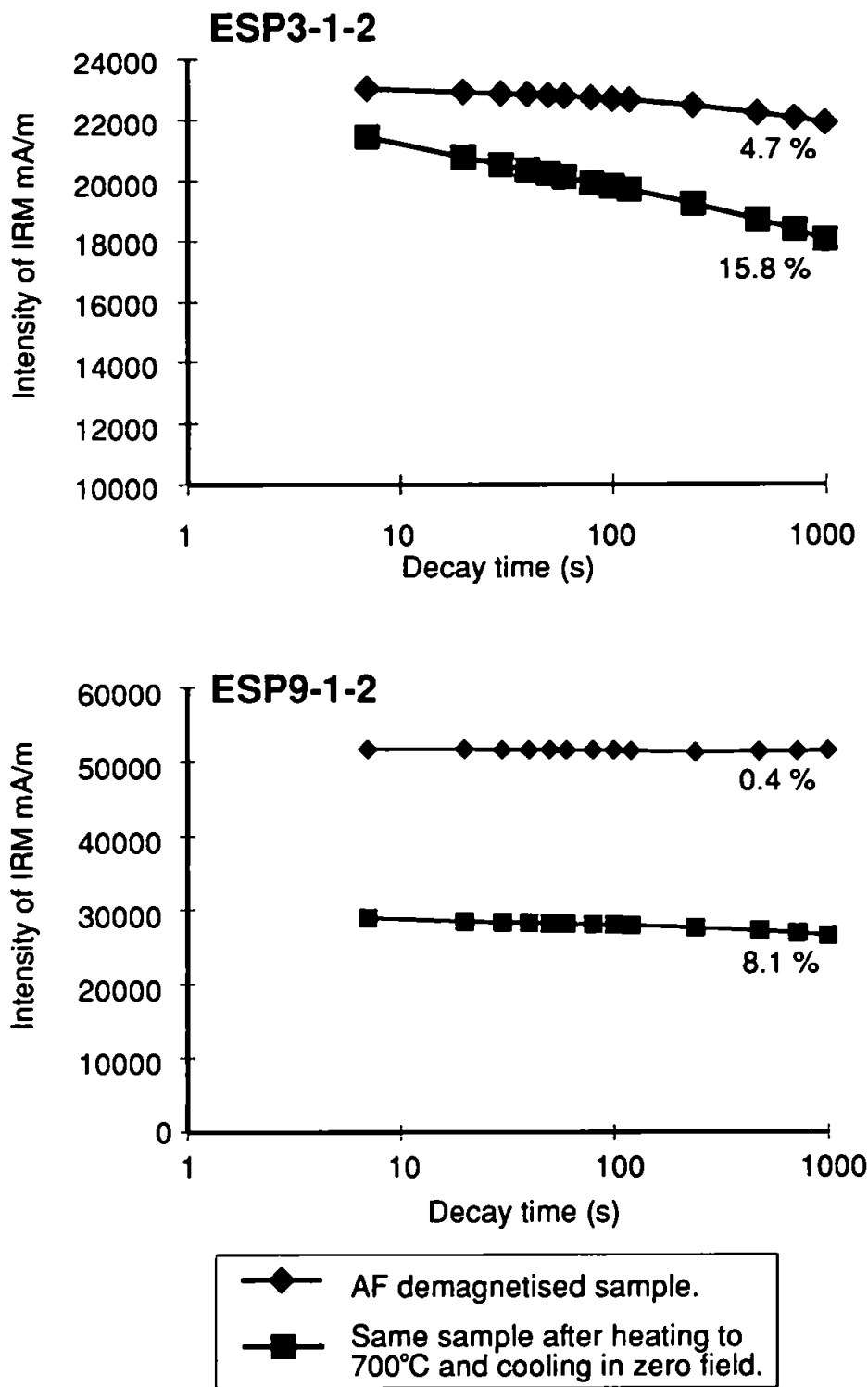


Figure 6.15. Graphs illustrating the presence of VRM in samples of the Quebrada Vicunita Formation. Graphs show the decay of IRM after exposure to a 5 mT field. Percentages are amount of intensity lost during decay time.

Site	Sampling site		Tilt correction	ChRM isolation mT	
	Long. W	Lat. S		Min.	Max.
<i>Northern Region</i>					
* ESP44	69°27'	26°21'	031/64	20	100
* ESP45	69°27'	26°21'	031/64	10	70
* ESP46	69°28'	26°23'	325/81	10	80
ESP48	69°28'	26°23'	151/22	10	50
* ESP50	67°28'	26°23'	151/22	10	80
ESP53	69°24'	26°24'	232/73	10	60
ESP55	69°24'	26°24'	186/40	50 (400°C)	80 (540°C)
* ESP56	69°23'	26°24'	205/28	NRM	50
* ESP57	69°23'	26°24'	205/28	20	60
ESP58	69°25'	26°20'	197/23	NRM→30	90
<i>Southern region</i>					
ESP1	69°26'	26°48'	165/16	30	70
ESP3	69°26'	26°48'	165/16	10	60
* ESP5	69°24'	26°47'	075/25	20	100
* ESP6	69°24'	26°47'	169/9	NRM→10	90
* ESP9	69°23'	26°46'	131/16	10	90
* ESP10	69°24'	26°49'	147/20	10	50→90

Table 6.5. Sampling and demagnetisation data from sites in the Quebrada Vicunita lavas. Tilt correction is given in right-hand-rule format, ChRM isolation is demagnetisation level at which ChRM is isolated in the site, a range with an arrow indicates a within site variation.

Site	n/No	Uncorrected		Corrected		k	α_{95}
		Dec.	Inc.	Dec.	Inc.		
Northern Region							
ESP44 (1)	3/3	168.0	35.2	159.1	-14.4	526.2	5.4
ESP44 (2)	3/3	217.5	62.8	151.3	25.9	634.4	4.9
* ESP44 (Both)	3/6	185.3	51.5	155.4	5.7	12.9	19.4
* ESP45	6/6	355.0	-35.7	342.9	9.9	31.1	12.2
ESP46 (2)	3/3	21.2	0.9	339.6	-54.9	66.5	15.2
* ESP46 (3)	3/3	335.6	-47.9	274.6	-28.8	293.6	7.2
ESP48	4/6	343.4	84.4	256.1	68.5	28.4	17.5
* ESP50	6/6	355.2	-36.7	6.9	-25.5	95.0	6.9
ESP53 (1)	3/3	296.6	-43.5	175.7	-55.9	1200.6	3.6
ESP53 (2)	3/3	237.1	-55.9	177.7	-16.8	76.7	14.2
ESP53 (Both)	6/6	271.2	-53.5	177.0	-36.5	13.4	19.0
ESP55	6/6	124.5	-10.7	126.1	22.2	20.4	17.8
* ESP56	6/6	358.2	-50.0	35.2	-54.3	48.9	9.7
* ESP57	6/6	348.3	-47.8	24.3	-57.4	175.6	5.1
ESP58 (1)	3/3	277.3	-41.0	270.5	-63.5	66.4	15.3
ESP58 (2)	3/3	167.0	-3.5	167.8	7.9	127.7	11.0
Mean	6/10	356.5	-45.0			105.9	6.5
				346.5	-32.7	3.6	41.0

Table 6.6a. Remanence data from the Quebrada Vicunita lavas in the northern domain. Numbers in brackets after site number indicate the hand sample number and are given where the directions from the individual blocks are significantly different; n/No. is number of samples included in site mean/number of samples demagnetised; dec. and inc. are declination and inclination of remanence vector; k is Fisherian precision parameter; α_{95} is semi-angle of 95% cone of confidence. Sites marked * are included in formation mean.

Site	n/No	Uncorrected Dec.	Inc.	Corrected Dec.	Inc.	k	α_{95}
<i>Southern Region</i>							
ESP1 (1 only)	3/6	250.8	76.5	253.0	60.6	95.7	12.7
ESP3	6/6	69.5	62.1	62.5	78.0	49.0	10.4
* ESP5	6/6	327.4	-48.2	332.3	-24.0	474.3	3.1
* ESP6	6/6	1.1	-49.9	10.9	-47.3	177.9	5.0
* ESP9	6/6	347.8	-24.4	352.2	-14.4	277.1	4.0
* ESP10	6/6	354.8	-54.3	13.0	-42.1	46.3	10.0
Mean	4/6	347.5	-44.9			23.6	19.3
				355.3	-33.0	13.6	25.9

Table 6.6 b. Remanence data from the Quebrada Vicunita lavas in the southern domain. Numbers in brackets after site number indicate the hand sample number and are given where the directions from the individual blocks are significantly different; n/No. is number of samples included in site mean/number of samples demagnetised; dec. and inc. are declination and inclination of remanence vector; k is Fisherian precision parameter; α_{95} is semi-angle of 95% cone of confidence. Sites marked * are included in formation mean.

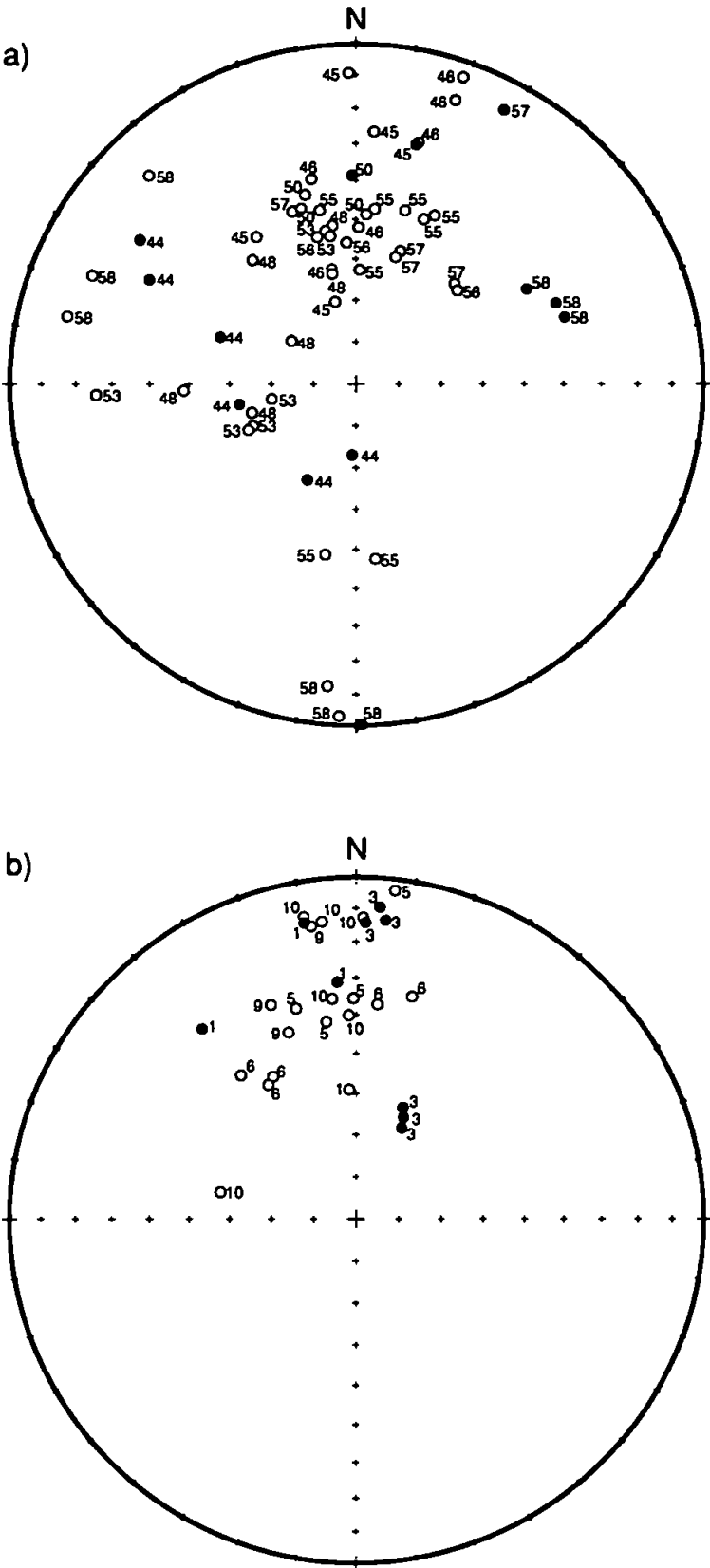


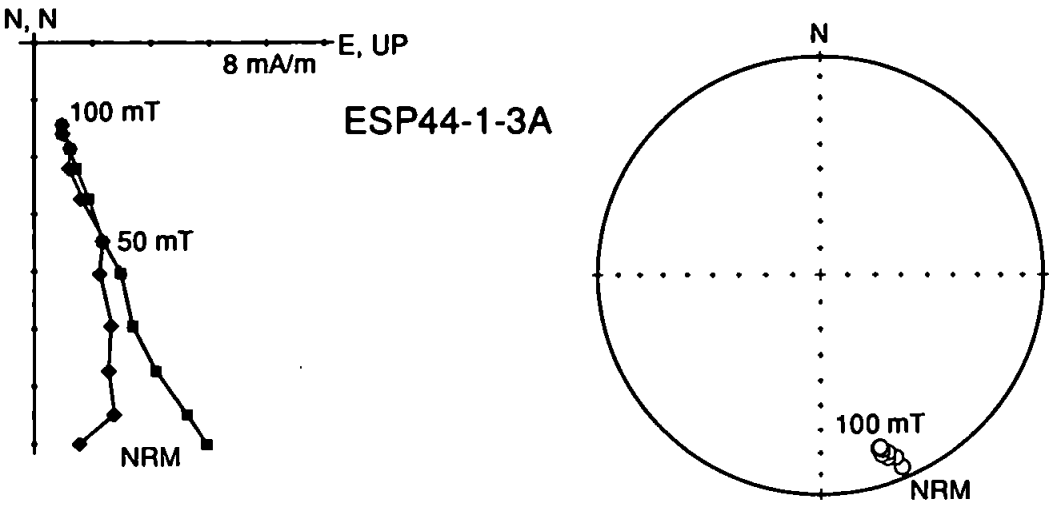
Figure 6.16. Equal area stereographic projection of low coercivity and unblocking temperature components from sites in the Quebrada Vicunita lavas. a) From the northern region b) From the southern region. Open (closed) symbols are upper (lower) hemisphere projections. Directions are *in situ* numbers are site numbers.

6.17a-d shows the range of demagnetisation behaviour seen in the sites. Samples from seven of the sites demagnetised exhibit similar behaviour to that of sample ESP44-1-3A (Figure 6.17a), a low coercivity component removed by 10 mT, and a higher coercivity, well defined component of magnetisation to the origin. The demagnetisation behaviour of samples ESP10-2-1A and ESP48-1-2A (Figures 6.17b and c) was also observed in seven sites. These are characterised by a low coercivity component which dominates much of the total NRM intensity, this component is removed by 20-30 mT. At higher demagnetisation levels a poorly defined higher coercivity component is isolated. In sites ESP55 and ESP56 (Figure 6.17d) a great circle distribution of directions on the stereographic plot indicates the presence of two or more components which are not being isolated. In site ESP56 only the lowest coercivity component recorded a stable direction of magnetisation, but in ESP55 the higher coercivity direction could be isolated as a linear segment between 50 and 80 mT.

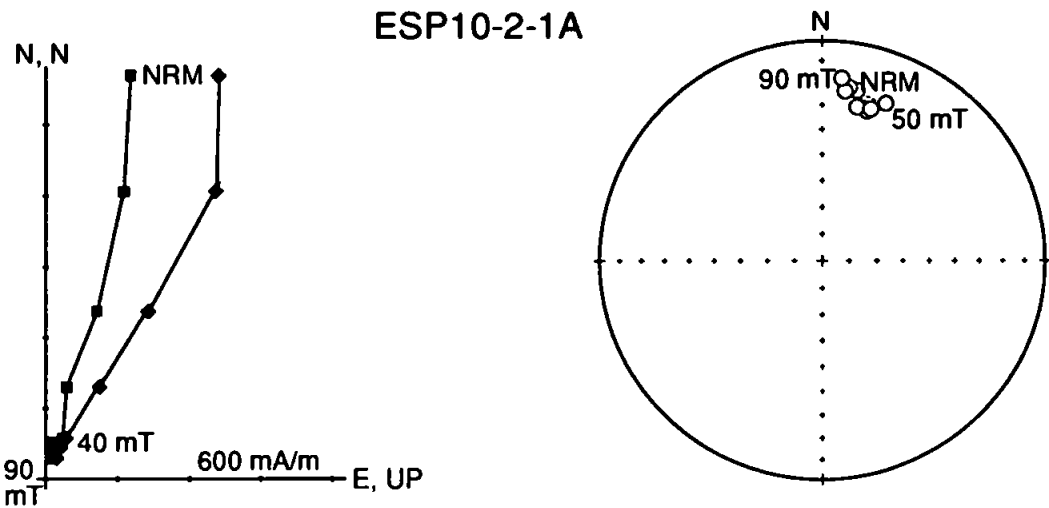
Mean directions for sites in the northern domain are shown in Table 6.6a and Figure 6.18, one site, ESP44, has reversed polarity. Four sites (ESP48, 53, 55, 58) have been excluded from the formation mean calculation as they have directions apparently unrelated to the mean. The cause of these directions is unknown, but samples from sites ESP53 and ESP58 have very high NRM intensities, up to 145 Am^{-1} in ESP58. In ESP58 this high intensity may be due to a lightening strike induced IRM, as this site was collected from an exposed ridge. The cause of the high intensity in site ESP53 is unknown, a lightening strike IRM seems unlikely as the samples were collected in a valley bottom.

The formation mean direction for the sites in the northern domain is shown in Table 6.6b and Figure 6.18. The site mean directions are best grouped *in situ*, and the increase in k after tilt correction fails the fold test ($k_1/k_2 = 0.16$, less than the statistically significant value of 2.98 at 95% confidence; McElhinny, 1964).

a)



b)



- Horizontal projection
- ◆ Vertical projection
- Upper hemisphere projection
- Lower hemisphere projection

Figure 6.17a, b. Examples of demagnetisation behaviour in samples from the Quebrada Vicunita lavas. All plots are tilt corrected.

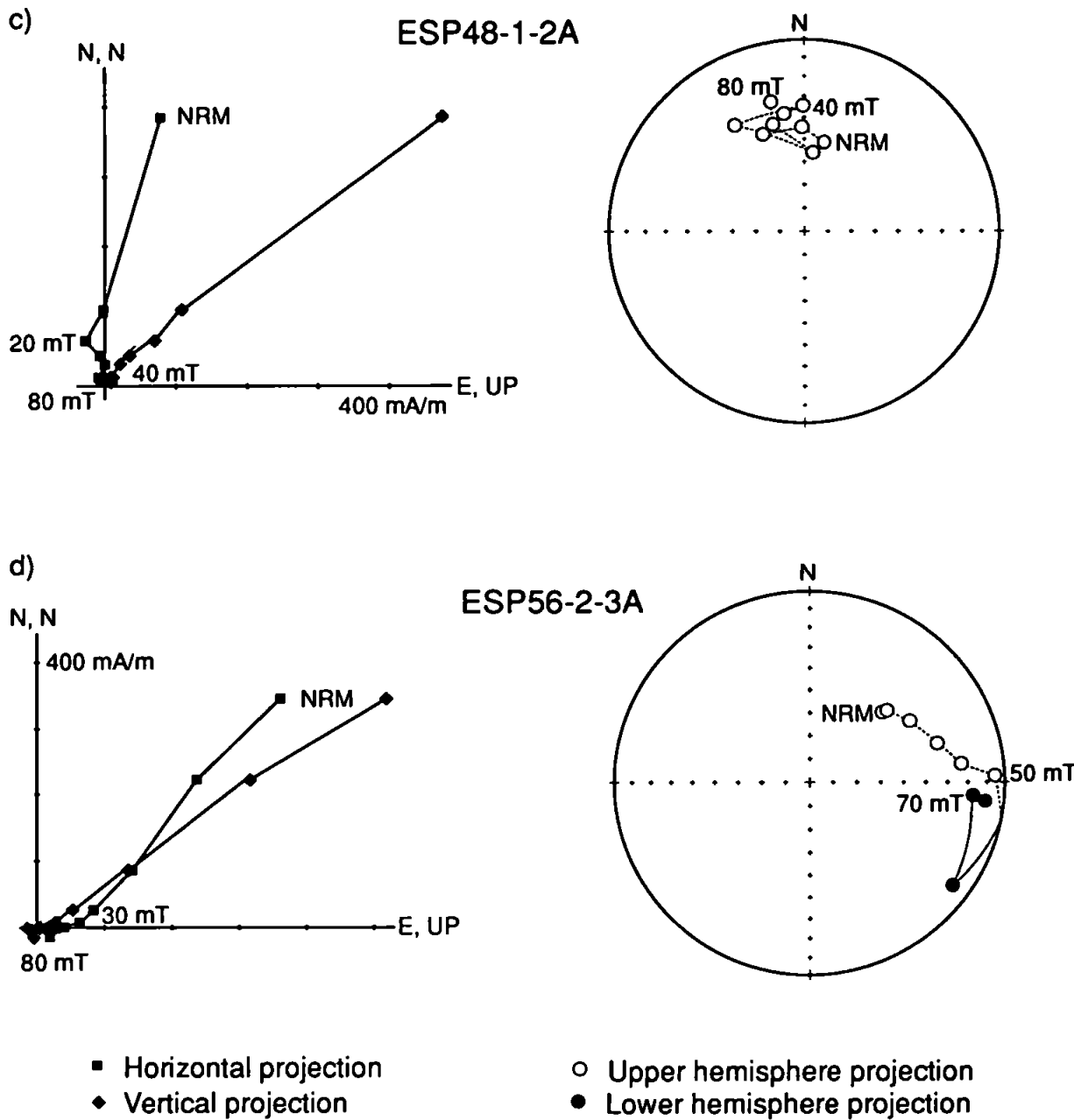


Figure 6.17c, d. Examples of demagnetisation behaviour in samples from the Quebrada Vicunita lavas. All plots are tilt corrected.

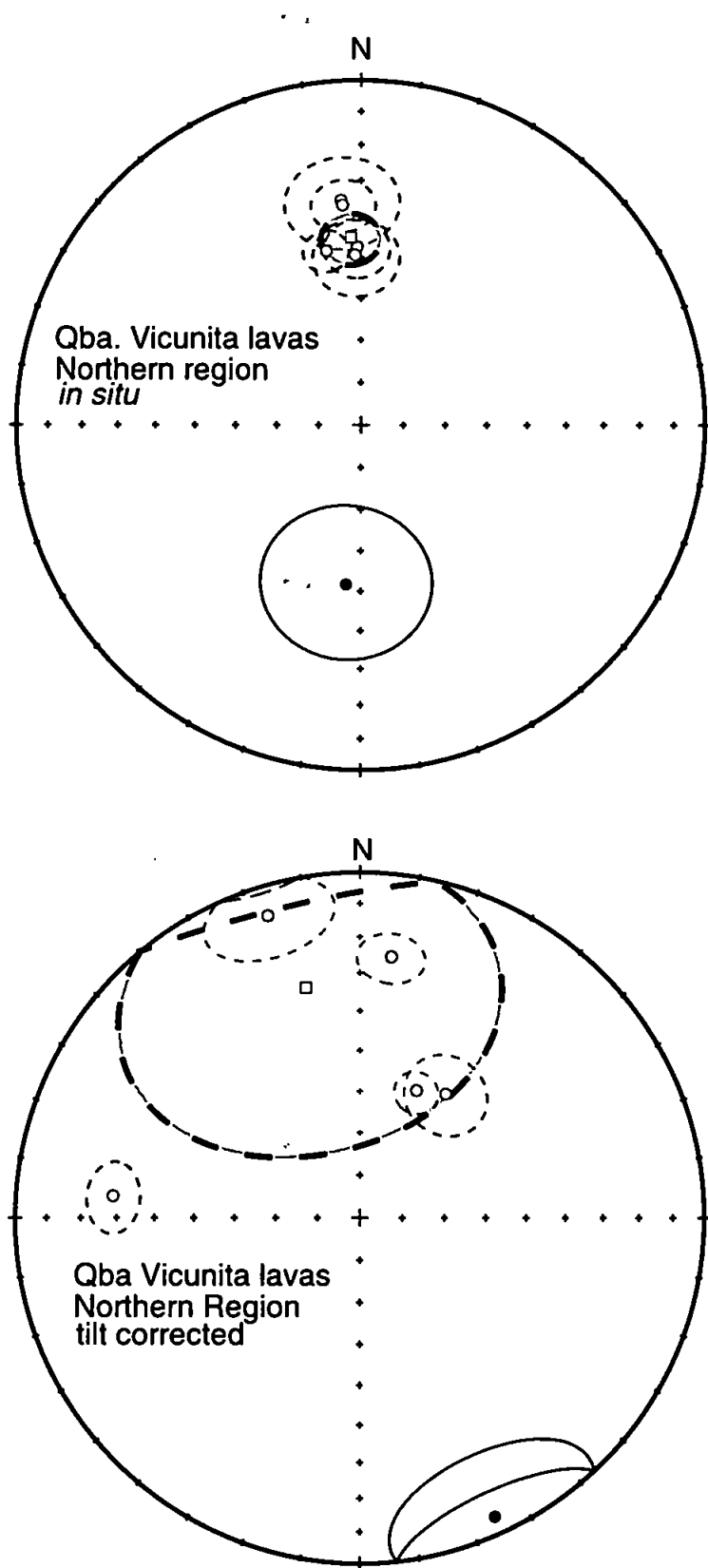


Figure 6.18. Stereographic projection of site mean directions from the Quebrada Vicunita lavas (circles) and the Formation mean directions (square) from the northern region. Error ellipses are 95% confidence. Open (closed) symbols are upper (lower) hemisphere projections.

Four of the six sites in the southern domain have been used to calculate the formation mean (Table 6.6b and Figure 6.19). The two excluded sites both have NRM intensities which are rapidly demagnetised by the AF technique, and the high coercivity components are not well isolated. Site ESP1 also has a high NRM intensity, possibly indicating the presence of a lightening strike induced IRM. As with sites in the northern domain, the site mean directions are best grouped *in situ*, and application of tilt correction results in an increase in k great enough to fail the fold test of McElhinny (1964); $k_1/k_2 = 0.58$ is less than 4.28, the statistically significant value at 95 % confidence.

iv) Discussion of results

The failure of the fold test for both the northern and southern mean directions indicates that the remanence was acquired after folding. In addition, the inclinations of the mean directions are closer to those expected for a South American locality before tilt correction. The timing of motion on both the fold-and-thrust belt in the northern domain, and the NW trending strike-slip faults in the southern domain is dated as Eocene-Oligocene. If the folding in the southern domain is synchronous with the fault motion, as may reasonably be expected, the age of remanence in the rocks from the Quebrada Vicuña Formation must be younger than Oligocene. The timing and origin of the remagnetisation is unknown, but the pervasive alteration of minerals identified in thin section indicates that low temperature hydrothermal alteration has been widespread. This hydrothermal action may be related to the emplacement of copper porphyry deposits in this region during the late Oligocene-early Miocene (Comejo *et al.*, 1993), and the magnetisation recorded in these rocks may be of this age. The presence of a reversed sample in the data set from the northern domain may indicate that the remagnetisation occurred over a long time period, or alternatively that the rocks have undergone several phases of less pervasive remagnetisation

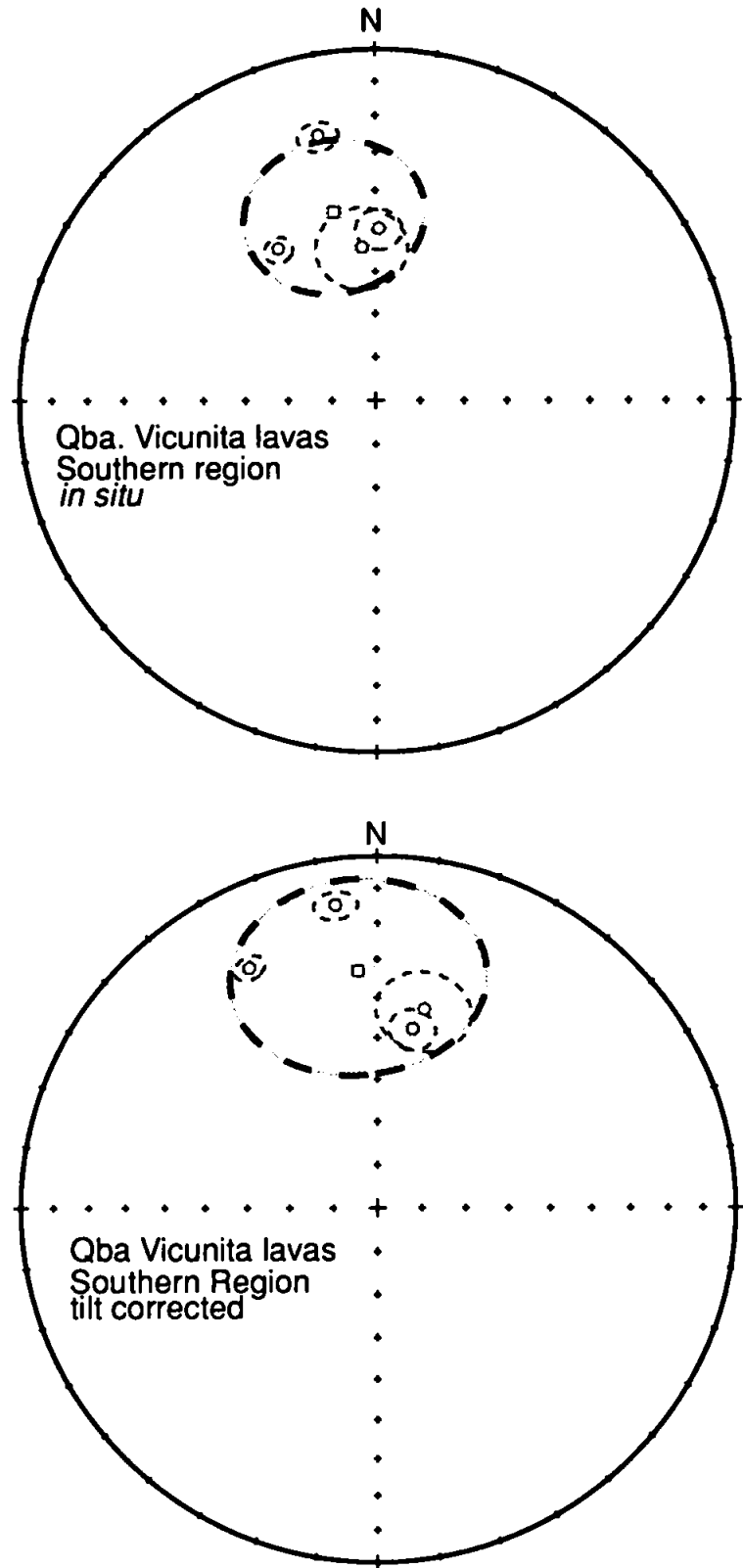


Figure 6.19. Stereographic projection of site mean directions from the Quebrada Vicunita lavas (circles) and the Formation mean directions (square) from the southern region. Error ellipses are 95% confidence. Open (closed) symbols are upper (lower) hemisphere projections

during their history. As discussed in Chapter 3, the time averaged field direction can be used as reference for comparison with remanences younger than Palaeocene. This direction is therefore used as reference for both mean directions from the Quebrada Vicuña Formation.

When considered *in situ*, the mean direction for the sites in the northern domain has a small α_{95} confidence limit, suggesting that secular variation may not be fully averaged by the data. Despite this the formation mean is close to the position of the time averaged present-day field, showing only a $3.5 \pm 5.4^\circ$ anticlockwise rotation with $0.0 \pm 5.2^\circ$ of latitudinal transport. Comparison of the southern domain mean direction with the reference direction indicates an anticlockwise rotation of $12.5 \pm 22.3^\circ$ with $0.1 \pm 15.4^\circ$ of northward displacement.

The amounts of rotation and latitudinal transport from both mean directions are within their associated errors and are therefore not statistically significant. These rotations are not considered further.

6.3.3 Quebrada Monardes Formation (Early Cretaceous)

i) Palaeomagnetic sampling localities

The Quebrada Monardes Sandstone Formation was sampled at a total of 25 sites in three localities, all in the southern and central parts of the study area (Figure 6.20). Sites ESP22-30 were collected from around a gently SW plunging open anticline in the southernmost part of the area. Sites ESP80-89 were collected further north, but still in the domain of NW trending strike-slip faults. The major structure at this locality is a NW-SE trending anticline, but there is also minor folding. Sites ESP74-79 come from a constantly dipping 20 m thick section at Mina Vieja near Portrerillos. This sampling locality lies in the area of overlap between the southern domain of strike-slip faults, and the northern fold-and-

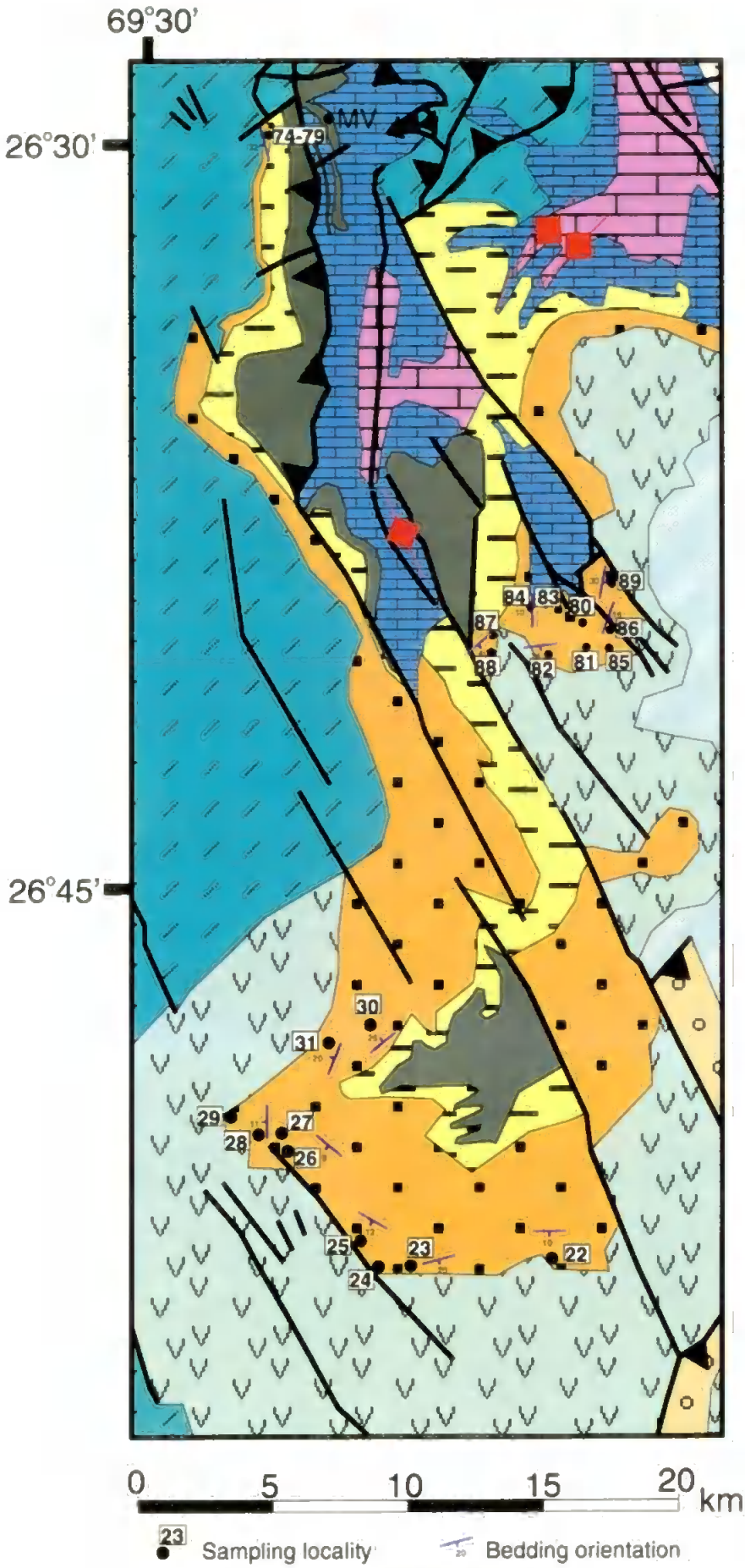


Figure 6.20. Sampling localities for the Quebrada Monardes Formation in the southern and central region of the study area. MV is Mina Vieja.

thrust belt domain. The area between the two domains has complex faulting and several small thrusts are seen. At all three collecting localities the sandstones are well bedded and good structural control could be obtained at each site. Sites ESP80-89 were collected as hand samples, all others were collected as drilled cores.

ii) Magnetic mineralogy

Visual inspection of samples from the Quebrada Monardes Formation shows a range of red colouring, indicating a variation in the amount of iron oxide present. Samples from four sites, selected to represent the colour range present, were used in IRM experiments following the method described in section 2.6.1. The results are shown in Figure 6.21a-d. Acquisition of IRM in sample ESP31-1 (Figure 6.21a) indicates both low and high coercivity carriers. The acquisition curves for samples ESP22-4, ESP24-4 and ESP76-3 (Figure 6.21b-d) also show a mix of carriers with an increasing dominance of the high coercivity component. Demagnetisation of IRM in this sample series is also consistent with an increasingly dominant high coercivity carrier which is demagnetised by 670°C. In all cases, demagnetisation of NRM was carried out by thermal treatment only. This showed a steady decay in intensity, sometimes with a large drop at 100-300°C and complete demagnetisation at 640-670°C. The data are therefore consistent with a haematite dominated magnetite and haematite mix of carriers for both the IRM and NRM. The rapid fall in NRM intensity between 100°C and 300°C may indicate that the magnetite is multi-domain or is a titanium rich titanomagnetite.

iii) Palaeomagnetic remanence measurements

Of the 25 sites collected from the Quebrada Monardes Sandstone Formation, 14 have been demagnetised. Demagnetisation of eight of the nine sites (not ESP23) from the

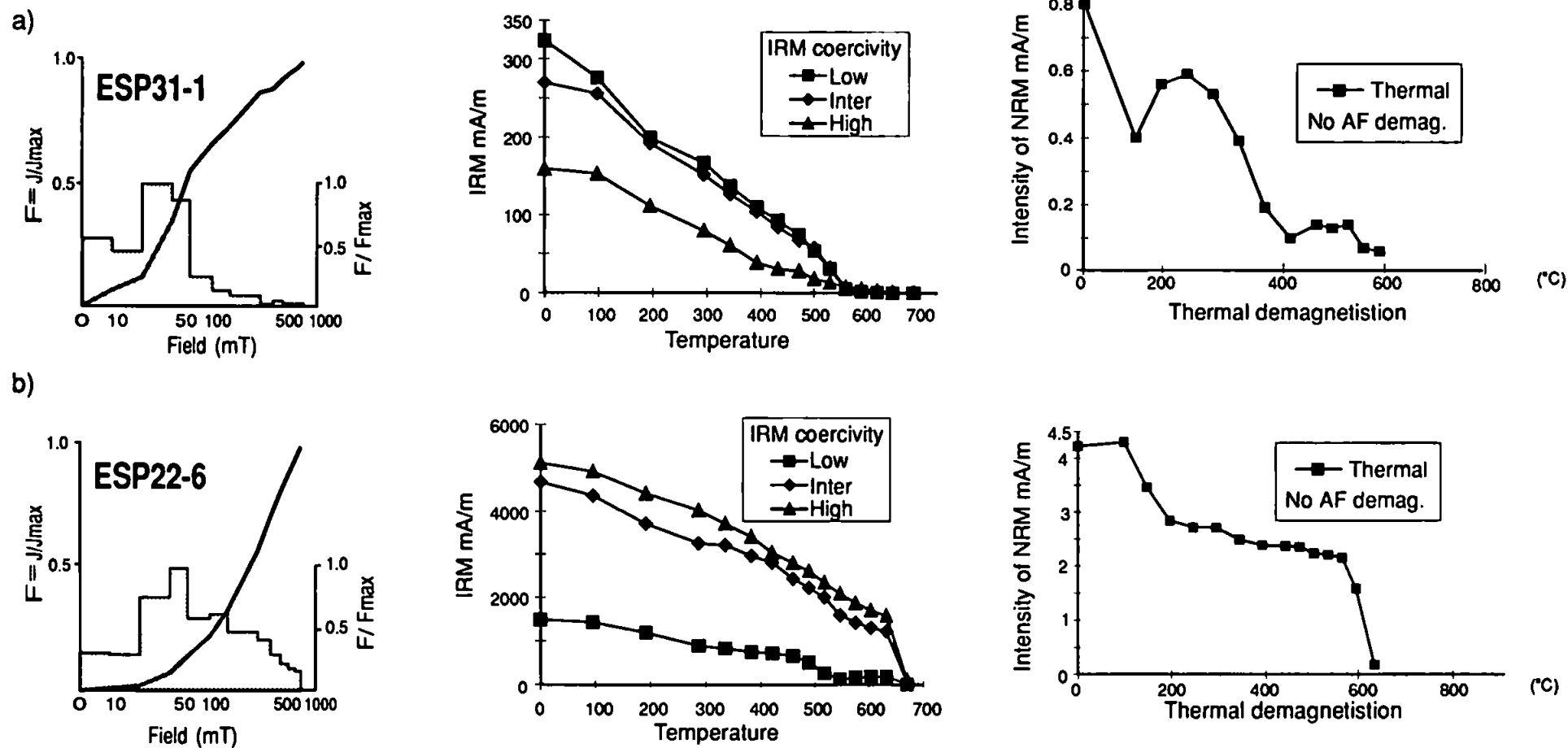


Figure 6.21a, b. Rock magnetic experiments on samples from the Quebrada Monardes Sandstone. Graphs show acquisition of IRM, demagnetisation of three-axis IRMs and demagnetisation of NRM.

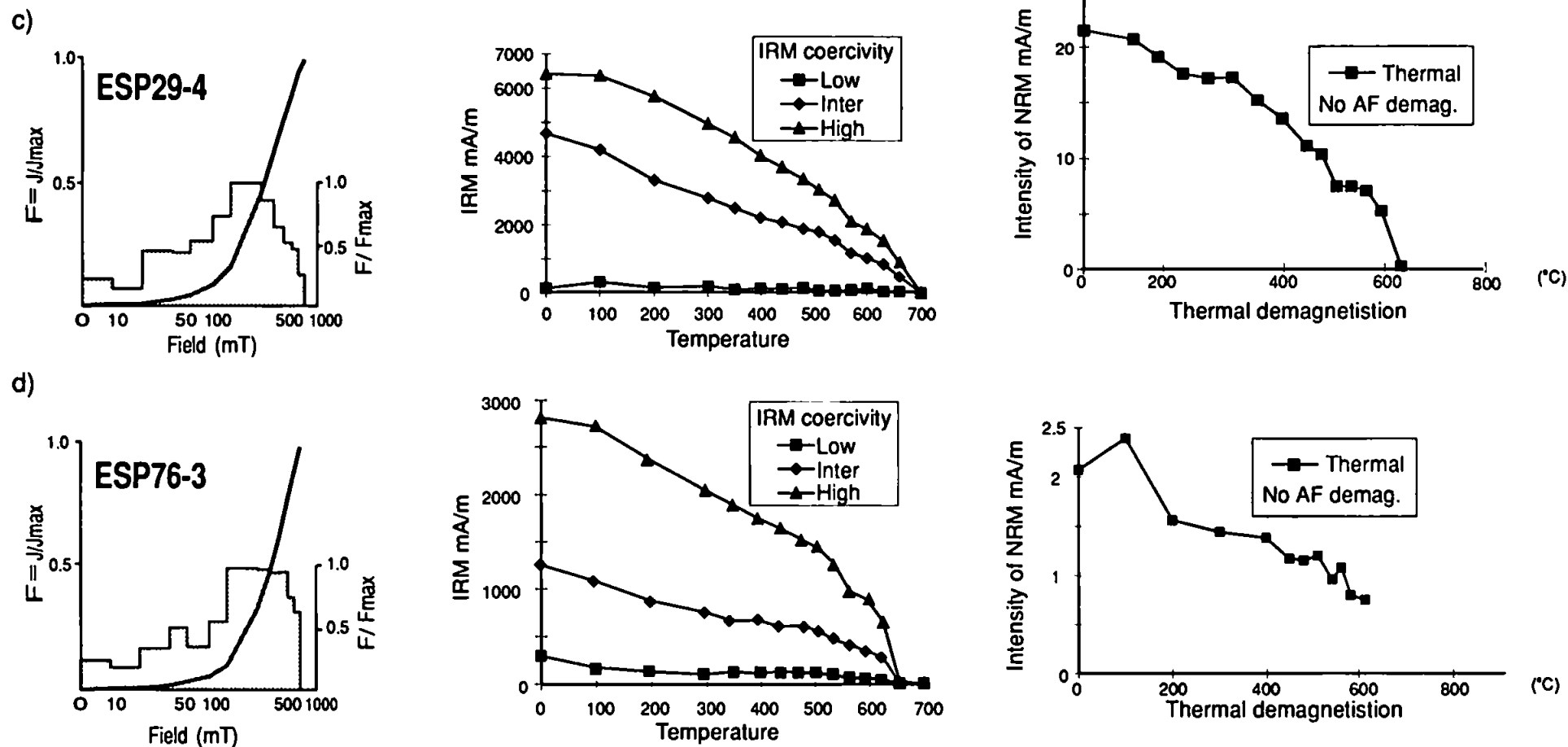


Figure 6.21c, d. Rock magnetic experiments on samples from the Quebrada Monardes Sandstone. Graphs show acquisition of IRM, demagnetisation of three-axis IRMs and demagnetisation of NRM.

southernmost sampling area, and all sites from the central region (ESP74-79) has been completed. The demagnetisation and remanence data from all sites is given in Tables 6.7 and 6.8. All of the sites display within site variability of demagnetisation components, but a stable, consistent mean direction of magnetisation is recovered from most sites.

The directions of the low unblocking temperature components for the two sampling areas are shown in Figure 6.22. Both plots are shown *in situ*, and the directions become slightly more scattered after tilt correction. For most sites, in both the southern and central sampling areas, the low components are not well grouped either within, or between sites, although there is a loose grouping of directions close to the present-day field direction in samples from the central region. The scattering of directions indicates that most of the low unblocking temperature components were acquired after the cores were removed from the host rock, and are therefore laboratory induced remanences.

Examples of demagnetisation behaviour from the Quebrada Monardes Formation are shown in Figure 6.23a-f. Although there are variations in magnetic intensities between sites, most have total NRM intensities of less than 3 mAm^{-1} . Demagnetisation behaviour is extremely variable, even within individual sites, for example Figure 6.23a and 6.23f are both from site ESP22. Commonly, the NRM is composed of several components which are often overlapping. As a result, the ChRM is only recognised as a linear segment in one or two samples from the site, the others require the use of remagnetisation circles. The demagnetisation plots shown in Figure 6.23 are representative of sites from both the southern and central sampling areas.

All eight sites from the southern sampling locality have a consistent direction, directed upwards in the NE quadrant or its antipode (Table 6.8 and Figure 6.24). The sites group better after tilt correction although the improvement in precision parameter, k , on tilt correction is not sufficient to pass the fold test of McElhinny (1964), $k_1/k_2 = 1.18$, less than

Site	Sampling site		Tilt correction	ChRM isolation °C	
	Long. W	Lat. S		Min.	Max.
<i>Southern Region</i>					
* ESP22	69°21'	26°52'	090/10	510	640
* ESP24	69°25'	26°52'	085/8	200	640
* ESP25	69°25'	26°52'	121/12	200	580
* ESP26	69°27'	26°50'	125/8	100→480	680
* ESP27	67°27'	26°50'	155/12	450→610	640
* ESP29	69°28'	26°48'	172/17	300	640
* ESP30	69°26'	26°46'	230/26	400	680
* ESP31	69°27'	26°46'	202/20	200→500	580
<i>Central region</i>					
* ESP74	69°26'	26°26'	181/34	NRM→300	610
* ESP75	69°26'	26°26'	180/39	400	610
ESP76	69°26'	26°26'	160/31	NRM→400	610
ESP77	69°26'	26°26'	158/31	Not isolated	
* ESP78	69°26'	26°26'	159/36	NRM→560	680
* ESP79	69°26'	26°26'	182/28	NRM→450	610

Table 6.7. Sampling and demagnetisation data from sites in the Quebrada Monardes Formation. Tilt correction is given in right-hand-rule, ChRM isolation is demagnetisation level at which ChRM is isolated in the site, a range with an arrow indicates a within site variation.

Site	n/No	Uncorrected Dec.	Inc.	Corrected Dec.	Inc.	k	α_{95}
<i>Southern Region</i>							
* ESP22	5/7	52.5	-34.5	47.8	-27.9	32.9	13.9
* ESP24	5/6	174.6	60.2	174.7	52.2	58.7	10.1
* ESP25	6/6	0.5	-45.7	5.4	-35.1	23.9	14.0
* ESP26	6/7	8.0	-50.1	9.8	-46.1	37.7	11.2
* ESP27	6/7	3.1	-60.4	11.9	-56.7	36.9	12.0
* ESP29	4/6	29.6	-52.7	37.0	-46.7	38.0	15.1
* ESP30	4/5	351.4	-32.2	6.6	-52.7	38.5	15.0
* ESP31	7/7	194.9	41.4	212.5	40.8	17.8	14.9
Mean	8/8	12.6	-48.9			20.6	12.5
				19.7	-46.2	24.3	11.5
<i>Central Region</i>							
* ESP74	4/4	310.1	-15.2	323.1	-39.5	14.5	24.9
* ESP75	3/6	320.5	-24.7	345.2	-43.5	44.1	18.8
ESP76	3/4	309.7	-29.0	330.3	-40.0	13.3	35.3
ESP77	Unstable, no within site direction						
* ESP78	5/6	303.2	-23.6	324.3	-39.8	43.4	11.7
* ESP79	3/4	317.3	-5.6	323.0	-24.6	67.3	15.1
Mean	4/6	312.8	-17.4			50.1	13.1
				328.4	-37.2	46.9	13.6

Table 6.8. Remanence data from the Quebrada Monardes Formation. n/No. is number of samples included in site mean/number of samples demagnetised; dec. and inc. are declination and inclination of remanence vector; k is Fisherian precision parameter; α_{95} is semi-angle of 95% cone of confidence. Sites marked * are included in formation mean.

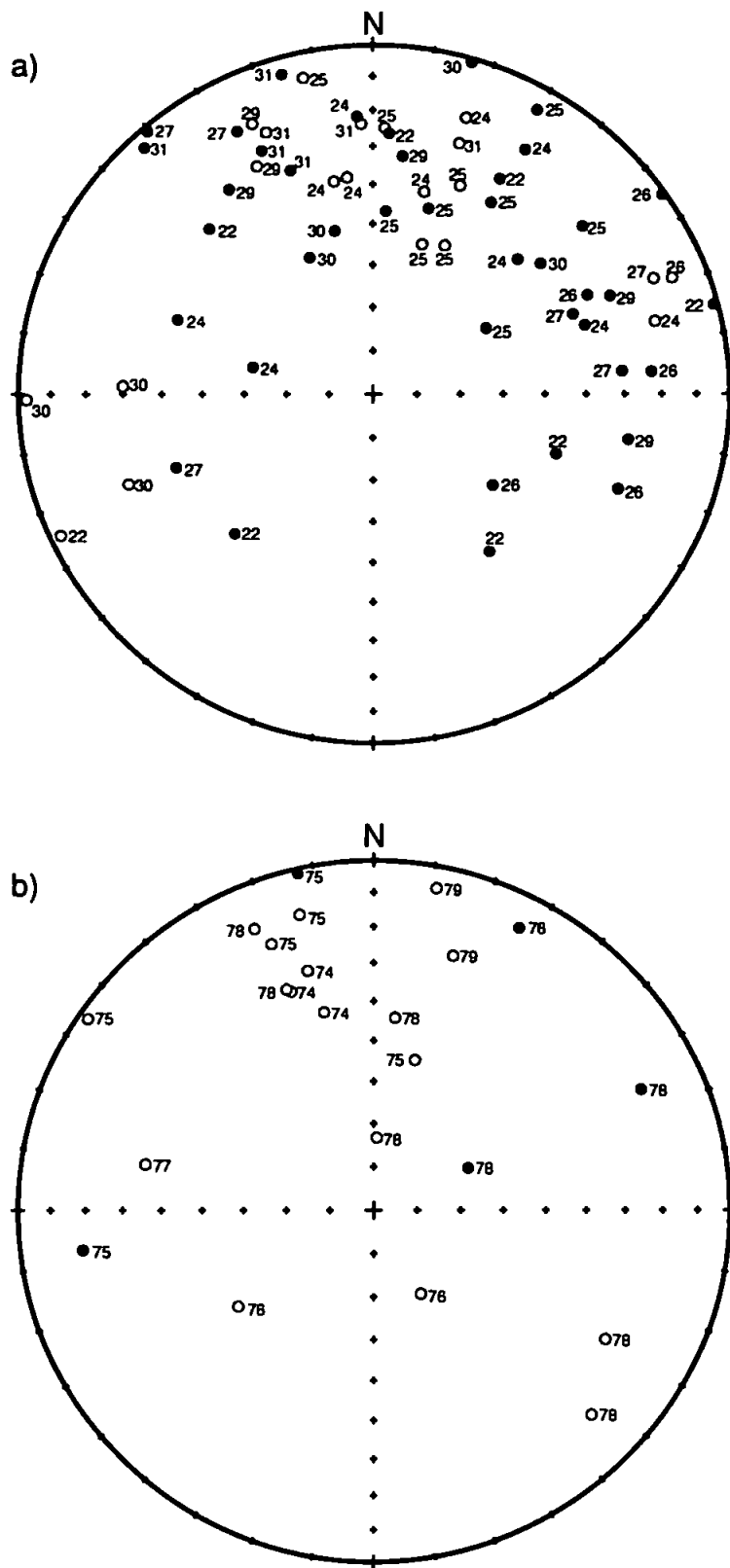


Figure 6.22. Equal area stereographic projection of low unblocking temperature components from sites in the Quebrada Monardes Sandstone. a) From the southern region b) From the central region. Open (closed) symbols are upper (lower) hemisphere projections. Directions are *in situ* numbers are site numbers.

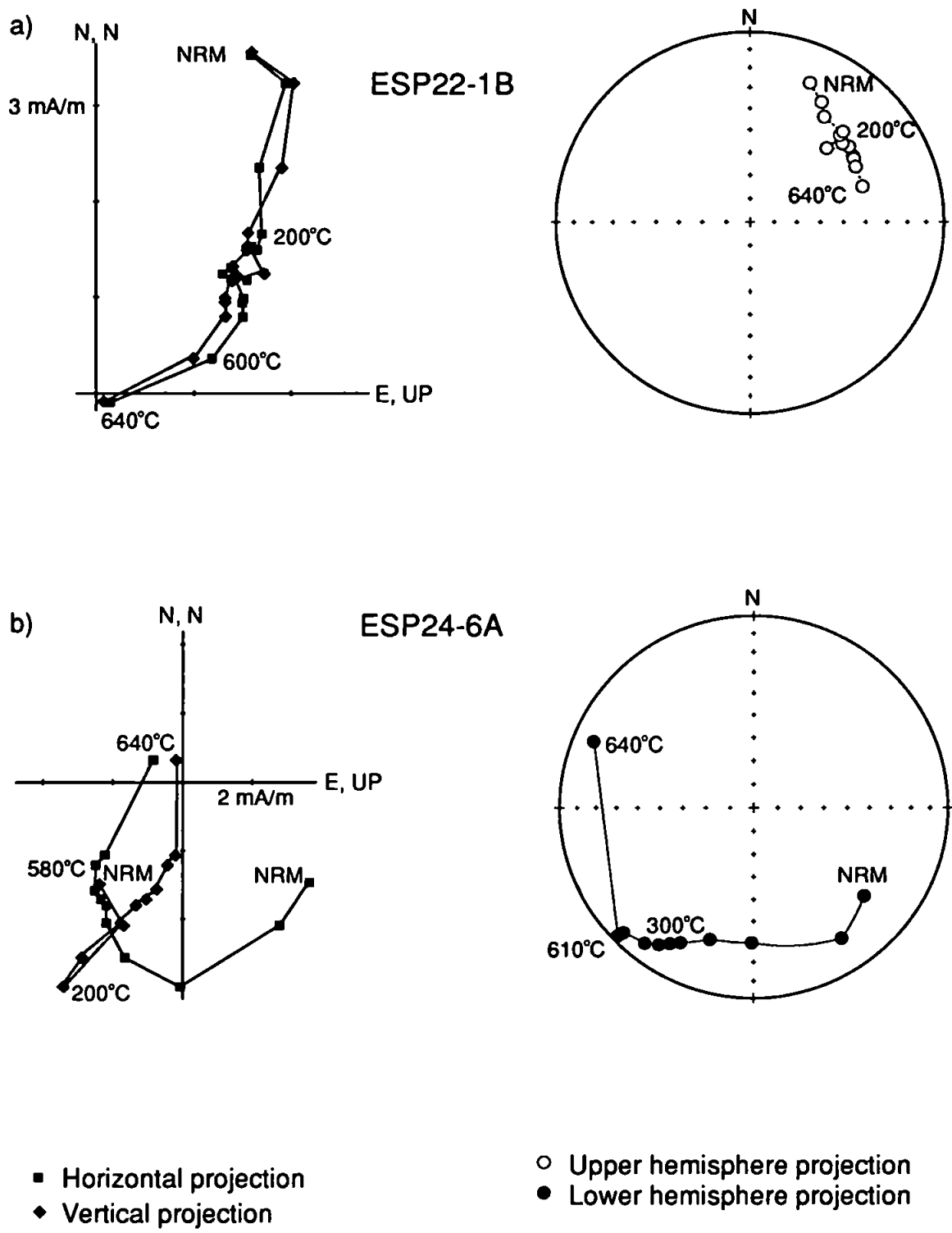


Figure 6.23a, b. Examples of demagnetisation behaviour in samples from the Quebrada Monardes Formation. All plots are tilt corrected.

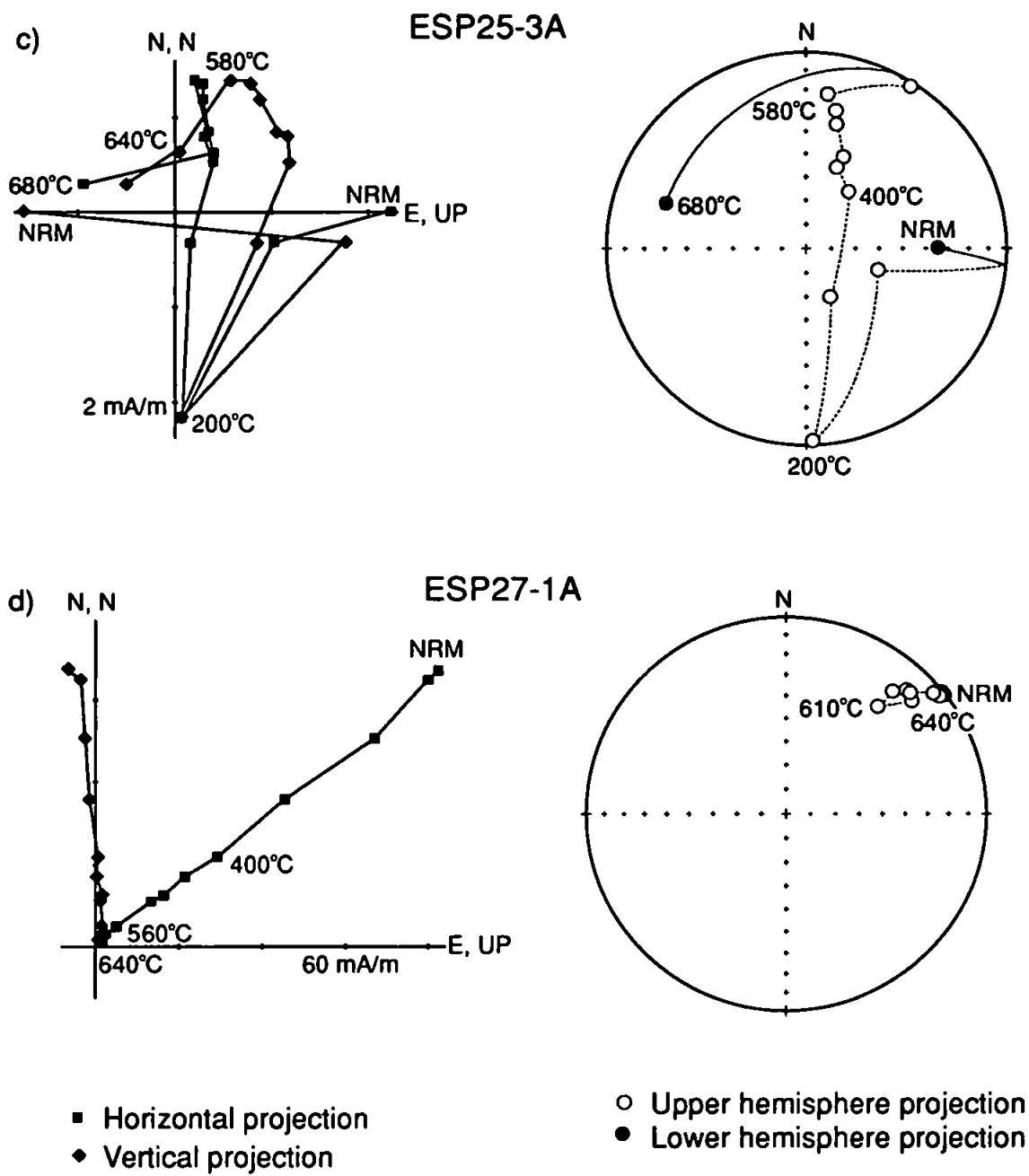


Figure 6.23c, d. Examples of demagnetisation behaviour in samples from the Quebrada Monardes Formation. All plots are tilt corrected.

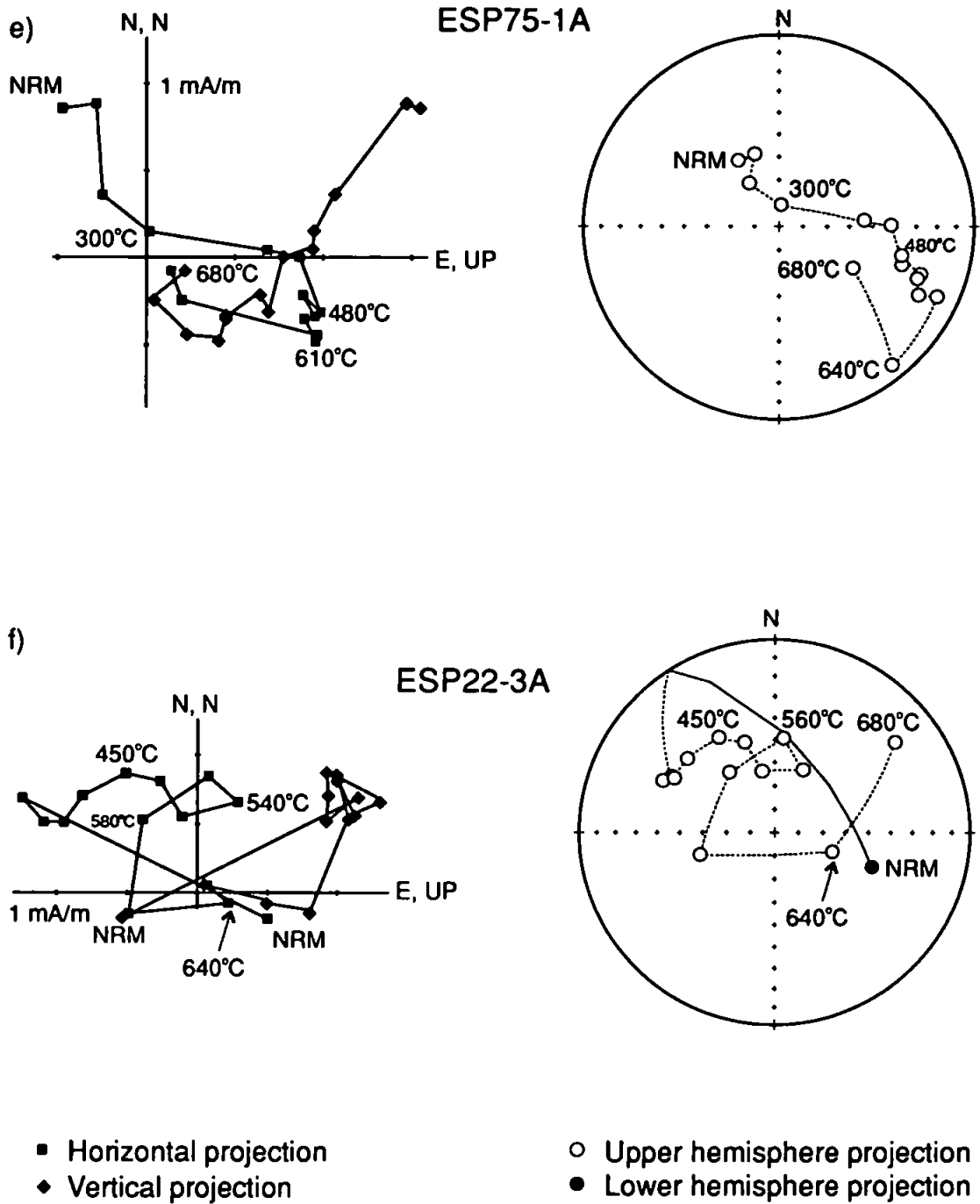


Figure 6.23e, f. Examples of demagnetisation behaviour in samples from the Quebrada Monardes Formation. All plots are tilt corrected.

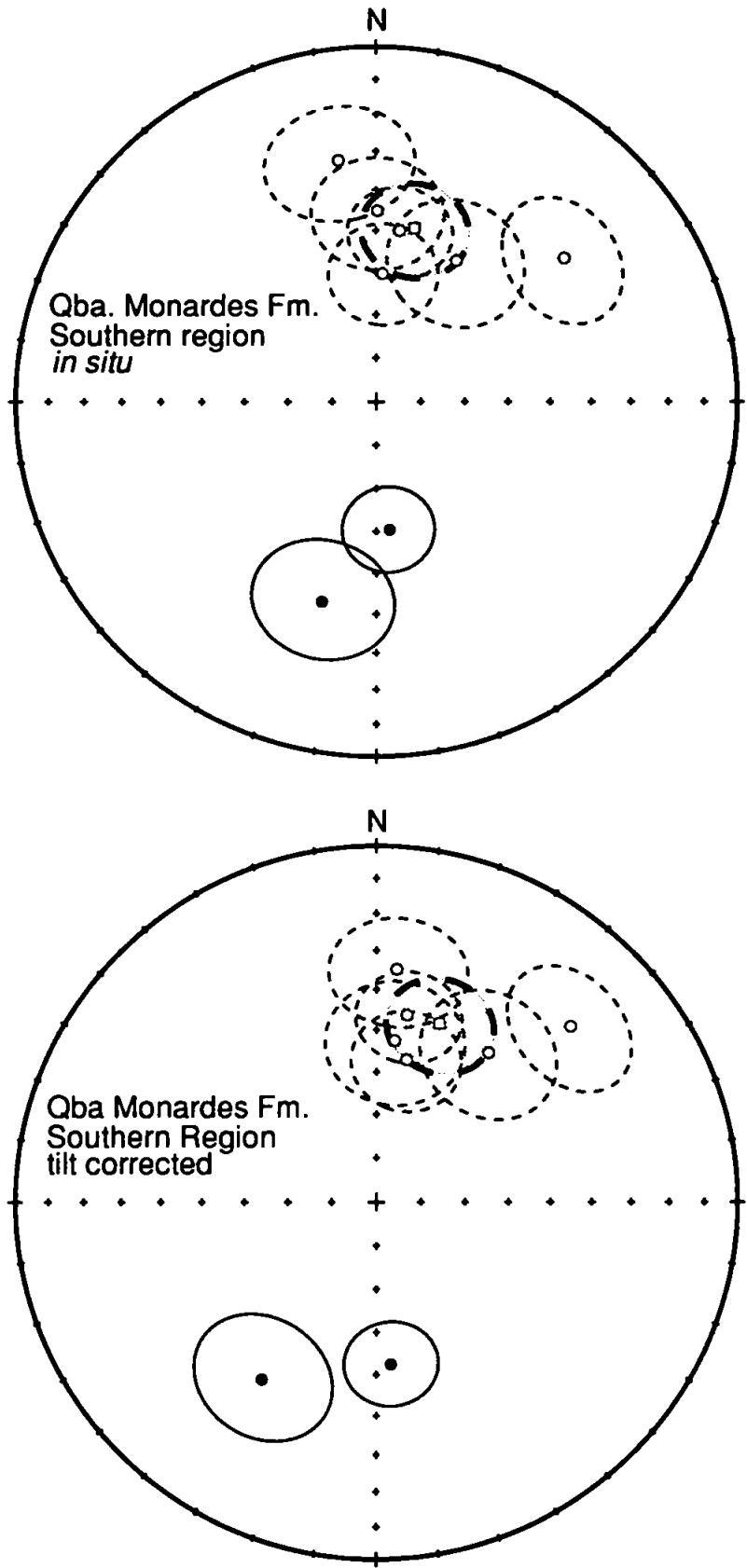


Figure 6.24. Stereographic projection of site mean directions from the Quebrada Monardes Formation (circles) and the Formation mean directions (square) from the southern region. Error ellipses are 95% confidence. Open (closed) symbols are upper (lower) hemisphere projections.

the statistically significant value of 2.47 at the 95 % confidence level. Removing the effects of the plunge on the fold does not increase the precision parameter on the tilt corrected mean enough to pass the test of McElhinny (1964).

Four of the six sites in the central area carry a consistent remanence direction, directed upwards in the NW quadrant (Table 6.8 and Figure 6.25). All of the sites included in the mean have normal polarity. The two sites excluded from the formation mean failed to yield a consistent or statistically acceptable site mean direction. As the tilt corrections are similar for all sites no fold test can be performed, but tilt correction steepens the formation mean inclination from -17.4° to -37.2° .

iv) Discussion of results

The demagnetisation of samples is both complex and variable, although a stable consistent direction can be obtained from both sampling localities. Although the directions from the southern sampling sites do not pass the fold test, k does improve on tilt correction. It is possible that the failure to pass the fold test is due to the dips on most of the tilt corrections being shallow, less than 20° , and because there are only two sites from the northern limb of the fold. More sites collected in a greater range of orientations may better constrain the mean direction and the precision parameter. Tilt correction does however improve the inclination in the central sites to one more consistent with the latitude expected for the sampling locality. Together these data suggests that the remanence in the Quebrada Monardes Formation is pre-folding, but more sites are required to confirm this.

Assuming that the remanence is pre-folding, and most likely primary or early diagenetic, the formation mean directions are compared against the Early Cretaceous reference direction. Comparison of the formation mean direction from the southern sampling sites with the reference direction yields a clockwise rotation of $23.7 \pm 13.7^{\circ}$, with a

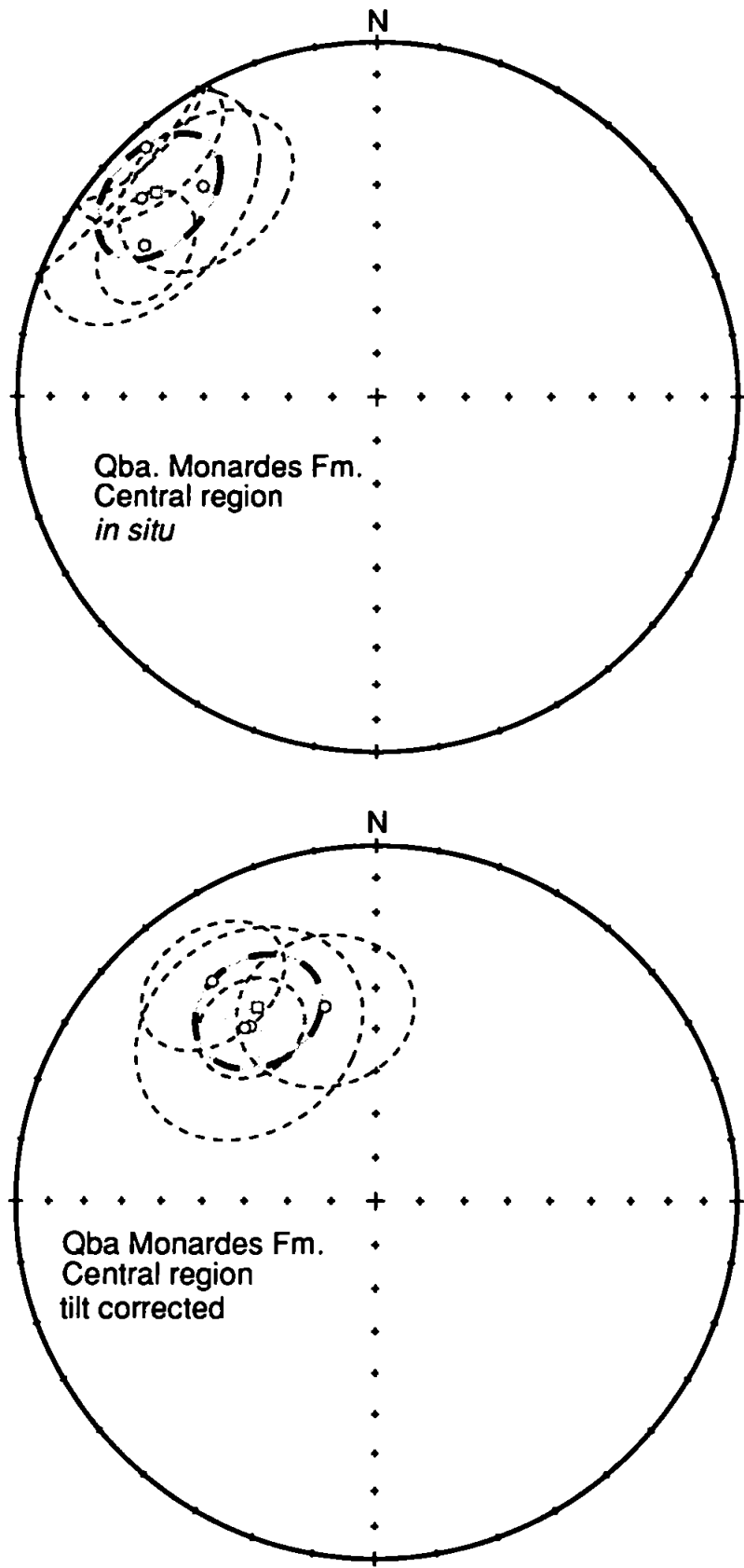


Figure 6.25. Stereographic projection of site mean directions from the Quebrada Monardes Formation (circles) and the formation mean directions (square) from the central region. Error ellipses are 95% confidence. Open (closed) symbols are upper (lower) hemisphere projections.

latitudinal displacement of $7.2 \pm 9.5^\circ$ southward. This magnitude of rotation is consistent with the results obtained by Riley *et al.* (1993) from the Quebrada Monardes Formation approximately 120 Km to the south of this study area. Their data indicate a clockwise rotation of $27.7 \pm 22.3^\circ$, with $1.9 \pm 16.6^\circ$ of southward latitudinal displacement, when compared with the Early Cretaceous direction from Chapter 3.

When the formation mean from the sites in the central area is compared to the reference direction an anticlockwise rotation of $27.6 \pm 14.1^\circ$ with a northward latitudinal displacement of $1.8 \pm 11.1^\circ$ is indicated. Although the α_{95} confidence limit on the formation mean direction is well constrained, the confidence limits on a number of the sites are much larger. This is in part due to some of the sites having only three samples, and suggests that better constrained results could be obtained by sampling more sites.

Overall the data from the Quebrada Monardes Formation indicates that although its magnetisation is complex, it probably carries a primary remanence. It may therefore be a suitable target for future palaeomagnetic work in the pre-Cordillera.

6.3.4 Cerro Valiente Sequence (Palaeocene)

i) Palaeomagnetic sampling localities

A total of 24 sites were collected from the Cerro Valiente lava sequence, 14 from the northern structural domain (ESP60-73), and 10 from the southern structural domain (ESP12-21). All sites were collected as hand samples except ESP73 which was drilled and orientated by both solar and magnetic compasses.

The northern sampling area is shown in Figure 6.26. Sites were collected from around an open syncline orientated roughly NE-SW. Palaeohorizontal control was obtained from boundaries between lava flows.

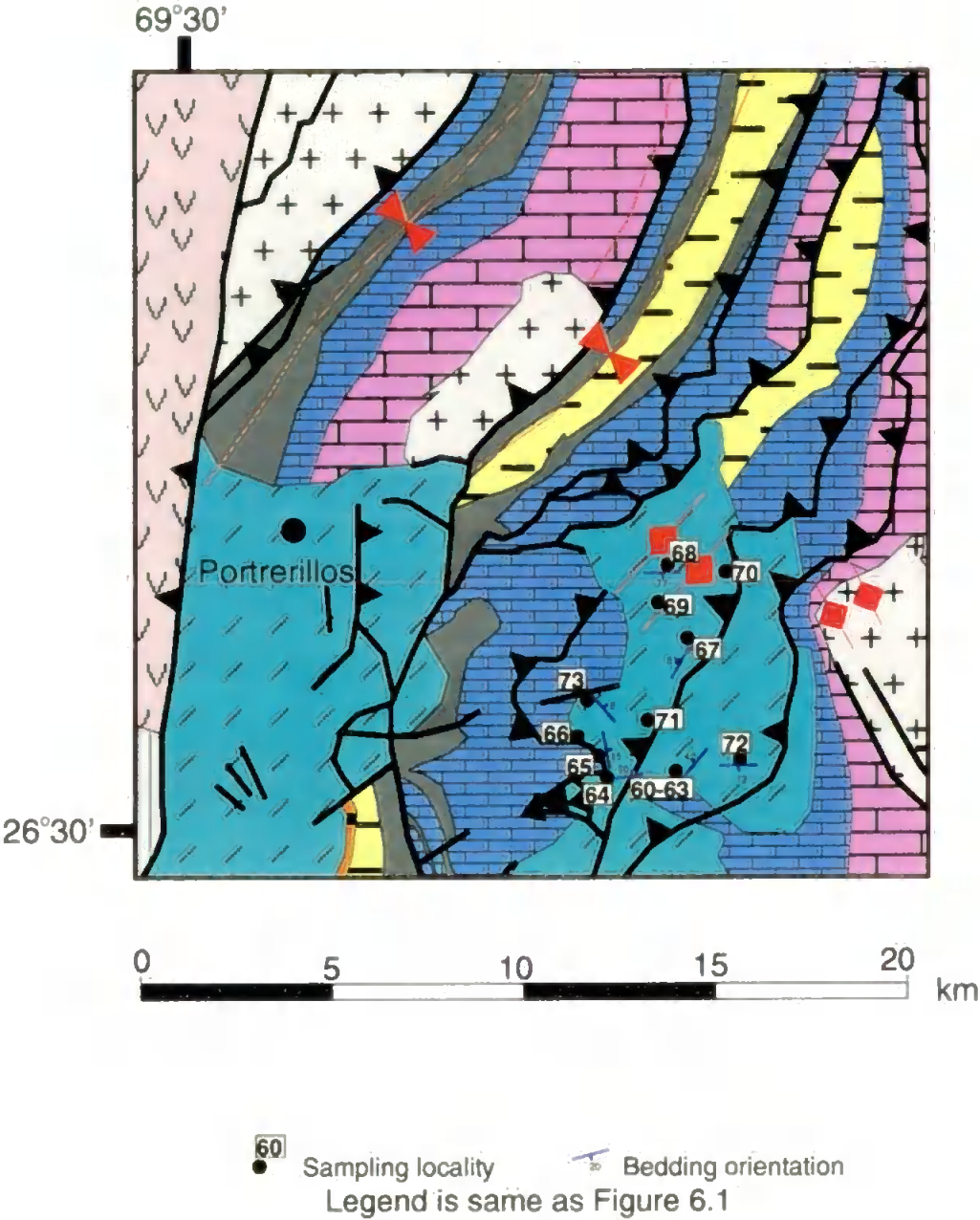


Figure 6.26 Sampling localities for the Cerro Valiente Formation in the northern region of the study area.

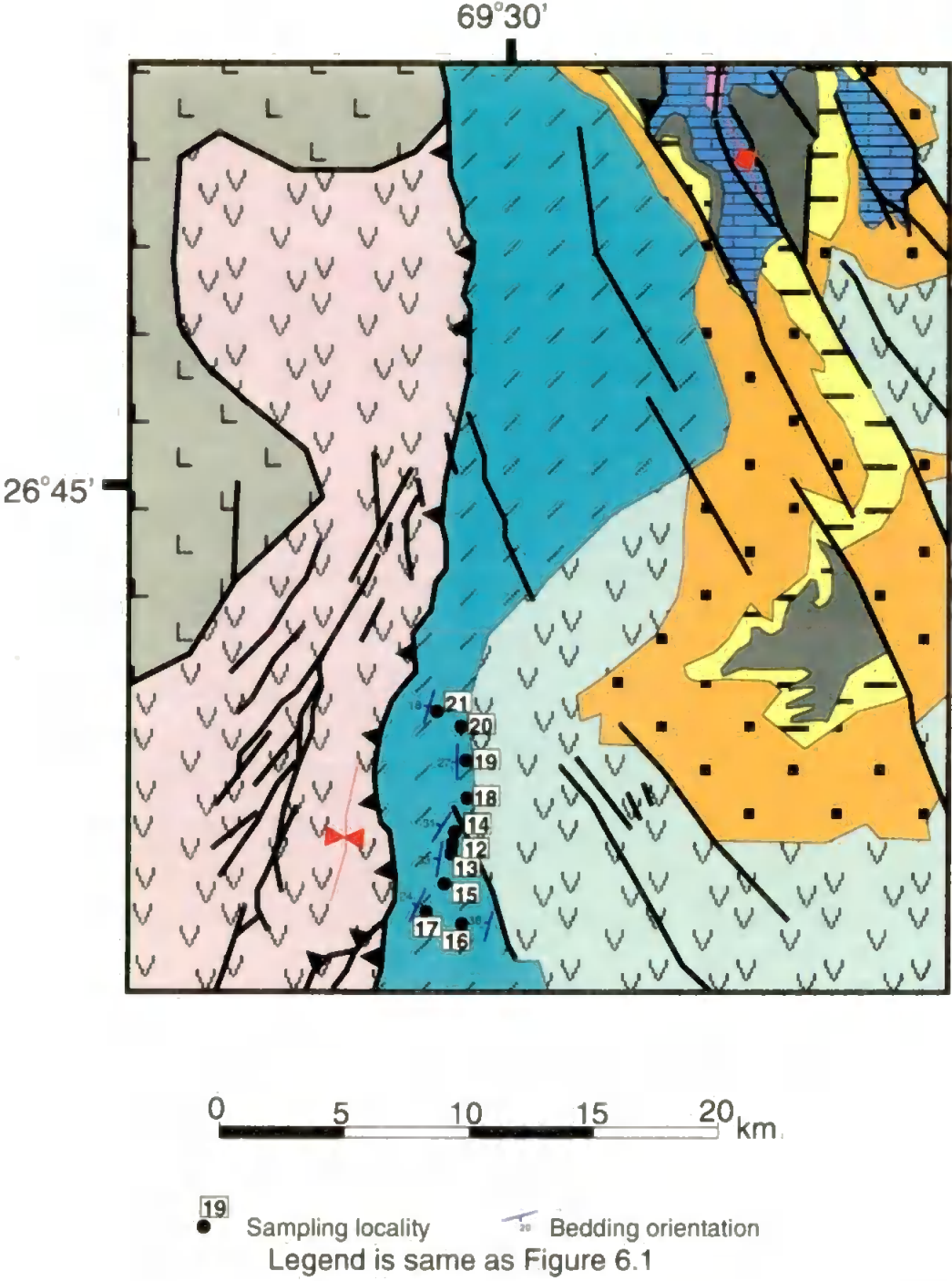


Figure 6.27. Sampling localities for the Cerro Valiente Formation in the southern region of the study area.

Sampling sites from the southern region are shown in Figure 6.27 . Here the lavas have a fairly consistent dip and palaeohorizontal control can be measured from limestone beds which are intercalated with the lavas.

ii) Magnetic mineralogy

IRM experiments (see section 2.6.1) were carried out on four samples, results from two are shown in Figure 6.28. Sample ESP20-1-3 (Figure 6.28a) shows an initial rapid rise in IRM, indicative of a dominant low coercivity carrier, but then a decrease. Repetition of the IRM acquisition by AF demagnetising the sample and re-applying the IRM showed that this intensity drop was a repeatable phenomenon, although the intensity of the IRM produced varied. After the decrease there is an unsteady rise in IRM which fails to saturate in the 800 mT applied field, this indicates a significant high coercivity component. IRM demagnetisation shows a dominant low coercivity component which is removed at $\sim 580^{\circ}\text{C}$, but also present is a high coercivity component which remains until $\sim 640^{\circ}\text{C}$. There is also a small fall in the low coercivity IRM component at $300\text{--}350^{\circ}\text{C}$, this may indicate the presence of some maghemite in the sample. These data are consistent with the sample having both magnetite and haematite carriers, possibly with some maghemite. The demagnetisation shows that the high coercivity component is only a minor constituent of the IRM, this appears to be inconsistent with the acquisition data which indicates a significant high coercivity contribution to the total IRM. AF demagnetisation of the NRM removes only 50% of the original intensity, indicating that both the magnetite and haematite were carriers of NRM. Attempts to isolate the higher coercivity component by thermal treatment failed, the demagnetisation directions became unstable and did not maintain a consistent direction.

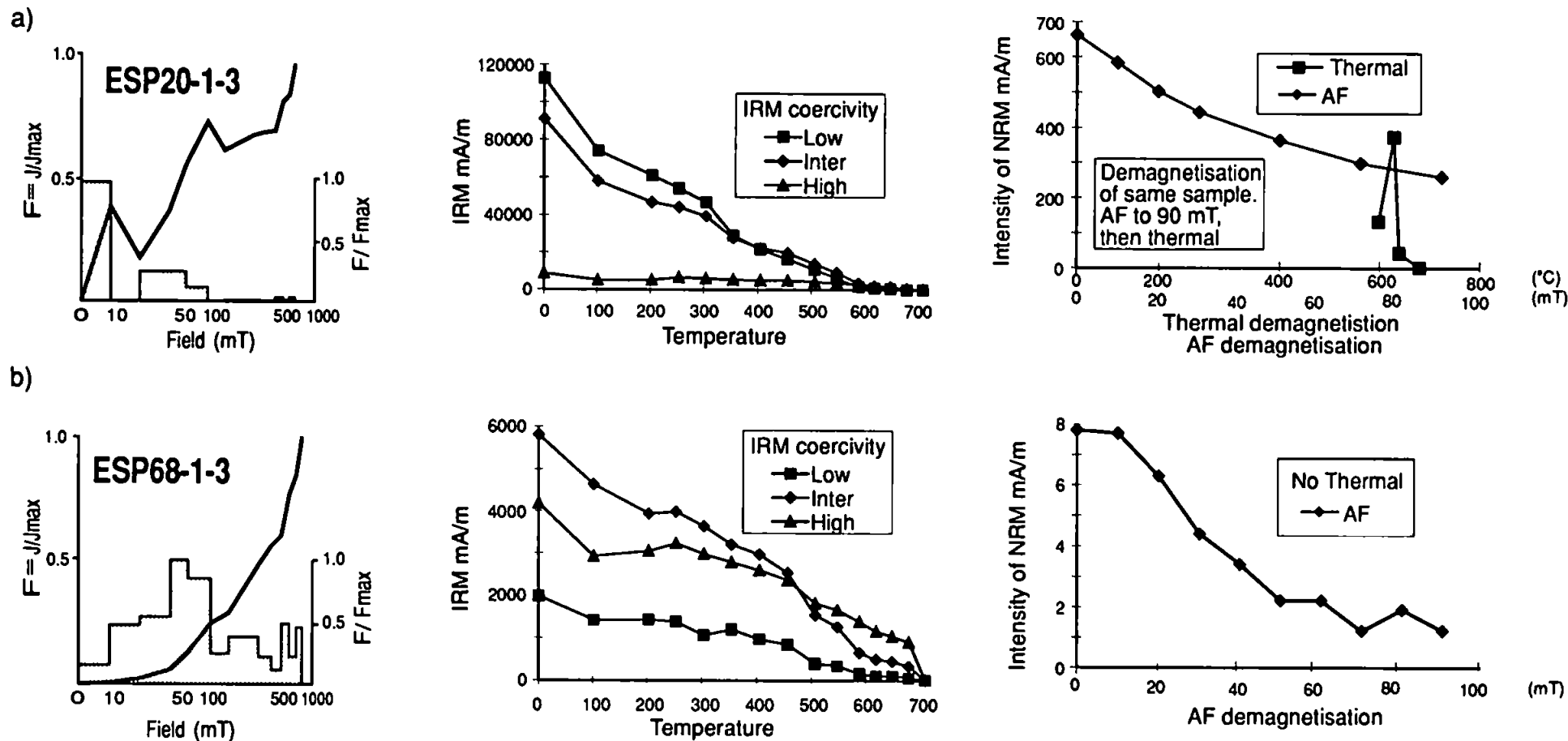


Figure 6.28a, b. Rock magnetic experiments on samples from the Cerro Valiente Formation. Graphs show acquisition of IRM, demagnetisation of three-axis IRMs and demagnetisation of NRM.

Sample ESP68-1-3 (Figure 6.28b) has an IRM acquisition curve consistent with a dominant high coercivity carrier. This is confirmed by the IRM demagnetisation where high and intermediate coercivities, demagnetised at $\sim 700^{\circ}\text{C}$ dominate. These data are consistent with a haematite dominated haematite/magnetite mix of carriers. Demagnetisation of the NRM was carried out by AF only and the sample became unstable by 50 mT. At this stage $\sim 15\%$ of the samples NRM intensity remains, significantly less than the 50 % remaining in ESP20-1-3. This suggests that in sample ESP68-1-3, haematite may not have been as important in carrying an NRM as it is an IRM.

The reasons for the erratic IRM acquisition and thermal demagnetisation behaviour in sample ESP20-1-3 are unclear. Experiments to ascertain the grain size of the magnetic fraction (section 2.6.2) were carried out on samples from the finest and coarsest lavas sampled from the Cerro Valiente Formation. The results are shown in Table 6.9 and suggest that the average particle size is in the pseudo-single domain size range and similar in both samples. It must be noted however, the presence of haematite in these samples causes a slight overestimate of the grain size (D. K. Potter, pers. comm., 1995). The results suggest that the samples should be capable of holding a stable remanence.

Sample	RRM mAm^{-1}	ARM mAm^{-1}	Effective field (Bg) μT	Particle size (d) μm
ESP15-2-1	401.5	1138.0	24.7	4.0
ESP60-2-3	337.4	1189.5	19.9	5.0

Table 6.9. Magnetic grain size analysis in the Cerro Valiente lavas using RRM and ARM acquisition as described in section 2.6.2.

Results of VRM experiments (section 2.6.3) carried out on samples ESP20-1-3 and ESP68-1-3 are shown in Table 6.10 and Figure 6.29. Both samples show more viscous behaviour after heating to 700°C and, in addition, samples are unable to acquire the same

Decay time (s)	<u>AF demagnetisation only</u>		<u>After thermal demag. to 700°C</u>	
	IRM (mA/m)	Normalised %	IRM (mA/m)	Normalised %
<u>20-1-3</u>				
7	16675	100.0	6744	100.0
20	16633	99.7	6686	99.1
30	16612	99.6	6656	98.7
40	16575	99.4	6635	98.4
50	16607	99.6	6630	98.3
60	16624	99.7	6635	98.4
80	16592	99.5	6614	98.1
100	16555	99.3	6626	98.3
120	16575	99.4	6600	97.9
240	16524	99.1	6547	97.1
480	16445	98.6	6484	96.1
720	16419	98.5	6414	95.1
1000	16368	98.2	6334	93.9
<u>68-1-3</u>				
7	77.5	100.0	20.5	88.9
20	74.2	95.7	19.5	84.6
30	73.3	94.6	19.7	85.4
40	72.2	93.2	19.8	85.8
50	71.8	92.6	20.1	86.8
60	71.8	92.6	20.1	86.9
80	71.0	91.6	20.0	86.5
100	70.3	90.7	20.1	87.0
120	71.8	92.6	20.6	89.0
240	71.2	91.9	21.7	94.0
480	70.4	90.8	23.1	100.0
720	70.7	91.2	22.0	95.4
1000	70.1	90.5	20.3	88.0

Table 6.10. Data for VRM experiments. Each sample was exposed to a 5 mT field to induce an IRM. The intensity of the IRM was measured at intervals up to 1000 s. Data is given as absolute measurement and normalised percentage of maximum intensity.

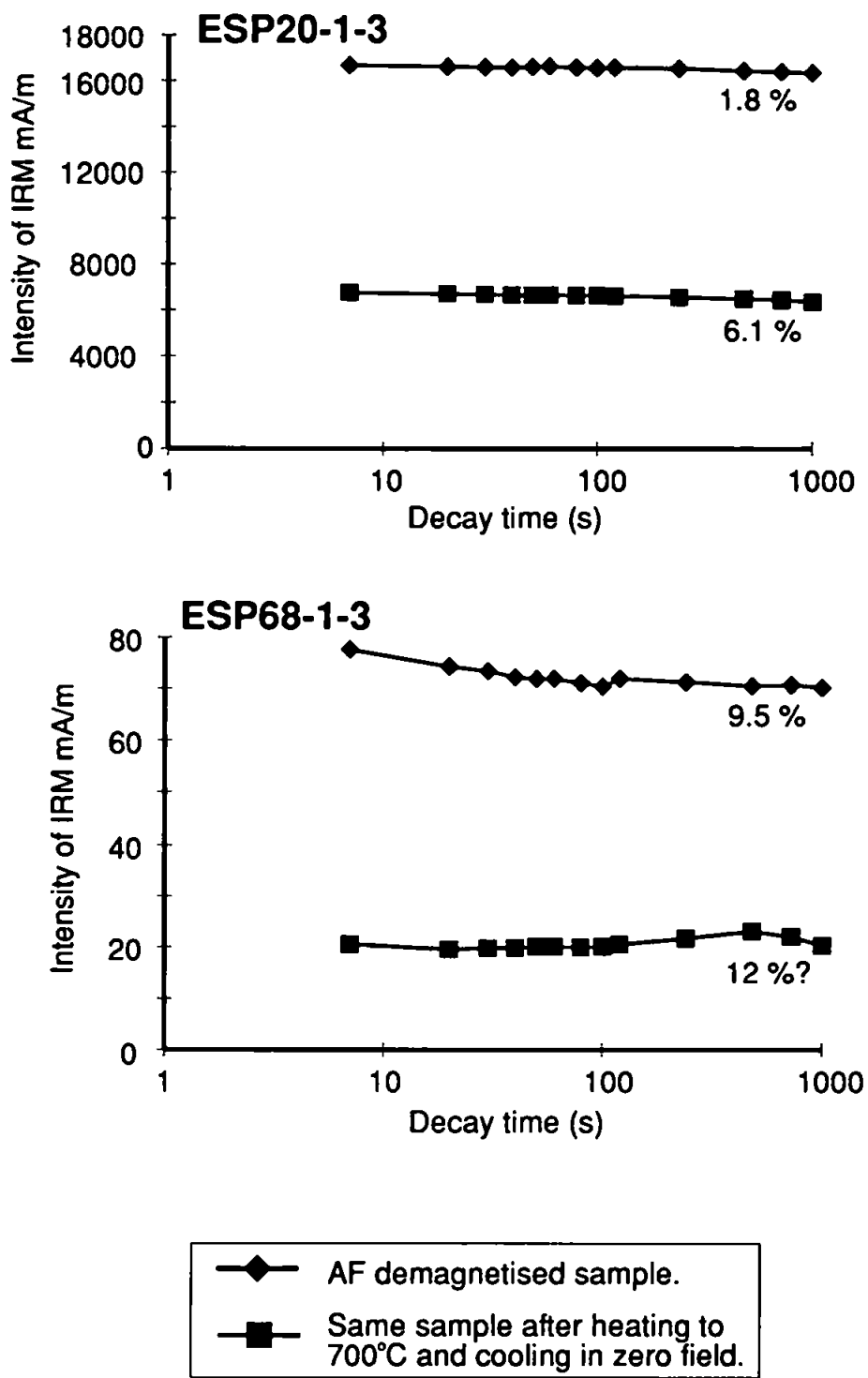


Figure 6.29a, b. Graphs illustrating the presence of VRM in samples of the Cerro Valiente Formation. Graphs show the decay of IRM after exposure to a 5 mT field. Percentages are amount of intensity lost over time period.

IRM intensity. This inability to acquire the same IRM after heating is interpreted as being due to mineralogical changes in the sample, probably oxidising magnetite to haematite. The decay of viscous remanence in sample ESP68-1-3 was unstable, this experiment was repeated with similar results, possibly indicating that the sample can rapidly acquire stray magnetic fields. During measurement however, the samples were not removed from the magnetometer, so the source of any stray field is unknown. Another possible source of error is due to instrument drift, although calibration before and after measurement suggested that this was minor. In conclusion therefore, the cause of the intensity rise in sample ESP68-1-3 is unknown. The results from both samples suggest that these rocks can undergo significant changes in magnetic mineralogy during heating. AF demagnetisation may therefore be better at isolating magnetic components than thermal treatment in samples from this formation.

The rock magnetic experiments suggest a dominant magnetite carrier for the NRM which has a grain size suitable for carrying a primary remanence. Although samples can behave in a viscous manner after heating, the loss of remanence due to VRMs is not significant in unheated samples.

iii) Palaeomagnetic remanence measurements

Of the 24 sites collected 11 have been demagnetised, six from the northern domain and five from the southern domain. All sites demagnetised carry a stable remanence direction within the site, sampling and demagnetisation data are given in Tables 6.11 and 6.12.

Low coercivity and unblocking temperature components from the measured sites are shown in Figure 6.30. Directions from sites in the northern domain (Figure 6.30a) do not have a consistent direction and there is no improvement in grouping after tilt correction.

Site	Sampling site		Tilt correction	ChRM isolation mT (°C)	
	Long. W	Lat. S		Min.	Max.
Northern Region					
* ESP60	69°23'	26°29'	210/43	10→30	100
* ESP64	69°23'	26°29'	260/30	30	100
* ESP65	69°23'	26°29'	320/35	30	100
* ESP67	69°23'	26°28'	208/61	NRM→10	100
ESP68	69°23'	26°27'	090/77	10→30	60
* ESP73	67°24'	26°28'	330/8	10	100
Southern Region					
* ESP14	69°31'	26°53'	202/31	20	90 (up to 670)
* ESP15	69°32'	26°55'	198/36	20	100
* ESP16	69°32'	26°56'	196/36	50 (510)	100 (670)
* ESP19	69°30'	26°52'	180/27	20→30	100 (up to 670)
* ESP20	69°30'	26°51'	195/28	30	90 (up to 670)

Table 6.11. Sampling and demagnetisation data from sites in the Cerro Valiente Formation. Tilt correction is given in right-hand-rule, ChRM isolation is demagnetisation level at which ChRM is isolated in the site, a range with an arrow indicates a within site variation.

	Site	n/No	Uncorrected		Corrected		k	α_{95}
			Dec.	Inc.	Dec.	Inc.		
				<i>Northern Region</i>				
*	ESP60	5/6	232.9	64.4	271.7	33.1	18.6	19.5
*	ESP64	6/6	183.0	43.2	201.0	71.4	347.0	3.6
*	ESP65	6/6	194.5	51.6	134.5	68.8	72.1	8.5
*	ESP67 (1)	3/3	213.4	15.8	224.4	3.0	163.6	9.7
	ESP67 (2)	3/3	47.0	11.6	26.6	22.1	45.7	18.5
	ESP68	6/6	301.4	56.1	212.6	28.0	50.6	10.2
*	ESP73	3/8	8.1	-22.3	23.3	-19.9	75.5	14.3
	Mean	5/7	199.9	40.6			11.1	24.0
					220.0	45.8	3.8	45.7
				<i>Southern Region</i>				
*	ESP14	6/6	288.3	-44.2	281.7	-75.1	53.5	9.2
*	ESP15	6/6	335.4	-56.6	43.0	-63.4	272.1	4.1
*	ESP16	6/6	277.1	-37.9	261.6	-72.7	181.0	5.0
*	ESP19	6/6	262.8	-79.5	94.5	-73.3	393.6	3.4
*	ESP20	6/6	304.2	-53.1	342.7	-76.5	226.5	4.5
	Mean	5/5	295.6	-56.2			14.7	20.6
					357.5	-83.5	17.8	18.6

Table 6.12. Remanence data from the Cerro Valiente Formation. Numbers in brackets after site numbers indicate the hand sample number and are given where the directions from the individual blocks are significantly different; n/No. is number of samples included in site mean/number of samples demagnetised; dec. and inc. are declination and inclination of remanence vector; k is Fisherian precision parameter; α_{95} is semi-angle of 95% cone of confidence. Sites marked * are included in formation mean.

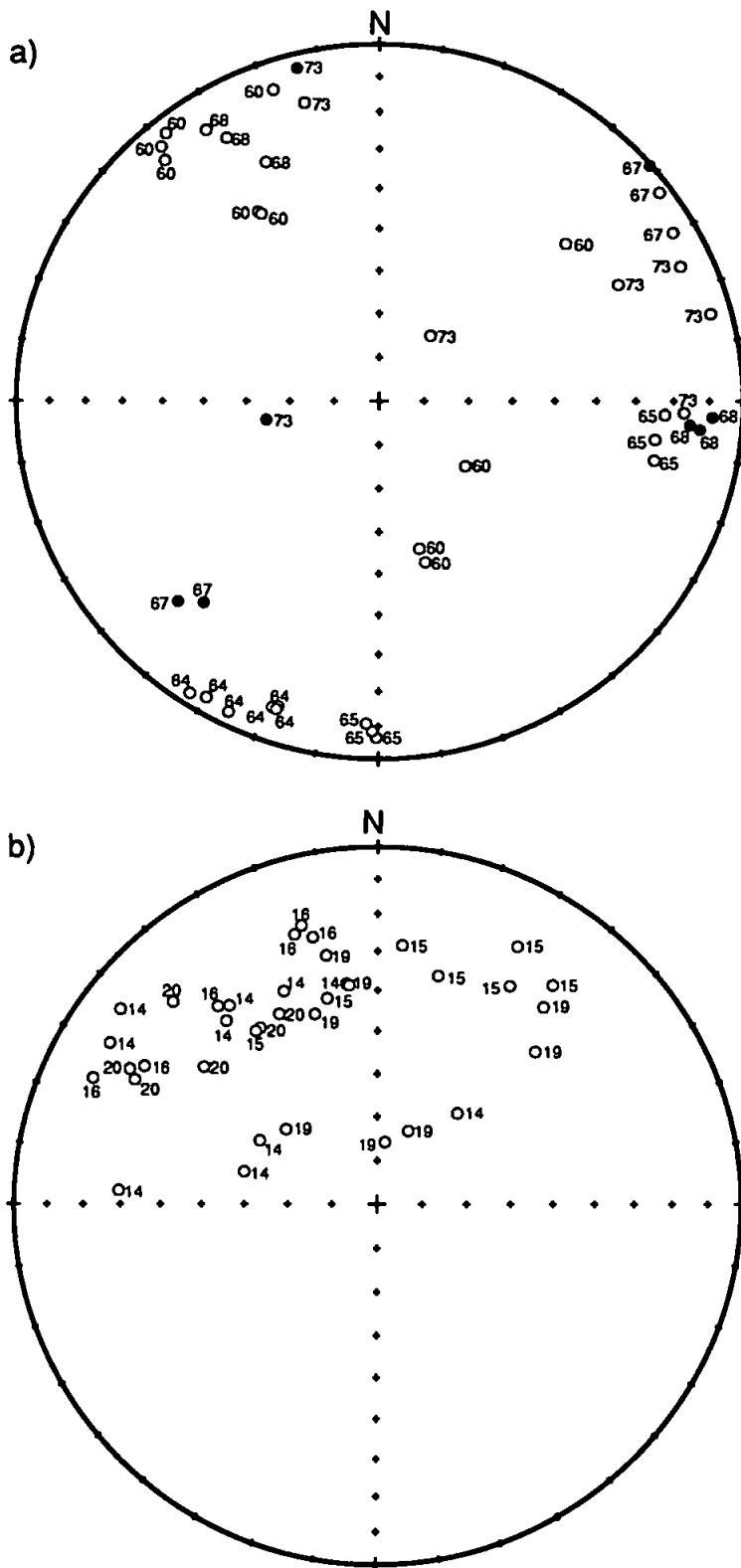


Figure 6.30. Equal area stereographic projection of low coercivity and unblocking temperature components from sites in the Cerro Valiente lavas. a) From the northern region b) From the southern region. Open (closed) symbols are upper (lower) hemisphere projections. Directions are *in situ* numbers are site numbers.

The components do, however, tend to group well within site, or at least within sample block. The samples from site ESP73, which was drilled in the field, are scattered. This would indicate that these components were acquired after the blocks and field drilled cores were collected, but before the cores were removed from the blocks in the laboratory. These low coercivity and unblocking temperature directions therefore seem to be the result of a laboratory or collection induced component.

The directions from sites in the southern domain are much better grouped overall, although directions from the individual sites are, in some cases, less well defined than from sites in the northern domain (Figure 6.30b).

Although the directions of magnetic components present vary between sites, the demagnetisation behaviour, in terms of the number and demagnetisation level of components, is similar. Sites have either a single component of magnetisation, the ChRM, or a major stable high coercivity/unblocking temperature ChRM component and a low coercivity/unblocking temperature component removed by 20 mT. In many cases the spectra of the low coercivity/unblocking temperature component overlaps with the sites ChRM. In sites from the northern domain, the ChRM is directed downwards toward the SW or its antipode. In the southern domain, the ChRM has a WNW direction with a moderate upwards directed inclination. Figure 6.31a-d are representative of the types of behaviour seen during demagnetisation. Five of the sites in the northern region have demagnetisation plots like Figure 6.31a or 6.31b, characterised by rapid demagnetisation during AF treatment, and ChRM isolation above ~30 mT. In site ESP68 (Figure 6.31c) the demagnetisation vector is much better defined, with the ChRM held between 20 and 60 mT. Site ESP68 is also different from others in the northern domain in that its NRM intensity is at least a factor of 100 less than all of the other sites. All of the sites collected in the southern domain display demagnetisation directions and plots similar to that shown in

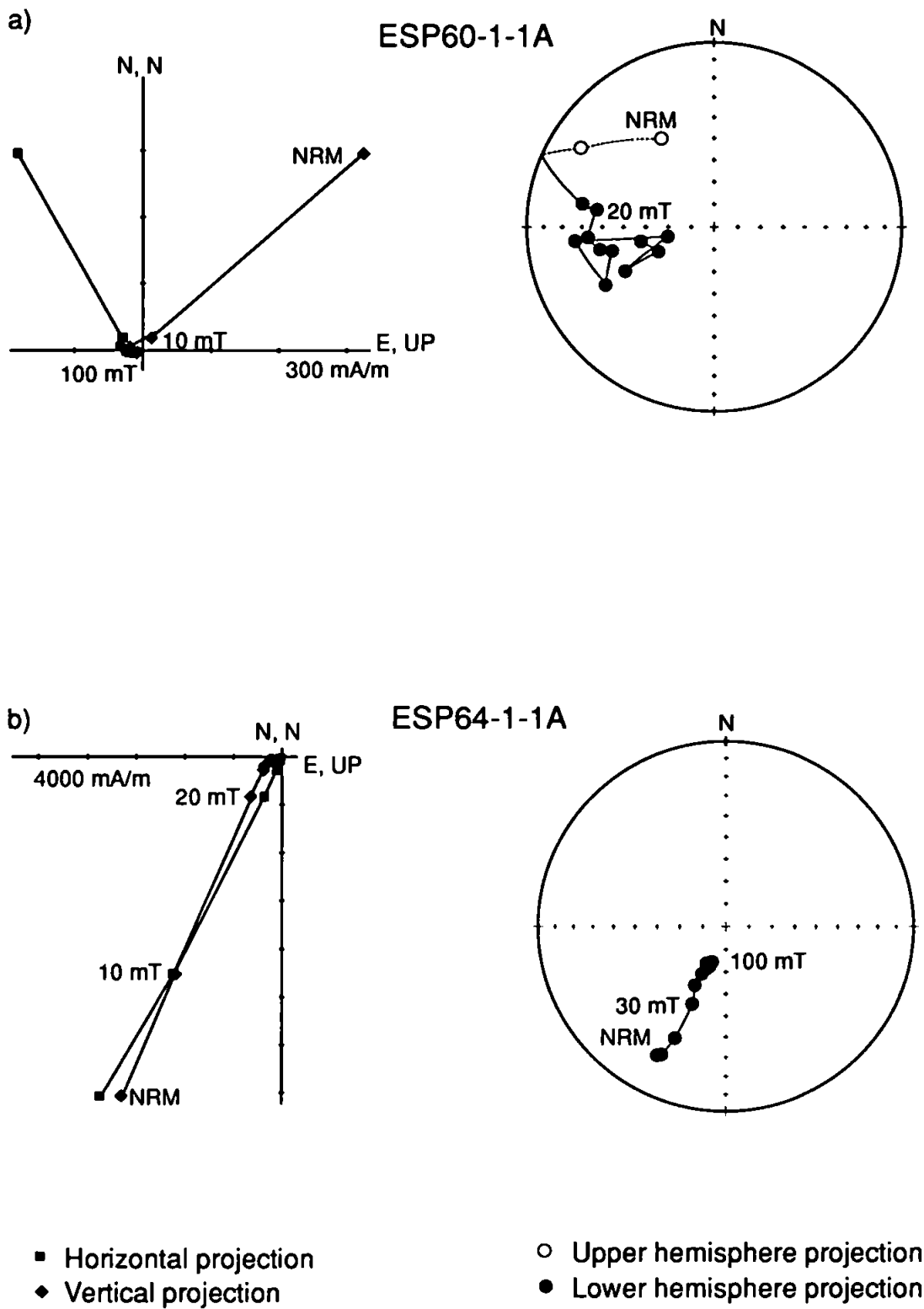


Figure 6.31a, b. Examples of demagnetisation behaviour in samples from the Cerro Valiente lavas. All plots are tilt corrected.

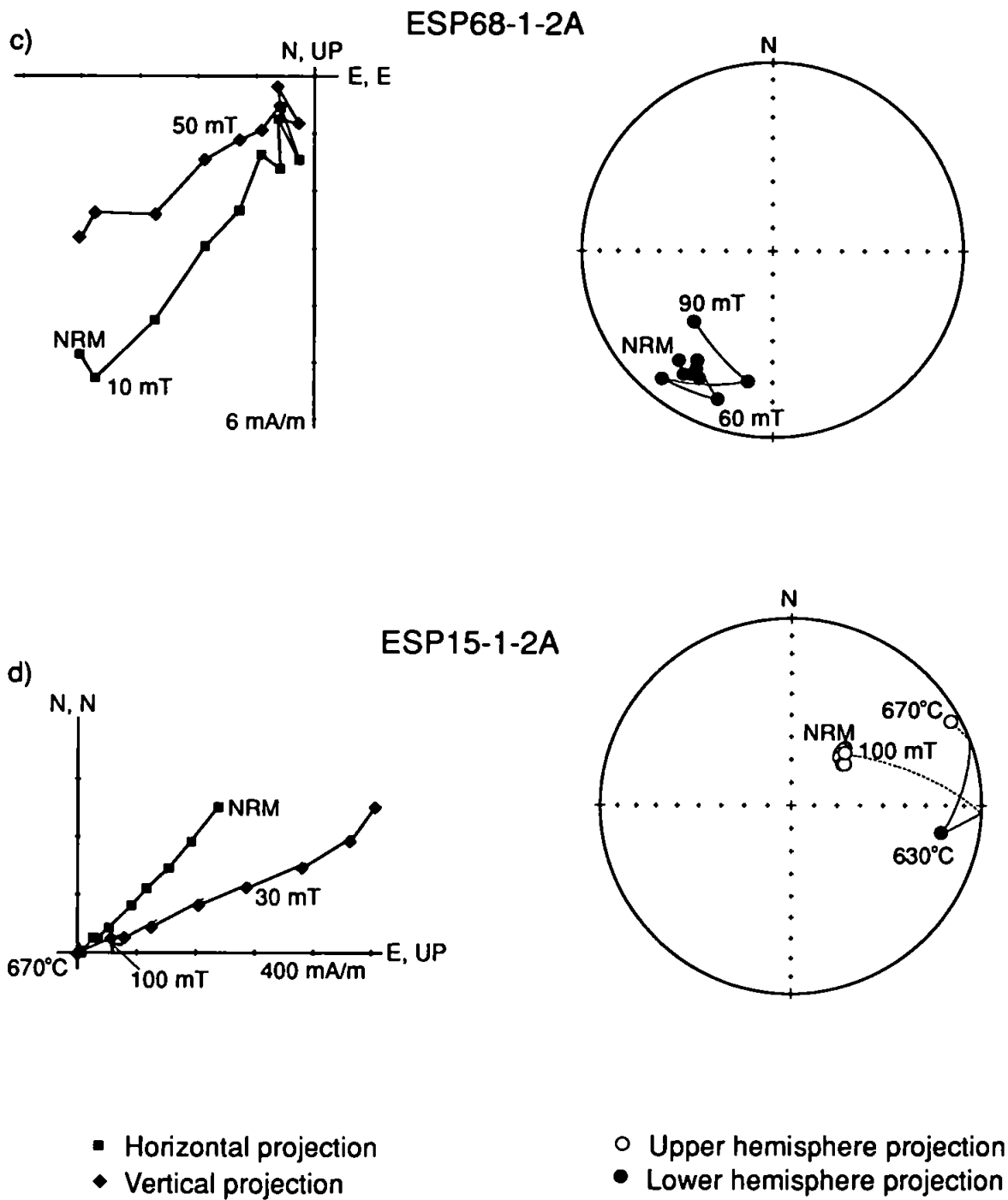


Figure 6.31c, d. Examples of demagnetisation behaviour in samples from the Cerro Valiente lavas. All plots are tilt corrected.

Figure 6.31d. A low coercivity/unblocking temperature component is removed by 10 mT. The ChRM is recovered at demagnetisation levels between 10 and 100 mT. In all sites some remanence remains after AF demagnetisation to 100 mT, but thermal demagnetisation caused significant and random increases in intensity as well as directional changes.

The site mean directions within the two domains are best grouped before tilt correction. Site mean directions for sites in the northern domain are shown in Figure 6.32. Site ESP68 is excluded from the mean calculation as it has a direction apparently unrelated to the formation mean direction. The site also displays different demagnetisation behaviour to the other sites, as described above. The site mean directions are better grouped when viewed *in situ* and the formation mean (Table 6.12 and Figure 6.32) is based on their *in situ* distribution. Four of the site mean directions are reversed. The decrease in precision parameter k on tilt correction ($k_1/k_2 = 0.53$ is less than the statistically significant value of 3.44 at 95% confidence) fails the fold test of McElhinny (1964).

Site mean directions from all five sites in the southern domain are shown in Figure 6.33, the formation mean is also shown and is given in Table 6.12. One of the most noticeable features in the data are the small α_{95} confidence limits on the site means. Because of the consistency of the tilt corrections on the sites mean directions a meaningful fold test cannot be performed, but the precision parameter, k , does show slight improvement after tilt correction.

iv) Discussion of results

The failure of the fold test for the sites in the northern domain indicates a post-folding remanence. As with the Quebrada Vicuña Formation, the timing of remagnetisation in these rocks is uncertain. Again the pervasive hydrothermal alteration seen in thin section may be related to the later stages of the tectonic activity in the area,

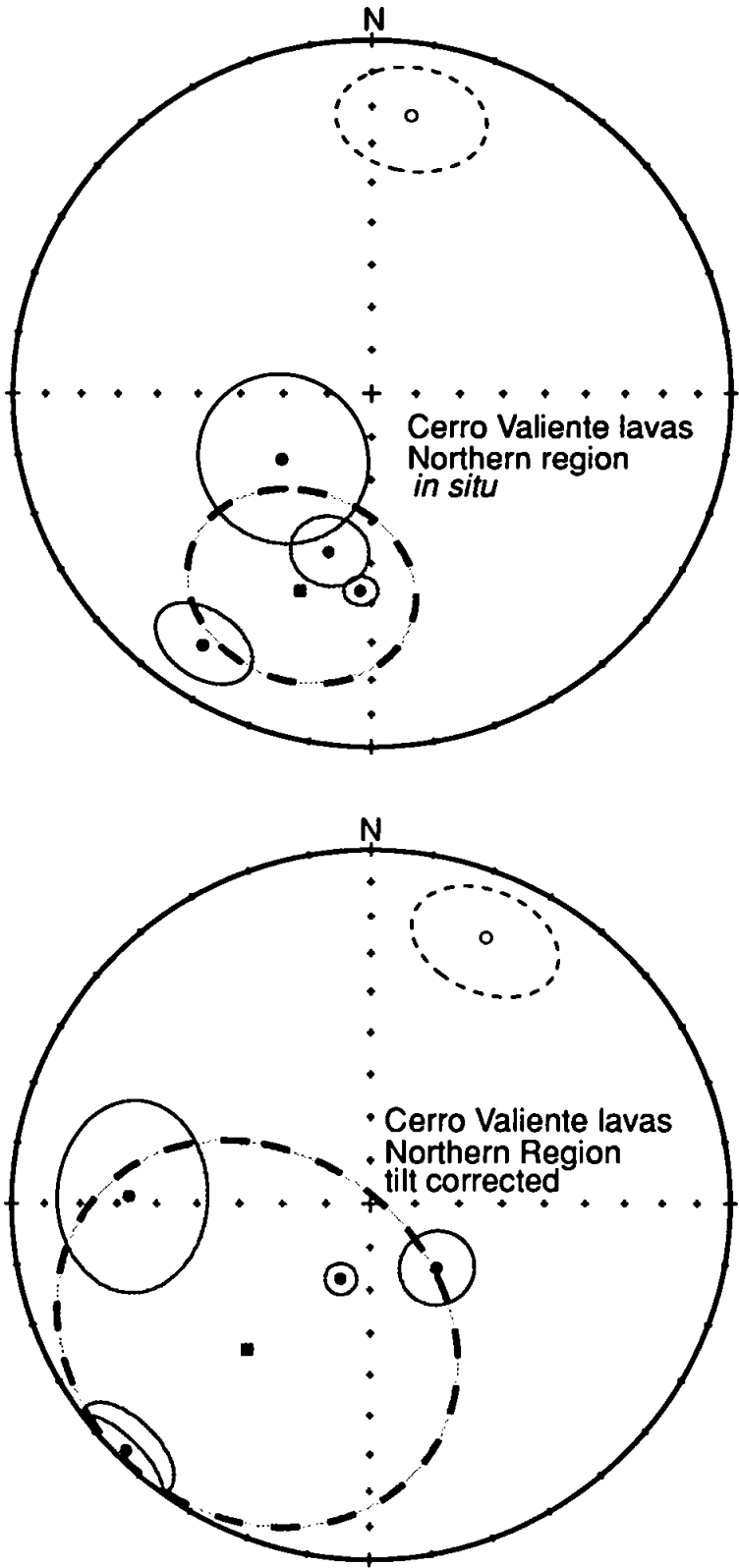


Figure 6.32. Stereographic projection of site mean directions from the Cerro Valiente lavas (circles) and the Formation mean directions (square) from the northern region. Error ellipses are 95% confidence. Open (closed) symbols are upper (lower) hemisphere projections.

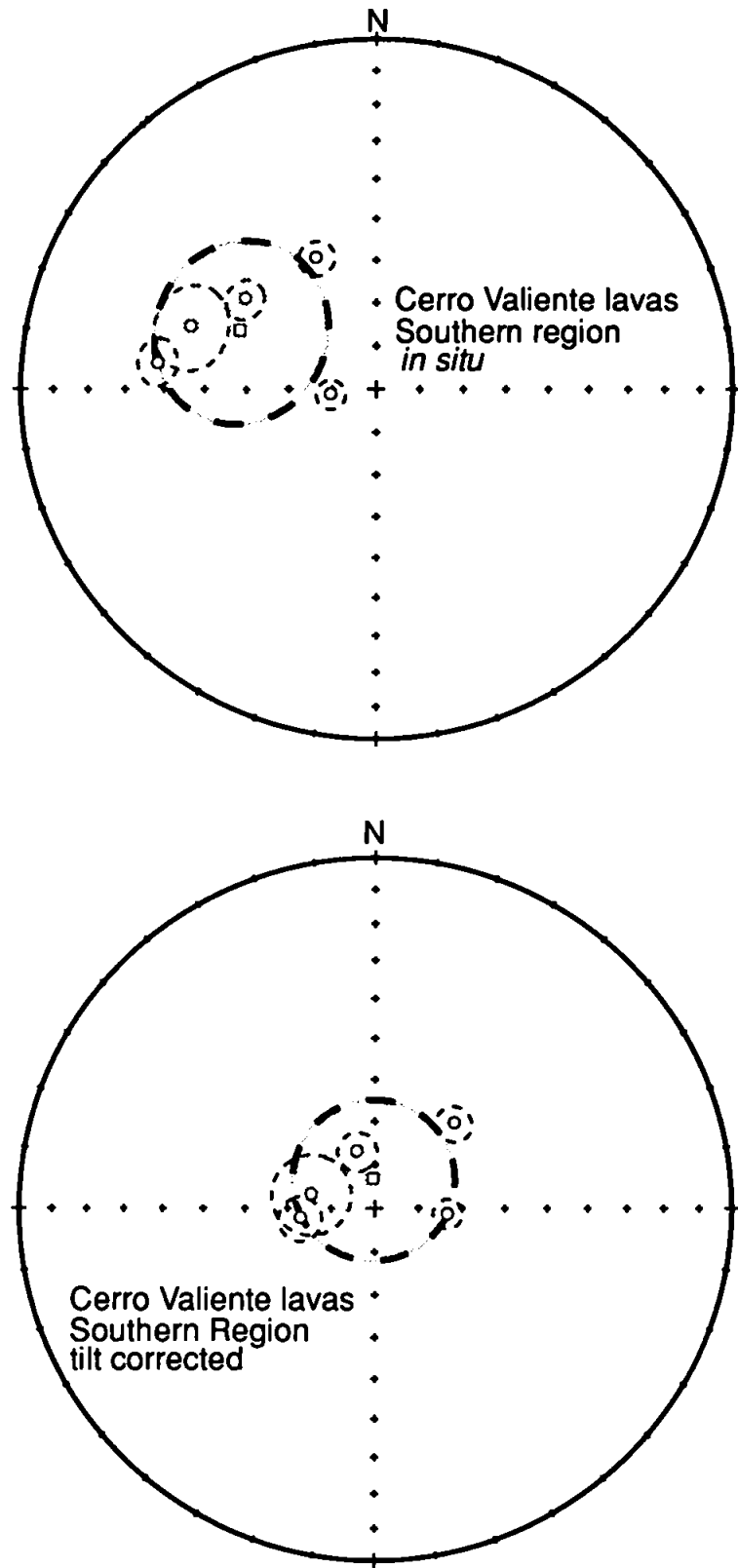


Figure 6.33. Stereographic projection of site mean directions from the Cerro Valiente lavas (circles) and the Formation mean directions (square) from the southern region. Error ellipses are 95% confidence. Open (closed) symbols are upper (lower) hemisphere projections.

dated as late Oligocene-early Miocene. The remanence carried by the Cerro Valiente Formation must be younger than this. The inclusion of four sites with reversed polarity in the formation mean direction for the northern domain, but with none in the southern domain may suggest that the remagnetisation of the formation occurred at different times. As discussed in Chapter 3, the time averaged field direction is an appropriate reference direction for remanences younger than Palaeocene and is used for reference.

The site mean directions from sites in the northern domain are best grouped *in situ*. This formation mean direction is poorly defined, having an $\alpha_{95} = 24^\circ$ *in situ* and $\alpha_{95} = 45.7^\circ$ after tilt correction, any interpretation made from the data must therefore be regarded as tentative. Comparison of the northern mean direction with the reference direction gives a clockwise rotation of $19.9 \pm 25.9^\circ$ with a flattening of $4.4 \pm 19.2^\circ$ for these sites. As the amount of rotation is within its associated error, it is not statistically significant.

As the structural corrections for the sites collected in the southern domain are constant, no meaningful fold test can be performed to determine the age of remanence relative to the deformation. When tilt corrected, the formation mean inclination increases from -56.2° to -83.5° , this is much too steep to be a true direction at this locality and suggests that the remanence is post-folding in age. The demagnetisation behaviour in these sites is, however, essentially single component and therefore much simpler than that observed in sites from any other formation. In addition, four of the sites have very small α_{95} confidence limits, suggesting that secular variation may not have been averaged within these sites. This is not consistent with the idea of complex remagnetisation over a long time period. Another possibility therefore is that the remanence is primary, and the steep inclination is the result of the remanence having been acquired rapidly during a geomagnetic excursion. It is, however, difficult to reconcile this with the pervasive alteration of the rocks, and the remagnetisation of the volcanic units in the rest of the sampling area. It is

more likely that the directions represent complete remagnetisation over a short time period, possibly as a result of a pulses of hydrothermal fluid associated with a porphyry deposit.

The *in situ* mean direction is therefore likely to be a result of a remanence younger than Oligocene and is compared with the time averaged field direction. This yields an anticlockwise rotation of $64.4 \pm 31.4^\circ$, with a flattening of $11.2 \pm 16.5^\circ$. This rotation is statistically significant, although poorly constrained in terms of its timing and confidence limit.

6.4 Discussion and Conclusions

Of the four formations and lithologies sampled in this area, it seems only the Quebrada Monardes Sandstone Formation may be carrying a pre-folding remanence. The volcanic units have all undergone significant remagnetisation since the age of folding, probably during the late Eocene to Miocene. The presence of both normal and reversely magnetised site mean directions in the Sierra Fraga, Quebrada Vicuña and Cerro Valiente Formations suggests that either the remagnetisation event occurred over a significant time period, or was the culmination of several phases of remagnetisation, some of which occurred during periods of reversed polarity.

Most of the units sampled in the volcanic rocks display statistically insignificant amounts of rotation or latitudinal displacement. Two of the formations in the volcanic units, the Sierra Fraga Formation and the southern Cerro Valiente Formation, have rotations which exceed their associated confidence limits and may therefore be recording post-folding rotations. As discussed in Section 6.3.1, the confidence limit of the *in situ* Sierra Fraga direction is extremely large and no geological interpretation is made from it. Although the confidence limits on the Cerro Valiente mean directions are better than that on

the Sierra Fraga direction, the rotation must be considered to be poorly constrained. Table 6.13 shows a summary of the rotations from this study, and those which are considered to be statistically significant and well constrained. As a result of the remagnetisation there are no statistically significant results from the northern domain, the fold-and-thrust belt.

Only four sites from the complex zone of deformation between the northern fold-and-thrust belt domain, and the southern domain of NW trending strike-slip faults record a stable magnetisation. Despite this the sites from the Quebrada Monardes Sandstone Formation define a fairly well constrained mean direction. The result from this small area indicates that a $\sim 27^\circ$ anticlockwise rotation has occurred.

The results from the southern strike-slip fault domain are conflicting; the result from the Quebrada Monardes Formation indicates a $\sim 24^\circ$ clockwise rotation since the Early Cretaceous, while the Cerro Valiente lavas indicate anticlockwise rotation of $\sim 64^\circ$ probably since the Oligocene or Miocene. It is difficult to envisage a situation where an anticlockwise rotation of $\sim 64^\circ$ could occur since this time, particularly as this time period post-dates the major tectonic activity in the region. This direction does not seem to be geologically sensible and the better constrained $\sim 24^\circ$ clockwise rotation recognised from the Quebrada Monardes Formations is taken as being representative of the rotation in the southern strike-slip fault domain. The reason for the Cerro Valiente direction lying so far from the reference direction is unknown, but it is possible that these sites may have been remagnetised over a short time period during a reversal or geomagnetic excursion.

In conclusion, the pervasive remagnetisation seen in the rocks in this area have made interpretation of any tectonic rotation difficult. Only the rotations from the Quebrada Monardes Sandstone Formation can really be regarded as well constrained, both statistically and in terms of age control. The rotations suggested by all of the volcanic units are either not statistically significant, or are difficult to explain geologically.

Formation name	Age of Formation	Age of Remanence	Rotation±error (°)	Flattening±error (°)
<i>Northern Domain</i>				
Quebrada Vicuña	L. Jurassic	Oligocene or younger	-3.5±7.4	0.0±5.2
Cerro Valiente	Palaeocene	Oligocene or younger	19.9±25.9	-4.4±19.2
<i>Central area between two domains</i>				
Quebrada Monardes*	E. Cretaceous	? E. Cretaceous	-27.6±14.1	-1.8±11.1
<i>Southern domain</i>				
Quebrada Vicuña	L. Jurassic	Oligocene or younger	-12.5±22.3	-0.1±15.4
Quebrada Monardes*	E. Cretaceous	? E. Cretaceous	23.7±13.7	7.2±9.5
Cerro Valiente*	Palaeocene	Oligocene or younger	-64.4±31.4	11.2±16.5
<i>Above Agua Amarga Thrust</i>				
Sierra Fraga	? M. Jurassic	? Oligocene or younger	-59.8±52.1	14.4±22.0

Table 6.13. Amount of rotation and flattening indicated by comparison of formation mean directions with stable reference directions. Rotation and flattening and associated errors calculated as described in section 2.7.1. In the rotation column, a negative value indicates anticlockwise and a positive clockwise rotation. In the flattening column, a negative value indicates northward and a positive southward latitudinal transport. * indicates that result is statistically significant and well constrained.

Chapter 7

MODELS FOR ROTATION IN THE ATACAMA AND DOMEYKO FAULT SYSTEMS

7.1 Introduction

As discussed previously, no consensus has been reached as to the mechanism responsible for the rotations observed in the Andean margin of South America (see Chapter 4). The palaeomagnetic data for studies carried out in Cenozoic and Mesozoic rocks in the margin between $\sim 5^{\circ}\text{S}$ and 35°S latitude are given in Table 7.1. To calculate the rotations the mean directions have been compared against the reference directions in Chapter 3. Although rotations have been recognised from palaeomagnetic studies outside this latitude range, they are not thought to be related to the tectonic processes operating around the Arica Deflection. For example, rotations further north are usually attributed to development of the Huancamba Deflection (e.g., Laj *et al.* 1989), and those from further south are thought to be localised and the result of motion on the Liquiñe-Ofqui fault zone (e.g., Cembrano *et al.*, 1992).

The distribution and pattern of rotations are shown in Figure 7.1 and listed in Table 7.1. In this chapter the applicability of both the large-scale rigid rotation, and large and small-scale *in situ* rotation models are discussed with reference to the palaeomagnetic data. Particular attention is given to the applicability of the models to the new data presented in this study. The possible relationship between palaeomagnetically identified rotations, and the Arica Deflection is discussed. Finally, new models are presented to explain the rotations observed in the two study areas covered during the course of this work.

Locality	Lat.	Long.	Age (Ma)	Ref.	Dec. (°)	Inc. (°)	α_{95} (°)	Rotation (°)	Reference
Cenozoic data									
<i>North of Arica Deflection (<17°S)</i>									
Cajamarca	6-7	79	E. Oligocene	ECn	333.4	-20.6	5.7	-15.6±13.6	Mitouard <i>et al.</i> (1990)
Volcanics	11-15	76-77	Eocene-Miocene	ECn	341.4	-27.3	4.7	-7.6±13.4	Macedo-Sanchez <i>et al.</i> (1992a)
Volcanics	11-13	76-78	Eocene	ECn	343.5	-29.0	8.6	-5.5±14.9	Macedo-Sanchez <i>et al.</i> (1992b)
Ocros	13.0	74.0	8.5	PD	345.8	-31.8	5.3	-14.2±5.0	Heki <i>et al.</i> (1983; 1985)
Sediments and volcanics	14.7	76.1	Miocene-Pliocene	PD	354.6	-22.9	6.7	-5.4±5.8	Tsunakawa <i>et al.</i> (1987)
Laguna Umayo	15.8	70.1	~60	ECn	139.2	24	10.4	-40.8±9.1	Butler <i>et al.</i> (1995)
Pto. Japones-Chama	16-17	68.5	Oligo-Miocene	PD	346.0	-34.0	10.0	-14.0±9.7	Roperch <i>et al.</i> (1993)
<i>Within hinge zone (17°-19°S)</i>									
Salla	17.0	67.0	28-24	ECn	353.4	-37.4	5.4	4.4±13.8	MacFadden <i>et al.</i> (1990)
Micaña	17.5	67.0	7.5-6.5	PD	355.2	-25.8	5.9	-4.8±5.2	MacFadden <i>et al.</i> (1990)
Tiupampa	18.0	65.5	60-58	ECn	167.2	38.1	7.9	-1.8±15.0	Butler <i>et al.</i> (1995)
Sucusuma	18.1	65.8	61-59	ECn	144.6	47.3	4.7	-24.4±13.8	Butler <i>et al.</i> (1995)
<i>South of Arica Deflection (>19°S)</i>									
Inchasi	19.7	65.3	4	PD	355.1	-30.1	8.5	-4.9±4.3	MacFadden <i>et al.</i> (1993)
Quehua	20.0	67.0	13-7	PD	15.3	-37.9	9.3	15.3±9.5	MacFadden <i>et al.</i> (1995)
Cerdas	21.0	66.0	16.5-15.5	PD	10.1	-39.1	7.0	10.1±7.2	MacFadden <i>et al.</i> (1995)
Lipez	22.0	65.0	20	PD	39.0	-38.0	11.0	39.0±11.2	Roperch <i>et al.</i> (1993)
Quebrada Honda	22.0	65.0	13-12	PD	17.8	-40.7	3.9	17.8±4.1	MacFadden <i>et al.</i> (1990)
Lipiyoc	22.5	67.0	9	PD	357.6	-34.3	7.9	-2.4±7.7	Somoza <i>et al.</i> (1996)
Paciencia group	22.6	68.3	~28	ECn	20.0	-27.0	13.5	31.0±17.5	Hartley <i>et al.</i> (1992a)
Cifuncho Fm.	25.6	70.6	? E. Cenozoic	ECn	40.3	-53.8	15.1	51.3±24.5	Forsythe <i>et al.</i> (1987)
Quebrada Vicuña Fm.	26.3	69.4	? Oligo-Miocene	PD	356.5	-45.0	6.5	-3.5±7.4	This study
Cerro Valiente Fm.	26.4	69.3	? Oligo-Miocene	PD	19.9	-40.6	24.0	19.9±25.9	This study
Quebrada Vicuña Fm.	26.8	69.4	? Oligo-Miocene	PD	347.5	-44.9	19.3	-12.5±22.3	This study
Cerro Valiente Fm.	26.9	69.5	? Oligo-Miocene	PD	295.6	-56.2	20.6	-64.4±31.4	This study

Table 7.1

Continued...

Locality	Lat.	Long.	Age (Ma)	Ref.	Dec. (°)	Inc. (°)	α_{95} (°)	Rotation (°)	Reference
Cordillera de Domeyko	27.5	70.1	? Cenozoic	ECn	26.1	-59.7	13.0	37.1±24.7	Riley <i>et al.</i> (1993)
Elquinos Fm.	29.5	70.5	? E. Cenozoic	ECn	356.0	-41.5	12.1	7.0±18.1	Palmer <i>et al.</i> (1980b)
Angualasto	30.0	69.5	10	PD	351.9	-48.4	9.7	-8.1±11.8	Ré and Barredo (1993)
Huaco	30.1	68.4	3	PD	8.6	-45.3	6.0	8.6±6.8	Johnson <i>et al.</i> (1986)
Río Azul sediments	30.6	68.9	~12.5-9.2	PD	5.3	-41.9	5.4	5.3±5.8	Jordan <i>et al.</i> (1990)
Mesozoic data									
<i>North of Arica Deflection (<17°S)</i>									
Yumagual Fm.	5.9	78.2	Cenomanian	mC	339.4	-32.5	5.1	-19.6±6.8	Kono <i>et al.</i> (1985)
Pariatambo Fm.	7.1	78.3	Albian	mC	307.5	-21.1	5.4	-53.5±6.7	Kono <i>et al.</i> (1985)
Chulec Fm.	7.1	78.3	Albian	mC	321.7	-22.7	10.2	-37.3±10.9	Kono <i>et al.</i> (1985)
Puente Piedra Fm.	11.9	77.1	~90	mC	343.2	-28.6	3.4	-15.8±5.7	May and Butler (1985)
Sediments/volcanics	12.0	76.9	~112-78	mC	334.9	-28.4	5.3	-24.1±6.8	Macedo-Sanchez <i>et al.</i> (1992b)
Chala	15.8	74.3	~170	MJ	290.5	-31.1	16.0	-71.5±16.4	Roperch and Carlier (1992)
Chala	15.8	74.3	~80	LC	324.9	-25.1	4.4	-31.1±7.5	Roperch and Carlier (1992)
Aréquiapa	16.5	71.8	~100	mC	299.5	-47.0	15.4	-59.5±18.9	Roperch and Carlier (1992)
<i>Within hinge zone (17°-19°S)</i>									
Ilo	17.5	71.4	~80	LC	330.9	-39.9	8.5	-25.1±10.9	Roperch and Carlier (1992)
La Yarada	18.1	70.7	~80	LC	330.6	-38.1	6.0	-25.4±8.8	Roperch and Carlier (1992)
Camaraca Fm.	18.5	70.3	M. Jurassic	MJ	352.1	-37.6	2.8	-9.9±7.2	Kono <i>et al.</i> (1985)
Camaraca Fm.	18.6	70.3	~157	MJ	339.4	-37.1	5.9	-22.6±8.8	Palmer <i>et al.</i> (1980a)
Arica Dykes	18.6	70.3	E. Cretaceous	EC	345.1	-25.6	4.1	-10.9±4.8	Heki <i>et al.</i> (1985)
Atajaña Dyke swarm	18.8	70.3	Cretaceous	mC	345.1	-25.6	4.1	-13.9±6.0	Kono <i>et al.</i> (1985)
<i>South of Arica Deflection (>19°S)</i>									
Camaraca/Cuya Dykes	19.2	70.3	M. Jur.-E. Cret.	MJ ¹	351.3	-39.8	6.7	-10.7±9.6	Scanlan and Turner (1992)
Cuya Dyke swarm	19.2	70.2	M. Jurassic	MJ	345.9	-21.1	7.8	-16.1±9.4	Kono <i>et al.</i> (1985)
La Palca	19.5	65.9	71-60	LC	212.9	42.1	4.4	36.9±7.9	Butler <i>et al.</i> (1995)

Table 7.1

Continued...

Locality	Lat.	Long.	Age (Ma)	Ref.	Dec. (°)	Inc. (°)	α_{95} (°)	Rotation (°)	Reference
Purilactis Fm.	22.8	68.4	L. Cret.-E. Cen.	LC	41.0	-36.0	8.9	45.0±10.9	Hartley <i>et al.</i> (1992a)
Coloso Fm.	23.0	71.0	E. Cretaceous	EC	26.2	-34.3	7.9	30.2±8.3	Turner <i>et al.</i> (1984)
Coloso and El Way Fm.	24.0	70.4	E. Cretaceous	EC	9.1	-25.3	6.4	13.1±6.5	Tanaka <i>et al.</i> (1988)
Coastal Cordillera	24.0	70.0	M. Jur.-E. Cret.	MJ	27.3	-29.2	7.7	25.3±9.6	Hartley <i>et al.</i> (1988)
Cordillera de Domeyko	24.5	69.0	Triassic	Tr ²	-	-	-	0.0±5.7	Jesinkey <i>et al.</i> (1987)
Coastal Cordillera	24.5	70.5	Jur.-Cret.	LC	27.8	-33.8	10.8	31.8±12.2	Forsythe and Chisholm (1994)
La Negra Fm.	25.8	70.4	M. Jurassic	MJ	42.0	-35.5	9.6	40.0±11.5	This study
Vetado Pluton Dykes	26.3	70.3	M. Jurassic	MJ	48.9	-49.6	12.1	46.9±16.5	This study
Flamenco Pluton Dykes	26.4	70.4	? 155	MJ	45.6	-43.0	8.8	43.6±11.7	This study
Animas Pluton Dykes	26.3	70.2	154	MJ	44.0	-48.6	11.2	42.0±15.2	This study
Las Tazas Pluton Dykes	26.5	70.2	129	mC	38.7	-41.5	12.0	39.7±13.8	This study
Quebrada Monardes Fm.	26.5	69.4	E. Cretaceous	EC	328.4	-37.2	13.6	-27.6±14.1	This study
Remolino Pluton Dykes	26.7	70.1	< 126	mC	37.2	-39.3	11.6	38.2±13.0	This study
Quebrada Monardes Fm.	26.8	69.4	E. Cretaceous	EC	19.7	-46.2	11.5	23.7±13.7	This study
Cordillera de Domeyko	27.6	69.5	E. Cretaceous	EC	23.7	-40.9	20.5	27.7±22.3	Riley <i>et al.</i> (1993)
Volcanics	29.5	70.5	E.-m. Cretaceous	mC	9.4	-53.0	4.5	10.4±7.7	Palmer <i>et al.</i> (1980b)
Coastal Cordillera	33.0	71.5	Jurassic	MJ	2.0	-49.2	11.9	0.0±16.1	Irwin <i>et al.</i> (1987)
Coastal Cordillera	33.0	71.5	E. Cretaceous	EC	11.4	-54.3	9.5	15.4±13.5	Irwin <i>et al.</i> (1987)
Central Valley	34.0	70.7	L. Cretaceous	LC	16.8	-50.2	6.0	20.8±9.9	Beck <i>et al.</i> (1986)

Table 7.1. Mesozoic and Tertiary palaeomagnetic data from around the Arica Deflection. Lat. and Long. are latitude (°S) and longitude (°E) of palaeomagnetic sampling sites; age is as quoted from original source, a question mark denotes uncertainty, usually with age of an over-print; Ref. denotes which age reference direction (from Chapter 3) is used for comparison, EJ, MJ, LJ are Early, Middle and Late Jurassic, EC, mC, LC are Early, mid and Late Cretaceous, ECn is Early Cenozoic, PD is present day; Dec., Inc. and α_{95} are declination, inclination and 95% cone of confidence for mean direction; rotation and associated error is calculated as described in Section 2.7.1. Notes: ¹ due to age range the Late Jurassic reference direction may be most appropriate, but the Middle Jurassic reference is used due to uncertainty about the accuracy of the Late Jurassic reference; ² as no Triassic reference direction is calculated in this thesis, the original quoted rotation is given.

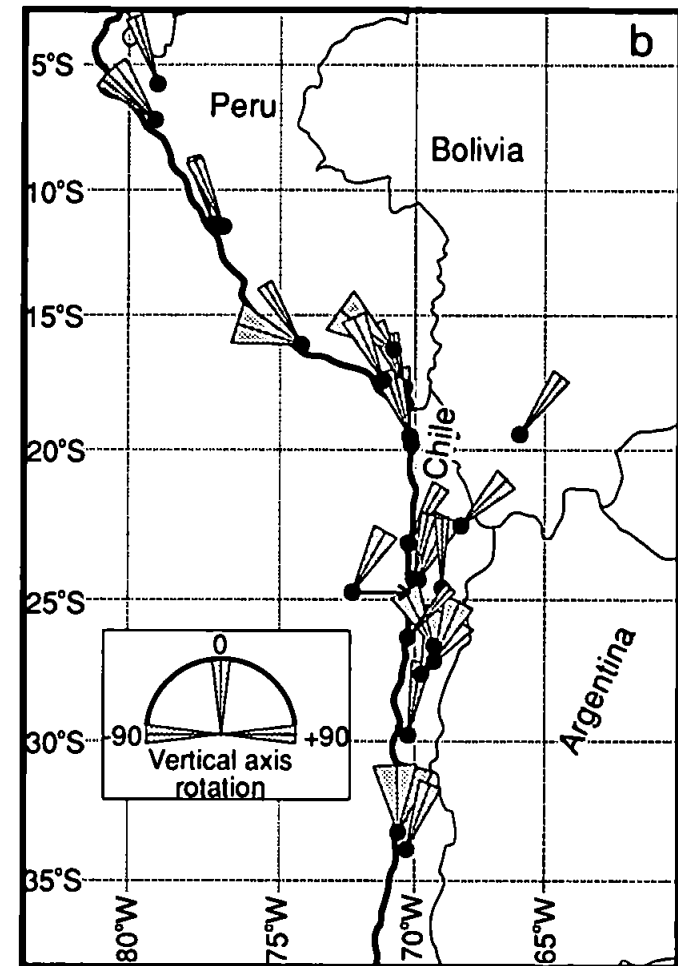
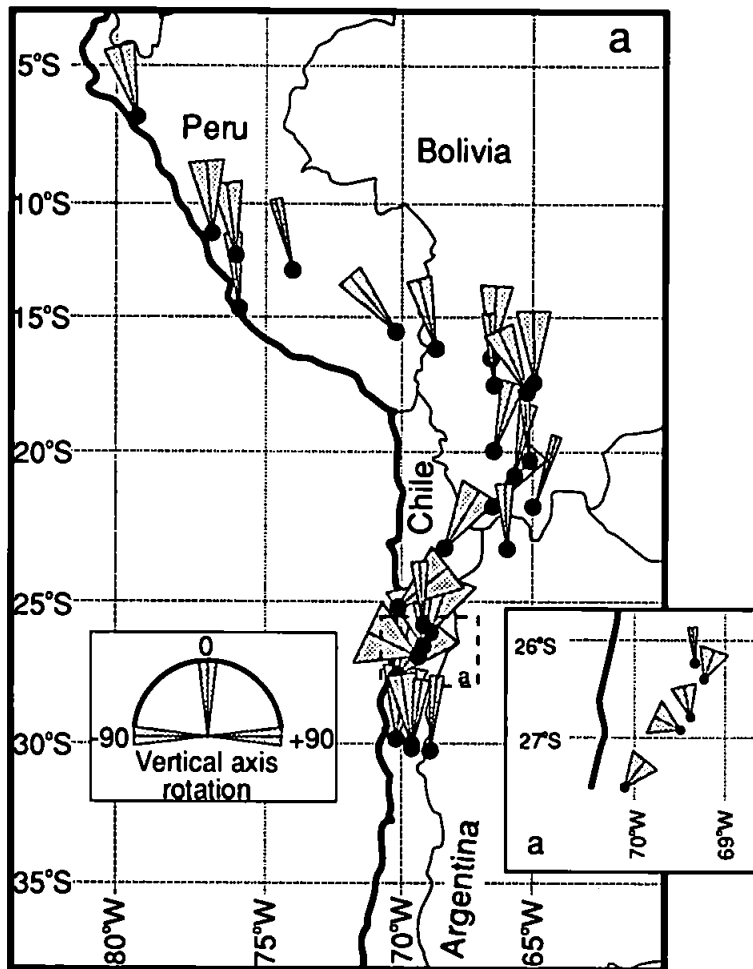


Figure 7.1. Maps showing rotations recorded around the Arica Deflection by previous workers and in this study. Data taken from Table 7.1. a) Cenozoic data. b) Mesozoic data. Errors α_{95} cone of confidence. On the Mesozoic map, directions from the Coastal Cordillera are plotted as one direction to reduce cluttering. This direction was calculated by taking a mean of the six formation rotations to give a rotation of $41.6 \pm 5.4^\circ$.

7.2 Rigid bending of the Andean margin

The oroclinal bending model of Carey (1958) considered that the Arica Deflection was the result of complementary and coeval rotation of two rigid limbs around a hinge zone. This rotation would lead to anticlockwise rotation in Peru and clockwise rotation in Chile, near to the hinge zone, approximately 17-19°S, there should be no rotation. As the limbs rotate in a single rigid motion, the amount of rotation should be consistent along the length of the limb. The change in geological strike and shoreline near to Arica is ~50-60° (Beck, 1988), this should also be reflected by the difference in palaeomagnetic rotations between the two limbs. This model has subsequently been supported by palaeomagnetic studies interpreted as showing opposite senses of rotation of approximately the correct magnitude on either side of the Arica Deflection (e.g., Palmer *et al.*, 1980a; Heki *et al.*, 1983; Kono *et al.*, 1985). Roperch and Carlier (1992) and Beck *et al.* (1994) also note that the general pattern of rotations around the Arica Deflection is broadly consistent with oroclinal bending, as shown by both the Cenozoic and Mesozoic directions of Table 7.1 and Figure 7.1

The data do not however, record a simple change in rotation either side of the hinge. Firstly, the amount of rotation is inconsistent within the limbs and some studies which are distant from the hinge zone indicate that no rotation has occurred (Irwin *et al.*, 1987; Jesinkey *et al.*, 1987), this is inconsistent with a rigid body rotation. Secondly, the Mesozoic data indicate that the change in sense of rotation does not coincide with the change in orientation of the coastline, but lies between 19.5°S and 22.5°S where there are no available data (Figure 7.2). Isacks (1988) notes however that the hinge in the Andean mountain chain and the forearc does not coincide exactly with the change in coastline orientation. When the studies from south of the coastal deflection are compared with the

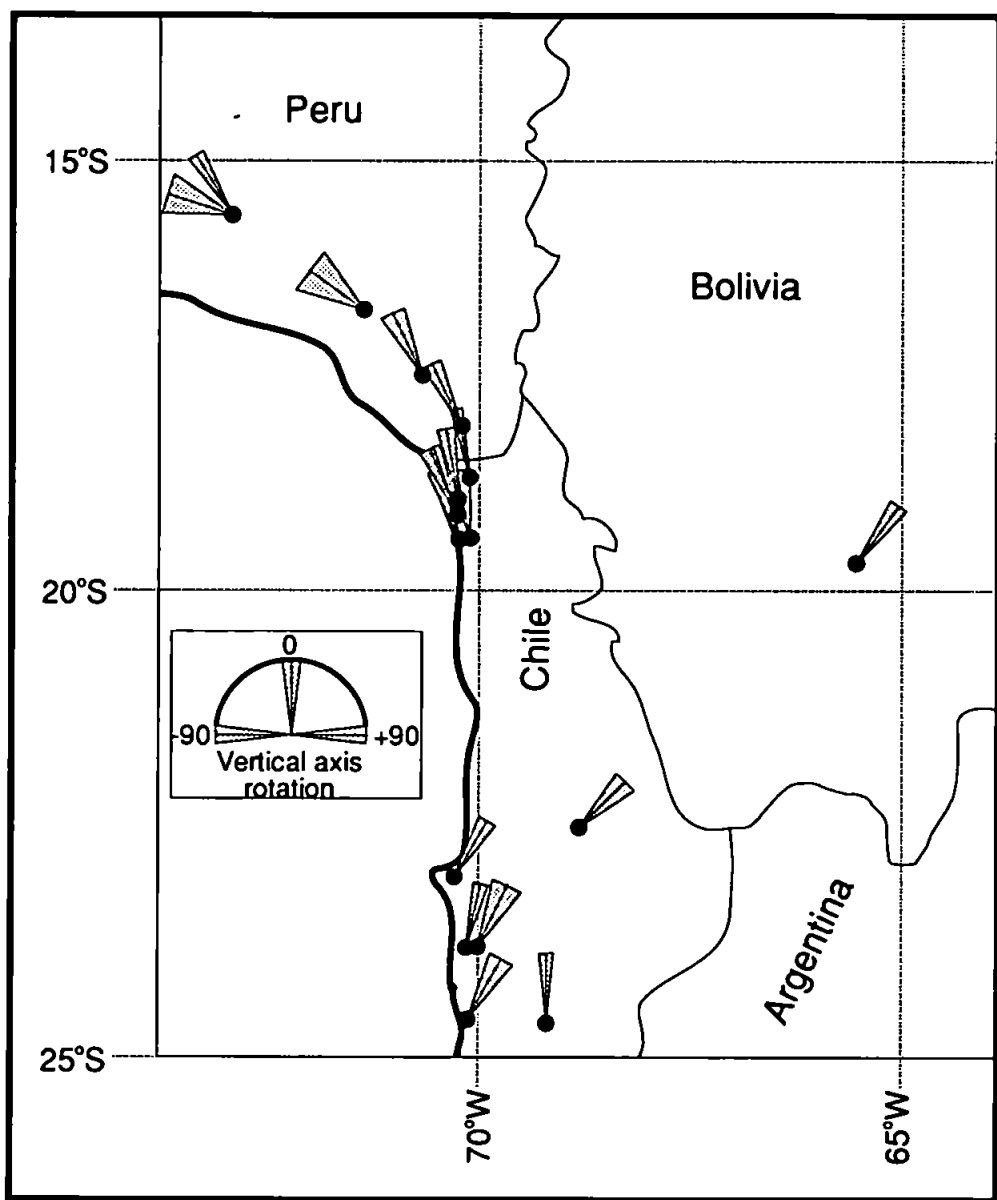


Figure 7.2. Large scale map of Mesozoic directions from around the Arica Deflection. Data are taken from Table 7.1. Errors are α_{95} cones of confidence.

hinge in the mountain chain they lie in the northern limb and would be expected to show anticlockwise rotation, consistent with the model. Thirdly, at the same latitude as the anticlockwise rotations in the Camaraca Formation and Cuya Dykes (Palmer *et al.*, 1980a; Kono *et al.*, 1985; Scanlan and Turner, 1992), the La Palca direction of Butler *et al.* (1995) shows a significant clockwise rotation. This indicates the possibility a spatial east-west change in the rotations which cannot be accommodated by a rigid rotation model. Finally, although the average amount of rotation within each limb is difficult to quantify due to the variation observed, several studies indicate rotation which exceeds the 60° maximum deflection suggested by the change in geological strike.

The rotations identified during this study are inconsistent with the oroclinal bending model. The amounts of rotation identified in the Coastal Cordillera and the pre-Cordillera are different and anticlockwise rotation has been recorded by the Quebrada Monardes Formation in the central region of the pre-Cordillera. Although Carey (1958) did not specify the amount of rotation in each limb, the amount of rotation identified in the Coastal Cordillera (~42°) is probably more than would be expected on one limb.

Although similar in concept, the differential shortening model (Isacks, 1988) is better constrained than the oroclinal bending model in that both the amount of rotation expected in the limbs, and the timing of their rotation is identified. Isacks (1988) suggests that an original bend in the Andean mountain chain was enhanced by differential shortening during the Miocene (23-5 Ma). The amount of rotation accommodated in the model is up to 10° on the southern limb and 15-22° on the northern limb (Figure 7.3). Other workers have suggested that differential shortening could account for more rotation, but do not detail the reasons or mechanisms for this (e.g., Watts *et al.*, 1995). As with the oroclinal bending model, the amount of rotation should be consistent along the length of both limbs. Isacks (1988) selected palaeomagnetic data from along the Andean margin

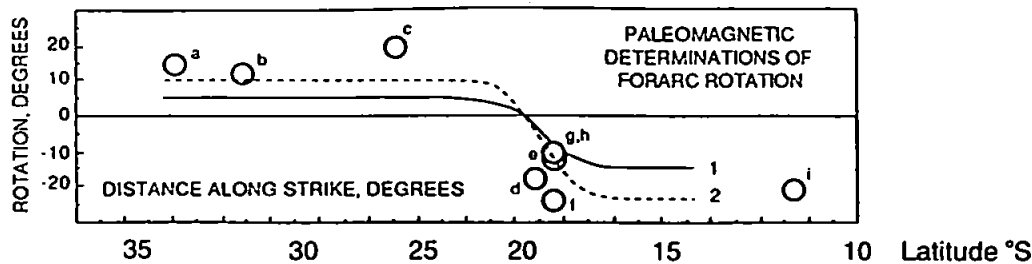


Figure 7.3. Maximum rotation predicted by differential shortening models. Solid and dashed lines show the two possible models suggested by Isacks (1988). The solid line represents Isacks' preferred model. Note that the latitude scale is not linear. This is because Isacks constructed the models with reference to a line drawn normal to the inferred maximum compressive stress direction rather than latitude. Circles show the location with respect to latitude and the amount of rotation recorded by the palaeomagnetic studies selected by Isacks to support the model. a, Palmer *et al.* (1980b); b, d, g, Kono *et al.* (1985); c, Turner *et al.* (1984); e, h, Heki *et al.* (1985); f, Heki *et al.* (1983) and Palmer *et al.* (1980a); i, May and Butler (1985). Modified from Isacks (1988), figure 6.

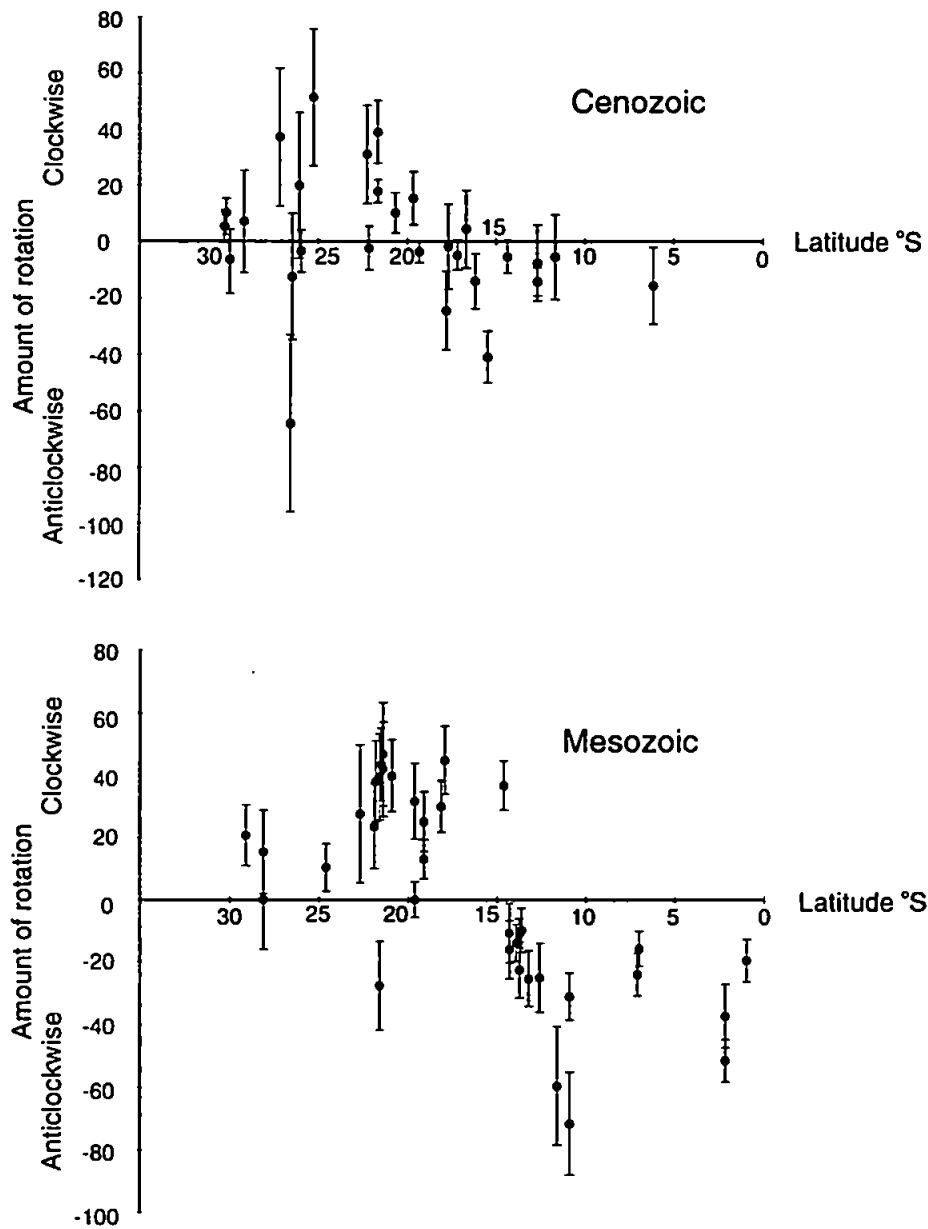


Figure 7.4. Rotation versus latitude plots for the data in Table 7.1.

to support the model (Figure 7.3) and some recent reviews of the Cenozoic database have also been interpreted as supporting both the mechanism and timing of the rotation (Butler *et al.*, 1995; MacFadden *et al.*, 1995).

Many of the problems with the oroclinal bending model also apply to the differential shortening model, particularly that the amount of rotation is inconsistent within the limbs and there are unrotated areas. An additional problem is that rotations much larger than those predicted by the model have been identified (Figure 7.4), this is particularly the case in the Chilean margin. This observation led Beck *et al.* (1994) and Butler *et al.* (1995) to suggest that rocks older than the Neogene may have undergone an additional component of *in situ* rotation as a result of another independent tectonic process.

Based on a review of the available Neogene directions, Somoza *et al.* (1996) suggest that if rigid body rotation operated as a mechanism, this process must have been completed prior to the middle Miocene as the younger poles from Peru are unrotated. However, rotations which also show a pattern of anticlockwise rotations north of and clockwise rotations south of Arica, have been interpreted from post-middle Miocene rocks in Chile, Bolivia and Argentina. The differential shortening model cannot therefore explain these rotations. This led Somoza *et al.* (1996) to conclude that rigid body rotation models do not explain the spatial and temporal variations in the rotations observed in the Andean margin.

The data from this study are inconsistent with the rotation predicted by the differential shortening model of Isacks (1988). All of the units in the Coastal Cordillera, and the Quebrada Monardes Formation in the pre-Cordillera display rotation in excess of the 10° maximum for the southern limb. Additionally, the anticlockwise rotation identified in this study from the Quebrada Monardes Formation cannot be explained by the model.

The data indicate therefore that rigid rotation is unlikely to be the major component to the rotation.

In conclusion, the magnitude and variability of the rotations recorded both in this study and in the Andean margin as a whole indicate that rigid body rotation cannot be a single process responsible for all rotations observed in the Andean margin. It is more likely that either all of the rotations are due to another mechanism, or that rotations, particularly those in the Chilean margin, are compound and the result of a small amount of rigid rotation operating after a more significant primary rotation mechanism. As there is no well dated unrotated unit in the studied areas a component of rigid body rotation cannot be excluded completely.

7.3 Large-scale *in situ* rotation models

The models of Hartley *et al.* (1988) and Beck *et al.* (1993) interpret the rotation of palaeomagnetic vectors as being due to *in situ* rotation as a consequence of large-scale tectonic processes operating in response to E-W extension of the forearc. In both of these models the Arica Deflection is presumed to be a primary feature pre-dating rotation.

In the model of Hartley *et al.* (1988) transtensional stress in the forearc resulting from retreating subduction generate rotation through subduction roll-back. The rotation is accommodated in rigid blocks, the size of which is confined by the trench and a crustal-scale, trench-linked, strike-slip fault (Figure 7.5). In the model, the block-bounding faults are sinistral and drive clockwise rotation as the forearc extends. Hartley *et al.* (1988) envisage the rotation as occurring in response to a phase of slow oblique convergence during the Late Cretaceous-early Tertiary. Hartley *et al.* (1988) acknowledge that rotation of this type would be localised and may only be applicable to small areas of the forearc.

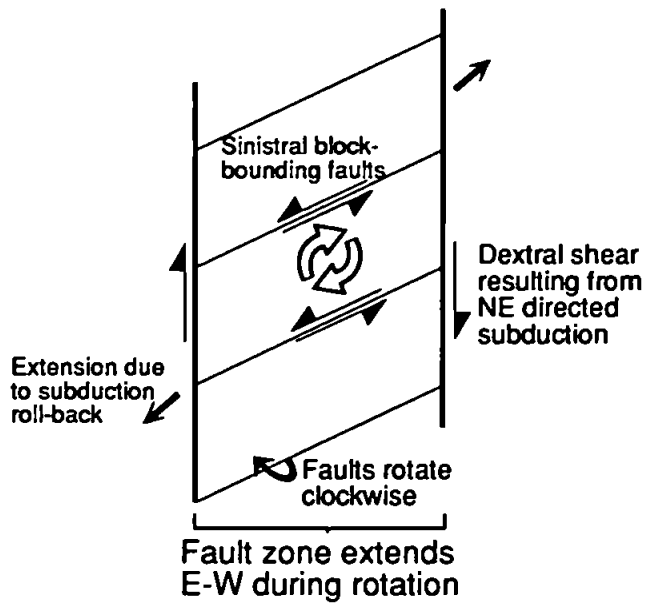


Figure 7.5. The transtensional rotation model of Hartley *et al.* (1988). Clockwise rotation on sinistral block-bounding faults in a dextral shear zone generates extension of the forearc.

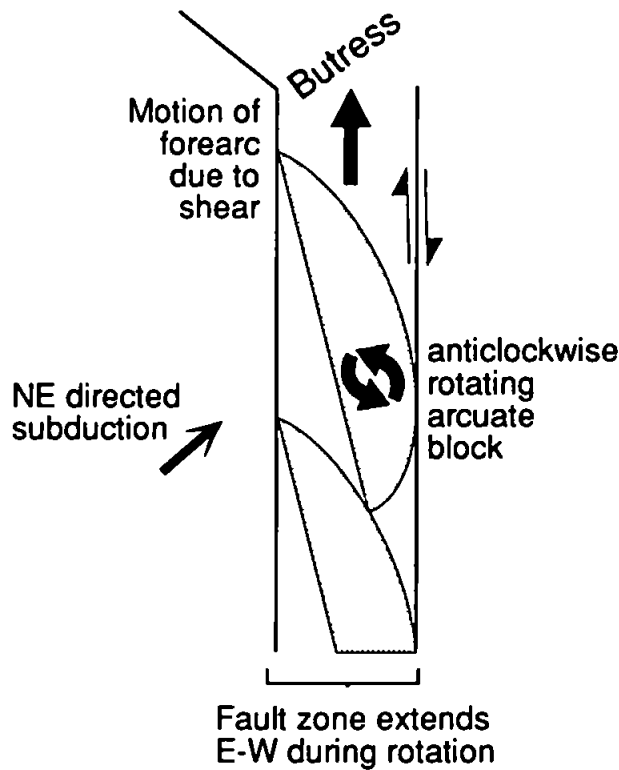


Figure 7.6. Proposed rotation of arcuate blocks in the model of Beck *et al.* (1993). The fault zone extends E-W due to dextral shear and anticlockwise rotation.

They note several problems with applying the model to the data set from the Andean margin. Firstly, the model cannot explain rotations identified inland from the forearc and secondly, the model has difficulty explaining the extent of rotation within the forearc. The third problem is that the model cannot resolve the anticlockwise rotations identified in the Peruvian margin.

In the current study area, the major structural feature in the Coastal Cordillera is the AFS which comprises a set of NW-SE directed sinistral faults block-bounding faults within a sinistral strike-slip fault system. This geometry is therefore incompatible with the transtensional model of Hartley *et al.* (1988). Additionally, SE directed subduction would have been required to generate sinistral shear and clockwise rotation, this is incompatible with the known plate configuration from the Late Cretaceous-early Tertiary. Also, the La Negra arc in the Coastal Cordillera was abandoned in the middle Cretaceous, and the AFS did not undergo significant strike-slip motion after this time, again this appears to be inconsistent with the transtensional model. As stated previously, the model cannot explain rotation inland of the trench-linked strike-slip fault, and cannot therefore explain the rotations in the pre-Cordillera as they lie to the east of the Domeyko fault Zone.

In conclusion, this transtensional model may be useful for explaining localised rotations under certain tectonic conditions within the Coastal Cordillera. The model cannot, however, be applied to explain the rotations identified in this study.

Beck *et al.* (1993) proposed that large blocks could be rotated *in situ* by restricting margin parallel motion of the forearc sliver by buttressing. The buttress can be overcome by extending the forearc normal to the slip direction on the margin parallel strike-slip faults. Beck *et al.* (1993) suggest this process operated in southern Chile and propose that the extension is achieved by rotating large arcuate blocks along a crustal scale strike-slip fault.

In the example given, NE directed subduction generates dextral shear and anticlockwise rotations (Figure 7.6).

The buttressing model is not, however, applicable to the rotations observed in northern Chile. The model relies on the buttressing effect of the Altiplano to generate the rotations and therefore requires NE directed subduction and dextral shear. As in southern Chile this would generate anticlockwise rotations, opposite to the general pattern observed. Additionally, the major strike-slip faults in northern Chile are dominantly sinistral, apparently implying southward directed subduction, this means that buttressing and subsequent forearc extension would not occur. The buttressing model is therefore incompatible with the palaeomagnetic data and geology of northern Chile and cannot explain the rotations observed either in this study, or in the margin as a whole.

7.4 Small-scale *in situ* rotation models

The observed palaeomagnetic rotations may be occurring as a result of blocks rotating *in situ* in response to motion on strike-slip faults in the overriding continental plate. These models are the vertical axis, domino and fault block rotation models discussed in Chapter 4. In these models the Arica Deflection is regarded as being a primary feature of the margin pre-dating the rotation, its origins are not therefore related to the palaeomagnetically identified rotations. The rotation pattern observed may, however, be controlled by the bend due to the different orientation of the margin either side of the bend with respect to the subducting plate (Figure 7.7; see also Beck, 1988). The presence of large-scale fault systems throughout the Andean margin suggests that discrete models of rotation are probably more appropriate than continuum models (see Section 4.3.2). Discrete *in situ* rotation models would not necessarily generate a coherent pattern of

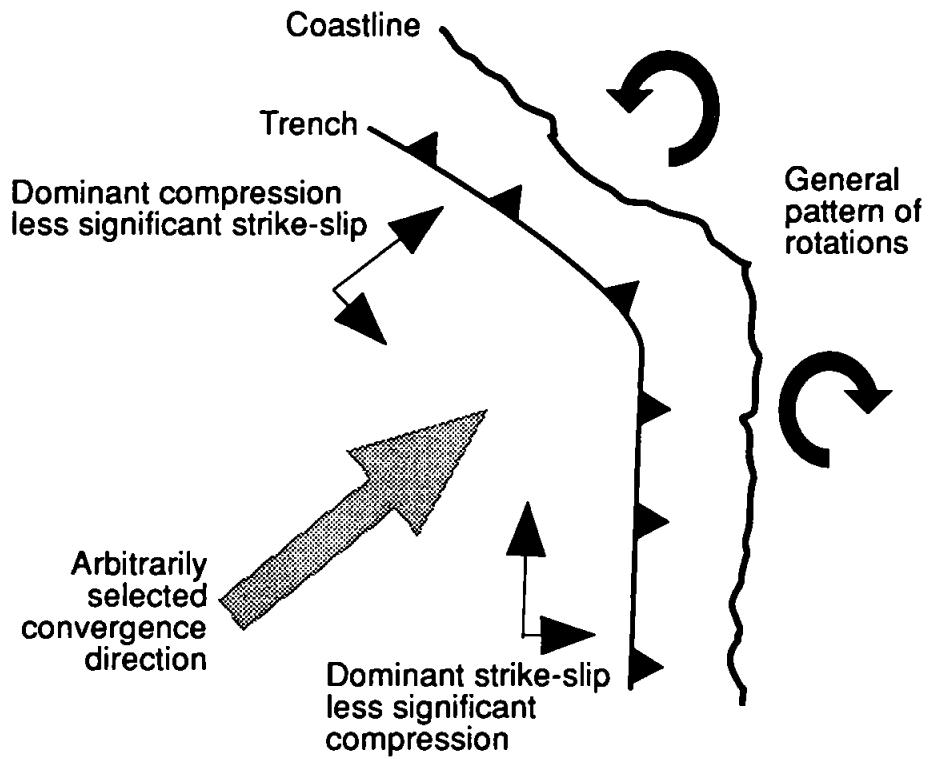


Figure 7.7. The deflection in the Andean margin causes a difference in the dominant stress regime in the margin due to the angle of plate convergence.

rotations in the Andean margin as the rotations occurring within each fault system will be localised.

In the ball-bearing rotation model of Beck (1988) circular blocks rotate due to distributed shear in the Andean margin driven by motion on trench parallel strike-slip faults. In the model as presented, NE directed subduction generates a northward trench-parallel shear component in the Chilean margin, resulting in presumed dextral faults, and a southward directed shear with sinistral strike-slip faults in Peru. Motion on the dextral faults in Chile would cause clockwise rotation and anticlockwise rotation in Peru on the sinistral faults. This means that the change in sense of rotation at the Arica Deflection is due to the pre-existence of the bend and is not a consequence of the formation of the bend itself.

This ball-bearing model fits the general pattern of rotations in the Andean margin, i.e., anticlockwise rotation in Peru and clockwise in Chile, but does have several problems. Firstly the model requires that the change in coastline orientation at Arica is fixed and is responsible for the change in sense of rotation. It cannot therefore account for the anticlockwise rotations found south of Arica. Secondly, the model implies that rotation is accommodated across the margin by progressive development of new strike-slip faults inland of the last. This implies that the amount of rotation between any two margin parallel faults should be consistent.

The data from this study do not support a ball-bearing type model. Although the palaeomagnetic rotations identified in the Coastal Cordillera are clockwise, the dominant fault systems are sinistral. According to Beck (1988), motion on these sinistral faults would generate anticlockwise rotation in the Chilean margin, opposite in sense to that observed. The anticlockwise rotation in the pre-Cordillera is also inconsistent with the model.

The variation in the amounts, and the spatial distribution of rotations observed in Andean margin as a whole do not support this model. Although the model accounts for the general pattern of rotations observed, its requirement for dextral fault systems in Chile is inconsistent with the geological evidence. Overall the model is too simplistic and in reality, the shapes of the blocks and interactions within the fault systems on a continent long scale will define a much more variable set of rotations than can be described by this model.

As stated in Chapter 4, most discrete models take the form of a set of parallel block-bounding faults between two system-bounding faults. Rotation results from motion on the system-bounding faults and is therefore localised and controlled by motion within the individual fault systems. These are termed block rotation models. Rotation occurs in the horizontal plane and the deformation zone extends parallel to the system-bounding faults. The exception to this are the slat models of McKenzie and Jackson (1983; 1986), where the deformation zone does not extend parallel to the system-bounding faults. Instead, there is dip-slip on the block-bounding faults to maintain the surface area. Another mechanism for generating *in situ* small-scale vertical axis rotation is by rotation on thrust sheets. If thrust sheets become pinned, or the amount of slip is variable along the length of the thrust, shortening across the deforming zone can cause differential migration and rotation of the thrust sheet. This mechanism has been reported from northern Chile where palaeomagnetic rotations can be linked to thrust sheets operating in a thin-skinned tectonic setting (Hartley *et al.*, 1992a). Small-scale *in situ* rotation models are specific to the tectonics of the sampling sites and can therefore explain the specific variations in the palaeomagnetic database from the Andean margin as being due to local controls.

Although several authors have suggested that *in situ* block rotation may be the dominant cause of rotations in the Coastal Cordillera of Chile (e.g., Riley *et al.*, 1993; Somoza, 1994, Somoza *et al.*, 1996), only one block rotation model has been published

which makes specific reference to the fault systems present. Forsythe and Chisholm (1994) suggest a model to explain clockwise rotations in the Paposo segment of the AFZ in northern Chile. They propose that clockwise rotation of blocks occurs in response to sinistral strike-slip motion in a NW-SE orientated secondary fault system to the west of the AFZ, which is also undergoing sinistral motion (Figure 7.8). In the model, the AFZ is kept in a fixed orientation and forms a buttress against which the rotation occurs. Although the subsidiary fault system and its relations to the AFZ are poorly defined, Forsythe and Chisholm (1994) support the model by showing that the amount of rotation predicted from the fault displacements is consistent with that observed from the palaeomagnetic study (Figure 7.8).

At first sight this model seems to fit the geology and the palaeomagnetic results obtained in the Coastal Cordillera during this study; sinistral motion on the AFZ with a set of sinistral NW-SE trending subsidiary faults to the west, and clockwise rotation. However, assuming that the AFZ as a buttress against which the subsidiary faults terminate and the rotation occurs is inconsistent with the geological evidence from the study area considered in this thesis as the subsidiary faults are known to cut and displace the AFZ. Additionally, clockwise rotations have been identified to the east of the AFZ (from the Remolino pluton dykes), suggesting that the AFZ cannot be the eastward boundary to the rotation. Forsythe and Chisholm (1994) also sampled units to the east of the AFZ and recorded clockwise rotations, but they ignore this in their model.

7.5 Proposed models for rotation in the Atacama and Domeyko Fault Systems

The rotations observed in the Coastal Cordillera and the pre-Cordillera can be best explained by models of *in situ* rotation. As was discussed in section 7.2, however, the effects of a component of rigid body rotation cannot be ruled out completely. The

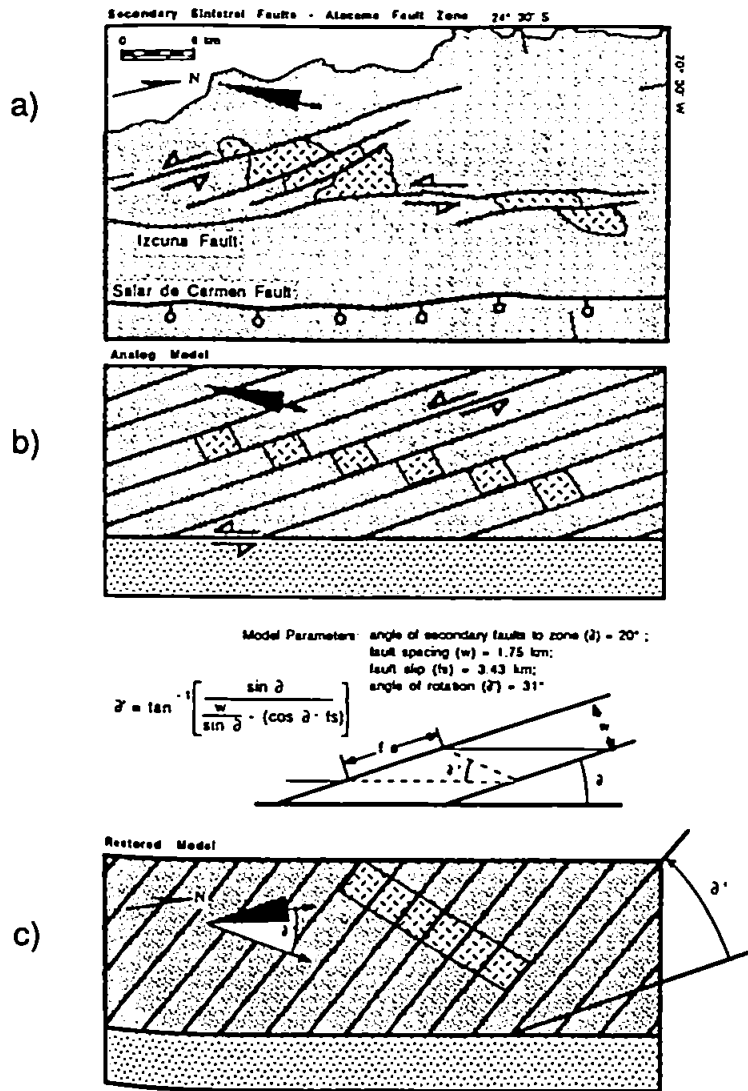
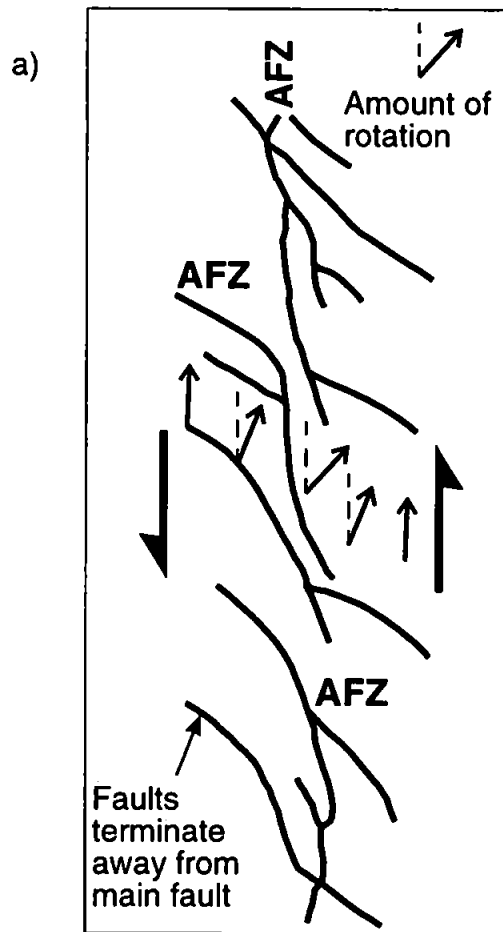


Figure 7.8. The *in situ* rotation model of Forsythe and Chisholm (1994). a) Clockwise rotation results from sinistral motion on NW-SE trending subsidiary faults to the west of the AFZ (Atacama Fault Zone, here termed the Salar de Carmen Fault). b) An analogue model of the rotation using the AFZ as a buttress against which the rotation occurs. c) The restored model using average fault spacing, slip and angle to AFZ along with the rotation angle from the palaeomagnetic study. The black arrows on diagrams a and b show the palaeomagnetic vector, on c, this is restored along with the faults. From Forsythe and Chisholm (1994), Figure 14.

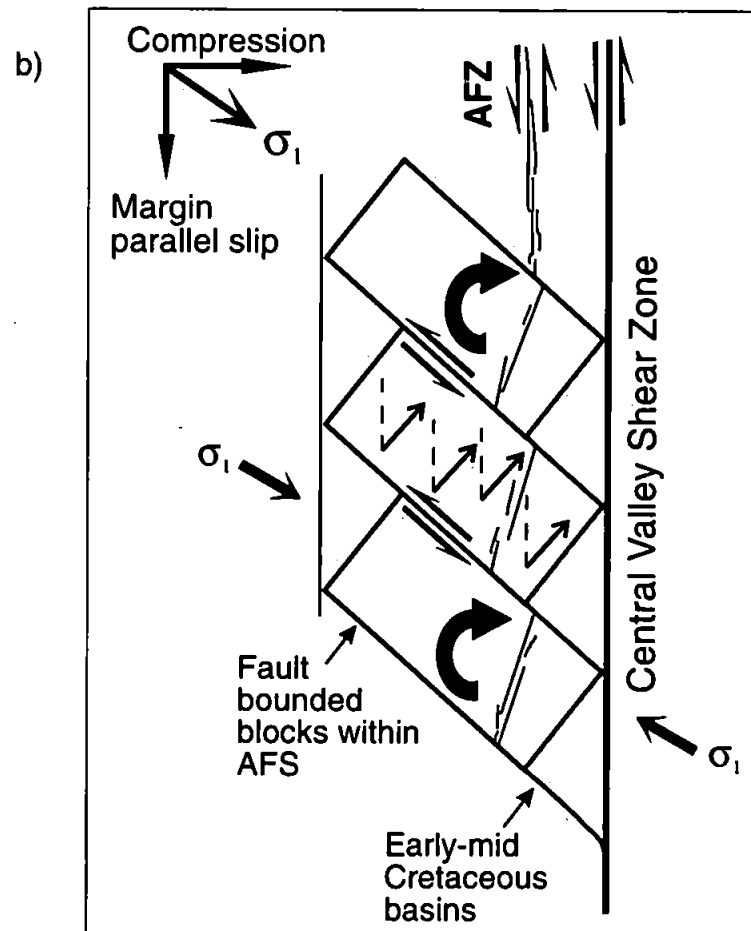
following sections present models for rotation in the Coastal Cordillera as a result of motion on the Atacama Fault System, and in the pre-Cordillera as a result of motion on the Domeyko Fault System. In both models, the rotation is accounted for by *in situ* rotation alone, ignoring any contribution from possible rigid rotation. If any rigid body rotation has affected the sampling regions the magnitude of its contribution cannot be easily quantified.

7.5.1 The Atacama Fault System

As discussed in Chapter 5, all of the sampled units in the Coastal Cordillera show a consistent clockwise rotation of $\sim 42^\circ$. Figure 7.9 shows two possible models to explain clockwise rotation in the Coastal Cordillera as a result of sinistral motion on the AFS. In model A (Figure 7.9a), the AFZ is regarded as being a large-scale fault in which the NW trending sinistral faults are synthetic and the NE trending dextral faults are antithetic. This type of model is known from theoretical and observed examples (Naylor *et al.*, 1986) and could lead to the fracture pattern observed in the Coastal Cordillera. In this model, the displacements on the NW faults, and the magnitude of the rotations increase toward the principal fault. This is opposite to the pattern observed where the displacement on the NW trending faults increases away from the AFZ and the plutons closest to the fault (i.e., the Las Tazas and Remolino plutons) show the least amount of rotation. Additionally, as discussed in section 5.2.2, the AFZ is cut and displaced by some of the NW trending faults, indicating that movement on these faults, at least in part, post-dated the principal phase of motion on the AFZ. Given the timing of motion on the AFZ most of the rotation would have to have been Early Cretaceous in age, almost synchronous with emplacement of the Remolino pluton. It is therefore difficult to resolve rotation of the dykes in the Remolino pluton with motion on the AFZ. This model does not therefore fit the geology, the timing of events, or palaeomagnetic data from the Coastal Cordillera.



Model A



Model B

Figure 7.9. Models of rotation for sites in the Coastal Cordillera. a) Rotation occurs in the AFZ, maximum rotation and displacement occurs with increasing distance from the principal fault. b) Rotation occurs in a crustal-scale shear zone bounded to the east by the Central Valley Shear Zone. The Atacama Fault Zone is displaced and rotated passively in the blocks. The amount of rotation is consistent across the region.

Model B (Figure 7.9b) is mechanically identical to that of Forsythe and Chisholm (1994) discussed above. The difference in this model is that during the major phase of rotation the AFZ is not considered to be the eastern system-bounding fault to the rotating blocks. Instead, it is suggested that the NW trending strike-slip faults, originally initiated by the AFZ, were reactivated and extended, hence they cut and displace the AFZ. The subsidiary faults extended eastwards and soled out into the Central Valley Shear Zone, (CVSZ) and define the AFS. Thus the AFS defines a large, crustal-scale duplex structure which is part of a much broader forearc sliver than was previously defined by the AFZ. The CVSZ formed the eastern system-bounding fault, and the block-bounding faults are the NW trending strike-slip faults. The complementary system-bounding fault to the west is unidentified, but may lie close to the trench, consistent with the rotation being accommodated across the whole of the forearc sliver. The blocks are rotated in the same manner as suggested by Forsythe and Chisholm (1994), where sinistral transpression across the shear zone drives clockwise rotations. As the AFZ is rotated passively, the timing of the rotation in this model is not constrained by the geochronological data from the AFZ, there is unfortunately also no upper age limit for the rotations defined by younger unrotated rocks. The only control on the timing of rotation therefore is that it is certainly younger than 126 Ma, the age of intrusion of the Remolino pluton, and probably post-dates the intrusion of the La Barrocha pluton at 106 Ma. The likely timing of the rotation is in the mid-Late Cretaceous, coincident with the abandonment of the Middle Jurassic to Early Cretaceous magmatic arc and its eastward migration. This change in the magmatic and tectonic configuration of the Andean margin coincided with a major compressional event, the Peruvian or 'Subhercynian' Orogeny (Coira *et al.*, 1982). This orogeny is recognised along the length of the Andean margin and marked the onset of the Andean orogenic cycle. This tectonic period is contemporaneous with increased spreading rates in the South Atlantic at

about 100 Ma (Larson and Pitman, 1972).

Model B fits the geology and palaeomagnetic data from the Coastal Cordillera much better than model A. In particular, model B can account for the clockwise rotations found on both sides of the AFZ, the offsets in the AFZ by NW trending strike-slip faults (up to 70 km, Brown *et al.*, 1993), and the clockwise rotation of offset segments of the AFZ (e.g., at 27°S segments of the AFZ trend at ~050, Arevalo, 1995).

As discussed in section 4.4.3, one of the problems with rotating rigid blocks is the development of triangular spenochasms as the blocks rotate away from the major system-bounding fault, this is demonstrated by the cartoon of the model in Figure 7.9b. It is suggested that in the Coastal Cordillera, the problem of spenochasms may be overcome in several ways. Firstly, the outcrop pattern of Early-mid Cretaceous sedimentary rocks in the east of the Coastal Cordillera suggests that these may be preserved in extensional zones created by the blocks rotating away from the CVSZ (Taylor *et al.*, in prep.). Secondly, the major NW trending faults have a small component of NE side down dip-slip displacement in addition to the sinistral strike-slip motion. This dip-slip displacement may be accommodating some change of block shape during rotation and extension of the shear zone due to E-W shortening. Thirdly, the blocks themselves deform during rotation, this manifests itself as minor folds and thrusts within the blocks and pervasive NW-SE minor faults with small displacements.

This model of block rotation, and the dominance of sinistral strike-slip faults parallel to the margin implies that the bulk shear during the mid-Late Cretaceous was driven by S-SE directed subduction beneath the Andean margin. There is no direct evidence to support this subduction direction, but plate reconstructions suggest that subduction may have been

E to SE at this time (Larson and Pitman, 1972; Duncan and Hargraves, 1984; Pardo-Casas and Molnar, 1987; Thiele and Pincheira, 1987).

In conclusion, the clockwise rotations in the Coastal Cordillera can be explained by a model which invokes sinistral transpression across the AFS, bounded to the east by the CVSZ. The rotation occurs in a domino fashion with the blocks bounded by NW trending sinistral strike-slip faults. It is suggested that this rotation occurred in response to the Peruvian or 'Subhercynian' Orogeny during the mid-Late Cretaceous.

7.5.2 The Domeyko Fault System

Constructing a model for the rotations observed in the pre-Cordillera is complicated by the problems of remagnetisation identified in the lavas and volcanic rocks. For this reason it is not possible to suggest a model for rotations in the fold-and-thrust belt of the northern domain. The only rotations which are considered well constrained and geologically sensible are those from the Quebrada Monardes Sandstone Formation which appear to carry a primary or early remanence. Samples from this unit show a clockwise rotation of $\sim 24^\circ$ in the southern domain, the NW trending strike-slip faults, and an anticlockwise rotation of $\sim 28^\circ$ in the area of overlap between the two domains. A simplified fault map of the DFS, and a possible model to explain the rotation observed in the southern domain, is shown in Figure 7.10.

In this model, the clockwise rotation in the southern domain is due to block rotation as a result of sinistral motion on the NW trending strike-slip faults (Figure 7.10). As the NW trending subsidiary faults do not cut the DFZ, this seems to be a tectonic buttress against which this rotation is occurring, and is therefore the system-bounding fault. There does not appear to be a second complementary system-bounding fault to the deformation zone. The rotation is occurring in response to compression across the DFS and the

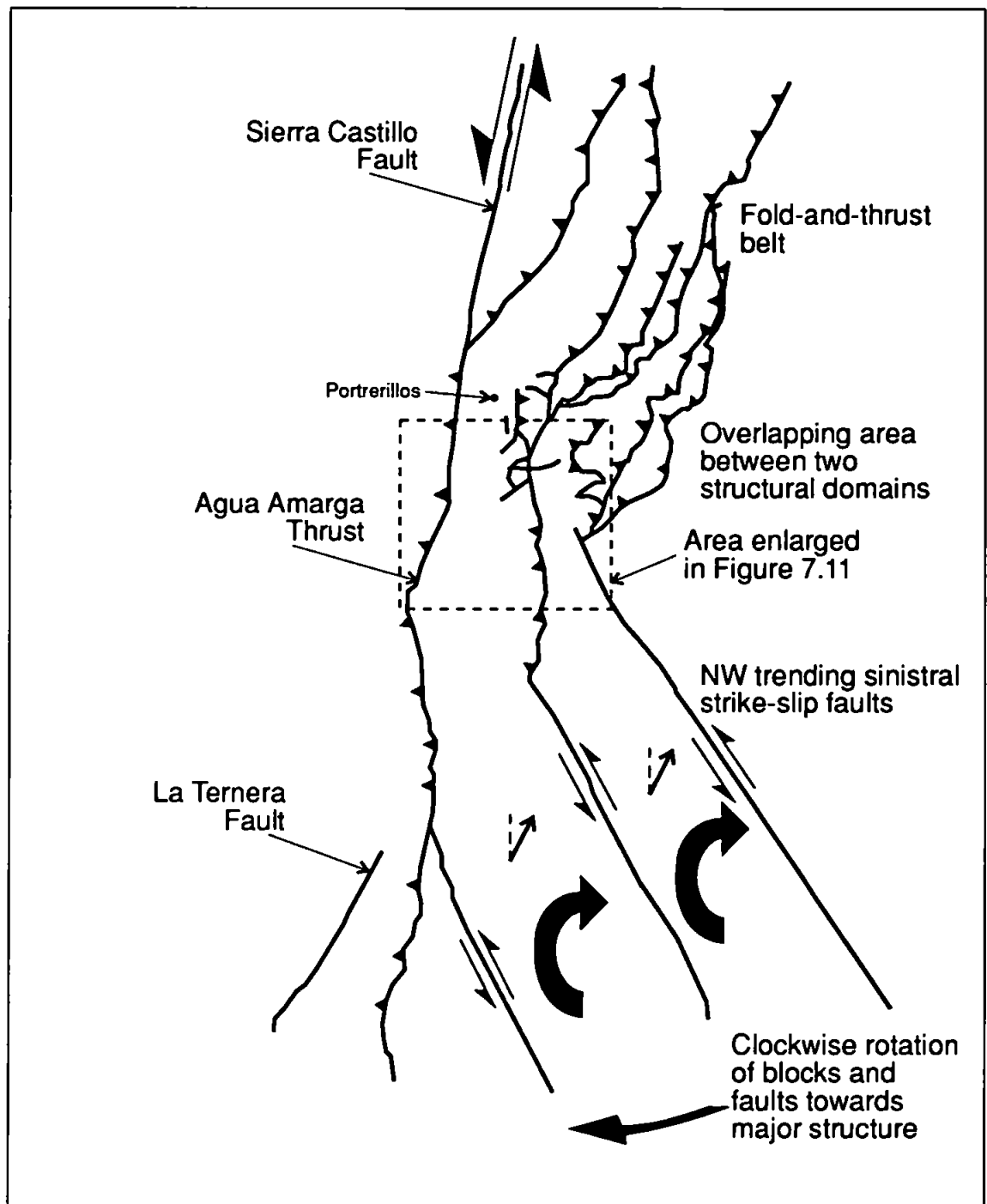


Figure 7.10. Model to explain the clockwise rotations identified in the Quebrada Monardes Formation in the southern domain of NW trending strike-slip faults. The area from the central region between the two domains is enlarged in Figure 7.11. This is the area where anticlockwise rotations were identified from samples of the Quebrada Monardes Formation.

subsidiary faults are rotating clockwise towards the major structure, as would be predicted from Coulomb failure criteria (Anderson, 1951). The rotation can therefore be due to compression alone with no requirement for strike-slip motion on the DFZ, although this is not precluded by the model. This would, however, require the NW trending strike-slip faults to be present prior to the rotation and main compressional phase of deformation. Between the major NW trending faults, folds and smaller strike-slip and reverse faults are observed (Cornejo *et al.*, 1993). These structures may be the result of block deformation during rotation to avoid the development of sphenochasms.

The samples from the Quebrada Monardes Formation which show an anticlockwise rotation are from an area of complicated deformation between the overlapping domains. An enlarged map of the central area and the location of the sampling sites is shown in Figure 7.11. Only the major structures are shown on the map so constructing a specific model for samples collected over a small area is difficult. The map shows a dominance of E-W directed dextral strike-slip faults around the sampling sites as well as several small thrusts. It is possible that the rotation identified in this area is locally controlled by block rotation as a result of motion on these small-scale structures. All of the samples collected from the Quebrada Monardes Formation were from a small ~20 m section. If more samples were taken from across this zone of complex deformation, rotations of different magnitudes and directions may have been found

The timing of the rotation and deformation in the two structural domains east of the DFZ is well constrained as the faults displace dated porphyry deposits. As discussed in Section 6.2.2, the timing of deformation on the DFZ itself is not well constrained as the fault was probably active for a much longer time period. The major phase of deformation both in the fold-and-thrust belt and the domain of NW trending strike-slip faults is dated as mid-Eocene-Oligocene. It is likely that the rotations were contemporaneous with this

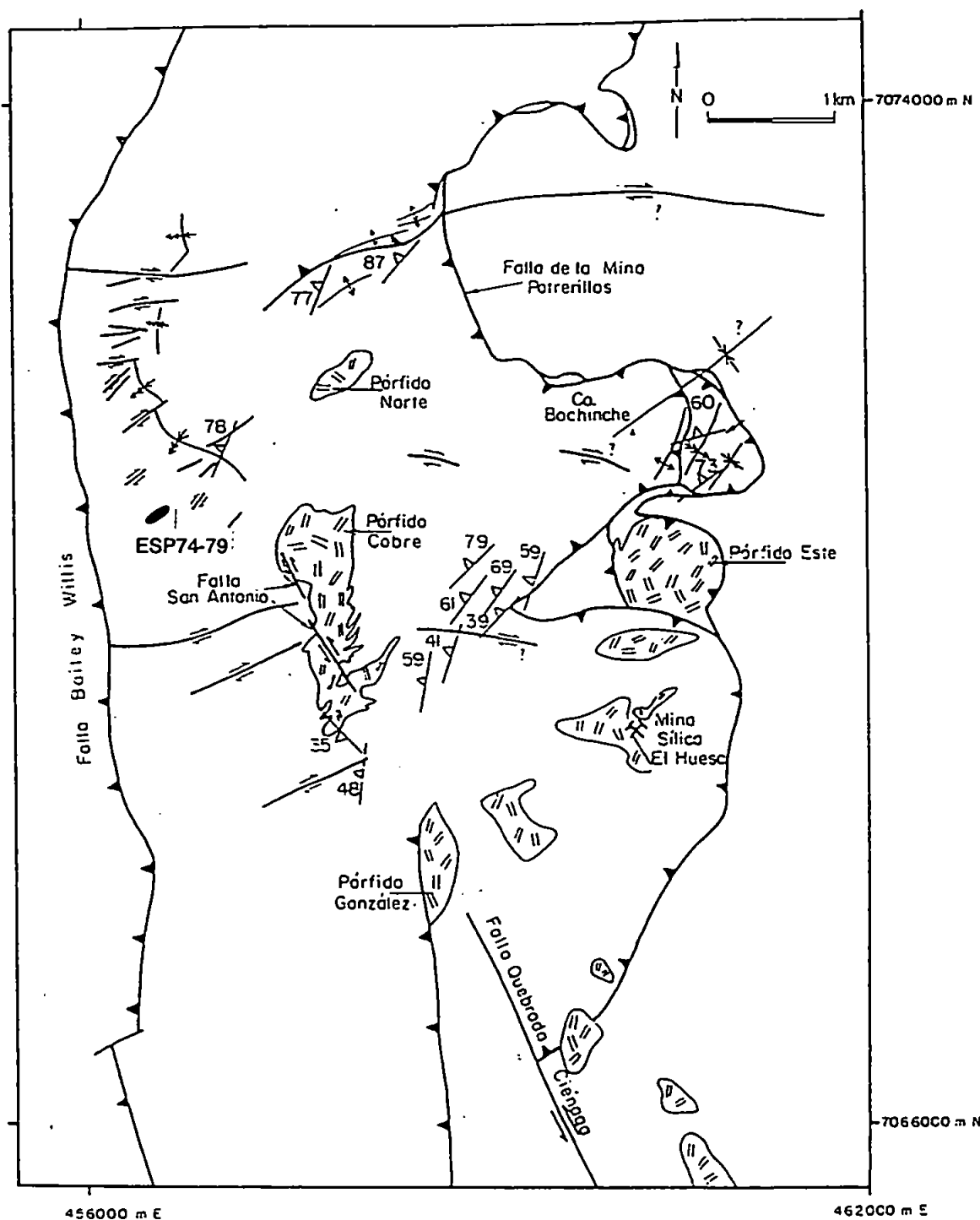


Figure 7.11. Enlargement of central region between the two overlapping structural domains. On this diagram only the major structures are shown. Note the dominance of E-W orientated dextral strike-slip faults around the sampling sites from the Quebrada Monardes Formation. (Taken from Comejo *et al.*, 1993, figure 44).

deformation. The timing of the deformation correlates with the Incaic Orogeny, recognised widely in northern Chile and Peru (Coira *et al.*, 1982). This compressional phase is coincident with a period of rapid convergence between the Nazca and South American plates (Pardo-Casas and Molnar, 1987).

The dominance of sinistral strike-slip motion on the DFZ is inconsistent with the suggested direction of bulk shear during the Tertiary (Pardo-Casas and Molnar, 1987). From the early Eocene, subduction has been directed NE-E which might be expected to produce dextral shear in the Chilean margin. The reason for the DFZ recording the opposite sense of motion is unclear. It is possible that ancient basement structures have, in part, controlled the development of the DFZ, and, to some extent its shear sense. There is however no evidence to support this hypothesis. A second possibility is that most of the sinistral motion on the DFZ could have occurred prior to the compressional phase which caused the rotation. During the Eocene-Oligocene development of the DFS, the DFZ may have not have undergone a substantial amount of strike-slip motion but merely acted as a buttress against which the deformation could be accommodated in the DFS. As the NW trending faults are rotating towards the DFZ as a result of compression across the deformation zone, there is no requirement for strike-slip motion on the major structure.

In conclusion, the rotations observed in the southern strike-slip fault domain can be explained by a model of compression across the DFS with the subsidiary structures rotating towards the major tectonic structure. The anticlockwise rotation in the area between the two domains may be explained in terms of localised tectonic rotation. It is suggested that the rotations are occurring in response to the Incaic Orogeny in the late Miocene-Oligocene.

7.6 Conclusions

The models of rotation previously presented for the Chilean segment of the South American margin have been discussed with respect to the data from the margin as a whole and the data presented in this study. Although the general pattern of rotations in the Andean margin is obvious, the models presented to account for this, namely oroclinal bending and differential shortening, suffer from a number of problems and are therefore regarded with some scepticism. It is believed that the rotations observed in the study areas covered in this work can be best explained in terms of discrete block rotations controlled by major fault systems within the margin. The deformational events causing these rotations correlate with regional compressional phases identified within the Andean margin.

Chapter 8

SUMMARY AND CONCLUSIONS

8.1 Introduction

In this study, samples for palaeomagnetic analysis have been collected from a variety of lithologies within two fault systems, both associated with major strike-slip fault zones in northern Chile. The tectonics of this part of the Andean margin is dominated by the Atacama Fault Zone and the Central Valley Shear Zone in the Coastal Cordillera, and the Domeyko Fault Zone in the pre-Cordillera. Two of these faults, the Atacama and Domeyko Fault Zones are interpreted as having been major trench-linked strike-slip faults during their main deformation phase. Although the Central Valley Shear Zone may also have been a trench-linked strike-slip fault, there is insufficient evidence to be certain of this. The aim of this project was to identify and quantify any vertical axis rotation, to try and relate this to the observed fault pattern and to the tectonics of the Andean margin as a whole. This chapter gives a brief summary of the results and conclusions from this work, and suggests some recommendations for future work in this part of northern Chile.

8.2 The Coastal Cordillera

The Coastal Cordillera formed the Jurassic to middle Cretaceous magmatic arc (the La Negra arc) in this part of northern Chile. The Coastal Cordillera is characterised by a basement of Palaeozoic rocks meta-sedimentary intruded by a suite of Permian to Triassic granitic rocks. The magmatic arc is represented by Late Triassic to middle Cretaceous plutons in the southern part of the study area, and a sequence of Triassic to ? Late

Cretaceous sedimentary and volcanic rocks covering the basement in the north and east. The major tectonic feature in this part of Chile is the Atacama Fault Zone (AFZ), and a set of NW-SE trending strike-slip subsidiary faults. Some clearly cut and displace the AFZ and sole out into the Central Valley Shear Zone (CVSZ) farther to the east. Together the CVSZ and the NW trending subsidiary faults define the Atacama Fault System (AFS). To identify and quantify any rotation associated with the AFS, samples for palaeomagnetic analysis were collected from the volcanic rocks of the La Negra Formation (Early-Late Jurassic) and a series of five dyke swarms which are intruded into a set of west to east younging granitic plutons. The dyke swarms are dated as probably Early-Middle Jurassic through to middle Cretaceous (<126 Ma). The main conclusions from this work can be summarised as:

- Thin section analysis of all of the lithologies sampled show evidence of low temperature hydrothermal alteration. Rock magnetic studies demonstrate that in the majority of samples, the magnetisation is carried by magnetite/titanomagnetite or haematite, or a combination of these.
- Structural analysis of dilation directions indicates that the dykes have undergone no significant post-emplacement tilting.
- Sites collected from the Early-Late Jurassic La Negra Formation pass both fold and reversal tests suggesting that they carry a primary or early remanence.
- Both normally and reversely magnetised sites are present in four of the five dyke swarms. The evidence suggests that all dyke swarms carry a primary or early remanence.
- Palaeomagnetic analysis of all units reveals a consistent clockwise rotation of $\sim 42^\circ$.
- The rotation can be explained by a model of *in situ* block rotation where the CVSZ is the eastern system-bounding fault and the NW trending strike-slip faults are the block-

bounding faults. The rotation occurred in response to sinistral transpression across the fault system.

- The rotation occurred during the mid-Cretaceous and was a result of the Peruvian or Subhercynian Orogeny. Contemporaneously the magmatic arc in the Coastal Cordillera was abandoned and the locus of magmatism migrated eastwards.

8.3 The pre-Cordillera

During the Late Triassic to Early Cretaceous, the pre-Cordillera formed the back-arc basin to the La Negra arc. The geology of the back-arc basin is characterised by sediments and volcanic rocks of Jurassic to Early Cretaceous age lying unconformably on a Palaeozoic igneous basement. During abandonment of the La Negra arc in the mid-Cretaceous the pre-Cordillera underwent a period of uplift and erosion, the area then became the Late Cretaceous-Palaeocene magmatic arc. The major tectonic structures of this part of the pre-Cordillera are the Domeyko Fault Zone (DFZ), comprising the Sierra Castillo Fault, the Agua Amarga Thrust and, possibly, the La Ternera Fault and a set of subsidiary faults to the east. The subsidiary faults define two distinct but slightly overlapping structural domains; a fold-and-thrust belt in the north, and a set of NW-SE trending sinistral strike-slip faults in the south. Together the DFZ and the subsidiary faults define the Domeyko Fault System (DFS). To identify and quantify any rotation associated with motion on the fault system, samples were taken from both structural domains to the east of the DFS, and one set of samples were taken from the west of the DFZ. Samples from the Sierra Fraga Formation (Jurassic) were collected from the west of the AFZ above the Agua Amarga Thrust. East of the DFZ, Early Cretaceous sandstones from the Quebrada Monardes Formation were collected from the southern domain, and the area of

overlap between the two domains. Samples were collected from the volcanic rocks of the Quebrada Vicuña (Jurassic) and Cerro Valiente (Palaeocene) Formation. These volcanic rocks were collected from both structural domains east of the DFZ. The main conclusions from this work are summarised as:

- Thin section analysis showed evidence of low temperature metamorphism/hydrothermal alteration in all of the volcanic units. Rock magnetic studies indicate a variety of magnetic carriers, dominated by a combination of magnetite/titanomagnetite or haematite in all units.
- The directions from sites in the Sierra Fraga Formation are scattered and do not record a coherent and geologically sensible mean direction.
- All sites from the volcanic rocks of the Quebrada Vicuña Formation east of the DFZ fail a fold test and appear to carry a post-folding remanence. The rotations suggested by the data are not statistically significant.
- The sites from the Quebrada Monardes Formation in the southern domain probably record a pre-folding remanence. The direction indicates a clockwise rotation of $\sim 24^\circ$.
- Sites from the Quebrada Monardes Formation in a small central area between the two domains indicate an anticlockwise rotation of $\sim 28^\circ$.
- The sites from the Cerro Valiente Formation appear to have been remagnetised. The small rotation identified in the northern domain is not statistically significant. The data from the southern domain suggest a statistically significant anticlockwise rotation of $\sim 64^\circ$. This rotation is, however, difficult to reconcile with the more statistically constrained clockwise rotation indicated by the Quebrada Monardes Formation.
- The rotation in the southern domain recognised from the Quebrada Monardes Formation can be explained by a model of *in situ* block rotation. In the model, the blocks are

bounded by the NW trending sinistral strike-slip faults and are rotating clockwise in response to compression/sinistral transpression across the deformation zone.

- The anticlockwise rotation recognised from the Quebrada Monardes Formation in the central region can be explained by invoking a model of small-scale localised rotation resulting from motion on thrust sheets or dextral strike-slip faults.
- The deformation and rotation in the pre-Cordillera are the result of the Incaic Orogeny in the late Miocene-Oligocene. This is a synchronous deformation event recognised along the length of the Andean margin.

8.4 The Andean margin

The pattern of palaeomagnetic rotations from around the Arica Deflection has previously been used to support the hypothesis of rigid body rotation. However, as has been demonstrated by this and other previous studies, rotation can also be explained by a number of other mechanisms unrelated to rigid body rotation. It is possible that rotations from studies interpreted as supporting the oroclinal bending theory could also be the result of locally controlled *in situ* rotation, but this may have not been recognised due to limited investigations of the tectonic controls in these sampling areas. If all rotations are the result of small-scale *in situ* rotation, the reason for the change in rotation sense around the Arica Deflection remains uncertain. There are three possible explanations for the change in sense of the rotations. Firstly, differential shortening along the length the margin may cause bending of the forearc and opposite senses of rotation. Secondly, rigid cratonic blocks behind the forearc may act as a buttress or backstop against which the younger more mobile forearc and magmatic arc bend and rotate. The third possibility is that the difference in the

orientation of the margin and deformation zone with respect to the subducting plate due to a primary bend may be a control.

Another problem with using studies in the Andean margin to support any generalised model are the poorly defined and constrained reference directions. Despite improvement and the addition of several new poles over the last few years, many parts of the South American APWP remain poorly defined, of particular note is the Late Jurassic to earliest Cretaceous. As many of the rotations identified from the Andean margin are quite small, variations in the choice of reference direction can make large differences to the interpretation.

8.5 Recommendations for future work

In the Coastal Cordillera, the rotation is fairly well constrained and consistent within the study area. The crucial test for the *in situ* rotation model presented for the Coastal Cordillera is to sample rocks up to and from the other side of the CVSZ. If the CVSZ is the eastern system-bounding fault, and the rotation is occurring in a block rotation type mechanism, there should be constant rotation up to the CVSZ, and a different magnitude of rotation on the other side of it. There are several units between the AFZ and the CVSZ which could be sampled to test the model.

In the DFS, remagnetisations rendered many of the lithologies sampled unsuitable for palaeomagnetic study. To get a comparison of the rotations in both of the structural domains it is ideal to have the same units sampled both in the north and south of the area. There is a small area of Quebrada Monardes Formation in the northern domain, close to Salar de Pedernales. Sampling this unit here may give more information about rotation in the northern domain, but, unfortunately, the only outcrop is on an isolated thrust sheet, so

there may be a problem with local thrust sheet rotation. Another possibility is to sample the Jurassic limestones, namely the Montandón, Asientos and Pedenaes Formations. Although these are likely to be permeable and will have been exposed to the same remagnetisation fluids as the volcanic rocks, it is possible that their remanence may be carried by different minerals which may be more stable.

In terms of studying the Andean margin as a whole, attention needs to be given to constraining the South American APWP. Reassessment of many of the previous studies with better defined reference directions may lead to changes in the pattern and magnitude of rotations. Only then can palaeomagnetic data covering a wide temporal and geographic span be used to constrain the large-scale variations in the tectonic processes operating along the Andean margin.

Appendices

Appendix 1

THIN SECTION DESCRIPTIONS

La Negra Formation

Site Number: AT69

General Description: Brown colour, very fine grained, glass shards present.

Alteration: Intense alteration, rock looks haematized.

Rock Type: Devitrified ignimbrite

Site Number: AT70

General Description: Purple-grey colour. Plag. and orth. phenocrysts (20%), including zoned phenocrysts. Feldspar often have reaction rims. Opaque minerals present, most appear secondary. Some may be primary as they appear to be associated with feld. laths.

Alteration: Feld. altered to sericite. Preferential alteration of high temp. Ca rich plag. fraction in zoned phenocrysts, low temp. Na rich parts are less altered. Range of secondary opq. present, inc. haematite and possible ilmenite.

Rock Type: Basic/andesitic

Site Number: AT74

General Description: Original feld. can still be identified and makes up 20%, also qtz. 10%. Ferromag. minerals present and opq. 5%.

Alteration: Feld. altered to sericite/epidote. Ferromag. minerals altered to chlorite. Lots of epidote present. Rock has been haematized, often seen as a ring on epidote alteration areas.

Rock Type: Basalt/andesite

Site Number: AT76

General Description: Alkali feld phenocrysts 5%, 20% disequilibrium qtz. phenocrysts, some contain remnants of other material now altered to epidote/chlorite. Also present is plag. 10%. Groundmass is de-vitrified glass, therefore pyroclastic rock.

Alteration: Feld. highly altered. Epidote pseudomorphs other minerals in groundmass, no evidence of the original mineral. Evidence of a lot of water/hydrothermal alteration.

Rock Type: Rhyolite (glassy)

Site Number: AT78

General Description: Equigranular feld. and qtz. dominate 70%, pyx.?

Alteration: Calcite is dominant secondary mineral 40%. In places heavily chloritized, also epidote present.

Rock Type: Basalt/andesite

Site Number: AT79

General Description: Equi-granular, very fine grained. Plag. 50%, opq. 30% and altered ferromag. minerals.

Alteration: Highly altered, difficult to identify due to grain size, probably epidote/chlorite.

Rock Type: Basalt/andesite (lava higher temp.?)

Site Number: AT80

General Description: Plag. phenocrysts 60%, +reaction rims. Ortho-Pyx. 20%, opq. 10%.

Alteration: Plag. to sericite. Chloritization of possibly biotite? in groundmass, v. diff. to see. Haematization seen.

Rock Type: Basaltic

Site Number: AT81

General Description: Large plag. phenocrysts, many with reaction rims. Many also broken and cracked, appears to be post-solidification of plag. xtals, but syn- or pre-solidification of groundmass. Intraformational rock fragments present. Flow fabric can be seen in the groundmass. Groundmass is very fine, glassy; plag., opq. (including haematite) and qtz.

Alteration: Feld. are altered, lots of carbonate, possibly calcite present.

Rock Type: Basalt (brecciated)

Site Number: AT82

General Description: Large plag. phenocrysts 5%. Very few large opq. 1-2%, but seem to be associated with the phenocrysts and patches of secondary epidote. Groundmass is very fine; opq. 20%, plag. 50%, epidote 20%? and others too fine to see. Glass originally?

Alteration: Feld. altered, as is groundmass, mostly to epidote.

Rock Type: Andesite/basalt

Site Number: AT83

General Description: V. similar to AT82. Plag. phenocrysts, also large masses of plag. with associated opq. and epidote, as in AT82. Groundmass as AT82.

Alteration: Intense alteration of plag. Lots of epidote 70%? in groundmass.

Rock Type: Andesite/basalt

Site Number: AT86

General Description: Altered plag. phenocrysts, fine groundmass epidote 60%, opq. 20%, chlorite 10%.

Alteration: Chlorite 20% and large calcite xtals + associated chlorite/epidote in vesicles.

Rock Type: Basalt/andesite

Site Number: AT88

General Description: Equi-granular essentially, but some larger altered plag. Groundmass 40% opq. and 40% plag. laths.

Alteration: Chlorite/epidote affects groundmass, lots of small qtz. veins.

Rock Type: Basalt/andesite

Vetado Pluton Dykes

Site Number: AT1

General Description: Grey-black colour. One large megacryst of plag. (labradorite).

Hornblende (actinolitic?) 40% dominates. 30% phenocrysts of plag./orth., some of the plag. has a perthitic texture. 10% opq.

Alteration: Plag. and amphibole? altered to sericite. Secondary biotite, epidote and sphene. Sphene is reacting from elongate opq. minerals, possibly ilmenite?

Rock Type: Micro-gabbro

Site Number: AT3

General Description: As 1, but coarser. Good zoning seen in plag.

Alteration: Amphibole altered to brown mineral, chlorite? More sphenes, again associated with elongate opaque, likely to be ilmenite. Same proportion of opq. as AT1.

Rock Type: Micro-gabbro (more intermediate than 1)

Site Number: AT5

General Description: As 1. Opq. 15%, plag. 60%, proportionally less amphibole 20%.

Alteration: More altered, especially chlorite. Less sphene and biotite.

Rock Type: Micro-gabbro - micro-diorite

Site Number: AT6

General Description: Porphyritic, zoned plag. phenocrysts 40%. One large phenocryst of hornblende also associated with clino-pyx. Groundmass is very fine inc. plag. 50%, opq. 20%, hornblende? 30%

Alteration: Fresher than previous samples, especially feld. Lots of chlorite.

Rock Type: Micro-gabbro - micro-diorite

De Las Animas Pluton Dykes

Site Number: AT17

General Description: Porphyritic. Dominant clino-pyx. 50%, some zoned. Definitely hyperthene, possible ortho-pyx. High extinction angle $\sim 38^\circ$. Plag. 40%, possibly olivine. Talc like texture seen in places, may be chlorite/sphene/calcite combination.

Alteration: Chlorite from pyx. and possibly olivine. In groundmass low proportions of epidote and qtz. are present.

Rock Type: Basalt/andesite

Site Number: AT18

General Description: Equi-granular. Lots of amphibole 40%, plag. 30%, calcite 10% (?secondary). More opq., get patches up to 30%, may be magnetite or pyrrhotite.

Alteration: Lots of secondary chlorite, cannot identify original minerals. Epidote replaces plag. Late stage opaque minerals, including possible magnetite, particularly with veins.

Rock Type: Micro-diorite

Site Number: AT19

General Description: Amphibole dom. 40%Pyx. 10%. Zoned plag. 20%. Opq. 10%.

Alteration: Highly altered. Amphibole altered to epidote and chlorite, plag. to sericite.

Secondary calcite and opq., particularly in vesicles.

Rock Type: Micro-diorite

Site Number: AT22

General Description: Very plag. rich, 60%. 30% amphibole. Opq. coarser than previous samples from pluton up to 1mm. Xtals of haematite identified.

Alteration: Highly altered. Lots of chlorite and carbonate affects 70% of rock, less epidote 10%. There is some secondary qtz. associated with veins.

Rock Type: Basalt

Las Tazas Pluton Dykes

Site Number: AT27

General Description: 40% plag. dom. Pyx. phenocrysts 20%. Often zoned, possibly azurine-augite. 30% amphibole. Opq. 10%. Groundmass is very fine, 5% muscovite (secondary?). Dom. amphibole 40% and plag. 40%.

Alteration: Epidote, carbonate and possibly muscovite.

Rock Type: Basalt/andesite

Site Number: AT29

General Description: Porphyritic amphibole dom. 50%, opq. 5-10%, also plag.

Groundmass is qtz., amphibole and opq., less than 27.

Alteration: Plag. highly altered to sericite. Epidote, chlorite and haematite also present.

Rock Type: Dacite

Remolino Pluton Dykes

Site Number: AT45

General Description: Plag. phenocrysts 60%. Concentrations of phenocrysts with associated opq., pyx. and amphibole. 20% opq. Groundmass amphibole 40%, plag. 40%.

Alteration: Highly altered. Chlorite replaces much of the plag. and pyx. Secondary opq.

Rock Type: Basalt

Site Number: AT46

General Description: Altered plag. phenocrysts 10%. Groundmass is fine grained 20% opq. Also plag. 40%, qtz. 40% and possibly hornblende.

Alteration: Highly altered, pseudomorphic replacement of plag., opq. and amphiboles? by chlorite. In a vein are coarser opq., evidence that secondary fluids deposited opq.

Rock Type: Dacite

Site Number: AT48

General Description: Phenocrysts originally amphibole 10%. Xenolith present, plag. and hornblende but no opq. Groundmass is opq. 10%, hornblende 50% and plag. 30%.

Alteration: Phenocryst have been completely replaced by chlorite. Epidote present.

Rock Type: Basalt/andesite

Site Number: AT49

General Description: Dom. plag. phenocrysts 30%, most are zoned, common reaction rims. Pyx. phenocrysts 20% also present. Opq. 10%, include magnetite/pyrrhotite? Groundmass is opq. 20%, plag., hornblende?, epidote? V. fine, diff. to estimate.

Alteration: Pyx. phenocrysts altered to chlorite, sometimes whole mineral is replaced, but often there is just an alteration rim. Groundmass is altered in patches.

Rock Type: Micro-gabbro - micro-diorite

Quebrada Monardes Sandstone

Site Number: ESP22

General Description: Poorly sorted F-M sand, dominated by qtz 70%, often with fluid inclusion tracks, also poly crystalline qtz. Plag. feld. 15%, lithic clasts 5%, containing feld., qtz., opq. Also minor opq., dom. haematite, and mica.

Alteration: Secondary haematite, particularly as rims on qtz. grains.

Rock Type: Sub-litharenite

Site Number: ESP29

General Description: Well sorted fine sand. Compositionally similar to ESP22, but with more mica. Occasionally large clasts of feld./lithic fragments.

Alteration: Secondary haematite, particularly as rims on qtz. grains.

Rock Type: Sub-litharenite

Sierra Fraga Formation

Site Number: ESP32

General Description: Porphyritic, feld. phenocrysts (anorthite) sometime zoned 30%. Lesser clino-pyx 20%. Groundmass originally of plag. 60%, opq. 30%, ?mica.

Alteration: Feld. to sericite. Groundmass contains lots of epidote, and secondary opq.

Rock Type: Basaltic lava

Site Number: ESP36

General Description: Equigranular, fine grained altered. Plag. 50%, qtz. 10% with undulose extinction, ? glass shards. Groundmass v. fine ?glass.

Alteration: Highly altered. Feld. to sericite, lots of secondary calcite present.

Rock Type: ?Tuff/ignimbrite

Site Number: ESP40

General Description: Porphyritic, 30% plag. phenocrysts which contain earlier opq. Also porphyritic clino-pyx 20%. Groundmass is fine, plag. 60%, opq. 30%, ?glass.

Alteration: Highly altered, feld. to sericite, some original inclusions in the feld. are altered to chlorite. Vesicle infilled with chlorite and later epidote. Also a large amount of epidote present in the groundmass.

Rock Type: Basaltic lava

Quebrada Viciñita Formation

Site Number: ESP50

General Description: Porphyritic, plag. 10% and smaller clino-pyx phenocrysts 10%.

Original groundmass probably of feld. 50%, pyx. 10%, opq. 10%.

Alteration: Feld. to sericite, epidote approx. 50% of the groundmass.

Rock Type: Basaltic lava.

Site Number: ESP53

General Description: Porphyritic, plag. (?andesine) 20% with 10% associated clino-pyx.

Large dark patches, may be haematite. Groundmass, glassy, brown. Also some plag. xtals.

Alteration: Feld. to sericite. Vesicle filled by, in order, chlorite, qtz. (drusy texture), calcite.

Sample, and vesicle fill, cut by veins. Filled with dom. calcite. In places secondary epidote with associated amphibole (?actinolite) fills vesicles.

Rock Type: Basaltic lava

Site Number: ESP58

General Description: Porphyritic, 40% plag. phenocrysts which contain small opq. and clino-pyx. Olivine also present 5%. Groundmass plag. 50% and opq. 20%, inc. haematite.

Alteration: Epidote replaces some large xtals., original mineral cannot be identified.

Epidote also abundant in the groundmass along with calcite.

Rock Type: Basalt lava

Cerro Valiente Sequence

Site Number: ESP62

General Description: ? porphyritic, difficult to tell altered xtals from infilled vesicles.

?Feld. present. Groundmass glassy, with some identifiable feld., opq.

Alteration: All xtals highly altered, haematite and epidote. Vesicle filled with qtz./calcite.

Rock Type: ?Basaltic Lava

Site Number: ESP64

General Description: Porphyritic, plag. 20% phenocrysts which show reaction rims. Inside felds. are opq. Also olivine present. Groundmass originally dom. feld. 60% and opq. 30%.

Alteration: Feld. virtually replaced by sericite and epidote. Groundmass altered to chlorite and epidote.

Rock Type: Basalt lava

Appendix 2

PALAEOMAGNETIC DATA

All of the palaeomagnetic data reported in this thesis is stored on computer disk at the Department of Geological Sciences, University of Plymouth, Drake Circus, Plymouth, Devon, PL4 8AA, UK.

REFERENCES

- Aguirre, L., B. Levi and J.O. Nystrom, The link between metamorphism, volcanism and geotectonic setting during the evolution of the Andes, in *Evolution of metamorphic belts, Geol. Soc. Special Publication*, vol. 43, edited by J.S. Daly, R.A. Cliff and B.W.D. Yardley, pp. 223-232, 1989.
- Allmendinger, R.W., V.A. Ramos, T.E. Jordan, M. Palma and B.L. Isacks, Paleogeography and Andean structural geometry, northwest Argentina, *Tectonics*, 2, 1-16, 1983.
- Anderson, E.M., *The dynamics of faulting*, Oliver and Boyd, Edinburgh, 1951.
- Andriamirado, C.R.A., Recherches paléomagnétiques sur Madagascar. Résultats et interprétations dans le cadre de la dialocation de la partie occidentale du Gondwana, PhD. thesis, 350 pp., Univ. of Strasbourg, Strasbourg, France, 1971.
- Apperson, K.D., Stress fields of the overriding plate at convergent margins and beneath active volcanic zones, *Science*, 254, 670-678, 1991.
- Arabasz, W.J., Geological and geophysical studies of the Atacama Fault Zone in northern Chile, Unpublished PhD. thesis, California Institute of Technology, 1971.
- Arevalo, C., Mapa geologico de la hoja Los Loros, Servicio Nacional de Geologia y Minería, Documentos de trabajo, No. 6, 1994.
- Arevalo, C., Mapa geologico de la hoja Copiapo, Servicio Nacional de Geologia y Minería, Documentos de trabajo, No. 8, 1995
- Aydin, A. and B.M. Page, Diverse Pliocene-Quaternary tectonics in a transform environment, San Francisco Bay region, California, *Geol. Soc. Am. Bull.*, 95, 1303-1317, 1984.
- Baker, P.E., O. González-Ferrán, and D.C. Rex, Geology and geochemistry of the Ojas del Salado volcanic region, Chile, *J. Geol Soc. Lond.*, 144, 85-96, 1987.

- Beck, M.E., Jr., Discordant paleomagnetic pole positions as evidence of regional shear in the Western Cordillera of North America, *Am. J. Sci.*, 276, 694-712, 1976.
- Beck, M.E., Jr., Paleomagnetic record of plate-margin tectonic processes along the western edge of North America, *J. Geophys. Res.*, 85, 7115-7131, 1980.
- Beck, M.E., Jr., Analysis of late Jurassic-Recent paleomagnetic data from active plate margins of South America, *J. South Am. Earth Sci.*, 1, 39-52, 1988.
- Beck, M.E., Jr., Model for Late Mesozoic-Early Tertiary tectonics of coastal California and western Mexico, and speculations on the origin of the San Andreas fault, *Tectonics*, 5, 49-64, 1986.
- Beck, M.E., Jr., R.R. Burmester, R.E. Drake and D. Riley, A tale of two continents: Some tectonic contrasts between the central Andes and the North American Cordillera, as illustrated by their paleomagnetic signatures, *Tectonics*, 13, 215-224, 1994.
- Beck, M.E., Jr., C. Rojas, and J. Cembrano, On the nature of buttressing in margin-parallel strike-slip fault systems, *Geology*, 21, 755-758, 1993.
- Bell, C.M. The origin of the Upper Palaeozoic Chañaral melange of N. Chile, *J. Geol. Soc. Lond.*, 144, 599-610, 1987.
- Bell, C.M., The relationship between sedimentary structures, transport directions and dune types in Mesozoic aeolian sandstones, Atacama region, Chile, *Geol. Mag.*, 38, 289-300, 1991.
- Bell, C.M. and M. Suárez, Late Triassic fluvial and marine shelf succession, Quebrada Doña Inés Chica, Atacama region, northern Chile, *J. S. Am. Earth Sci.*, 4, 287-293, 1991.
- Berg, K. and C. Breitzkreuz, Mesozoische Plutone in der nordchilenischen Küstenkordillere: Petrogenese, Geochronologie, Geochemie und Geodynamik mantelbetonter Magmatite, *Geotektonische Forschungen*, 66, 1-107, 1983.
- Besse, J. and V. Courtillot, Paleogeographic maps of the continents bordering the Indian Ocean since the Early Jurassic, *J. Geophys. Res.*, 93, 11,791-11,808, 1988.

- Besse, J. and V. Courtillot, Revised and synthetic apparent polar wander paths of the African, Eurasian, North American and Indian plates, and true polar wander since 200 Ma, *J. Geophys. Res.*, 96, 4029-4050, 1991.
- Briden, J.C., A new paleomagnetic result for the Lower Cretaceous of East Central Africa, *Geophys. J. R. Astron. Soc.*, 12, 375-380, 1967.
- Briden, J.C. and B.A. Duff, Pre-Carboniferous palaeomagnetism of Europe North of the Alpine orogenic belt, in *Palaeoreconstruction of the Continents*, AGU Geodyn. ser., 2, edited by M.W. McElhinny and D.A. Valencio, pp. 137-149, 1981.
- Brock, A., Paleomagnetism of Africa and Madagascar, in *Palaeoreconstructions of the Continents*, Geodyn. ser, no. 2, edited by M.W. McElhinny and D.A. Valencio, pp. 389-404, 1981.
- Brown, M., Geochemistry of the granitic complexes, 26°S-27°S, northern Chile, 5th *Congresso Geologico Chileno*, Santiago, 3, 153-1166, 1988.
- Brown, M., Relationship between magmatism and tectonics in northern Chile: Geochemical evidence from 25°30'-27°00'S, 6 *Congresso Geologico Chileno*, Actas, 1, 129-132, 1991.
- Brown, M., F. Diaz and J. Grocott, Displacement history of the Atacama Fault System 25°00'S-27°00'S, northern Chile, *Geol. Soc. Am. Bull.*, 105, 1165-1174, 1993.
- Buddin, T.S., I.G. Stimpson and G.D. Williams, North Chilean forearc tectonics and Cenozoic plate kinematics, *Tectonophysics*, 220, 193-203, 1993.
- Bussell, M.A., A simple method for the determination of the dilation direction of intrusive sheets, *J. Struc. Geol.*, 11, 679-687, 1989.
- Butler, R.F., *Paleomagnetism: Magnetic Domains to Geologic Terranes*, Blackwell Scientific, Cambridge, Mass., 1992.
- Butler, R.F., F. Hervé, F. Munizaga, M.E. Beck, Jr., R.F. Burmester and E.S. Oviedo, Paleomagnetism of the Patagonian Plateau Basalts, southern Chile and Argentina, *J. Geophys. Res.*, 96, 6023-6034, 1991.

- Butler, R.F., D.R. Richards, T. Sempere and L.G. Marshall, Paleomagnetic determinations of vertical-axis tectonic rotations from Late Cretaceous and Palaeocene strata of Bolivia, *Geology*, **23**, 799-802, 1995.
- Cande, S.C., J.L. LaBrecque and W. Haxby, Plate kinematics of the South Atlantic: Chron C34 to present, *J. Geophys. Res.*, **93**, 13,479-13,492, 1988.
- Carey, S.W., The orocline concept in geotectonics, *Proc. R. Soc. Tasmania*, **89**, 255-288, 1958.
- Castillo, J., W.A. Gose and A. Perarnau, Paleomagnetic results from Mesozoic strata in the Mérida Andes, Venezuela, *J. Geophys. Res.*, **96**, 6011-6022, 1991.
- Cembrano, J., M.E. Beck Jr., R.F. Burmester, C. Rojas, A. Garcia, and F. Herve, Paleomagnetism of Lower Cretaceous rocks of the Liquine-Ofqui fault zone, southern Chile: evidence of small in-situ clockwise rotations, *Earth and Plan. Sci. Lett.*, **113**, 539-551, 1992.
- Cobbold, P.R. and D. Gapais, Slip-system domains. 1. Plane-strain kinematics of arrays of coherent bands with twinned fibre orientations, *Tectonophysics*, **131**, 113-132, 1986.
- Coira, B., J. Davidson, C. Mpodozis and V.A. Ramos, Tectonic and magmatic evolution of the Andes of northern Argentina and Chile, *Earth Sci. Rev.*, **18**, 303-332, 1982.
- Collinson, D.W., *Methods in palaeomagnetism and rock magnetism*, Chapman and Hall, London, 1983.
- Cornejo, P.P., Mpodozis, C.M., C.F.R. Ramírez and A.J. Tomlinson, Estudio Geológico de la region de Portrerillos y El Salvador (26°-27° Lat. S), *Servicio Nacional de Geología y Minería*, 1993.
- Dallmeyer, R.D., J. Grocott, M. Brown, G.K. Taylor and P.J. Treloar, Mesozoic magmatic and tectonic events within the Andean plate boundary zone, 26°-27°S, north Chile: Constraints from ^{40}Ar - ^{39}Ar mineral ages, *J. Geol.*, **104**, 19-40, 1996.

- Dalrymple, G.B., C.S. Grommé and R.W. White, Potassium-argon age and palaeomagnetism of diabase dikes in Liberia: Initiation of central Atlantic rifting, *Geol. Soc. Am. Bull.*, 86, 399-411, 1975.
- Daly, M.C., Correlations between Nazca/Farallon plate kinematics and forearc basin evolution in Ecuador, *Tectonics*, 8(4), 769-790, 1989.
- Dalziel, I.W.D., Collision and Cordilleran orogenesis: an Andean perspective, in *Collision Tectonics, Geol. Soc. Special Publication*, no. 19, edited by M.P. Coward and A.C. Ries, pp. 389-404, 1986.
- Dalziel, I.W.D. and R.D. Forsythe, Andean evolution and the terrane concept, in *Tectonostratigraphic terranes of the Circum-Pacific Region, Circum-pacific Council for energy and mineral resources*, edited by D.G. Howell, 565-581, 1985.
- Delaney, P.T. and D.D. Pollard, Solidification of basaltic magma during flow in a dike, *Am. J. Sci.*, 282, 856-885, 1982.
- Delaney, P.T., D.D. Pollard, J.I. Ziony and E.H. McKee, Field relations between dikes and joints: Emplacement processes and paleostress analysis, *J. Geophys. Res.*, 91, 4920-4938, 1986.
- Demarest Jr., H.H., Error analysis for the determination of tectonic rotation from paleomagnetic data, *J. Geophys. Res.*, 88, 4321-4328, 1983.
- Dibblee Jr, T.W., Strike-slip tectonics of the San Andreas Fault and its role in Cenozoic basement involvement, in *Late Mesozoic and Cenozoic Sedimentation and Tectonics in California: Bakersfield, California, San Joaquin Geological Society*, edited by T.H. Nilsen, 26-38, 1977.
- Duncan, R.A. and R.B. Hargraves, Plate tectonic evolution of the Caribbean region in the mantle reference frame, *Geol. Soc. Am. Mem.*, 162, 81-93, 1984.
- Emmerman, S.H. and R. Marrett, Why dikes?, *Geology*, 18, 231-233, 1990.

- England, P and D. McKenzie, A thin viscous sheet model for continental deformation, *Geophys. J. R. Astron. Soc.*, 70, 295-321, 1982.
- Ernesto, M., I.G. Pacca, F.Y. Hiodo and A.J.R. Nardy, Palaeomagnetism of the Mesozoic Serra Geral Formation, southern Brazil, *Phys. Earth Planet. Inter.*, 64, 153-175, 1990.
- Ernesto, M., P. Renne, G. Martins, I.G. Pacca, and J.W.P. Macedo, Palaeomagnetic and Ar-Ar data on the Ceará-Mirim Mesozoic dyke swarm, Northeastern Brazil, In prep.
- Fisher, R.A., Dispersion on a sphere, *Proc. R. Soc. London*, 217, 295-305, 1953.
- Forsythe, R.D., D.V. Kent, C. Mpodozis and J. Davidson, Paleomagnetism of Permian and Triassic rocks, Central Chilean Andes, *Gondwana Six: Structure, tectonics, and geophysics*, AGU *Geophys. Mon.*, 40, edited by G.D. McKenzie, pp. 241-252, 1987.
- Forsythe, R.D. and L. Chisholm, Paleomagnetic and structural constraints on rotations in the northern Chilean coastal ranges, *J. S. Am. Earth Sci.*, 7, 279-294, 1994.
- Freund, R., Kinematics of transform and transcurrent faults, *Tectonophysics*, 21, 93-134, 1974.
- Garcia, F., Geologica del Norte Grande de Chile. Santiago Soc. Geol. de Chile. *Symposium sobre el Geosinclinal Andino 3*, p.138, 1967.
- Garfunkel, G., Regional deformation by block translation and rotation, in *Paleomagnetic rotations and continental deformation*, NATO ASI series, vol. 254, edited by C. Kissel and C. Laj, 181-208, 1989.
- Gidskehaug, A., K.M. Creer and J.G. Mitchell, Paleomagnetism and K-Ar ages of the south-west African basalts and their bearing on the time of initial rifting of the South Atlantic, *Geophys. J. R. Astron. Soc.*, 42, 1-20, 1975.
- Gordon, R.G., A. Cox and S. O'Hare, Paleomagnetic Euler poles and the apparent polar wander and absolute motion of North America since the Carboniferous, *Tectonics*, 3, 499-537, 1984.

- Gouda-Hussein, A., A. Schult and H. Soffel, Paleomagnetism of the basalts of Wadi Abu Tereifiya, Mandisa and dioritic dykes of Wadi Abu Shihat, Egypt, *Geophys. J. R. Astron. Soc.*, 56, 55-61, 1979.
- Gough, D.I. and A. Brock, The paleomagnetism of the Shawa ijolite, *J. Geophys Res.*, 69, 2489-2493, 1964.
- Gough D.I. and N.D. Opdyke, The paleomagnetism of the Lupata alkaline volcanics, *Geophys. J. R. Astron. Soc.*, 7, 457-468, 1963.
- Grocott, J., M. Brown, R.D. Dallmeyer, G.K. Taylor and P.J. Treloar, Mechanisms of continental growth in extensional arcs: an example from the Andean plate boundary zone, *Geology*, 22, 391-394, 1994.
- Hailwood, E.A. and J.G. Mitchell, Palaeomagnetic and radiometric dating results from Jurassic intrusions in south Morocco, *Geophys. J. R. Astron Soc.*, 24, 351-364, 1971.
- Hammerschmidt, K, R. Döbel and H. Friedrichsen, Implication of $^{40}\text{Ar}/^{39}\text{Ar}$ dating of Early Tertiary volcanic rocks from the north-Chilean Precordillera, *Tectonophysics*, 202, 55-81, 1992.
- Hargraves, R.B., Paleomagnetism of Mesozoic kimberlites in southern Africa and the Cretaceous apparent polar wander curve for Africa, *J. Geophys Res.*, 94, 1851-1866, 1989.
- Harland, W.B., R.L. Armstrong, A.V. Cox, L.E. Craig, A.G. Smith and D.G. Smith, *A geological Timescale*, Cambridge University Press, 1989.
- Harrington, H., Geology of parts of Antofagasta and Atacama provinces of northern Chile, *Am. Ass. Pet. Geol. Bull.*, 45, 169-197, 1961.
- Harrison, C.G.A. and T. Lindh, A polar wandering curve for North America during the Mesozoic and Cenozoic, *J. Geophys. Res.*, 87, 1903-1920, 1982.

- Hartley, A.J., P. Turner, G. Williams and S. Flint, Paleomagnetism of the Cordillera de la Costa, northern Chile: Evidence for local forearc rotation, *Earth Planet Sci. Lett.*, **89**, 375-386, 1988.
- Hartley, A.J., E.J. Jolley and P. Turner, Paleomagnetic evidence for rotation in the Precordillera of northern Chile: structural constraints and implications for the evolution of the Andean forearc, *Tectonophysics*, **205**, 49-64, 1992a.
- Hartley, A.J., P. Turner, D.C. Rex and S. Flint, Palaeomagnetic, geochronological and geological constraints on the tectonic evolution of the Mejillones Peninsula, northern Chile, *Geol. Jour.*, **27**, 59-74, 1992b.
- Heki, K., Y. Hamono and M. Kono, Rotation of the Peruvian block from palaeomagnetic studies of the Central Andes, *Nature*, **305**, 514-516, 1983.
- Heki, K., Y. Hamano, H. Kinoshita, and M. Kono, paleomagnetic study of Cretaceous rocks of Peru, South America: Evidence for rotation of the Andes, *Tectonophysics*, **108**, 267-281, 1984.
- Heki, K., Y. Hamano, M. Kono and T. Ui, Palaeomagnetism of Neogene Ocosingo dyke swarm, the Peruvian Andes: Implication for the Bolivian Orocline, *Geophys. J. R. Astron. Soc.*, **80**, 527-534, 1985.
- Herve, M., Movimiento sinistral en el Cretácico Inferior de la Zona de Falla de Atacama, Chile, *Rev. Geol. Chile*, **31**, 37-42, 1987.
- Irving, E. and G.A. Irving, Apparent polar wander paths Carboniferous through Cenozoic and the assembly of Gondwana, *Geophys. Surv.*, **5**, 141-188, 1982.
- Irwin, J.J., W.D. Sharp, R.R. Spangler and R.E. Drake, Some paleomagnetic constraints on the tectonic evolution of the Coastal Cordillera of central Chile, *J. Geophys. Res.*, **92**, 3603-3614, 1987.
- Isacks, B.L., Uplift of the Central Andean plateau and bending of the Bolivian orocline, *J. Geophys. Res.*, **93**, 3211-3231, 1988.

- Jackson, P. and D.J. Sanderson, Scaling of fault displacements from the Badajoz-Córdoba shear zone, SW Spain, *Tectonophysics*, 210, 179-190, 1992.
- Jaeger, J.C., Temperature outside a cooling sheet, *Am. J. Sci*, 257, 44-54, 1959.
- Jarrard, R.D., Relations among subduction parameters, *Rev. Geophys.*, 24, 217-284, 1986.
- Jelineck, V., Characterization of the magnetic fabric of rocks, *Tectonophysics*, 79, 63-67, 1981.
- Jesinkey, C., R.D. Forsythe, C. Mpodozis and J. Davidson, Concordant late Paleozoic paleomagnetizations from the Atacama Desert; implications for tectonic models of the Chilean Andes, *Earth Plan. Sci. Lett.*, 85, 461-472, 1987.
- Johnson, N., T. Jordan, P. Johnsson, and C. Naeser, Magnetic polarity stratigraphy, age and tectonic setting of fluvial sediments in an eastern Andean foreland basin, San Juan Province, Argentina, *Spec. Pub. int. Ass. Sediment.*, 8, 63-75, 1986.
- Jordan, T.E. and R.N. Alonso, Cenozoic stratigraphy and basin tectonics of the Andes mountains, 20°-28° South latitude, *Am. Ass. Pet. Geol. Bull.*, 71(1), 49-64, 1987.
- Jordan, T.E., P.M. Rutty, L.E. McRee, J.A. Beer, K. Tabbutt and J.F. Damanti, Magnetic polarity stratigraphy of the Miocene Río Azul section, PreCordillera thrust belt, San Juan Province, Argentina, *J. Geology*, 98, 519-539, 1990.
- Jupp P.E. and J.T. Kent, Fitting smooth paths to spherical data, *App. Stats.*, 36(1), 34-46, 1987.
- King, G., D. Oppenheimer and F. Amelung, Block versus continuum deformation in the Western United States, *Earth and Plan Sci. Lett.*, 128, 55-64, 1994.
- Kirschvink, J.L., The least-square line and plane and the analysis of paleomagnetic data, *Geophys. J. R. Astron. Soc.*, 62, 699-718, 1980.
- Kono, M., K. Heki and Y. Hamano, Paleomagnetic study of the central Andes: Counterclockwise rotation of the Peruvian block, *J. Geodyn.*, 2, 193-209, 1985.

- Kretz, R., The dilation direction of intrusive sheets, *J. Struc. Geol.*, **13**, 97-99, 1991.
- Laj, C., P. Mitouard, P. Roperch, C. Kissel, T. Mourier, and F. Magard, Paleomagnetic rotations in the coastal areas of Ecuador and northern Peru, in *Paleomagnetic rotations and continental deformation, NATO ASI series*, vol. 254, edited by C. Kissel and C. Laj, 489-511, 1989.
- Lamb, S., A model for tectonic rotations about vertical axis', *Earth Plan. Sci. Lett.*, **84**, 75-86, 1987.
- Larson, R.L. and W.C. Pitman, World-wide correlation of Mesozoic magnetic anomalies and its implications, *Geol. Soc. Am. Bull.*, **83**, 3645-3662, 1972.
- Lawver, L.A. and C.R. Scotese, A revised reconstruction of Gondwana, in *Gondwana Six: Structure, tectonics, and geophysics, AGU Geophys. Mon.*, **40**, edited by G.D. McKenzie, pp. 17-23, 1987.
- Linares, E. and D.A. Valencio, Paleomagnetism and K-Ar ages of some trachybasaltic dikes from Rio de Los Molinos, Province of Córdoba, Republic of Argentina, *J. Geophys. Res.*, **80**, 3315-3321, 1975.
- Lowrie, W., Identification of ferromagnetic minerals in a rock by coercivity and unblocking temperature properties, *Geo. Res. Lett.*, **17**, 159-162, 1990.
- Lucassen, F and G. Franz, Arc related Jurassic igneous and meta-igneous rocks in the Coastal Cordillera of northern Chile/Region Antofagasta, *Lithos*, **32**, 273-298, 1994.
- Luyendyk, B.P., Crustal rotation and fault slip in the continental transform zone in southern California, in *Paleomagnetic rotations and continental deformation, NATO ASI series*, vol. 254, edited by C. Kissel and C. Laj, 229-246, 1989.
- Luyendyk, B.P., M.J. Kamerling and R. Terres, Geometric model for Neogene crustal rotations in southern California, *Geol. Soc. Am. Bull.*, **91**, 211-217, 1980.
- MacDonald, W.D., Net tectonic rotation, apparent tectonic rotation, and the structural tilt correction in paleomagnetic studies, *J. Geophys. Res.*, **85**, 3659-3669, 1980.

- MacDonald, W.D. and N.D. Opdyke, Triassic paleomagnetism of northern south America, *Am. Ass. Pet. Geol. Bull.*, 58, 208-215, 1974.
- Macedo-Sánchez, O., J. Surmont, C. Kissel and C. Laj, New temporal constraints on the rotation of the Peruvian central Andes obtained from paleomagnetism, *Geophys. Res. Lett.*, 19, 1875-1878, 1992a.
- Macedo-Sánchez, O., J. Surmont, C. Kissel, P. Mitouard and C. Laj, Late Cainozoic rotation of the Peruvian Western Cordillera and uplift of the central Andes, *Tectonophysics*, 205, 65-78, 1992b.
- MacFadden, B.J., F. Anaya, H. Perez, C.W. Naeser, P.K. Zietler and K.E. Campbell Jr, Late Cenozoic paleomagnetism and chronology of Andean basins of Bolivia: Evidence for possible oroclinal bending, *J. Geol.*, 98, 541-555, 1990.
- MacFadden, B.J., F. Anaya and J. Argollo, Magnetic polarity stratigraphy of Inchasi: A Pliocene mammal-bearing locality from the Bolivian Andes deposited just before the Great American Interchange, *Earth Plan. Sci. Lett.*, 114, 229-241, 1993.
- MacFadden, B.J., F. Anaya and C.C. Swisher III, Neogene paleomagnetism and oroclinal bending of the central Andes of Bolivia, *J. Geophys. Res.*, 100, 8153-8167, 1995.
- Mandl, G., Tectonic deformation by rotating parallel faults: the "bookshelf" mechanism, *Tectonophysics*, 141, 277-316, 1987.
- May, S.R. and R. Butler, Paleomagnetism of the Puente Piedra Formation, central Peru, *Earth and Plan Sci. Lett.*, 72, 205-218, 1985.
- May, S.R. and R.F. Butler, North American Jurassic apparent polar wander: Implications for plate motion, paleogeography and Cordilleran tectonics, *J. Geophys. Res.*, 91, 11,519-11,544, 1986.
- McElhinny, M.W., Statistical significance of the fold test in palaeomagnetism, *Geophys. J. R. Astron. Soc.* 8, 338-340, 1964.

- McElhinny M.W. and D.L. Jones, Paleomagnetic measurements on some Karoo dolerites from Rhodesia, *Nature*, 206, 921-922, 1965.
- McFadden, P.L. and M.W. McElhinny, The combined analysis of remagnetisation circles and direct observations in palaeomagnetism, *Earth and Plan. Sci. Lett.*, 87, 161-172, 1988.
- McFadden, P.L. and M.W. McElhinny, Classification of the reversal test in paleomagnetism, *Geophys. J. Int.*, 103, 725-729, 1990.
- McKenzie, D. and J. Jackson, The relationship between strain rates, crustal thickening, palaeomagnetism, finite strain and fault movements within a deforming zone, *Earth and Plan. Sci. Lett.*, 65, 182-202, 1983.
- McKenzie, D. and J. Jackson, A block model of distributed deformation by faulting, *J. Geol Soc. Lond.*, 143, 349-353, 1986.
- McKenzie, D. and J. Jackson, The kinematics and dynamics of distributed deformation, in *Paleomagnetic rotations and continental deformation*, NATO ASI series, vol. 254, edited by C. Kissel and C. Laj, 17-31, 1989.
- Mena, M., Correlation paleomagnetica de diversos afloramientos del complejo Marifil (Provincia de Rio Negro), *Revista de la Ass. Geol. Argentina*, XLV, 136-144, 1990.
- Mendia, J.E., Palaeomagnetism of alkaline lava flows from El Salto-Almafuerte, Córdoba Province, Argentina, *Geophys. J. R. Astron. Soc.*, 54, 539-546, 1978.
- Mercado, M., Geologia de la Cordillera de la costa entre Chañaral y Caldera, *Instituto de Investigaciones Geologicas*, Carta Geologica de Chile (escala 1:100 000), 1978.
- Merrill, R.T. and M.W. McElhinney, *The Earth's magnetic field*, Academic press, London, 1983.
- Mitouard, P., C. Kissel and C. Laj, Post-Oligocene rotations in southern Ecuador and northern Peru and the formation of the Huancamba deflection in the Andean Cordillera, *Earth and Plan Sci. Lett.*, 98, 329-339, 1990.

- Montes-Lauar, C.R., I.S. Pacca, A.J. Melfi, E.M. Piccirillo, G. Bellieni, R. Petrini and R. Rizzieri, The Anari and Tapirapuã Jurassic formations, western Brazil: Paleomagnetism, geochemistry and geochronology, *Earth and Plan. Sci. Lett.*, 128, 357-371, 1994.
- Montes-Lauar, C.R., I.S. Pacca, A.J. Melfi and K. Kawashita, Late Cretaceous alkaline complexes, southeastern Brazil: Paleomagnetism and geochronology, *Earth and Plan. Sci. Lett.*, 134, 425-440, 1995.
- Mpodozis, C. and V.A. Ramos, The Andes of Chile and Argentina: Circum Pacific Council for Energy and Mineral Resources, *Earth Science Series*, 11, 59-90, 1989.
- Mpodozis, C. and R. Allmendinger, Extensión cretácica a gran escala en el norte de Chile (Puquios-Sierra Fraga, 27°): Significado para la evolución tectónica de los Andes, *Rev. Geol. de Chile*, 12, 167-197, 1992.
- Naranjo, J.A., Zona interior de la Cordillera de la Costa entre 26°00'S y 26°20'S, *Instituto de Investigaciones Geológicas*, Carta Geologica de Chile No. 34 (escala 1:100 000), 1978.
- Naranjo, J.A., Interpretación de la actividad cenozoica superior a lo largo de la zona de falla Atacama, norte de Chile, *Rev. Geol. de Chile*, 31, 43-55, 1987.
- Naranjo, J.A. and A. Puig, Hojas Taltal y Chañaral, *Instituto de Investigaciones Geológicas*, Carta Geologica de Chile No. 62-63 (escala 1:250 000), 1984.
- Naylor, M.A., G. Mandl, and C.H.K. Sijpesteijn, Fault geometries in basement-induced wrench faulting under different initial stress states, *J. Struct. Geol.*, 8, 737-752, 1986.
- Nelson, M.R. and C.H. Jones, Paleomagnetism and crustal rotations along a shear zone, Las Vegas Range, southern Nevada, *Tectonics*, 6, 13-33, 1987.
- Nicholson, C., L. Seeber, P. Williams, and L. Sykes, Seismic evidence for conjugate slip and block rotation within the San Andreas Fault System, southern California, *Tectonics*, 5, 629-648, 1986.

- Odonne, F. and G. Massonnat, Volume loss and deformation around conjugate fractures: comparison between a natural example and analogue experiments, *J. Struc. Geol.*, **14**, 963-972, 1992.
- Olson, S.F., The stratigraphic and structural setting of the Portrerillos porphyry copper district, northern Chile, *Rev. Geol. de Chile*, **16**, 3-29, 1989.
- Opdyke, N.D. and W.D. MacDonald, Paleomagnetism of Late Cretaceous Poços de Caldas alkaline complex, southern Brazil, *Earth Plan. Sci. Lett.*, **18**, 37-44, 1973.
- Oviedo, E.S., D.A. Valencio and J.F. Vilas, Palaeomagnetism of Jurassic and Cretaceous rocks from south America and the tectonics of the central Andes, in *Andean magmatism and its tectonic setting*, *Geol. Soc. Special Publication*, vol. 265, edited by R.S. Harmon and C.W. Rapela, pp. 291-299, 1991.
- Palacios, C.M., A.A. Lahsen and H. Sylvester, Low-sulfur gold mineralization at Inca de Oro, northern Chile: Mineralogy and fluid inclusions, *J. S. Am. Earth. Sci.*, **6**, 183-189, 1992.
- Palmer, H.C., A. Hayatsu, and W. MacDonald, The Middle Jurassic Camaraca Formation, Arica, Chile: Paleomagnetism, K-Ar dating, and tectonic implications, *Geophys. J. R. Astron. Soc.*, **62**, 155-172, 1980a.
- Palmer, H.C., A. Hayatsu and W. MacDonald, Palaeomagnetic and K-Ar studies of a 6 km-thick Cretaceous section, from the Chilean Andes, *Geophys. J. R. Astron. Soc.*, **62**, 133-153, 1980b.
- Pardo-Casas, F and P. Molnar, Relative motion of the Nazca (Farallon) and South American plates since Late Cretaceous time, *Tectonics*, **6**(3), 233-248, 1987.
- Peacock, D.C.P., Displacement and segment linkage in strike-slip fault zones, *J. Struc. Geol.*, **13**, 1025-1035, 1991.
- Peacock, D.C.P., M.W. Anderson, A. Morris, D.E. Randall, and J.D. Rogers, Implication of the fractal nature of faults for models of block rotation, *in prep.*

Piccirillo, E.M. and A.J. Melfi, *The Mesozoic flood volcanism of the Paraná Basin:*

Petrogenic and geophysical aspects, Instituto Astronômico e Geofísico, Universidade de São Paulo, 1988.

Platzman, E.S., J.P. Platt, C. Trapirdamaz, M. Sanver and C.C. Rundle, Why are there no clockwise rotations along the North Anatolian Fault Zone?, *J. Geophys. Res.*, **99**, 21,705-21,715, 1995.

Pollard, D.D., P. Segall and P.T. Delaney, Formation and interpretation of dilatent echelon cracks, *Bull. Geol. Soc. Am.*, **93**, 1291-1303, 1982.

Potter, D.K. and A. Stephenson, The detection of fine particles of magnetite using anhysteretic and rotational remanent magnetizations, *Geophys. J. R. Astron. Soc.*, **87**, 569-582, 1986.

Price N.J. and J.W. Cosgrove, *Analysis of Geological Structures*, University Press, Cambridge, 1990.

Ramos, V.A., T. Jordan, R.W. Allmendinger, C. Mpodozis, S. Kay, J. Cortes and M. Palma, Paleozoic terranes of the central Argentine-Chilean Andes, *Tectonics*, **5**, 855-880, 1986.

Rapalini, A.E., J. Vilas and D. Valencio, New evidence for an allochthonous plate in southwestern Argentina, *Comunicaciones, Departamento de Geologia, Universidad de Chile*, **35**, 195-196, 1985.

Rapalini, A.E., Vilas, J.F., Preliminary data from the Sierra Grande Formation: Tectonic consequences of the first mid-Paleozoic paleopoles from Patagonia, *J. S. Am. Earth Sci.*, **4**, 25-41, 1991.

Rapalini, A.E., A.L. Abdeldayem and D.H. Tarling, Intracontinental movements in western Gondwana: a palaeomagnetic test, *Tectonophysics*, **220**, 127-139, 1993.

Raposo, M.I.B., Paleomagnetism of a mid-Cretaceous mafic dike swarm from south-east Brazil, *J. Geophys. Res.*, In press.

- Raposo, M.I.B. and M. Ernesto, An Early Cretaceous paleomagnetic pole from Ponta Grossa Dikes (Brazil): Implications for the South America Mesozoic apparent polar wander path, *J. Geophys. Res.*, 100, 20,095-20,109, 1995.
- Ré, G. and S. Barredo, Estudio magnetotratigráfico y tasa de sedimentación del Grupo Iglesia en sus afloramientos aledaños a la localidad de Angualasto (Prov. de San Juan), *Actas XII Congreso Geológico Argentino*, 2, 148-155, Mendoza, 1993.
- Renshaw, C.E. and D.D. Pollard, Are large differential stresses required for straight fracture propagation paths?, *J. Struc. Geol.*, 16, 817-822, 1994.
- Ressetar, R., A.E.M. Navin and J.R. Monrad, Two phases of Cretaceous-Tertiary magmatism in the eastern desert of Egypt: Paleomagnetic, chemical and K-Ar evidence, *Tectonophysics*, 73, 169-193, 1981.
- Riley, P.D., M.E. Beck, Jr. and R.F. Burmester, Paleomagnetic evidence of vertical axis block rotations from the Mesozoic of northern Chile, *J. Geophys. Res.*, 98, 8321-8333, 1993.
- Rocha-Campos, A.C., U.G. Cordani, K. Kawashita, H.M. Sonoki and I.K. Sonoki, Age of the Paraná flood volcanism, in *The Mesozoic flood volcanism of the Paraná Basin: Petrogenic and geophysical aspects*, Instituto Astronômico e Geofísico, Universidade de São Paulo, edited by, E.M. Piccirillo and A.J. Melfi, 1988.
- Rogers, G and C.J. Hawkesworth, A geochemical traverse across the north Chilean Andes: evidence for crust generation from the mantle wedge, *Earth Plan. Sci Lett.*, 91, 271-285, 1989.
- Ron, H., R. Freund, Z. Garfunkel and A. Nur, Block rotation by strike-slip faulting: Structural and paleomagnetic evidence, *J. Geophys. Res.*, 89, 6256-6270, 1984.
- Ron, H., A. Aydin and A. Nur, Strike-slip faulting and block rotation in the Lake Mead fault system, *Geology*, 14, 1020-1023, 1986.

- Roperch, P. and G. Carlier, Paleomagnetism of Mesozoic rocks from the central Andes of southern Peru: Importance of rotations in the development of the Bolivian Orocline, *J. Geophys. Res.*, 97, 17,233-17,249, 1992.
- Roperch, P., M. Fornari and G. Hérail, A paleomagnetic study of the Altiplano (extended abstract), *2nd International Symposium on Andean Geodynamics, Program and abstracts*, 241-244, 1993.
- Royden, L.H., The tectonic expression slab pull at continental convergent boundaries, *Tectonics*, 12, 303-325, 1993.
- Rutter, E.H., On the nomenclature of mode of failure transitions in rocks, *Tectonophysics*, 122, 381-387, 1986.
- Sanderson, D.J. and W.R.D. Marchini, Transpression, *J. Struc. Geol.*, 6, 449-458, 1984.
- Sanderson, D.J., S. Roberts, J.A. McGowan and P. Gumiel, Hercynian transpressional tectonics at the southern margin of the Central Iberian Zone, west Spain, *J. Geol. Soc. Lond.*, 148, 893-898, 1991.
- Scanlan, P. and P. Turner, Structural constraints on paleomagnetic rotations south of the Arica bend, northern Chile: Implications for the Bolivian Orocline, *Tectonophysics*, 205, 141-154, 1992.
- Scheuber, E. and P.A.M. Andriessen, The kinematic and geodynamic significance of the Atacama Fault Zone, northern Chile, *J. Struc. Geol.*, 12, 243-257, 1990.
- Scheuber, E. and K.-J. Reutter, Magmatic arc tectonics in the central Andes between 21° and 25°S, *Tectonophysics*, 205, 127-140, 1992.
- Schreurs, G., Experiments on strike-slip faulting and block rotation, *Geology*, 22, 567-570, 1994.
- Schult, A. and S.D.C. Guerreiro, Palaeomagnetism of Mesozoic rocks from the Maranhão Basin, Brazil, and the opening time of the south Atlantic, *Earth Plan. Sci. Lett.*, 42, 427-436, 1979.

- Schult, A. and S.D.C. Guerreiro, Palaeomagnetism of Upper Cretaceous volcanic rocks from Cabo de Sto. Aghostino, Brazil, *Earth Plan. Sci. Lett.*, 50, 311-315, 1980.
- Schult, A., A. Hussain and H.C. Soffel, Paleomagnetism of Upper Cretaceous volcanics and Nubian sandstones of Wadi Natash, SE Egypt, and implications for the polar wander path for Africa in the Mesozoic, *J. Geophys.*, 50, 16-22, 1981.
- Scotese, C.R., Atlas of Phanerozoic plate tectonic reconstructions, International lithosphere program (IUGG-IUGS), *Paleomap project technical report, no. 10-90-1*, 1990.
- Segall, P. and D.D. Pollard, Mechanics of discontinuous faults, *J. Geophys. Res.*, 85, 4337-4350, 1980.
- Segerstrom, K., Cuadrángulo Quebrada Paipote, *Instituto de Investigaciones Geológicas, Santiago, Carta Geológica de Chile*, 2, pp 35, 1960.
- Sepúlveda, P. and J.A. Naranjo, *Hoja Carrera Pinto (Región de Atacama)*, Servicio Nacional de Geología y Minería, Carta Geológica de Chile (1:250 000), Santiago, 1982.
- Sichler, B., J.L. Olivet, J.M. Auzende, H. Jonquet, J. Bonnin and A. Bonofray, Mobility of Morocco, *Can. J. Earth Sci.*, 17, 1546-1588, 1980.
- Skewes, M.A. and C.R. Stern, Tectonic trigger for the formation of Late Miocene Cu-rich breccia pipes in the Andes of central Chile, *Geology*, 22, 551-554, 1994.
- Smith, A.G. and J.C. Briden, *Mesozoic and Cenozoic Palecontinental maps*, University Press, Cambridge, 1977.
- Somoza, R., South American reference pole for the mid-Cretaceous: Further constraints in the interpretation of Andean paleomagnetic data, *Geology*, 22, 933-936, 1994.
- Somoza, R., S. Singer and B. Coira, Paleomagnetism of Upper Miocene ignimbrites at the Puna; An analysis of vertical axis rotation in the central Andes, *J. Geophys. Res.*, 101, 11,387-11,400, 1996.
- Sonder, L.J. and P.C. England, Vertical averages of the rheology of continental lithosphere: Relation to thin sheet parameters, *Earth and Plan. Sci. Lett.*, 77, 89-90, 1986.

- Sonder, L.J., C.H. Jones, S.L. Salyards and K.M. Murphy, Vertical axis rotations in the Las Vegas Valley Shear Zone, southern Nevada: Paleomagnetic constraints on kinematics and dynamics of block rotations, *Tectonics*, 13, 769-788, 1994.
- Spence, D.A. and D.L. Turcotte, Magma-driven propagation of cracks, *J. Geophys. Res.*, 90, 575-580, 1985.
- St. Amand, P. and C.R. Allen, Strike-slip faulting in Northern Chile, *Geol. Soc. Am. Bull.*, 71, 1965, 1960.
- Stephenson, A, S. Sadikun and D.K. Potter, A theoretical and experimental comparison of the anisotropies of magnetic susceptibility and remanence in rocks and minerals, *Geophys. J. R. Astron. Soc.*, 84, 185-200, 1986.
- Storedvedt, K.M., V. Monstad, S. Asse and R. Lovlie, Paleomagnetism and early magmatic history of Fuerteventura (Canary Islands), *J. Geophys.*, 46, 319-331, 1979.
- Suárez, M. and C.M. Bell, Sabkhas continentales y costeros en el Triásico Superior-Cretácico Inferior de Atacama, Chile, *Rev. Geol. de Chile*, 24, 145-153, 1985.
- Suárez, M. and C.M. Bell, Braided rivers, lakes and sabkhas of the Upper Triassic Cifuncho Formation, Atacama Region, Chile, *J. S. Am. Earth Sci.*, 7, 25-33, 1994.
- Sylvester, A.G., Strike-slip faults, *Geol. Soc. Am. Bull.*, 100, 1666-1703, 1988.
- Tanaka, H., H. Tsunakawa, and K. Amano, Palaeomagnetism of the Cretaceous El Way and Coloso Formations from the northern Chilean Andes, *Geophys. J.*, 95, 195-203, 1988.
- Taylor, G.K., J. Grocott, A. Pope and D.E. Randall, Mesozoic fault systems, deformation and fault block rotation in the Andean forearc 25°-27°S: A crustal scale strike-slip shear zone in the Coastal Cordillera of northern Chile, *Earth Planet Sci. Lett.*, In prep.
- Tchalenko, J.S., Similarities between shear zones of different magnitudes, *Geol. Soc. Am. Bull.*, 81, 1625-1640, 1970.
- Thiele, R., and M. Pincheira, Tectónica transpresiva y movimiento de desgarre en el segmento sur de la zona de falla Atacama, Chile., *Rev. Geol. Chile*, 31, 77-94, 1987

- Thompson, R. and R.M. Clark, 'Fitting polar wander paths', *Phys. Earth Planet Int.*, 27, 1-7, 1981.
- Tikoff, B. and C. Teyssier, Crustal-scale, en echelon "P-shear" tensional bridges: A possible solution to the batholithic room problem, *Geology*, 20, 927-930, 1992.
- Tomlinson, A., C. Mpodozis, P. Comejo, and C. Ramirez, Structural geology of the Sierra Castillo-Agua Amarga fault system, Precordillera of Chile, El Salvador-Portrerillos, 2nd *International Symposium on Andean Geodynamics, Program and abstracts*, 259-262, 1993.
- Tsunakawa, H., H. Tanaka, K. Amano and M. Kono, Paleomagnetic study of Late Miocene and Early Pliocene rocks from southern Peru, Central Andes, *J. Geomag. Geoelectr.*, 39, 477-486, 1987.
- Turner, P., Clemmy, H., and S. Flint, Palaeomagnetic studies of a Cretaceous molasse sequence in the central Andes (Coloso Formation, Northern Chile), *J. Geol. Soc. Lond.*, 141, 869-876, 1984.
- Valencio, D.A., El paleomagnetismo de algunas magmatitas del Triasico superior, Grupo Cacheuta Prov. de Mendoza, Rep. Argentina, *Revista de la Ass. Geol. Argentina*, XXIV, 191-198, 1969.
- Valencio, D.A. and J.F. Vilas, Palaeomagnetism of some Middle Jurassic lavas from south-east Argentina, *Nature*, 225, 262-264, 1970.
- Valencio, D.A., Palaeomagnetism of the Lower Cretaceous Vulcanitas Cerro Colorado Formation of the Sierra de los C6ndores group Province of C6rdoba, Argentina, *Earth and Plan. Sci. Lett.*, 16, 370-378, 1972.
- Valencio, D.A. and J.F. Vilas, Palaeomagnetism of Late Palaeozoic and Early Mesozoic rocks of South America, *Earth and Plan. Sci. Lett.*, 15, 75-85, 1972.

- Valencio, D.A., J.E. Mendia, A. Giudici and J.O. Gascon, Palaeomagnetism of the Cretaceous Pirgua Subgroup (Argentina) and the age of the opening of the South Atlantic, *Geophys. J. R. Astron. Soc.*, **51**, 47-58, 1977.
- Valencio, D.A., J.F. Vilas, P. Solá and M.G. López, Palaeomagnetism of Upper Cretaceous-Lower Tertiary igneous rocks from Central Argentina, *Geophys. J. R. Astron Soc. Lond.*, **73**, 129-134, 1983a.
- Valencio, D.A., J.F. Vilas and I.G. Pacca, The significance of the paleomagnetism of Jurassic-Cretaceous rocks from South America: Predrift movements, hairpins and magnetostratigraphy, *Geophys. J. R. Astron Soc. Lond.*, **73**, 135-151, 1983b.
- Van der Voo, R., Jurassic paleopole controversy: Contributions from the Atlantic-bordering continents, *Geology*, **20**, 975-978, 1992.
- Van der Voo, R., *Paleomagnetism of the Atlantic, Tethys and Iapetus Oceans*, University Press, Cambridge, 1993.
- Vickery, S. and S. Lamb, Large tectonic rotations since the Early Miocene in a convergent plate-boundary zone, South Island, New Zealand, *Earth and Plan. Sci. Lett.*, **136**, 43-59, 1995.
- Vilas, J.F., Palaeomagnetism of some igneous rocks of the Middle Jurassic Chon-Aike Formation from Estancia La Reconquista, Province of Santa Cruz, Argentina, *Geophys. J. R. Astron. Soc.*, **39**, 511-522, 1974.
- Vilas, J.F., Palaeomagnetism of the Lower Cretaceous Sierra de los Condores Group Cordoba Province Argentina, *Geophys. J. R. Astron. Soc.*, **46**, 295-305, 1976.
- Vilas, J.F. and D.A. Valencio, Palaeomagnetic and K-Ar dating of the Carboniferous Andacollo Series (Argentina) and the age of its hydrothermal overprinting, *Earth and Plan. Sci. Lett.*, **40**, 101-106, 1978.
- Warsi, W.E.K., T.W.C. Hilde, and R.C. Searle, Convergence structures of the Peru trench between 10°S and 14°S, *Tectonophysics*, **99**, 313-329, 1983.

- Watts, A.B., S.H. Lamb, J.D. Fairhead and J. Dewey, Lithospheric flexure and bending of the Central Andes, *Earth Plan. Sci. Lett.*, 134, 9-21, 1995.
- Wilcox, R.E., T.P. Harding and D.R. Seely, Basic wrench tectonics, *Am. Ass. Petrol. Geol. Bull.*, 57, 74-96, 1973.
- Woodcock, N.H., The role of strike-slip fault systems at plate boundaries, *Phil. Trans. R. Soc. Lond.*, A317, 13-29, 1986.
- Zijderveld, J.D.A., A.C. demagnetisation of rocks: Analysis of results, in *Methods in palaeomagnetism*, Elsevier, Amsterdam, edited by D.W. Collinson and S.K. Runcorn, 254-286, 1967.